STELLARATORS

STATUS AND FUTURE DIRECTIONS

JOINT US-EURATOM REPORT

JULY 1981

Published for the
JOINT US-EURATOM STEERING COMMITTEE ON STELLARATORS
by
MAX-PLANCK-INSTITUT FÜR PLASMAPHYSIK
D-8046 Garching, F.R. Germany

REPORT IPP 2/254

STELLARATORS

STATUS AND FUTURE DIRECTIONS

JOINT US-EURATOM REPORT

JULY 1981

Published for the
JOINT US-EURATOM STEERING COMMITTEE ON STELLARATORS

W.F.DOVE	Washington
G.GRIEGER, Chairman	Garching
J.L.JOHNSON	Princeton
D.J.LEES	Culham
P.A.POLITZER	Cambridge
J.L.SHOHET	Madison
H.WOBIG	Garching
F.RAU, Scientific Secretary	Garching

by

MAX-PLANCK-INSTITUT FÜR PLASMAPHYSIK
EURATOM Association
D-8046 Garching, Federal Republic of Germany

REPORT IPP 2/254

PREFACE

This joint US-EURATOM report was prepared as a data base assessment in order to demonstrate the promising and challenging prospects of the stellarator as a candidate for the optimum toroidal magnetic confinement system. The outline of an intesified cooperative US-EURATOM program for stellarators is given in the Executive Summary of this document.

In the meeting between DOE and EURATOM at Washington D.C. on May 6 and 7, 1980, the officials discussed in detail the existing alternatives to tokamaks. As one result of this discussion, a Joint Steering Committee on Stellarators was formed and given the initial task to write this document within one year, starting after the 1980 IAEA Brussels Conference. Four meetings of the Steering Committee were held, two in the United States and two in Europe. At these meetings, the outline and then the text of this report were thoroughly discussed. The contributions to this document were made by members of the Steering Committee and by the following individuals:

T.K.CHU	Princeton
J.A.DERR	Madison
R.A.KRAKOWSKI	Los Alamos
L.M.LIDSKY	Cambridge
R.L.MILLER	Los Alamos
J.NÜHRENBERG	Garching
D.PFIRSCH	Garching
H.RENNER	Garching
A.SCHLÜTER	Garching
I.N.SVIATOSLAVSKY	Madison

The editing was done by

F. RAU	Garching

CONTENTS

I. EXECUTIVE SUMMARY

Introduction

The stellarator concept was one of the first proposed for the confinement of thermonuclear plasmas and is one of the few approaches capable of steady-state reactor operation. A stellarator is a toroidal magnetic confinement system. Toroidal devices with nested magnetic surfaces have demonstrated their potential for the containment of hot, dense plasmas by providing thermal insulation of the plasma from its surroundings. The tokamak is the best-known representation of this class. Its field configuration requires currents flowing in external coils and a net current flowing in the plasma. The stellarator, on the other hand, is the only concept which retains the property of nested magnetic surfaces without need for a net current in the plasma, and is thus inherently suited for steady-state operation. The concept is also compatible with the use of ohmic heating for plasma generation and heating, and the stabilizing effects of stellarator fields have clearly been demonstrated for such operation. The real potential of the stellarator concept could be demonstrated only after powerful alternate heating sources became available, since they make the ohmic heating current superfluous. Excellent confinement properties with substantial plasma parameters have been found under these conditions.

There also has been essential progress in analytical and computational work. Extensive work has produced stellarator configurations promising stable average betas of 5-10%, with aspect ratios large enough to facilitate reactor maintenance, but small enough to yield reasonable fusion output power. Monte Carlo calculations tend to show that, in the reactor regime, losses by transport seem to be tolerable.

Progress has also been made in engineering. Classical stellarator fields have been created by two sets of coils; toroidal-field coils provide most of the field energy and helical windings the required field geometry. For large devices massive structure is needed to support the electromagnetic forces between the two coil systems. Other effective coil systems have been developed which avoid the problems of excessive forces and await testing. Most of the technology problems and development areas, expected for stellarator reactors appear to be generic to magnetic fusion in general, and many of these problems are being addressed by main-line tokamak programs. Where major problems are shared between the stellarator and other approaches to magnetic fusion, they appear to be reduced in magnitude for the stellarator. Certain key problems for the main-line approaches in fact seem to be eliminated by the stellarator approach.

In summary, during the last several years worldwide progress has occurred in stellarator development. Prospects are not bad for the stellarator to become the optimum reactor concept. These advances make it necessary to assess the present data base and to recommend future directions for the program.

I.1 Special Properties of Stellarators

Stellarators have many properties that are common to tokamaks, but since a net current in the plasma is not required for equilibrium, a number of their features are distinct and exciting:

i) steady magnetic fields with nested surfaces which provide confinement from start-up and potential for self-sustained steady-state operation;

ii) no major disruptions that could lead to an abrupt and excessive energy dump on the first wall;

iii) moderate plasma and coil aspect ratios which can improve access and allow the use of higher fields at the plasma for the same limiting field at the coil, thereby allowing high plasma power density already for lower average beta;

iv) possibility for producing the full magnetic field with only one set of coils and no need for feedback position control;

v) several potential methods for impurity control and ash removal including divertors, limiters, and profile control.

Difficulties associated with the stellarator concept are addressed in the discussion of future tasks in Section 3.

I.2 State of the Art - Recent Advances

During the last few years large and steady progress has been achieved in stellarator experiment, theory, advanced-coil concept development and reactor understanding. This gain in experience provides a solid and, with respect to tokamaks, challenging basis for the next steps to be taken.

A. Experiments

There are now several experiments, mainly WENDELSTEIN VII-A, CLEO, L-2, and HELIOTRON E, which give consistent and promising results:

i) no major disruptions are observed in ohmically heated discharges, provided the external transform is large enough;

ii) the energy confinement essentially follows the drift parameter scaling for ohmically heated discharges, i.e. it improves with decreasing plasma current;

iii) net-current-free operation has been achieved with neutral beam injection, and by application of radio frequency heating;

iv) in WENDELSTEIN VII-A ion temperatures of 700 eV, densities of 10^{14} cm^{-3}, beta values not far from 1%, and $n\tau$-values of $3\text{-}4 \cdot 10^{12}$ cm^{-3} have been achieved for magnetic fields of 3 T and plasma radii of only 10 cm;

v) net-current-free discharges showed no MHD activity, no major disruptions, and an extremely low level of small-scale turbulence;

vi) transport losses in net-current-free discharges are smaller than those in ohmically heated discharges with similar conditions;

vii) experiments with high-power near-perpendicular injection indicate good confinement of high-energy particles;

viii) in HELIOTRON E the afterglow of a radio-frequency heated discharge yielded an energy confinement time of 35 msec, and electron and ion temperatures of 200 and 150 eV, respectively, at densities of about $5 \cdot 10^{12}$ cm^{-3}.

B. Theory

Theoretical progress is concentrated in three essential fields:

i) numerical codes for three-dimensional plasma equilibrium and stability have been developed; present indications are that realistic $\ell = 2,3$ stellarator and torsatron equilibria exist with beta as high as 5%;

ii) plasma configurations with reduced secondary currents can be achieved by superposition of helical fields with different helicities; compared to classical stellarators with identical rotational transform and aspect ratio much higher equilibrium betas are obtained; a configuration of this type with an average magnetic well seems to promise stability betas up to 10 % at a plasma aspect ratio of about 20;

iii) recently established Monte Carlo codes for collisional transport yielded smaller losses than predicted analytically for simple model fields in the low-collisionality regime; further reduction of plasma losses due to radial electric fields is confirmed by these codes.

C. Coil Systems

Progress has been made in obtaining simple stellarator coil systems in which the radial components of the electromagnetic force are moderate and directed radially outward:

i) stellarator fields with large transform, reduced secondary currents in the plasma, or with other attractive properties are produced by modular coil systems without a net toroidal current;

ii) in modular configurations there are no toroidally continuous windings.

iii) torsatron fields produced by helical windings with currents in the same direction do not need separate coils for the compensating vertical fields; the current loops can be configured as a set of modules; or the coils can be net force-free.

D. Reactor Understanding

Earlier studies of stellarator reactors were based on coil concepts no longer favored today. For this reason, their projections of stellarator reactors as very large, low power-density and costly systems with untenable coil-force problems are no longer valid. Only a few studies based on the torsatron geometry or modular coils have been undertaken. These more contemporary studies concentrate on recently-resolved, key stellarator features and indicate that very acceptable solutions can be found. More thorough studies must be performed before such statements can be made with full justification.

An important question is the achievable distance between the coils and the plasma surface. This distance impacts on the embodiment of the first-wall, blanket, and shield configuration, the use of magnetic divertor versus a pumped-limiter for impurity control, and the problem of economical engineering power density. The unique interdependence of plasma physics, magnetics and coil-set design in stellarators and the wide range of configurational options make the stellarator reactor a fertile but difficult to optimize system. Nevertheless, in stellarator experiment, theory, development of advanced coil concepts, and, to some extent, reactor understanding, the recent gains provide a solid and, with respect to tokamaks, challenging basis for the next steps to be taken.

I.3 Future Tasks

There are a number of well identified tasks to be addressed in the future program. The most essential ones, which have to be treated theoretically and experimentally in a well coordinated fashion, are:

i) investigate transport properties in the long-mean-free-path, net-current-free regime, and the existence of diffusion-driven current;

ii) determine the extent that confinement can be optimized by the reduction of secondary current and drift optimization; study the available stable beta;

iii) investigate self-consistent electric fields and their effects on orbits and particle confinement;

iv) determine the mechanism of impurity control, release and transport;

v) examine the effects of the magnetic geometry, shear, harmonic content, and magnetic well;

vi) develop efficient heating methods.

These tasks have to be tackled under reactor-relevant conditions, i.e. especially at long-pulse operation with substantial plasma parameters.

I.4 Recommendations

It follows from the data base documented in this report that the stellarator program is ready to advance and to investigate systems promising further essential improvements. New and major decisions should be taken in the following fields:

A. Experiments

New and modern stellarator devices are required to allow access to regimes adequate for properly investigating the relevant issues. They should incorporate advanced stellarator-configuration ideas or techniques that drive the classical stellarator to its full advantage. They should be able to operate in the collision-free regime and have ample separation between the plasma boundary and the wall. Sufficient heating power must be provided. Utilization of modern diagnostics is essential.

The program should incorporate parallel development and use of several experimental devices and subsequently at least one large feasibility experiment. This should have hydrogen operation with plasma parameters envisaged in a fusion reactor in order to prove the reactor potential of the stellarator.

B. Theory

Configuration studies are producing significant results at an acceptable rate. The level of effort on beta limits and transport properties, with all their three-dimensional implications, is inadequate and needs to be expanded. Adequate manpower and computer time must be provided and a proper balance between numerical and analytic approaches has to be ensured.

C. Reactor Studies

Questions regarding engineering and reactor developments have been, and are, of prime importance for stellarators. Therefore, some stellarator reactor studies with modest industrial involvement are necessary to identify the most essential reactor properties and to provide a focus for the theoretical and experimental programs.

D. Technology

No special technology program is required for stellarators at this time because the basic technologies can be transferred from other parts of the fusion development program. Some small-scale work might be required, however, to include the specific stellarator geometry into these technologies.

I.5 Role of Stellarators in the Fusion Program

A. Schedule

There is general agreement that, apart from a demonstration of basic physics, the essential task of the next big step in the development of fusion as a whole is to provide a device for the development and demonstration of fusion-relevant technology. This requires sufficient neutron flux and fluence and thus reliable operation of the machine. There is little need to use reactor-relevant considerations for selecting the confinement system used for this purpose. Therefore the tokamak will be used since its data base is most complete and its performance is most predictable. Optimization of the reactor concept is then the task for the following step.

This provides a unique situation for the development of the stellarator concept:

i) as an alternative system it has many basic features different from the tokamak which promise essential improvement. Since the basic requirements of stellarator technology are similar to those of other toroidal systems, the stellarator program can concentrate on its physics issues and a continuing assessment of reactor potential.

ii) as follows from above, the target date for selecting the optimum reactor concept occurs after operation of the engineering test reactor, i.e. in the early nineties. This provides sufficient time for two sequential generations of new stellarator experiments, with the second one to prove the full feasibility.

B. International Cooperation

Increased international cooperation has become a major driving force for the development of stellarators. There exists a well established foundation as this report demonstrates. The combined EURATOM and US stellarator activities have the potential to yield a well coordinated and sufficiently thorough program to achieve a sound feasibility demonstration of the stellarator concept in proper time. The extension of this cooperation will be of particular benefit to both partners since the ideas of the next-generation devices are rather complementary. This cooperation should be open to other potential partners.

II. HISTORY OF STELLARATOR RESEARCH

A stellarator is a closed steady-state toroidal device for confining a hot plasma in a magnetic field where the rotational transform is produced externally, from torsion or coils outside the plasma. This concept was one of the first approaches proposed for obtaining a controlled thermonuclear device. It was suggested and developed at Princeton in the 1950's. Worldwide efforts were undertaken in the 1960's. The United States stellarator commitment became very small in the 1970's, but recent progress, especially at Garching and Kyoto, together with some new insights for attacking both theoretical issues and engineering concerns have led to a renewed optimism and interest as we enter the 1980's.

The stellarator concept was born in 1951. Legend has it that Lyman Spitzer, Professor of Astronomy at Princeton, read reports of a successful demonstration of controlled thermonuclear fusion by R. Richter in Argentina, when he was on a ski trip. As he rode up the ski lift he pondered over how this could be achieved. He considered the possibility of mirror containment but dismissed it because of scattering into the loss cone. He preferred steady-state operation and chose not to use internal currents to set up the magnetic fields in closed devices as in pinches or tokamaks. He recognized the problem with toroidal confinement due to $E \times B$ drifts, where the electric field is set up by the $B \times \nabla B$ drifts of the ions and electrons. This led to a need for a rotational transform so that the electrons could flow along the magnetic field lines from regions of accumulation to regions of positive charge, thus eliminating the electric field. Spitzer's big achievement was to recognize that this could be accomplished by bending the torus into a figure-eight shape. Then the electrons would drift upwards in one end of the system and downwards in the other so that the charge could be neutralized by flow along the magnetic field lines. At this time he developed an understanding of most of the problems associated with thermonuclear containment-auxilliary heating since ohmic heating to ignition is difficult, need for a divertor to protect the plasma from impurities sputtered from the wall, etc. Spitzer's proposal to develop the stellarator concept was supported, and stellarator studies began in the summer of 1951.

A conceptual plan evolved leading to a four stage stellarator program: Model A, a small, low-field, table-top device would demonstrate the feasibility of the idea with confinement of the electrons. Plasma confinement, heating, and divertor action would be demonstrated on one or more Model B devices which would have roughly a two inch tube diameter and a 30 kG field. The Model C Stellarator with an 8 inch diameter vessel and 50 kG field would essentially be a quarter-scale pilot model of a power producing prototype, Model D.

The Model A Stellarator was built in 1952 and showed that breakdown could be achieved more easily in a figure-eight device with a rotational transform than in a pure torus. Although cross field diffusion seemed higher than expected, it confirmed the theoretical expectations.

The Model B1 Stellarator became operational in 1954 and met significant difficulties with forces on the coils and impurities. After being rebuilt with a stainless steel vessel and incorporating state of the art high-vacuum techniques, this device became quite reliable. Plasma diagnostic techniques, particularly using spectroscopic and microwave methods, were developed on it. Its noteworthy results concerned MHD instabilities. In particular, it was found that if the plasma current associated with Ohmic heating exceeded the Kruskal limit, the discharge became violently turbulent and the plasma was rapidly lost to the walls. Instabilities were also observed at lower currents. These are now considered to be tearing modes, but, at the time, there were questions concerning whether they were associated with a loss of equilibrium due to the rotational transform becoming rational.

As B1 was starting to work, a reactor study, the Model D Report, was initiated to determine whether or not the device would be economically interesting if the physics problems could be solved. It found that β, the ratio of material to magnetic pressure, would have to be very high ~ 0.7, largely because of the energy dissipated in the coils, and the total power would be large ~ 5GW. On the basis of this design, studies for the Model C device were initiated in 1954.

In 1954 Edward Teller raised the question of magnetohydrodynamic instabilities. It was quickly recognized that, with the bulges provided for a magnetic pumping region and for a divertor and with the magnetic field lines twisting with the same pitch, the stellarator was clearly unstable with respect to interchange modes. This quickly led to two actions. First, design efforts for the Model C device were stopped. Second, a major effort on MHD stability was initiated. Again, Spitzer quickly provided the answer: by making the twist or rotation of the magnetic field lines different on neighboring magnetic surfaces, one could make it necessary to bend the field lines to interchange them, thus stabilizing the mode. His technique for providing this shear led to the development of helical windings. Since these provided a rotational transform as well as shear, it was no longer necessary to utilize the figure-eight geometry.

The need for a well-designed bakable device for impurity control led to the design and construction of B3. One of the many significant results emerging from this machine was the measurement of plasma recycling from the walls, leading to a good determination of particle confinement. This confirmed the earlier indications of much poorer plasma confinement than is predicted classically and led to a major study of pumpout.

The improved stability picture with shear stabilization, although with much lower β values than previously hoped for, together with the observation that pumpout was so large in the small devices that the particles could not be held long enough to be heated to an interesting temperature, led to reinitiating work on Model C. This device, with an eight inch vacuum vessel, helical windings, a divertor, and an ICRF heating port was started in 1957. It was planned strictly as a research device.

Other devices made contributions to the program in this period. Magnetic pumping was investigated on B2 with good energy absorption observed from the power supply but so many impurities introduced that the plasma was actually cooled. The first demonstrations of the efficacy of a divertor for impurity control and of the use of helical windings to provide a rotational transform were made on B64 and B65, modular stellarators proposed by Thomas Stix. Drift waves were identified and phase correlations between density and electric field fluctuations investigated on ETUDE, a steady-state torus with helical windings.

This first phase of the stellarator program came to a close at the first United Nations Conference on the Peaceful Uses of Atomic Energy in Geneva in 1958 when the wraps of secrecy were removed from the United States, the Soviet Union, and European controlled nuclear fusion programs. These results were presented there with the Model B2 Stellarator providing a working demonstration. Although large problems remained to be solved, it was clear that considerable progress had been made and the concept was viable. The interest generated there stimulated worldwide interest in stellarators.

The second phase of the stellarator program started with the declassification and was marked by increased interest and activity around the world.

The only stellarator experiments reported at the First International Conference on Plasma Physics and Controlled Nuclear Fusion Research, held at Salzburg in 1961, concerned work on the B1 and B3 Stellarators and initial operation of Model C. The most important result was the observation of Bohm diffusion, with the containment time scaling as B/T and the magnitude no more than a factor of three better than Bohm's formula.

The stellarator concept was picked up at the Max-Planck Institut in Munchen Germany (later Garching) immediately after declassification in the United States. An essential impact on this program occurred at the Salzburg Conference, where comparison of the Model C results with classical confinement of a thermal cesium plasma in a straight Q-machine indicated that running a thermal, collisional cesium plasma with a "perfect" Maxwellian distribution in a stellarator configuration should give decisive information on the viability of the stellarator confinement concept. A series of experimental devices were built along this line. The first one, WENDELSTEIN I-A, a small $\ell = 3$ race-track machine ($R = 35$ cm, $a \approx 2$ cm, $B < 20$ kG) showed high losses. Introducing some curvature into the magnetic field in a linear Q-machine showed some increase in the loss rates, but this effect could be explained by $\int d\ell/B$ not being constant when the lines were bent. The WENDELSTEIN I-A results were explained by the Pfirsch-Schluter model according to which the r^2-dependence of the $\ell = 3$ rotational transform was not sufficient to provide equilibrium. In order to check this, WENDELSTEIN I-B an $\ell = 2$ stellarator with higher central transform but otherwise the same dimensions as WENDELSTEIN I-A was built.

More work was reported at the Second IAEA conference at Culham in 1965. The big theoretical development in this period was the discovery of resistive instabilities which grow on a much faster time scale than that of transport and thus are particularly dangerous for steady-state devices. Because the magnetic field lines are reconnected by the interchange, magnetic shear provides no stabilization. Thus it appears to be necessary to obtain configurations with minimum average B. Several papers describing techniques for achieving this were reported at this conference, but they all required complicated field configurations.

The Model C Stellarator studies continued to demonstrate Bohm diffusion, with drift waves associated with the ohmic heating current being ruled out as the major loss mechanism. Favorable results for ion cyclotron radio frequency heating were reported. Plasma guns were used to inject plasma into L-1, an $\ell = 2$ stellarator at the Lebedev Institute in Moscow. Good confinement was observed in current-free discharges. The Garching group reported excellent confinement of cesium plasmas, with classical diffusion being the main loss process perpendicular to B. These losses were so small that even tiny probes, 0.1 mm in diameter, provided a major disturbance. The results in WENDELSTEIN I-B were extremely sensitive to the proper adjustment of correction fields, which effect was felt to be connected with its race-track type shape and the presence of circularisers at the transitions from the curved to the straight sections. This led to the construction of the somewhat larger, circular WENDELSTEIN II-A device ($\ell = 2$, $R = 50$ cm, $a \approx 5$ cm, $B \approx 12$ kG).

The success of the Lebedev L-1 stellarator with gun-injected plasmas reported at the Culham Conference prompted the setting up of a stellarator program at the Culham Laboratory. Because of the uncertainty over the existence of magnetic surfaces in a high shear, truly toroidal stellarator and their significance in trapping plasma, it was decided to build the well-engineered, high-shear $\ell = 3$ single-particle experiment CLASP. In this device it was demonstrated that electrons generated by the β-decay of tritium, if passing particles, could be contained for more than 10^7 orbits around the system (i.e., sufficient for a reactor). Simultaneously, the CLEO experiment, a large apparatus with neutral injection, was proposed. It was decided that to build such a device was premature and PROTO-CLEO ($R = 40$ cm, $a = 5$ cm, $B = 5$ kG), a stellarator which could use either $\ell = 2$ or $\ell = 3$ coils and operate with medium or high shear, was built. This was a rather unconventional experiment, with the helical winding inside the vacuum vessel. This was necessary to remove the wall-plasma interaction, since the plasma would be produced by gun injection. This experiment was successful in that a tenuous plasma could be contained for a period as long as predicted by neoclassical theory, provided that account was taken of the finite ion gyro-radius (comparable with the density gradient scale length). Simultaneously, a turbulent heating program was carried out using TWIST, a slightly smaller $\ell = 3$ stellarator. In this experiment, a large Ohmic heating current induced

electrostatic instabilities and successfully heated the plasma by turbulence, although the magnetic field was too weak to confine the plasma.

A large number of experiments were reported at the Third International Conference at Novosibirsk in 1968. As in the earlier conferences, the major effect reported on the Model C Stellarator was in documenting and understanding the Bohm-like dependence of plasma transport. Studies with washer-gun plasmas and RF generated zero-current plasmas, both with longer mean free paths than before, gave confinement at about five times Bohm. It was noted in passing that significantly better results were being obtained with the B3 and ETUDE Stellarators. In contrast, good confinement was observed on the WENDELSTEIN II-A device at Garching. This $\ell = 2$ stellarator with little magnetic shear contained a barium plasma well enough that plasma loss could be accounted for classically, as in its predecessor, WENDELSTEIN I-B. Since in that device the losses had been so small that even tiny probes provided a major disturbance, the density in WENDELSTEIN II-A was measured by resonance flour-escence and probes could be avoided. Confinement was found to decrease markedly whenever ι is a rational fraction, where one should expect difficulties with equilibrium. Similar results related to enhanced loss when the rotational transform is rational were observed in L-1. The experiments emphasized the deterioration of the plasma properties if the magnetic surfaces have island structure.

Several new stellarator groups reported results at this meeting, including the encouraging results from Culham and some interesting work in the U.S.S.R. The Kharkov group used the SIRIUS stellarator (an $\ell = 3$, L = 600 cm, B = 20 kG racetrack device) to investigate turbulent heating. As with the TWIST work, they found regimes with high anomalous conductivity but observed that large microwave and x-ray emission was responsible for much of the energy balance. The Novosibirsk group described a small (R = 50 cm, a = 5 cm, $\ell = 3$, B ~ 2-6 kG) device which they used to study plasma diffusion.

On the theoretical front the developments in this period were relatively pessimistic. Several techniques were developed for constructing systems with minimum average B. On the other hand, new trapped-particle instabilities were discovered that indicated difficulties with three-dimensional systems. The development of neoclassical transport theory showed extremely bad confinement of collisionless plasmas. Difficulties of obtaining equilibria with well defined magnetic surfaces were discussed, with serious questioning of the severity of magnetic island problems and magnetic field line ergodicity.

All these problems emerged just at the time the Soviet researchers were obtaining good results with the T-3 Tokamak. Thus it is not at all surprising that, when the Culham group set up a Thomson scattering experiment on the T-3 device at Kurchatov and verified the high temperature claims, the United States abandoned its stellarator program and converted the Model C Stellarator into the ST Tokamak shortly after the 1969 Dubna meeting. Worldwide stellarator enthusiasm dwindled at this time as well, so that the research that continued was made more difficult by the problems associated with obtaining good diagnostic support and reasonable funding for new devices and improvements. The second phase of the stellarator program ended at this time with the program in a discouraging position.

Nevertheless, a number of new devices entered the scene as the program began its third phase. It was recognized by the Culham group that the stellarator configuration should be tested under circumstances as comparable with then existing tokamaks as possible (e.g., with T-3 and ST). The CLEO experiment (R = 90 cm, a = 11 cm, B = 20 kG) was thus designed to have an $\ell = 3$ helical winding similar to that on PROTO-CLEO and to be capable of conversion to a tokamak, so that a comparison between stellarators and tokamaks could be made in the same apparatus. At the 1971 Madison meeting, work on collisionless plasmas was reported on the Novosibirsk device, the Lebedev TOR-1 device (with $\ell = 2$, R = 60 cm, a = 8.5 cm, B = 15 kG and a large transform), and PROTO-CLEO with confinement time one fourth to one twentieth that predicted by neoclassical theory. Probably the most important stellarator experiment reported at the meeting was the demonstration in PROTO-CLEO that bootstrap currents were not seen and are thus at least an order of magnitude smaller than was predicted theoretically. Toroidal plasma motion was investigated on L-1. The Lebedev group also reported work on magnetic surfaces and island control in TOR-2 (an $\ell = 2$, R = 62.5 cm, a = 3.6 cm, B = 25 kG device). The SATURN device ($\ell = 3$, R = 35.6 cm, a = 8.6 cm, B = 6 kG) at Kharkov was used for magnetic surface studies in stellarators and torsatrons. This group reported initial operation of URAGAN (a 10 meter race track device with R = 110 cm, a = 10 cm, B = 10 kG, $\ell = 2$) and looked at the nature of anomalous conductivity with large ohmic heating current in SIRIUS, as well as investigated RF heating in OMEGA (R = 44 cm, a = 10 cm, B = 10 kG). Studies of turbulent heating in TWIST were continued. The JIPP-1 Stellarator ($\ell = 3$, R = 20 cm, a = 8.4 cm, B = 4 kG) at Nagoya was commissioned and confinement an order of magnitude better than Bohm was reported. The HELIOTRON D device (an $\ell = 2$, R = 105 cm, a = 10 cm, B = 2 kG torsatron with an auxiliary toroidal field) began operation at Kyoto. The WENDELSTEIN II-A group reported detailed studies of convection in their zero-shear device. This ended the successful work with "model-plasmas" in Garching and WENDELSTEIN II-B was built to investigate higher temperature plasmas. It was identical with WENDELSTEIN II-A but equipped with an ohmic heating transformer because among the available means this was the only one powerful enough to overcome the radiation threshold. The WENDELSTEIN VII-A stellarator (R = 200 cm, a ≈ 10 cm, $B \leq 40$ kG) was constructed in parallel. It is an $\ell = 2$ machine for avoiding resonances and has some average magnetic well for stability. The device is capable of housing a larger vacuum tube with at least twice the linear plasma dimensions. Some work was reported on high-β stellarators at Garching and Los Alamos at this meeting.

The situation was not drastically different at the 1974 Tokyo meeting. Ohmic heating experiments were carried out in WENDELSTEIN II-B, where the effect of rational magnetic surface resonances, reduced by the shear arising from the ohmic current, was seen. The electron confinement was found to be tokamak-like with some improvement of stability by the external transform, the ion confinement was close to neoclassical, and $T_e \approx 300$ eV was reached. Ohmic heating plasmas were also studied in URAGAN 1, JIPP-1B ($\ell = 2 + 3$, R = 50 cm, a = 7 cm, B = 4 kG), HELIOTRON D, and TORSO (an $\ell = 3$ ultimate torsatron successor to TWIST with R = 40 cm, a = 6.5 cm, B = 20 kG), resulting in confinement times comparable to pseudoclassical predictions. The torsatron, with its large helical ripple, was chosen at Culham as an appropriate device for study of the effect of superbananas. The ratio of electron drift velocity to electron thermal velocity was the principal parameter found to characterize the plasma containment. At low collisionality, superbanana diffusion effects were masked by turbulent diffusion due to the high drift velocity. Radio frequency heating studies were reported in URAGAN 1 and HELIOTRON D. CLEO had just begun operation. The ASPERATOR T-3 at Sendai was built to investigate the use of helical windings to heat and stabilize tokamak instabilities. Stringer reported an anomalous particle loss model associated with ion loss cones. Voitsenya and his colleagues made a comparison of confinement work on PROTO-CLEO, SATURN, VINT-20 (a Kharkov torsatron with $\ell = 1$, R = 32 cm, a ~ 3 cm, B = 17 kG), SPAK-1 (a Nagoya torsatron with $\ell = 2$, R = 40 cm, a ~ 6 cm, B = 2 kG), and HELIOTRON D. They found that diffusion increases with decreasing collisionality, but not as rapidly as predicted by neoclassical theory. A reactor study based on the Heliotron concept was reported. The m = 1 axisymmetric instability that had been predicted theoretically for high-beta stellarators was observed on SCYLLAC and ISAR, leading to the abandonment of this approach. The PROTO-CLEO device had just been moved to the University of Wisconsin so that work on stellarators in the United States was resumed.

The next IAEA conference on Plasma Physics and Controlled Nuclear Fusion was held in Berchtesgaden in 1976. Several new devices became operational at this time. The three that would dominate stellarator research were CLEO at Culham, WENDELSTEIN VII-A at Garching and L-2 ($\ell = 2$, R = 100 cm, a = 17.5 cm, B = 20 kG) at Lebedev. They all reported studies with ohmic heating. The CLEO team found confinement at least as good as in an equivalent tokamak. Comparison of TORSO and CLEO showed no significant difference between stellarators and torsatrons. The WENDELSTEIN VII-A experiments started with ohmic heated plasmas and showed that the external transform provides for mode stabilization and completely avoids major current disruptions. Radio frequency heating was investigated in HELIOTRON D, RO-2 (an $\ell = 2$, R = 65 cm, a = 4 cm, B = 15 kG torsatron at Sukhumi), and in URAGAN 2 (an improvement of the device at Kharkov). HELIOTRON DM ($\ell = 2$, R = 45 cm, a = 6 cm, B = 10 kG) at Kyoto and JIPP T-2 ($\ell = 2$, R = 91 cm, a = 14 cm, B = 30 kG) at Nagoya also began operation. The figure-eight approach was resurrected at Kurchatov in M-8, a machine with L = 270 cm, R = 20 cm, a = 4 cm, and B = 15 kG. Pease pointed out in his closing summary that stellarator results were quite promising.

Experimental results were presented at the Innsbruck 1978 meeting from six groups, CLEO, L-2, WENDELSTEIN VII-A, HELIOTRON D and DM, RO, and PROTO-CLEO. It was becoming well established that helical fields improve the confinement properties of ohmically sustained discharges, with energy confinement increased by a factor of two to ten above that of comparable tokamaks. If the externally imposed transform is sufficiently large, disruptions can reliably be avoided. Ion heat conductivity appears to be neoclassical. A particularly important and well documented conclusion is that the energy containment improves with decreasing current, and closely follows the drift parameter scaling. Radio frequency heating studies were continued at Sukhumi and Kyoto. An interesting experiment at Kharkov, not reported at the conference, showed that white noise lowered the ion heat transport, presumably by imposing a higher effective collisionality.

Only five experimental groups reported on stellarator experiments at the 1980 Brussels meeting. Probably the most exciting was the work on WENDELSTEIN VII-A, where the availability of about 1 MW of neutral injection for plasma heating and careful programming the helical currents made current-free operation possible. Pure stellarator operation was achieved by starting with an ohmic heating target plasma. Significant plasma parameters $T_i \approx 700$ eV, $\bar{n} \approx 10^{14}\text{cm}^{-3}$, $\tau_E \approx 35$ ms, together with a strong reduction in fluctuation level and vanishing of the MHD activity, were obtained. Currentless plasmas were also obtained in CLEO using ECRH heating. JIPP T-2, HELIOTRON D and DM, and PROTO-CLEO also studied plasmas with auxiliary heating techniques. A new larger device HELIOTRON E ($\ell = 2$, R = 220 cm, a ~ 28 cm, B = 20 kG) began operation at this time.

There were several conceptual advances reported in this period leading to a very positive outlook for stellarators as this third era drew to a close. Further studies with WENDELSTEIN VII-A current-less discharges gave very favorable confinement times. Initial operation of HELIOTRON E with ohmic heating produced very respectable plasmas. With 10 msec pulses of 200 kW ECRH excitation, currentless plasmas with $n_e \approx 5 \times 10^{12}\text{cm}^{-3}$, $T_e \approx 500$ eV, $T_i \approx 100$ eV, and in the afterglow $\tau_E \approx 40$ msec have been obtained, with near neoclassical thermal conductivity for both the electron and ions. Theoretical studies indicate that transport should be significantly lower than that calculated from earlier neoclassical models. This is partially due to the effects of radial electric fields. More importantly, in the earlier work the number of particles in trapped orbits and the time they stayed in them were overestimated. On the engineering side, new ideas emerged for building modular coils that significantly reduce the problems associated with forces on the coils. Preliminary results from reactor studies are encouraging. In theoretical studies at Garching advanced stellarator configurations were identified which promise a considerable reduction of the

secondary currents and thus an increase of the equilibrium beta. They also give strong hope to increase the stability beta for not too small aspect ratios in such configurations.

Thus the stellarator program is entering its fourth period with enthusiasm and optimism.

A good introduction to the early years can be found in Bishop's book.[1] A review of the basic MHD considerations of equilibrium and stability was prepared by Greene and Johnson.[2] A comprehensive analysis of the results obtained on the Model C stellarator was given by Young.[3] The second and third phases of the program were well summarized in Miyamoto's excellent review paper.[4] His list of references is especially extensive. A good discussion of stellarators was recently given by Shohet.[5] The flavor of the work was caught well in Shafranov's recent anniversary paper[6] in Nuclear Fusion.

References

1. A. S. Bishop, "Project Sherwood; the U.S. Program in Controlled Fusion". (Addison-Wesley Publishing Co., Reading, Mass., 1958.)
2. J. M. Greene and J. L. Johnson, in Advances in Theoretical Physics, (Academic Press Inc., New York, 1965) Vol. 1, p. 195.
3. K. M. Young, Plasma Physics, 16, 119, (1974).
4. K. Miyamoto, Nuclear Fusion, 18, 243 (1978).
5. J. L. Shohet, in "Fusion". (Edward Teller, Ed., Academic Press, Inc., New York, to be published) Chapter 4.
6. V. D. Shafranov, Nuclear Fusion, 20, 1075 (1980).

III. REACTOR STUDIES

Introduction

1. Physics of Reactor
2. Engineering Considerations
   - A. Magnet Design
   - B. Blanket and Shield
   - C. Impurity Control
   - D. Maintenance
3. Summary

Introduction

The stellarator system offers a distinct alternative to the mainline approaches to magnetic fusion power and has several potentially major advantages which are summarized in Table I. The steady-state magnetic fields simplify superconducting magnet design, remove the need for pulsed superconducting coils, and eliminate energy storage required to drive pulsed coils. Plasma confinement during startup is aided by the presence of magnetic surfaces at all times during this phase. Steady-state plasma operation at ignition is a clear potential advantage of the stellarator concept. Such operation would simplify blanket design, since fatigue problems would be eliminated. Steady-state operation, however, implies a need to refuel continually the plasma. Also, impurity control and ash removal are needed for steady-state burn, and several options exist to achieve both requirements. The stellarator configuration naturally possesses a magnetic limiter and a helical divertor which can be used to advantage for impurity control. Alternatively, the magnetic separatrix can be positioned near the coil and the plasma boundary set by a pumped limiter which also acts as the impurity control mechanism.

TABLE I

Advantages of a Stellarator versus Tokamak Reactor

1. Steady state-magnetic fields.
2. Steady-state plasma operation at ignition or high Q.
3. No energy storage and low recirculating power requirements.
4. Moderate plasma aspect ratio (10-20) which can improve access.
5. Start-up on existing magnetic surfaces with confinement at all times.
6. No significant positioning or field shaping coils.
7. No major disruptions that could lead to an energy dump on the first wall.
8. Several potential methods for impurity control and ash removal including:
   a. Plasma profile control by means of gas puffing and use of a pumped limiter.
   b. Magnetic limiter or helical divertor.
9. A possibility for confinement in outer plasma zone rather than in plasma core. This can facilitate impurity and ash removal, provided the net confinement is not significantly affected.
10. No net current in the plasma required.

A stellarator can have a relatively high aspect ratio and does not require expensive complicating auxiliary magnets (e.g., ohmic heating, field shaping, and position control coils). Its coil configuration permits access to the device from all sides and facilitates a modular approach to blanket and shield design. Since stellarators and torsatrons can operate free of net toroidal current and do not exhibit major plasma disruptions, the major concern of an excessive energy dump on the first wall can be eliminated for the reactor.

III.1 Physics of Reactor

In order to make an effective reactor, it is necessary that the plasma achieve certain basic conditions, as reflected by the parameters, $n\tau$, T_e, T_i and β. These conditions are in turn governed by the magnetics parameters chosen for the reactor, as reflected by the rotational transform, shear, well depth, aspect ratio and harmonic content of the surfaces. In turn, these magnetics parameters are affected by the choice of the magnetic coil configuration used. The coupling between plasma performance, magnetic topology and magnet design is particularly intimate and flexible for the stellarator configuration, leading to a wide range of potential reactor options.

The question of operational mode for any magnetically confined fusion reactor is centered around the following issues: pulsed versus steady-state plasma; driven high-Q versus ignited operation; refueling mechanism; impurity-control scheme; and plasma startup and rundown procedure. Each of these issues will strongly impact the reactor design and cost of electricity, and each is determined by physical phenomena that to date are computed or extrapolated from experimental observation. The uniqueness of the stellarator in this respect rests with the generation of the full magnetic field topology solely be external currents. Other toroidal approaches require a plasma current, as in a tokamak, or energetic electron rings, as in EBT. In fact, in stellarators the vacuum field topology is expected to remain relatively unperturbed by the presence of the plasma under reactor conditions. These factors impinge on the reactor mode of operation by suggesting a steady-state plasma that would more than likely be achieved through a low-density startup on existing closed and nested magnetic surfaces.

In order to determine the actual dynamics and the operating point of a stellarator reactor, one needs to adopt a transport model and solve energy and particle conservation equations for the plasma. Simple point model calculations indicate that, with neoclassical (axisymmetric) ion heat transport and Alcator scaling for electron heat transport, operation at 15-20 keV is feasible. This projection needs to be confirmed, however, with more detailed transport codes where the three-dimensional stellarator magnetic field is taken into account. A big uncertainty related to transport in the reactor regime is the effect of helical magnetic field ripple on the ion thermal conductivity. The analyti-

cal result[1] for the ion thermal conductivity is given by

$$\chi_i = \frac{46.5\ \varepsilon_H^{3/2}}{\nu_{ii}} \frac{(T_i)^2}{eBR},$$

where ν_{ii} is the ion-ion collision frequency, and ε_H is the helical field ripple. The magnitude of this estimate of χ_i at lower values of ν_{ii} is important. Numerical calculations by Potok[2] and Boozer[3], however, have yielded much lower values for the effect of ripple on χ_i and with a scaling which is closer to ν_{ii}-independent rather than ν_{ii}^{-1}. In this case, the effect of magnetic field ripple would be much more benign.

The magnetic field ripple can also have an effect on the fast (3.5 MeV) alpha particles, which are crucial to any ignited D-T plasma. A certain fraction will be born on drift surfaces that reach the walls. Since the drift time scale for these energetic alpha particles is much faster than the collision time scale, they will be lost almost immediately from the plasma and hence not contribute to plasma self-heating. A fraction of the remaining alpha particles will scatter onto these drift surfaces and be lost during the slowing down process. The severity of these effects has not yet been fully assessed, but can be mitigated by utilizing drift optimized systems as described in Section V.2 and V.3 or by tailoring the magnetic field ripple. The need for adjusting the magnetic field ripple and the requirement for closed magnetic surfaces coupled with minimum coil aspect ratios of $\sim 4-5$ and the finite blanket and shield thickness cause stellarator reactors to have rather high plasma aspect ratios ($A \sim 10-20$) in comparison with tokamaks.

When combined with the goal to generate electricity at power levels near ~ 1 GWe with a fusion-neutron first-wall loading of $\geq 1-2$ MW/m^2, the stability/equilibrium scaling of beta and plasma aspect ratio used for stellarator reactors generally leads to plasma densities of $\sim 10^{20}$m^{-3}, moderate temperature (8-15 keV) and minor radii in the range of 1-2 m. For these conditions, edge refueling may not be possible and high velocity ($> 10^4$ m/s) pellet injectors may be needed. Pellet refueling is also advantageous for peaking the density profile; this improves the power density for a given volume-averaged beta.

Heating a stellarator reactor to ignition will use methods similar to those envisaged for a reactor based on other concepts. Several combinations of ohmic heating, radio frequency heating and neutral-beam injection are possible to produce a target plasma first and then provide the heating to ignition. The choice of a particular mode of operation depends upon the efficiency of the various processes as a function of temperature and density. A possible advantage for stellarators with respect to neutral-atom injection is based on the inherent helical ripple. If the neutral atoms are injected along the same radial coordinate through which ripple-trapped particles might drift from the device, it may be possible to permit the neutral beam to penetrate well into the body of the plasma at a lower beam energy than could otherwise be acquired (perhaps $\simeq$ 100 keV in a reactor).

Stellarators possess a natural helical divertor if the separatrix region outside the last of the nested closed flux surfaces is positioned within the vacuum wall. The flux of particles lost through the separatrix occurs primarily at the apices of the magnetic separatrix, then focusses into narrow beams which emerge between adjacent helical windings. Inside the separatrix, the enclosed magnetic flux links all of the coils. Outside the separatrix, however, the flux links some, but not all, of the coils. Thus, magnetic flux must emerge somewhere between adjacent coils. This forms the basis for the divertor topology, which can be expected in any toroidal system which possesses a magnetic separatrix. Since modular stellarators can have such a separatrix, they also can have naturally-occurring divertors.

Figure 1 shows a typical cross section of the divertor region computed for an ℓ=3 modular stellarator. An ergodic region surrounds the last closed magnetic surface. The field lines in this region emerge from the torus in narrow bundles through the gaps between the modular coils. The flux bundle which emerges from each gap then wraps around a leg of the coil and re-enters the torus through an adjacent gap. For a modular stellarator with multiplicity ℓ and N coils, ℓ x N discrete bundle divertors will be distributed over the entire torus.

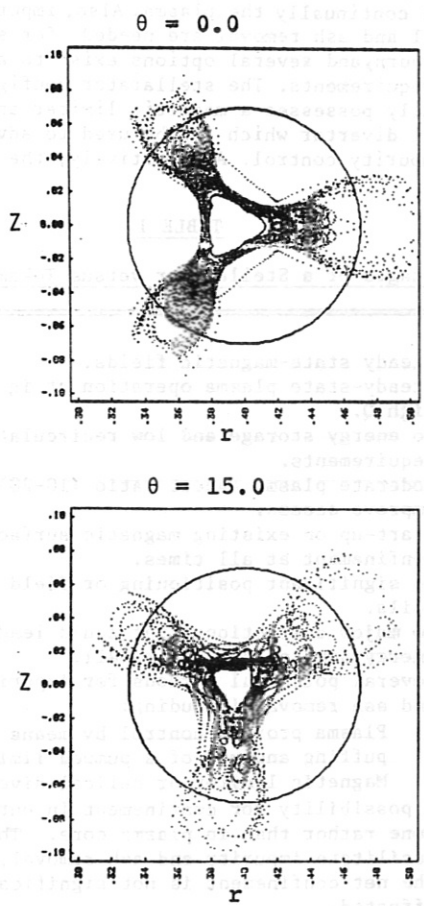

Fig.1 Trajectories of divertor field lines close to the modules of an ℓ= 3 modular stellarator .

An alternative to the divertor is to determine the plasma boundary using a pumped limiter.[4,5] This allows one to use magnetic configurations where the separatrix is outside the first wall (i.e., near the coil) and thus permits more variety in the choice of the coil configuration. This additional variety may offer some advantage in maximizing the plasma volume within the first wall and minimizing the complexity of the blanket and shield design. Although there is some experience with magnetic divertors on present tokamak experiments, both of these impurity control concepts are largely untested for long pulse, high power density operation.

In summary, those unique characteristics of the stellarator approach that are related to low-beta plasma confined within an externally-produced topology almost certainly will lead to a steady-state operating mode for the reactor. The issue of driven versus ignited operation depends crucially upon the energy transport scaling, the related thermal stability of the burn, and the ability to refuel and control impurity levels by external means. As with most approaches to magnetic fusion, the latter issue remains to be fully understood and quantified in the reactor context. The choice between (natural) magnetic divertors (i.e., separatrix near the first wall) versus pumped limiters (i.e., separatrix near magnets) represents an option for the stellarator.

III.2 Engineering Considerations

A. Magnet Design

The technical feasibility of a stellarator as a power producing reactor depends strongly on the magnet system. Classical stellarators, torsatrons, ultimate torsatrons, and modular systems would employ steady-state superconducting magnets similar to magnets for other fusion devices such as tokamaks and mirrors. The geometry of modular coils is more complex than a toroidal field coil for a tokamak, but the benefits of steady-state operation and the absence of linked pulsed poloidal field coils result. Magnetic fields in stellarator reactors are also similar to those of other devices. Most designs utilize magnetic fields on axis in the neighborhood of 5-6 T, with fields on the coils about 10 - 11 T. Since the magnetic fields are steady, monolithic conductors can be considered, which would have prohibitive losses if pulsed fields were present. Typical current densities do not exceed 3000 A/cm^2. Considering the available technology, NbTi is mainly chosen as superconductor with possible alloying additions to improve high field performance, and Nb_3Sn for use at still higher fields. It is also noted that because of the higher aspect ratio in stellarators, the magnetic field in the plasma is higher for a given field at the coil, thereby allowing similar plasma power densities (i.e., $\sim\beta^2B^4$) for somewhat lower beta in the stellarator.

Different methods exist for generating the confining magnetic fields in stellarators, as is described in more detail in Chapter VI. In the "classical" stellarator, the poloidal field is produced by a set of continuous helical coils. The oppositely directed currents in the helical coils of a classical stellarator generate forces directed inward in the minor radial direction. This could result in an undesirable support structure.

The "ultimate" torsatron configuration is known to have favorable physics properties and improved access when compared to the conventional torsatron helix[6]; on the basis of computation, the ultimate system also possesses remarkable stability properties under the influence of perturbing fields, and the engineering tolerances required for this concept may be relaxed, since the forces can be made everywhere outward in the minor radial direction. Also this design eliminates the need for large externally-generated vertical fields.

Recently, modular stellarator concepts have evolved based on the twisted coil concept[7]. Another design is a newly developed modular torsatron[8]; both designs can have forces that are directed radially outward. In both of these modular configurations, access equal to that of the ultimate torsatron is possible with the added advantage of coil modularity for construction and repairs. The properties of a plasma confined by these modular coil systems, however, are less understood than for the ultimate torsatron. Initial studies indicate that these systems can produce fields with acceptable physics properties, but some concern exists over sensitivity to field errors, and ripple characteristics that differ from those of continuous coil systems.

Since stellarator coil configurations operate in steady-state and with reasonable field strength, the engineering problems are primarily centered around support of the forces and maximization of the overall coil current density (i.e., miminizing the coil cross section and coil interference). Two principal contributions to forces on stellarator reactor windings can be identified: self forces resulting from the helical or twisted coil windings and interactive forces exerted between these coils and other external coils (e.g., toroidal or vertical field coils). Typical values for these forces are in the range 100 MN/m for a wide range of configuration . The poloidal and toroidal forces change direction with azimuthal angle while the radial force is always positive. The total force on the individual coils varies between 70 to 200 MN/m, which is comparable to forces considered in tokamak reactor coils.

In summary, therefore, these new approaches to stellarator/torsatron systems promise open and moderate-force systems that can lead to accessible and supportable engineering systems.

B. Blanket and Shield

As for other magnetically-confined fusion reactors, the stellarator requires a blanket/shield system interposed between the plasma and superconducting coil systems to: a) breed tritium, multiply neutrons and energy, recover the fusion energy, and provide radiation and thermal protection to the life-of-plant coil structure. Over the past several years, many different designs of blankets and shields have been proposed for magnetically-confined fusion power reactors. In principle, most of these designs are also applicable to stellarators. The main differences lie in four areas:

- Stellarators are steady-state devices, thus considerably reducing the problem of thermal fatigue.

- Stellarators are not subjected to plasma disruptions, thus somewhat relaxing the requirements on the first wall.

- The plasma cross-sectional shapes are different, leading to somewhat different blanket geometries, although these differences can be minimized if a pumped limiter is used with the magnetic separatrix located at the coil rather than at the first wall.

- Equilibrium and stability considerations may restrict the allowed separation between the plasma and the coils.

These differences can have a major impact on the design of the first-wall/blanket/shield. In a pulsed tokamak, for example, a primary failure mode in the first wall has been identified as a crack propagation due to thermal fatigue[9]. The steady-state stellarator burn will essentially nullify this effect. Similarly, plasma disruptions can deposit enormous amounts of energy on localized first wall areas, necessitating special precautions both with passive protection and special cooling systems; this does not appear to be necessary in stellarators.

The non-axisymmetric geometry of the stellarator plasma does lead to a unique difference. The natural divertor in these devices causes flux bundles along which particles travel to exit between windings everywhere along the toroid. In the modular stellarator, the flux bundles are discrete[10], and exit through penetrations which follow the effective helices generated by the twisted coils. In this case, blanket modules must be fitted between these penetrations, perhaps assuming somewhat unusual shapes. Further, the large number of penetrations will require a greater amount of shielding in order to reduce the effect of neutron streaming. If a pumped-limiter impurity control scheme is used, the first-wall/blanket/shield becomes less complicated, although the limiter slot may have to be helical. In any event, a more careful analysis of the neutron streaming in the stellarator configuration must be performed in order to assure the needed protection to the coils and other reactor components.

Because radiation damage will necessitate the periodic replacement of the blanket modules, it is important that they be designed for accessibility and easy replacement. The first wall is usually the most highly stressed component of the blanket. Both thermal loading and radiation damage peaks at the first wall and decreases rapidly into the blanket. First wall lifetime in pulsed fusion systems is generally dictated by thermal fatigue phenomena that promote crack propagation in a material already embrittled by radiation damage. The potential for steady-state burn in the stellarator will reduce thermal fatigue and thus prolong the life of the first wall by as much as 2-3 times. The economic implications of this added lifetime are significant; not only will the availability be higher because of the steady-state burn, but the cost and time of the first wall blanket replacement will be substantially reduced.

C. Impurity Control

The two systems presently considered for stellarators to remove impurities and alpha-particle ash are the magnetic divertor and the pumped limiter. In the magnetic divertor, the separatrix defines the plasma boundary, and the particles leave the reaction chamber along field lines before neutralization and removal. The pumped limiter[4,5] design operates with the separatrix displaced further from the plasma, perhaps as far as the coil radius. The limiter edge-plasma skims particles in a scrape-off zone and directs them to a vacuum duct. The buildup of neutral gas at the limiter base is computed to allow a higher helium pressure at the limiter and should facilitate its pumping; this process also occurs in the divertor chamber. Both magnetic divertors and pumped limiters require high heat-flux surfaces or collector plates. The heat load on these surface plates is sufficiently high to require special design. Sputtering of these surfaces is expected to aggravate the design complexity.

The integration of either pumped limiters or divertors into the overall blanket, shield, magnet, and supporting structure design of a stellarator reactor presents many problems which require further study before definitive answers can be given. Among these are neutron streaming through divertor or vacuum pumping channels, possible interference between these channels and the magnet support structure and the impact of internal limiters versus external divertor chambers on maintenance requirements. All of these problems have to be considered within the context of specific designs. It is premature at this time to choose between these two different approaches.

D. Maintenance

As for other approaches to fusion power, maintainability of stellarator power reactors will undoubtedly be a major criterion in determining their viability as future sources of energy. Furthermore, it is imperative to demonstrate that specific reactor components can be maintained remotely. Modularity of not only the blanket and shield, but the coil as well becomes extremely important. Power reactor maintainability can be divided into two categories, routine and unscheduled. Only the area of routine or scheduled maintenance is qualitatively described.

Certain high-performance reactor components (e.g., first wall and blanket) are subjected to high nuclear and thermal fluxes and will have to be periodically replaced. Other components have a finite life for other reasons and will also require preventative maintenance. Such maintenance is usually performed during scheduled shutdown of the reactor prior to the failure of the component. Only the replacement of first wall, blanket modules and the collector plates are addressed, since they will constitute the bulk of the routine maintenance.

There are four major problems encountered in routine first wall and blanket maintenance:

- Providing accessibility
- Making seals between adjacent blanket modules
- Disconnecting and connecting coolant lines
- Moving bulky and sometimes heavy blanket modules.

Providing accessibility for extracting blanket modules is one of the most crucial problems. In tokamaks, this problem was addressed by making the toroidal field coils oversized in order that blanket and shield segments could be taken out radially. This has an impact on the economics of the reactors because the coils comprise a major fraction of the capital costs. Accessibility in tokamaks is further hampered by poloidal field coils and by neutral beams which are usually in the way.

In a modular stellarator, it does not appear possible to provide accessibility for blanket/shield extraction without moving the coils. However, it may not be necessary to move all the coils to gain access to the entire blanket. If one coil is moved out radially, access may be provided for adjacent blanket modules. The large aspect ratio of the stellarator is a significant advantage to providing the required accessibility. The specific procedure for moving the blanket modules depends on the specific design. Obviously, smaller modules would be easier to handle. Liquids (e.g., coolants, breeders) can be drained out prior to handling the blanket module. Straight radial translation on guide rails, even small circumferential excursions, may be tolerable. Provided with guide rails, positive stops, and air bearings, even very heavy coils (500-700 tonne) can be moved for short distances.

The divertor plates and limiter blades will also require routine maintenance. The high particle fluxes will erode the surfaces of the plates requiring them to be periodically replaced. If the lifetime of these components can be matched to that of the blanket, then both can be replaced on the same schedule. However, since the divertor plates in a stellarator will be essentially on the outside of the blanket and shield, unlike the pumped-limiter blades, they can in principle be maintained without disturbing the coils. Generally, these operations can be characterized only by means of a sufficiently detailed reactor design, and must await the results of ongoing studies.

III.3 Summary

In summary, most of the technology problems and development areas, expected for stellarator reactors appear to be generic to magnetic fusion in general, and many of these problems are being addressed by main-line tokamak programs. Where major problems are shared between the stellarator and other approaches to magnetic fusion, they appear to be reduced in magnitude for the stellarator. Certain key problems for the main-line approaches in fact seem to be eliminated by the stellarator approach.

References

1. J.W. Connor and R.J. Hastie, Phys. Fluids 17, 114 (1974).

2. R.E. Potok, P.A. Politzer, and L.M. Lidsky, Phys. Rev. Lett. 45 16, 1328 (1980).

3. A.H. Boozer, Phys. Fluids 23 5, 904 (1980).

4. J.F. Schivell, "Method of Plasma Impurity Control without a Magnetic Divertor," Princeton Plasma Physics Lab. PPPL-1342, June (1977).

5. R.W. Conn, I.N. Sviatoslavsky and D.K. Sze, "Limiter Pumping System for Divertorless Tokamaks," Nuclear Engineering Dept. UWFDM-339, IEEE Meeting on Engineering Problems of Fusion Research, San Francisco, November (1979).

6. "WISTOR-U, A Superconducting Ultimate Torsatron," Engineering Experiment Station, University of Wisconsin, Madison, (1979).

7. S. Rehker and H. Wobig, Proc. 7th Symp. on Fusion Technology, Grenoble, 343, (1972); and T.K. Chu, H.P. Furth and C. Ludescher, Modular Torus with Twisted Coil Ends, PPPL, Princeton, NJ, (1979).

8. D.T. Anderson, et al., Proc. IAEA Conference on Plasma Physics and Controlled Fusion Research, Brussels, paper BB-1, (1980).

9. B.A. Cramer, J.W. Davis, R.C. Kinder, D.A. Bowers, "An Approach for Determining the Lifetime of a First Wall Structure in a Tokamak Reactor," McDonnell Douglas Astronautics Co., 2nd Topical Meeting on the Technology of Controlled Nuclear Fusion, Richland, Washington, September (1976).

10. J.A. Derr, "A Modular Stellarator Divertor", University of Wisconsin, Report ECE-80-36, October (1980)
and
"UWTOR-M , A Modular Stellarator Reactor Study", University of Wisconsin, Nucl. Eng. Dept. Madison (1981)

IV. EXPERIMENTS

Introduction

This section summarizes experimental results of major stellarators; these include the smaller CLEO, JIPP T-2, WENDELSTEIN VII-A ($a_p \approx 10$ cm) and the more recent device HELIOTRON E ($a_p = 21$-40 cm). Heating methods in these experiments include ohmic heating, ohmic plus auxiliary heating (neutral beam) and zero-net current experiments sustained by ECRH (in CLEO and HELIOTRON E) and high-power neutral beam (in WENDELSTEIN VII-A). The plasma parameters are in the plateau regime, and could not be extended yet to the collisionless regime.

i) In ohmically heated stellarator discharges MHD tearing modes can be stabilized by the externally applied rotational transform ι_o; this stabilizing effect preserves the plasma equilibrium and eliminates plasma disruption. In shearless vacuum configurations, plasma disruption is prevented with tokamak-like transform profiles at $\iota_o > 0.14$ (JIPP T-2, WENDELSTEIN VII-A). In high-shear devices (CLEO, L-2, HELIOTRON E) the high transform at the edge ($\iota_o > 0.5$) restricts the spreading of islands to the wall and therefore disruptions have never been observed. The suppression of disruptions enables the stellarator discharge to have higher density than that in tokamaks (the Murakami limit).

ii) Energy confinement in ohmically heated discharges is strongly affected by island formation at resonance surfaces. Thus, the appearance of strong (1,1), (3,2), and (2,1) modes leads to a significant reduction of the gross energy confinement time. In general, based on empirical scaling, energy confinement times in stellarators are comparable to or better than those in tokamaks of similar device parameters.

iii) In WENDELSTEIN VII-A, electron heat conductivity χ_e determined from profile analysis in regions without strong MHD effects shows a scaling close to that of the drift parameter:

$$\chi_e \sim I_p / B\, n\, T_e^{0.6} \quad .$$

iv) In zero-net current experiments, ECRH has been successfully used to initiate and sustain a discharge in HELIOTRON E. With modest power (200 kW incident, 80 kW absorbed) at 28 GHz for 10 kG field, a discharge with an initial electron temperature $T_e \approx 500$ eV was achieved, followed by an electron ion equilibrium stage in which $T_e \approx 200$ eV and $T_i \approx 150$ eV. In this afterglow region the observed particle confinement time ($\tau_p \approx 160$ msec), the ion as well as the electron thermal conductivity are close to predictions of neoclassical theory. The electron energy confinement time in the afterglow is ≈ 35 msec.

v) In the zero-net current experiment sustained by high-power neutral beams in WENDELSTEIN VII-A, a $\beta(0)$ larger than 0.6 % has been attained. The heating efficiency of these experiments is better than ordinarily expected for the nearly perpendicular injection, indicating reduced orbital loss of energetic particles because of the radial electric field. The power balance indicates a substantial reduction of electron thermal conduction loss from that of an ohmically heated plasma; this is consistent with the observation of significant reduction of low-frequency electrostatic and MHD fluctuations. Radiation at the core of the plasma column appears to be the dominant loss.

Section IV.1 lists parameters of major devices. Section IV.2 describes results of ohmic heating, and the effect of ohmic-heating current on equilibrium, stability, transport, impurities and attainable density and temperature is discussed. These experiments were carried out in all stellarators. Section IV.3 presents results with auxiliary heating and section IV.4 describes operation without net plasma current.

IV.1 Existing Major Facilities

A complete list of stellarators is given in the review paper [1] by K. Miyamoto and in the Annex. More recent report has been given at Oxford [2]. The progress of experiments in the US has been outlined at Brussels [3]. The most characteristic parameters of the major facilities are given as follows:

CLEO (UK, Culham, closed 1980) — Fig. 1a

Stellarator $\ell = 3$, $m = 7$

$R = 0.9$ m $\quad B_o = 2$ T

$a = 0.1$ m $\quad \iota_o \rightarrow 0.6$ shear; separatrix

Heating:

- OH
  - $I_p \rightarrow 25$ kA
  - $\bar{n} = 3 \cdot 10^{12} - 5 \cdot 10^{13}$ cm^{-3}
  - $T_e = 100 - 1000$ eV
  - $T_i = 80 - 300$ eV
  - $\tau_E < 10$ ms
- NI
  - $P_{inj} = 150$ kW, 20 kV, pulse duration <100 ms
- ECRH
  - 17.5 GHz/15 kW at $B_o = 0.63$ T
  - $n_e \approx 10^{13}$ cm^{-3}
  - $T_e = 30 - 50$ eV
  - $\tau_E = 1 - 2$ ms
- Laser Pellet
  - $T_e < 15$ eV

JIPP T-2 (Japan, Nagoya) — Fig. 1b

Stellarator $\ell = 2$, $m = 4$

$R = 0.91$ m $\quad B_o \leq 3$ T

$a = 0.17$ m $\quad \iota_o \leq 0.3$ low shear, limiter

Heating:

- OH
  - $I_p \rightarrow 100$ kA
  - $\bar{n} \leq 3 \cdot 10^{13}$ cm^{-3}
  - $T_e \rightarrow 1$ keV
  - $T_i < 250$ eV
- LHH
  - 0.8 GHz/280 kW
- NI
  - 100 kW / 70 kV
- ECRH
  - 3.5 GHz/20 kW
- ICRH
  - 300 kW

L-2 (USSR, Moscow)

Stellarator $\ell = 2$, $m = 14$

$R = 1$ m $\quad B_o \leq 2$ T sinusoidal < 20 ms

$a = 0.11$ m $\quad \iota_o = 0.2 \rightarrow 0.7$ shear; separatrix

Heating:

- OH
  - $I_p = 10 - 25$ kA
  - $\bar{n} = 5 \cdot 10^{12} - 2 \cdot 10^{13}$ cm^{-3}
  - $T_e < 400$ eV
  - $T_i < 100$ eV
  - $\tau_E \leq 8$ ms
- ICRH (operational 1981)

Personnel: appr. 12 physicists

URAGAN III (USSR, Kharkov; operational 1981)

Torsatron $\ell = 3$, $m = 9$

$R = 1$ m $\quad B_o \leq 3$ T

$a = 0.15$ m $\quad \iota_o \rightarrow 0.7$ separatrix; divertor

Heating:

- OH
- ICRH > 2 MW
- NI > 1.5 MW

FIG. 1a

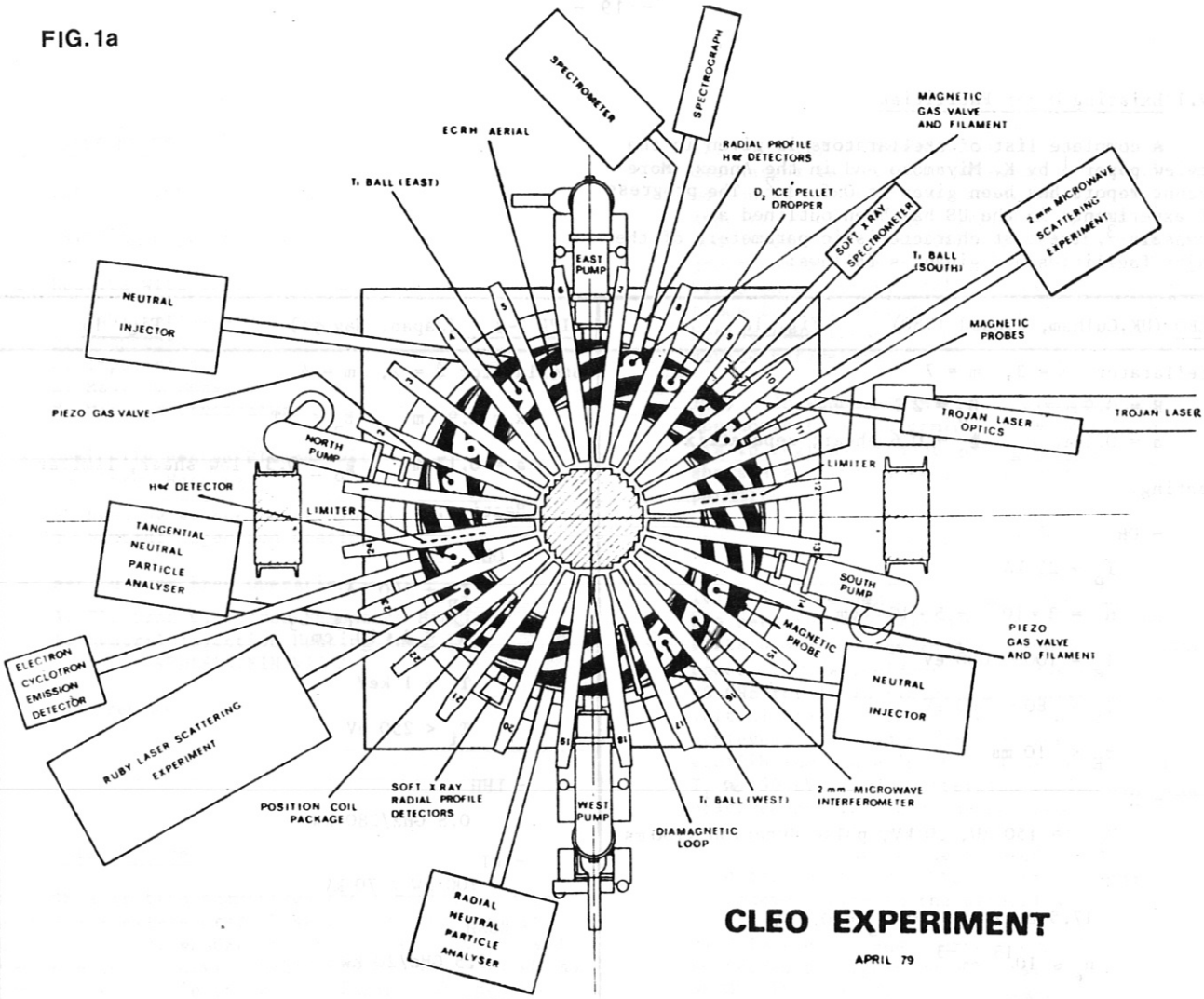
SPECTROMETER
SPECTROGRAPH
ECRH AERIAL
MAGNETIC GAS VALVE AND FILAMENT
RADIAL PROFILE Hα DETECTORS
T_i BALL (EAST)
D_2 ICE PELLET DROPPER
SOFT X RAY SPECTROMETER
2 mm MICROWAVE SCATTERING EXPERIMENT
EAST PUMP
T_i BALL (SOUTH)
NEUTRAL INJECTOR
MAGNETIC PROBES
PIEZO GAS VALVE
TROJAN LASER OPTICS
TROJAN LASER
NORTH PUMP
LIMITER
Hα DETECTOR
LIMITER
TANGENTIAL NEUTRAL PARTICLE ANALYSER
SOUTH PUMP
MAGNETIC PROBE
PIEZO GAS VALVE AND FILAMENT
ELECTRON CYCLOTRON EMISSION DETECTOR
NEUTRAL INJECTOR
RUBY LASER SCATTERING EXPERIMENT
POSITION COIL PACKAGE
SOFT X RAY RADIAL PROFILE DETECTORS
WEST PUMP
T_i BALL (WEST)
2 mm MICROWAVE INTERFEROMETER
DIAMAGNETIC LOOP
RADIAL NEUTRAL PARTICLE ANALYSER
CLEO EXPERIMENT
APRIL 79

FIG. 1b

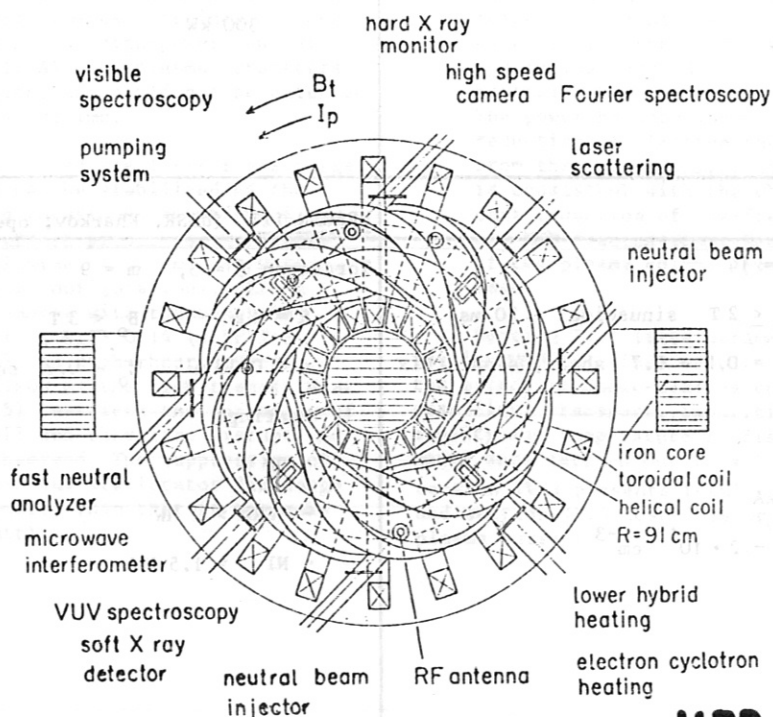
hard X ray monitor
visible spectroscopy
Bt
Ip
high speed camera
Fourier spectroscopy
pumping system
laser scattering
neutral beam injector
iron core toroidal coil
helical coil
R=91 cm
fast neutral analyzer
microwave interferometer
VUV spectroscopy
soft X ray detector
neutral beam injector
RF antenna
lower hybrid heating
electron cyclotron heating
JIPP T-2

FIG.1c

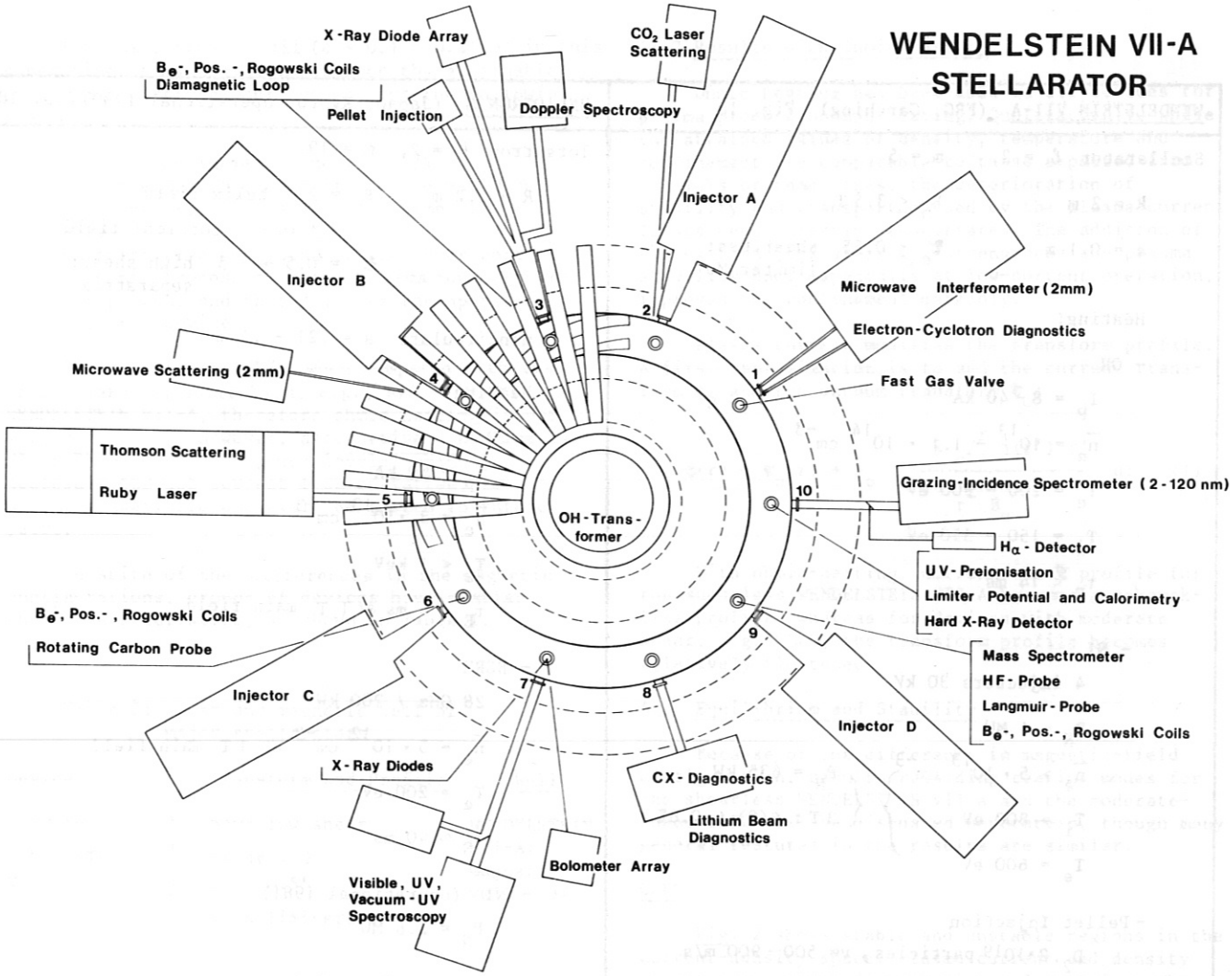
WENDELSTEIN VII-A
STELLARATOR
X-Ray Diode Array
B_θ-, Pos. -, Rogowski Coils
Diamagnetic Loop
Pellet Injection
CO_2 Laser
Scattering
Doppler Spectroscopy
Injector A
Injector B
Microwave Interferometer (2mm)
Electron-Cyclotron Diagnostics
Microwave Scattering (2mm)
Fast Gas Valve
Thomson Scattering
Ruby Laser
Grazing-Incidence Spectrometer (2-120 nm)
OH-Trans-
former
H_α-Detector
UV-Preionisation
Limiter Potential and Calorimetry
Hard X-Ray Detector
B_θ-, Pos.-, Rogowski Coils
Rotating Carbon Probe
Mass Spectrometer
HF-Probe
Langmuir-Probe
B_θ-, Pos.-, Rogowski Coils
Injector C
Injector D
X-Ray Diodes
CX-Diagnostics
Lithium Beam
Diagnostics
Bolometer Array
Visible, UV,
Vacuum-UV
Spectroscopy
1
2
3
4
5
6
7
8
9
10

FIG.1d

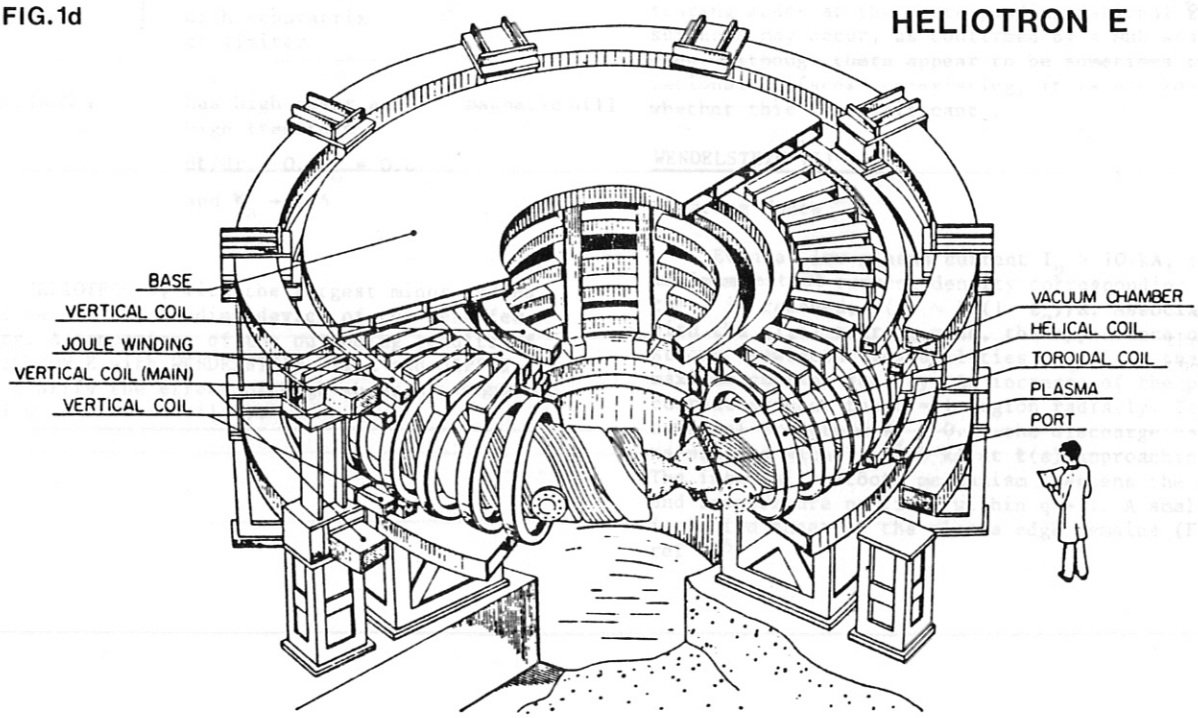
HELIOTRON E
BASE
VERTICAL COIL
JOULE WINDING
VERTICAL COIL (MAIN)
VERTICAL COIL
VACUUM CHAMBER
HELICAL COIL
TOROIDAL COIL
PLASMA
PORT

WENDELSTEIN VII-A (FRG, Garching) Fig. 1c

Stellarator $\ell = 2$, $m = 5$

$R = 2$ m $\quad B_o \leq 3.5$ T

$a = 0.1$ m $\quad \iota_o \leq 0.55$ shearless; limiter Mo

Heating:

- OH

  $I_p = 8 - 40$ kA

  $\bar{n}_e = 10^{13} - 1.1 \cdot 10^{14}$ cm^{-3}

  $T_e = 200 - 900$ eV

  $T_i = 150 - 350$ eV

  $\tau_E \leq 14$ ms

- NI

  4 injectors 30 kV

  $P_N > 1$ MW

  $\bar{n}_e > 5 \cdot 10^{13}$ cm^{-3}, $T_i = 800$ eV, $T_e = 600$ eV } { $P_N = 635$ kW; 3 T: $\beta(0) = 0.6\%$

- Pellet Injection

  D_2, $2 \cdot 10^{19}$ particles, v= 500 - 900 m/s

Personnel: 26 physicists, 3 engineers

HELIOTRON E (Japan, Kyoto; operational 1980) Fig. 1d

Torsatron $\ell = 2$, $m = 19$

$R = 2.2$ m $\quad B_o = 2$ T helix field

± 0.6 T toroidal field

$\iota_o = 0.5 \rightarrow 2.5$ high shear; separatrix

noncircular: a = .21 - .4 m

Heating:

- OH

  $I_p \rightarrow 90$ kA

  $\bar{n}_e < 3 \cdot 10^{13}$ cm^{-3}

  $T_e < 1$ keV

  $\tau_E < 6$ ms at 1 T main field

- ECRH

  28 GHz / 200 kW

  $\bar{n}_e = 5 \cdot 10^{12}$ cm^{-3} at 1 T main field

  $T_e = 200$ eV

  $\tau_E \sim 40$ ms

- NI (operational 1981)

  $P_N = 2.6$ MW

Personnel: 17 physicists

The small minor radii (a = 0.1 - 0.21 m) in this generation of stellarators restrict the attainable energy and particle confinement, for the following reasons:

- Short confinement time $\tau \sim a^2/\chi$
- high energy flux density to the wall $p \sim P/a$
- strong wall interaction with impurity release
- ineffective shielding of the inner core $\sim \bar{n}\, a$
- atomic processes in the plasma boundary are important and thus dominate the operation of the device.

The aspect ratio R/a when compared with that of tokamaks is quite high, e.g., R/A = 20 for WENDELSTEIN VII-A, therefore ohmic heating is not very effective. However, alternative heating by NI or RF at reasonable power levels, which is necessary for net current free operation, is becoming available and will be tested in future years.

In spite of the differences in the magnetic configurations, groups of devices have similar shear characteristics, as shown in Table I.

Table I: shear and magnetic well of major stellarators

Device	Transform and Profile	Well
JIPP T-2 WENDELSTEIN VII-A	have low shear $d\iota/dr \sim 0$ $\iota_o \leq 0.55$ with limiters	WENDELSTEIN VII-A: magnetic well < 3%
CLEO L-2 URAGAN III	have moderate shear $d\iota/dr > 0$, $\iota_o \to 0.8$ with separatrix as limiter	
HELIOTRON E	has high shear and high transform $d\iota/dr > 0$, $\iota_o = 0.6$ and $\iota_a \to 2.5$	magnetic hill

HELIOTRON E, with the largest minor radius, will become the leading device of the next few years. A comparison of the outcoming results of HELIOTRON E with WENDELSTEIN VII-A and JIPP T-2 may clarify the effect of high shear or magnetic well on plasma stability.

IV.2 Results with Ohmic Heating

Ohmic heating has been used in all devices for plasma production and heating. Qualitatively, while the attained values of density, temperature and confinement are comparable to those expected from tokamaks of same sizes, the deterioration of stability and transport caused by the plasma current I_p has been clearly demonstrated. The addition of the external transform ι_o, strengthens the plasma stability and, especially at low-current operation, improves the confinement markedly.

Plasma current modifies the transform profile. A first approximation is to add the current transform ι_p and the vacuum transform ι_o:

$$\iota(r) = \iota_o(r) + \mu_o \frac{R}{r^2 B_o} \int_o^r \frac{j(r')\, r'}{} dr' \quad (1)$$

With ohmic-heating current the ι profile for the shearless WENDELSTEIN VII-A becomes a tokamak-like profile, whereas for devices with moderate shear, e.g. CLEO, the transform profile becomes relatively flattened.

A. Equilibrium and Stability

Because of the difference in magnetic-field configuration, results regarding tearing modes for the shearless WENDELSTEIN VII-A and the moderate-shear CLEO will be discussed separately, though many general features in the results are similar.

CLEO

Fig. 2 shows stable and unstable regions in the current-density space. Plasma current and density affect the current distribution and therefore the onset conditions for various tearing modes (2,1), (3,1), and (5,2). When shear is reduced unstable tearing modes at the corresponding rational ι surfaces may occur, as confirmed by a MHD stability code. Although there appear to be sometimes two rational surfaces co-existing, it is not known whether this is significant .

WENDELSTEIN VII-A

-Tearing Modes

Even at low plasma current $I_p > 10$ kA, the maximum central current density corresponding to $\iota = 1$ is reached; $j(0) \sim B_o(1 - \iota_o)/R$. Associated with the (1,1) tearing mode, the appearance of strong "sawteeth" instabilities restricts the maximum current density. An increase of the plasma current extends the q = 1 region radially. For high external transform $\iota_o > 0.14$ the discharge can be maintained with $I_p = 45$ kA at $\iota(a)$ approaching to 1. The internal sawtooth mechanism flattens the density and temperature profiles within q = 1. A small isolation sheet at the plasma edge remains (Fig. 3), ref [4,5].

Fig. 2 CLEO

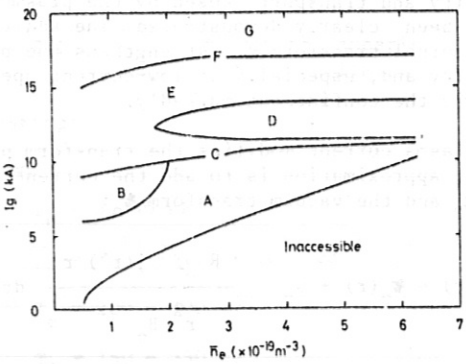

Fig. 2a Schematic diagram of operating conditions for CLEO with B_T = 1.85 T and ι_v = 0.4, showing regions of MHD instability.
A - m = 3, n = 1 stable; B - unstable m = 3, n = 1 near axis; C - development of large m = 3, n = 1 island; D - m = 2, n = 1 stable (m = 5, n = 2 possibly unstable); E - m = 2, n = 1 unstable near axis; F - development of large m = 2, n = 1 island; G - inaccessible at ι_v = 0.4.

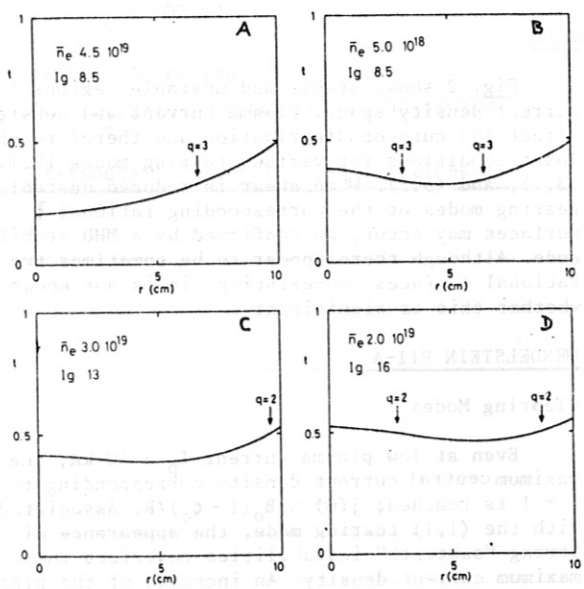

Fig. 2b Profiles of total rotational transform showing positions of rational-q surfaces for conditions in regions A, B, D and E in Fig. 2a.

Fig. 3 WENDELSTEIN VII-A

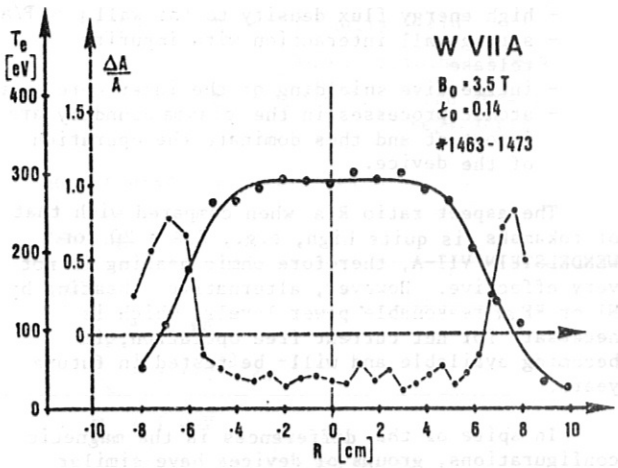

Fig. 3a Intensity of sawtooth oscillations measured by X-ray diodes. Comparison with the electron temperature profile.

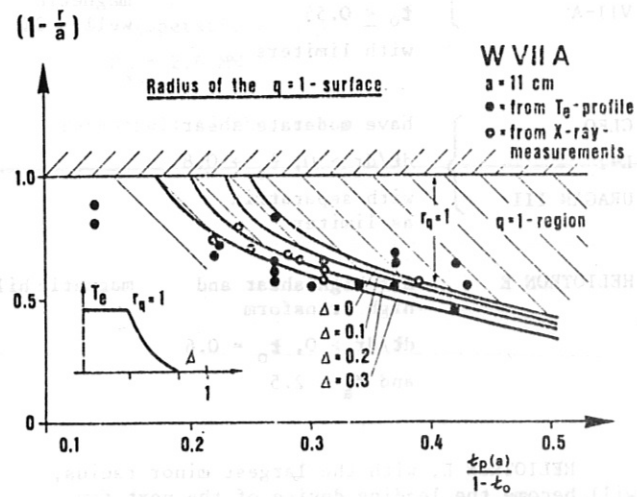

Fig. 3b Radius of the confinement region $a - r_{q=1}$ as a function of $\iota_p(a)/1-\iota_o$. The experimental data are derived from $T_e(r)$ profiles and X-ray measurements.

The onset of various tearing modes localized at resonant surfaces outside the q = 1 region depend on the current density profile, while the mode amplitude is affected by the plasma current, the external transform and density. For the most dangerous (2,1) tearing mode, saturation amplitude based on an analysis of the energy principle (Δ') has been calculated as a function of the measured current density profiles. Fig. 4 shows the width of the (2,1) mode for different profiles. Fig. 5 illustrates the agreement of the experiments and calculations [6].

Fig. 4 WENDELSTEIN VII-A

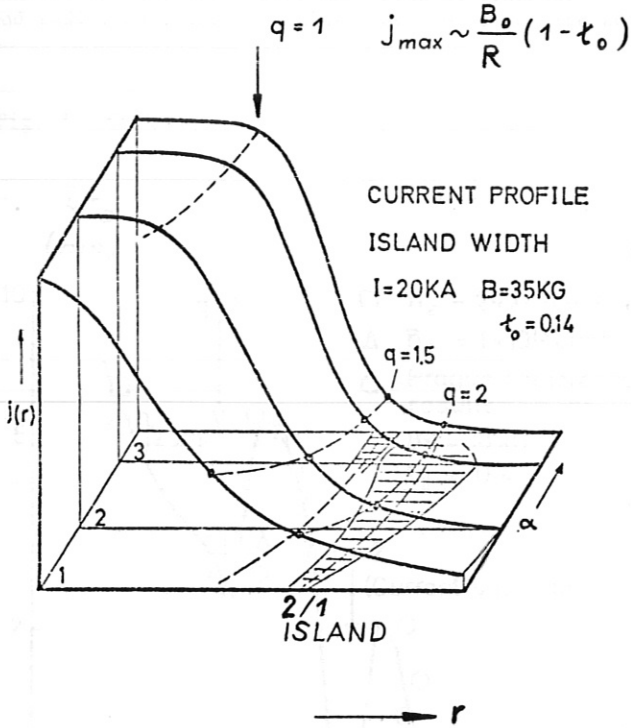

Fig. 4 Extension of the islands at resonant surfaces for different current density profiles with various α from the temperature profile $T_e(r) = T_e(o)\ 1/1 + (r/a)^{2\alpha}$. Discharges at $I_p = 20$ kA for $B_o = 3.5$T, $t_o = 0.14$.

Fig. 5 WENDELSTEIN VII-A

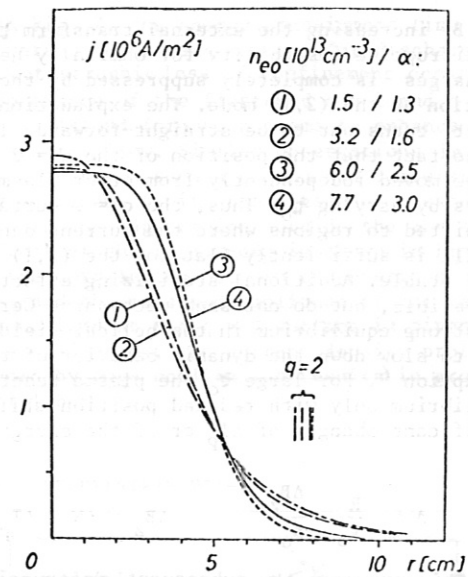

Fig. 5a Radial current density profiles calculated from measured electron temperature profiles for helium discharges with constant plasma current, for different electron densities. Discharge parameters: $B_o = 3.5$ T, $t_o = 0.14$, $I_{pl} = 20$ kA. q(a) = 2.9. n_{eo} is the central electron density calculated from the microwave line density by assuming a parabolic profile. α is a profile parameter which has been fitted to the electron temperature profiles, and which increase with n_e.

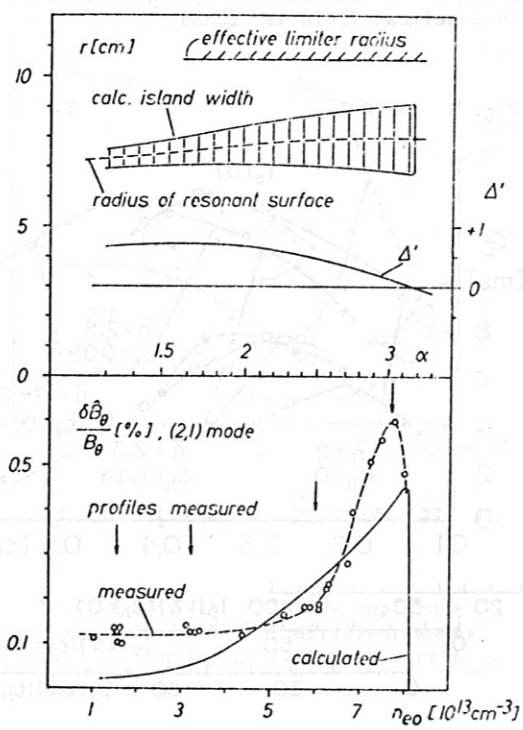

Fig. 5b For the discharge parameters given in Fig. 5a the relative amplitude $\delta\hat{B}_\theta/B_\theta$ of the (2,1) mode calculated as a function of α is shown. For comparison also the measured mode amplitude is presented as a function of the density n_{eo}. In the upper half, the corresponding calculated island width and the stability parameter Δ' are given.

- Disruptive Instability

By increasing the external transform $\iota_o > 0.14$, the disruptive instability for ohmically heated discharges is completely suppressed by the stabilization of the (2,1) mode. The explanation of this effect turns out to be straight-forward. It is due to the fact that the position of the q = 2 surface can be moved independently from other plasma parameters by varying ι_o. Thus, the q = 2 surface can be shifted to regions where the current density profile is sufficiently flat for the (2,1) mode to be stable. Additional stabilizing effects can be possible, but do not seem necessary. Certainly, the strong equilibrium in the helical fields will help to slow down the dynamic behavior of the disruption [6]. For large ι_o the plasma reacts in the equilibrium only with reduced position shifts for significant changes of ΔI_p or of the energy content ΔW.

$$\Delta \sim \frac{R}{\iota_o} \frac{\Delta B_z}{B_o} \qquad \Delta B_z \sim \Delta W \sim \Delta I_p \qquad (2)$$

This prevents the subsequent destruction of the plasma by limiter or wall contact after ergodization of a large confinement area. At sufficiently high ι_o, even operation without an applied vertical field is possible.

A suppression of the disruptive instabilities is also confirmed by JIPP T-2, if the transform $\iota_o > 0.14$ for the helical field is reached. In Fig. 6 a comparison for discharges at different ι_o and plasma current at comparable density is shown [7]. Theoretically a reduction of the linear growth rate of the m = 2 tearing mode by superposition of an ℓ = 2 helical field is found [8].

Fig. 6 JIPP T-2

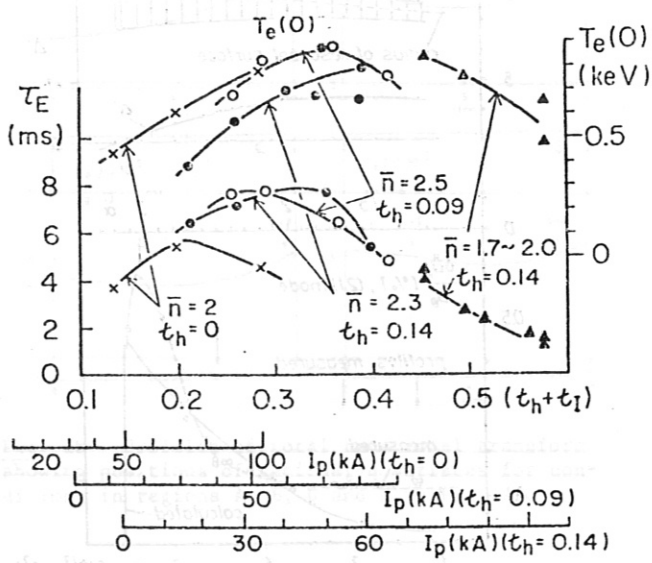

Fig. 6 Energy confinement time τ_E and central electron temperature versus $\iota_o + \iota_p$ for various values of the external transform ι_o and plasma current. JIPP T-2.

HELIOTRON E

In this device the ι = 1 boundary can be exceeded. Plasma currents 90 kA could be maintained with contribution of the current transform $\iota_p > 1$ at the plasma edge. Thus even the current density j seems not restricted to $j \sim B/R$ by the m = 1 mode. No disruptive instability was observed under these conditions.

B. Transport

Most of the results to date have concentrated on the global scaling of containment time

$$\tau_E = 3/2 \int \frac{\sum_k n_k T_k}{P_{OH}} dV$$

which experimental parameters. The values obtained in stellarators are in agreement with tokamak scaling or even better, see Fig. 6 or ref [9]. However, it is becoming evident that a knowledge of physics in stellarator plasmas can only be gained from a detailed study of the energy balance and transport coefficient. MHD effects, transport and radiation losses certainly have to be considered.

Effect of MHD Tearing Modes, Island Formation

In Fig. 7, the energy containment time τ_E is given versus the plasma current for discharges in CLEO. A catastrophic loss of confinement occurs with the appearance of the flattened q = 2 and q = 3 profiles. Island formation seems to enhance the radial energy flow. Similar observations in WENDELSTEIN VII-A show a pronounced decrease of energy confinement with the presence of extended islands in the edge region outside the q = 1 surface. The effect of the (2,1) mode is shown in Fig. 8, where the correlation between the energy containment time τ_E and the measured amplitude of the tearing mode localized at the q = 2 surface is given. With increasing density, the current density profile is steepened by edge cooling and results in growing (2,1) islands [10].

Fig. 7 CLEO

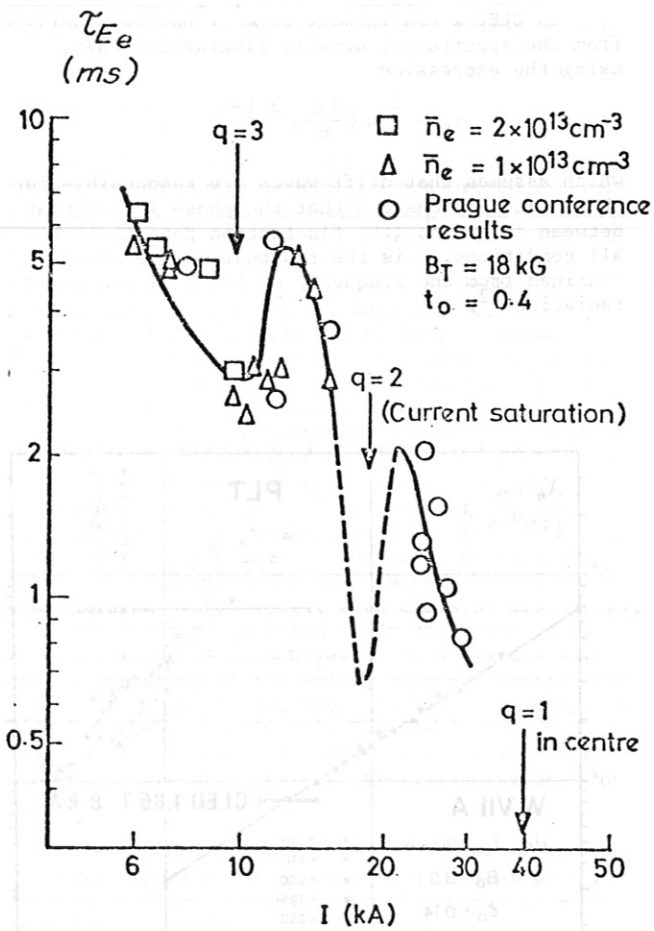

Fig. 7

Effect of flat q = 2 and q = 3 profiles on the electron energy confinement. CLEO

Fig. 8 WENDELSTEIN VII-A

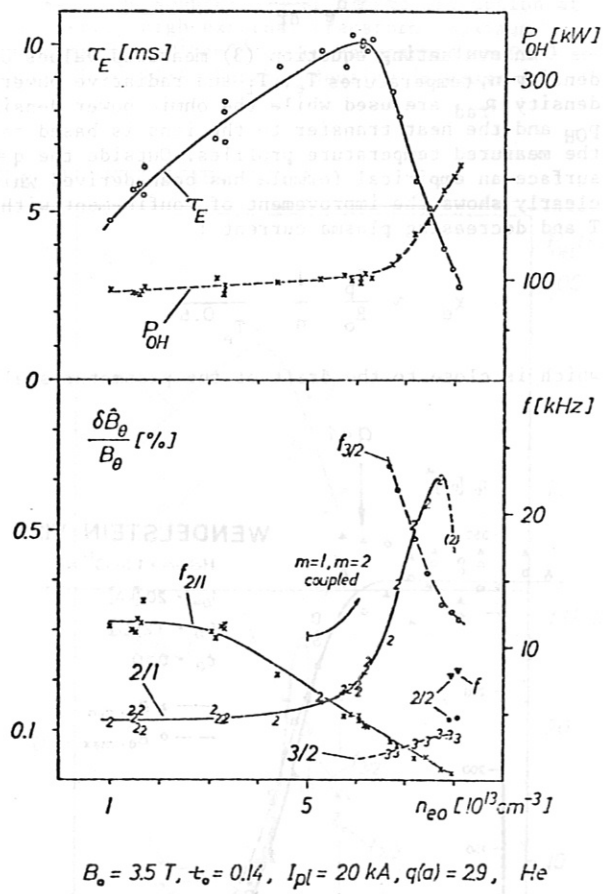

Fig. 8 Variation of the relative amplitude $\delta B_\theta / B_\theta$ and the frequency f of different modes observed with increasing central densities n_{eo}.

Measurements of temperature profiles by Thomson scattering and synchronized to the minimum and the maximum of the poloidal field fluctuations have been obtained. In agreement with the calculations based on the current density profile, the islands extend to 2 cm width (Fig. 9). The perturbation of the narrow confinement region outside the extended turbulent q = 1 core by the islands impairs the confinement [11].

Electron Thermal Conduction χ_e

The results of WENDELSTEIN VII-A at low densities $n_e < 5 \cdot 10^{13} cm^{-3}$ indicate a drift parameter scaling: $\chi_e \sim I_p / n_e \sqrt{T_e}$ in the regime where strong tearing modes are absent. The local heat conduction coefficient derived from the electron energy balance has been calculated outside the q = 1 area with enhanced transport [11].

$$\chi_e = \frac{\int_0^r (p_{OH}(r') - p_{rad}(r') - p_{ei}(r'))r'dr'}{r\, n_e \frac{dT_e}{dr}} \quad (3)$$

In evaluating equation (3) measured values of density n, temperatures T_e, T_i and radiative power density p_{rad} are used while the ohmic power density p_{OH} and the heat transfer to the ions is based on the measured temperature profiles. Outside the q = 1 surface an empirical formula has been derived which clearly shows the improvement of confinement with n, T and decreasing plasma current :

$$\chi_e \sim \frac{I_p}{B_o} \frac{1}{n} \frac{1}{T_e^{0.6}} \quad (4)$$

which is close to the drift of the parameter scaling.

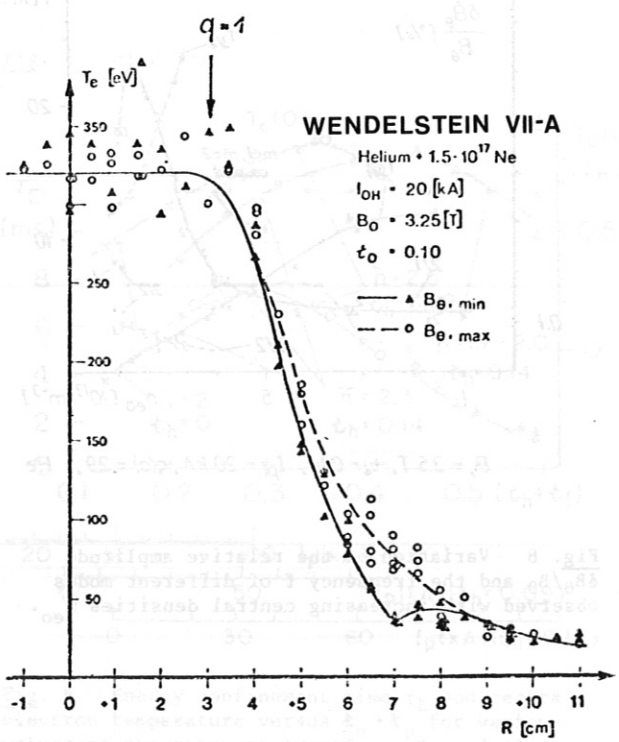

Fig. 9 Temperature profiles measured at the maximum and minimum of the poloidal field fluctuations B_θ for the (2,1) mode.

In Fig. 10 some data of $n\chi_e$ normalized to 20 kA/3.5 T are given. Also shown are PLT results. The deterioration of $n\chi_e$ with increasing current could be verified in a range I_p = 10 - 35 kA. In this respect, currentless operation may lead to a significant reduction of the anomalous electron heat losses. Because the derived scaling follows the drift parameter $\xi \sim I_p / n\sqrt{T}$, a current driven instability may be indicated for this anomalous loss. However, results from microwave scattering do not show a clear correlation between density fluctuations and drift parameters. Preliminary results with CO_2 laser scattering, at $k \sim 100\ cm^{-1}$ indicate however a correlation between the gross energy containment time τ_E and $(\delta n/n)^2$.

Away from any resonant surface effects, detailed energy balances show that for CLEO χ_e scales as $1/n_e$ with a value of $\chi \cdot n_e$ of $0.7 \cdot 10^{19} m^{-1} s^{-1}$. It is not possible to say if there is a drift parameter scaling, since the accessible current range is not sufficiently large [12].

In CLEO a confinement time τ_f has been derived from the spectrum of density fluctuation $\delta n/n$, using the expression

$$\tau_f \sim \left| \omega \left(\frac{\delta n}{n} \right)^2 \right|^{-1} ,$$

which assumes that drift waves are responsible for these fluctuations and that the phase is constant between δn and $\delta\phi$ (the fluctuation potential) for all conditions. ω is the fluctuation frequency obtained from the frequency of the 2 mm scattered radiation [12].

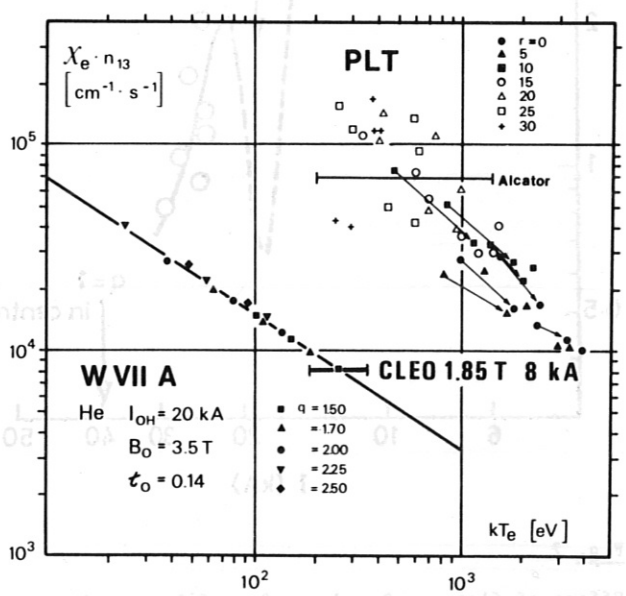

Fig. 10 Normalized local electron heat conductivity $\chi_e \cdot n$ versus temperature T_e.
n_{13} = local electron density in units of $10^{13} cm^{-3}$.
For comparison data from PLT and CLEO are indicated.

Ion Heat Conduction

The ion heat losses are found to be consistent with neoclassical predictions [13]. For WENDELSTEIN VII-A , in the plateau regime, the neoclassical value is approached with increasing density and temperature T_i. In CLEO, agreement is found at low current within a factor 2.

Diffusion Coefficient D_{exp}

It is difficult to measure particle losses, since the recycling must be accurately known and gas puffing localizes the sources of particles. However, the WENDELSTEIN VII-A results show that the particle confinement time τ_p has a dependence similar to that of the energy containment time τ_E. The values of D_{exp} appear about 2 orders of magnitude greater than the neoclassical predictions [14].

In CLEO τ_p thus determined increases linearly with the density up to a value of $\sim$ 70 ms at $n_e \sim 5 \cdot 10^{13} cm^{-3}$. This value agrees within a factor of 2 with neoclassical calculations.

C. Impurities

The small minor radius restricts the experiments in all existing stellarators. The short confinement time $\tau_E \sim a^2/\chi_e$ leads to high energy flux densities at the wall and subsequent release of impurities. The low $\bar{n} \cdot a$ screening length is not a sufficient protection of the inner core against impurity contamination. Wall effects have not yet been investigated in the same detail as in tokamaks. However, there is evidence that arcing and sputtering at the wall is much less than in tokamaks. Except at high currents, high Z material does not contribute significantly to the radiation losses. During plasma current buildup the external applied helical field centers the position of the discharge and the existence of magnetic surfaces reduces the loop voltage. Therefore, runaways and the influx of high Z material are diminished. The dominant impurities appear to be low Z oxygen and carbon. By careful conditioning of the vessel with cleaning discharges, i.e. for WENDELSTEIN VII-A under quasistationary conditions, 50 Hz discharges using a mixture Ne/H_2 and Ti gettering of the walls, oxygen concentrations $n_o/n_e < 5 \cdot 10^{-3}$ are reached. The use of He compared with H_2 appears beneficial. The chemical process leading to a release of oxygen from the wall via the production of water with the impinging atomic hydrogen can be avoided.

The current density distribution is influenced by small impurity concentrations. Small amounts of 1 - 2% Ne have been added to the discharge to prove that low concentration of low-Z impurities radiating from the edge can severely influence the current density profiles and the confinement. Fig. 11 shows the energy containment as a function of the density for the conditions of WENDELSTEIN VII-A. If a critical radiative power density p_{rad} (which is proportional to n_e, n_{imp}) is reached at the edge, the subsequent increase of the (2,1) tearing mode degrades the confinement, [13]. Compared to the condition in Fig. 8 the onset of a growing (2,1) mode is shifted to lower densities because of the added Ne, which increases the radiative power density at the edge. A radiative limiter is formed at high density, which constricts the current channel.

Bolometric measurements show radiative losses localized at the edge region up to 90% of the ohmic input power. The maximum of the energy confinement time corresponds at low external transform to the density limit by disruptive instability. Only the stabilizing effect of the external transform $\iota_o > 0.14$ prevents the disruptive instability at higher densities [13].

In the L-2 device discharges with separatrix operation and discharges with inserted material limiter have been compared [15]. With limiter introduced about 3 cm the wall interaction of the plasma is reduced and the radiative losses decrease. But this did not lead to an essential change of Z_{eff}. In contrast to WENDELSTEIN VII-A and CLEO high Z impurities seem to contribute almost entirely to Z_{eff}.

D. Maximum Density

With the suppression of plasma disruption at sufficiently high external transform, maximum densities $\bar{n}_e = 10^{14} cm^{-3}$ could be reached in CLEO and WENDELSTEIN VII-A. Further density increase is

Fig. 11 WENDELSTEIN VII-A

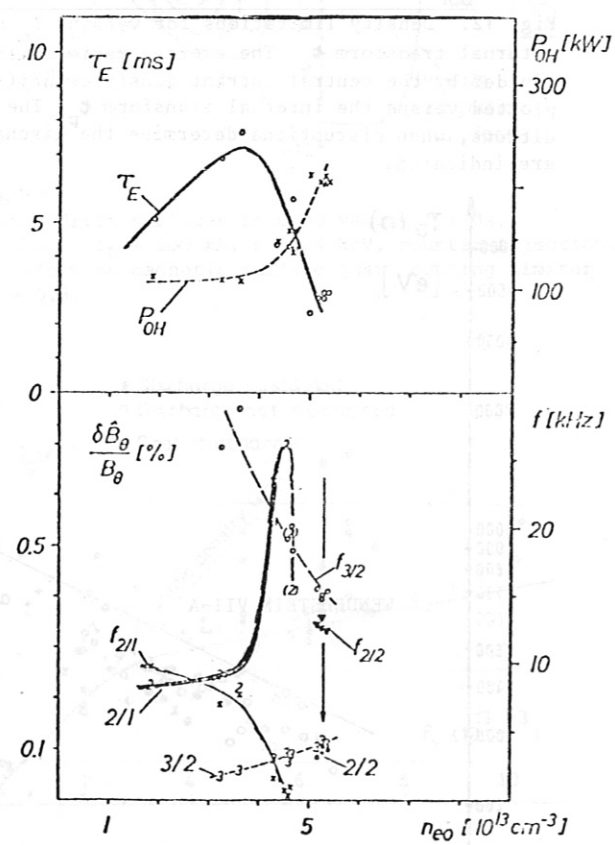

$B_o = 3.5\,T$, $\iota_o = 0.14$, $I_{pl} = 20\,kA$, $q(a) = 2.9$, He + Ne

Fig. 11 Effect of Ne ($2 \cdot 10^{17}$ particles) on the energy confinement and the (2,1) tearing mode for different central densities. Compare to Fig. 8.

limited by higher radiative losses, the concomitant deterioration of the confinement by edge cooling, and finally the depletion of ohmic power. Fig. 12 shows the ratio of density to the maximum current density for WENDELSTEIN VII-A corresponding to the q = 1 condition for various values of the external transform ι_o. The achievable density exceeds the Murakami limit for tokamaks:

$$\frac{\bar{n}}{j_{max}} \sim \frac{\bar{n}\,R}{B_o(1-\iota_o)} \leq 3\cdot10^{19}\,m^{-2}\,T^{-1} \qquad (5)$$

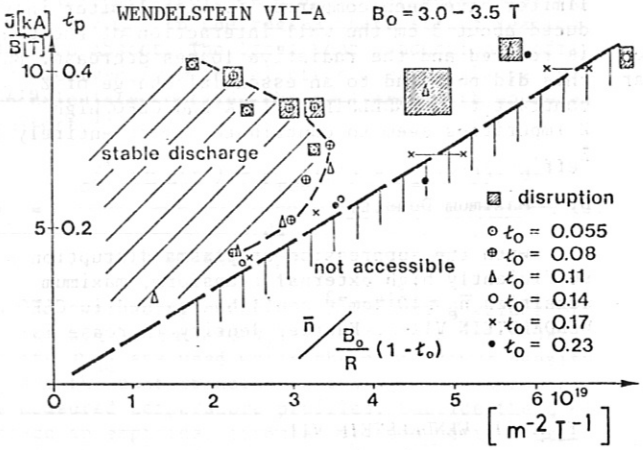

Fig. 12. Density limitations for various I_p and external transform ι_o. The average maximum densities divided by the central current densities $\bar{n}/j(o)$ are plotted versus the internal transform ι_p. The conditions, when disruptions determine the discharge, are indicated.

In CLEO for discharges free from MHD activity the particle confinement increases with density, whereas at high densities the average confinement time is independent of the density. Heat transport is determined by ion conduction in the core. The power returns to the electrons in the edge region and is lost by radiation.

E. Maximum Temperature

If radiation losses and ion heating by the electrons are negligible, the maximum attainable electron temperature with ohmic heating is determined by the electron heat conductivity and the restriction of the maximum current density. Based on the semiempirical formula [16] for χ_e which follows closely the drift parameter scaling

$$\chi_e \propto \frac{a}{R^{3/2}}\,\frac{I_p}{B}\,\frac{1}{r^2\,n\sqrt{T}}$$

the highest achievable temperature $T_e(o)$ is given by

$$T_e(0) \sim \left[Z_{eff}\,\frac{B}{R}\,[1-\iota_o]\,\frac{4}{3}\,\left(1-\frac{\iota_p}{1-\iota_o}\right)\right]^{1/2} \qquad (6)$$

In deriving this equation it is assumed that ι_o is independent of radius and that q = 1 on axis due to the current driven sawtooth oscillations. Fig. 13 shows values of $T_e(o)$ for WENDELSTEIN VII-A at different ι_o and $n_e < 5\cdot10^{13}cm^{-3}$ as well as those for several tokamaks. In stellarators the large aspect ratio and therefore a lowered maximum current density by a factor $(1-\iota_o)$ reduces the temperatures.

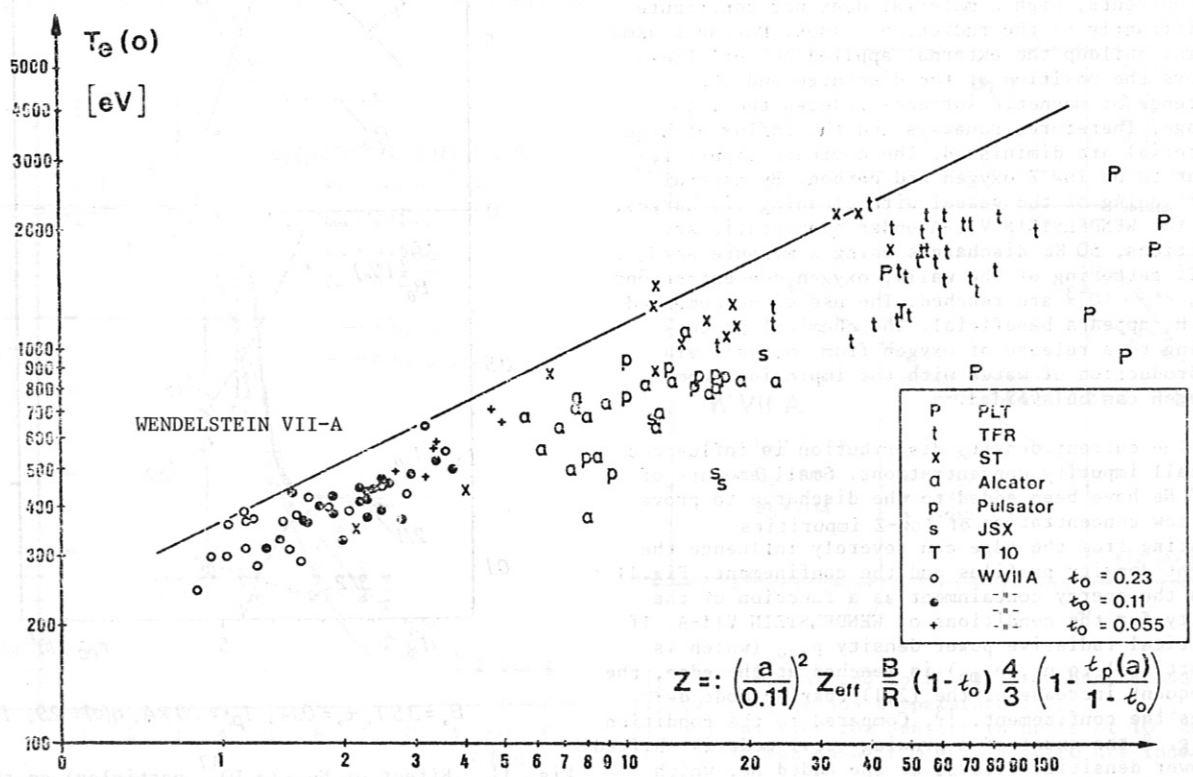

Fig. 13. Maximum electron temperature $T_e(o)$ versus $Z_{eff}\,\frac{B}{R}\,(1-\iota_o)\frac{4}{3}\,(1-\frac{\iota_p}{1-\iota_o})$ for ohmically heated discharges. Since most of the tokamak data are from the regime q = 4 - 6, the factor $\frac{4}{3}\,(1-\frac{\iota_p}{1-\iota_o})$ is set to 1.

IV.3 Ohmically Heated Plasmas with Auxiliary Heating

As outlined in section IV.2 the induced plasma current can lead to strong MHD activity with a deleterious effect on the confinement. A reduction of the plasma current almost eliminates the perturbation, but because of the corresponding decrease in ohmic heating power the accessible parameter range is narrowed. Auxiliary heating of an ohmically heated target plasma has been performed with neutral beams (CLEO, JIPP T-2, WENDELSTEIN VII-A), and lower hybrid frequency (JIPP T-2). In those experiments in which the ohmic heating power is a significant fraction of the total heating power, the heating results are in general agreeing with what can be expected from estimates based on the energy confinement time in an ohmically heated plasma.

A. Heating at the Lower Hybrid Frequency: LH

Heating at lower hybrid resonance has been investigated in JIPP T-2. The source had 160 kW at 800 MHz. At $B_o = 2.2$ T and $\bar{n} \sim 1.5 \cdot 10^{13} cm^{-3}$, both tokamak and stellarator operations showed an ion temperature heating rate ~ 1 eV/kW. In the stellarator mode, for $\iota_o = 0.14$ the heating efficiency decreased when $P_{LH} > 50$ kW. The loop voltage increased slightly. The reduction of heating efficiency was suggested to be caused by the loss of fast ions due to the helical ripples.

B. Neutral Injection Heating

Neutral Injection has been tested in CLEO and JIPP T-2, and in WENDELSTEIN VII-A at high power.

JIPP T-2, ref [7]

The injected power at 22 keV is 60 kW for coinjection and 30 kW counterinjection. The heating efficiencies in target plasmas at 2.2 T have been compared in tokamak and stellarator cases at the same value for $\iota_o + \iota_p \sim 0.3$ at the edge. In the tokamak case: $I_p = 60$ kA $|\bar{n}_e = 1.8 \cdot 10^{13} cm^{-3}$, $a = 15$ cm$|$ $\Delta T_i/P_N = 1.9$ eV/kW is measured for coinjection. For the stellarator $|\iota_o = 0.14$, $I_p = 45$ kA, $\bar{n}_e = 2.3 \cdot 10^{13} cm^{-3}$, $a_{eff} = 14$ cm $|$ $\Delta T_i/P_N = 1.6$ eV/kW is obtained, while heating efficiencies of counterinjection are equal in both cases $\Delta T_i/P_N = 1.6$ eV/kW. Because differences of trapping efficiency and direct orbit loss are estimated to be less than 5%, enhanced loss due to helical ripple may be used to explain this decrease.

CLEO, ref [17]

In CLEO, the neutral injection power has been increased to 150 kW at 20 keV with pulse lengths up to 100 ms. According to code calculations, without ohmic current and at $n \sim 2 \cdot 10^{13} cm^{-3}$, only 30% of the beam is ionized on confined orbits, because of the $\ell=3$ configuration with zero transform in the center. An induced plasma current $I_p = 6$ kA increases the efficiency to 50%.

For a target plasma produced with $I_p = 6$ kA at $\bar{n}_e = 2 \cdot 10^{13} cm^{-3}$ and $T_e = 150$ eV, $T_i = 130$ eV a significant rise of temperature is found: $\Delta T_e/P_{in} = 2.7$ eV/kW, $\Delta T_i/P_{in} = 2.3$ eV/kW. Analysis of the increase in the energy content W at switch on, dW/dt, shows that about 1/3 of the injected power seems to be transferred to the plasma. Orbit effects, charge exchange or additional losses as radiation may account for this rate.

Parameter range

For plasma currents $I_p > 6$ kA and neutral injection, significantly higher densities can be maintained by gas puffing than by ohmic heating alone (see Fig. 14). The maximum β is increased up to 0.75%. For lower currents $I_p > 6$ kA the density range cannot be extended. Close to the density limit, a gradual rise in loop voltage and impurity is seen. After a narrowing of the temperature profiles, the central temperature falls to $T_e \sim 15$ eV. With a timescale ~ 10 ms the density decays to $2 \cdot 10^{13} cm^{-3}$ and is maintained for the injection pulse length.

Fig. 14. CLEO.

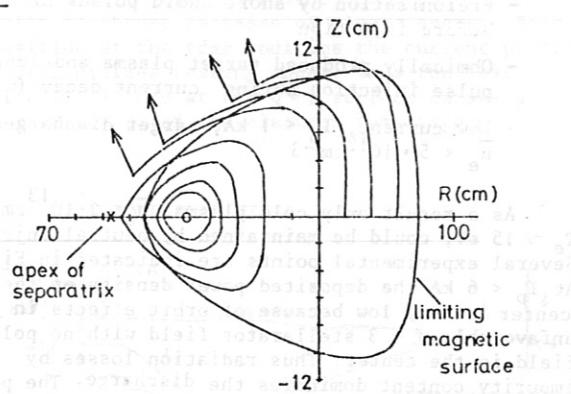

Fig. 14a
Proton drift surfaces in CLEO vacuum fields. $B_\phi = 20$kG, $I_L = 100$ kA, E = 24 keV, counter-injection. Transform on magnetic surface just touching limiter $\iota = 0.3$.

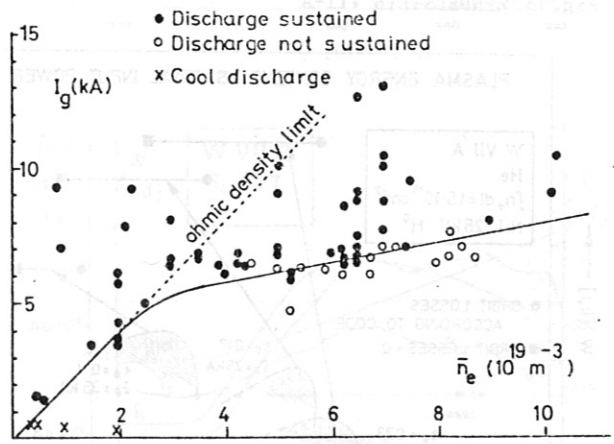

Fig. 14b
Operating diagram with 140 kW injection at 20 kV. $B_\phi = 18.4$ kG, $I_L = 100 - 120$ kA, $\iota = 0.35 - 0.55$. The solid line is the boundary of the operating region with injection. The dotted line is the boundary for ohmic discharges.
The line average density is taken assuming 1 interferometer fringe to be equivalent to $\bar{n}_e = 5 \times 10^{18}$ m^{-3}.

Confinement

The calculated energy containment time τ_{eE} for injection dominated discharges falls with increasing neutral injection power for constant $\bar{n}_e$. With increased density τ_{eE} stays constant. This behavior violates the drift parameter scaling. Certainly, ion conduction losses and radiation become important. No restriction by MHD phenomena has so far been observed. It should be noted that because of the ion heating, ion thermal conduction is increased. Radiation losses are increased by impurities possibly introduced by the beam. No MHD limit for the density attainable during neutral injection is seen: $\beta(o) \leq 0.75\%$ has been calculated for the central region.

Approach to Currentless Operation

Three methods for transition to currentless operation have been investigated:

- Preionization by short ohmic pulses $\Delta t < 20$ ms before injection
- Ohmically produced target plasma and long pulse injection during current decay ($\sim$100 ms)
- Low current, $I_p < 1$ kA, target discharges at $\bar{n}_e < 5 \cdot 10^{12} cm^{-3}$

As a result only cold plasma, $\bar{n}_e < 2 \cdot 10^{13} cm^{-3}$, $T_e \sim 15$ eV, could be maintained by neutral injection. Several experimental points are indicated in Fig. 14 b At $I_p < 6$ kA the deposited power density at the center is very low because of orbit effects in the unfavorable $\ell = 3$ stellarator field with no poloidal field in the center. Thus radiation losses by impurity content dominates the discharge. The power absorbed at low density conditions is not sufficient even to cross the radiation barrier. There are indications of significant radiation at the injection area due to impurity influx with the beam.

Fig. 15 WENDELSTEIN VII-A

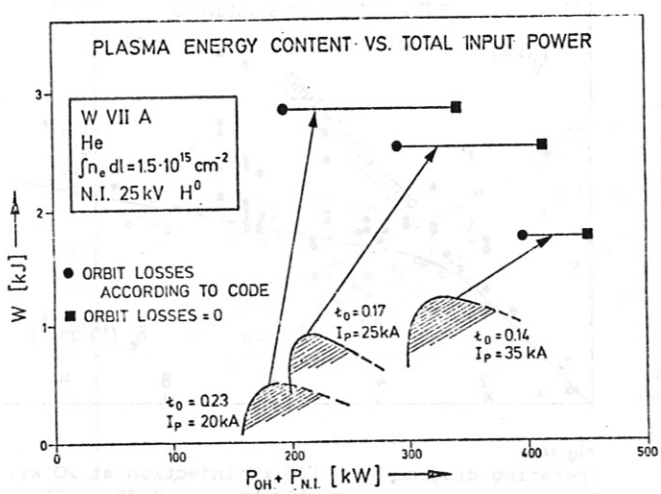

Fig. 15 Plasma energy versus input power: P_{OH} ohmic power, P_{NI} neutral injection power; the accessible region for ohmic heating at different plasma currents I_p and external transform ι_o are indicated.

WENDELSTEIN VII-A, ref [18]

In WENDELSTEIN VII-A the limited access restricts the injection angle to nearly perpendicular (6° injection). At this injection angle, the interaction length is short (0.2 m) and the density must be kept above $\bar{n}_e > 5 \cdot 10^{13} cm^{-3}$ for efficient absorption. In addition, significant orbit loss can be expected to occur. To describe the power deposition profiles, a computer code ODIN has been developed specifically for stellarator conditions. Four injectors of the CULHAM type for H_2 injection at 30 kV are available and deliver a total injection power of $P_N > 1$ MW. More detailed studies are done with two injectors delivering $P_N \sim 400 - 600$ kW. Even for high line densities $\int ndl > 10^{15} cm^{-2}$, with $n_{eo} > 10^{14} cm^{-3}$, the calculated power P_{in} transferred to the plasma is about 30% of the injection power.

Parameter Range

Compared to the accessible parameters of ohmically heated discharges, as indicated in Fig. 15 for different plasma currents, the application of neutral injection permits higher plasma pressure to be maintained. With residual plasma current both density and temperature can be increased. For discharges with $\int ndl = 1.5 \cdot 10^{15} cm^{-2}$ and $\iota_o + \iota_p(a) = 0.5$ the energy confinement time

$$\tau_E = \frac{W}{P_{OH} + P_{in}}$$

improves significantly at the reduced plasma current, even if uncertainties in the injection power P_{in} due to estimation of the orbit losses are allowed for. Because $\int ndl = 1.5 \cdot 10^{15} cm^{-2}$ as a target plasma can only be produced with high ohmic power at 35 kA, gas puffing must be used during neutral injection for lower current to build up comparable densities for sufficient beam absorption.

IV.4 Net Current Free Operation

Much work has been done in small devices such as the C-Stellarator, WENDELSTEIN II-A, PROTO-CLEO, HELIOTRON D, SATURN and VINT 20 with quasistationary and decaying plasmas at low densities and low temperatures. In his review paper Miyamoto summarizes some of the attempts to study the transport under currentless conditions. These small-radius devices can only reach the regimes of low density and temperature. Difficulties in the diagnostics and the analysis of the plasma parameters further complicate the interpretation of the results.

Progress in the application of RF and neutral injection heating, with the high power level now available, allows plasmas to be produced in a parameter range comparable to that of tokamaks. This section describes the zero net current experiments in discharges sustained by ECRH (CLEO, JIPP T-2, HELIOTRON E) and the high power neutral beam experiment of WENDELSTEIN VII-A.

A. Electron Cyclotron Resonance Heating

Quasistationary currentless plasmas were produced [17] in CLEO by ECRH power of 15 kW, at 17.5 GHz ($B_o = 0.625$ T), and pulse length 50 - 100 ms: Peak densities $\bar{n} \simeq 2.5 \cdot 10^{12} cm^{-3}$, $T_e \simeq 100$ eV. The optimum coupling efficiency for the ordinary mode was reached at $B_o = 0.57$ T. For

$\bar{n}_e = 2 \cdot 10^{12} cm^{-3}$ and $T_e \sim 60$ eV, $\tau_{Ee} \sim 1$ ms, the absorption efficiency is 20%. Fig. 16 shows these data related to the drift parameter scaling of ohmically heated discharges. The values compare well with those obtained by OH alone. The temperature increase is proportional to P_{in}. The measured confinement time is less than given by neoclassical theory. The coupling of the electrons to the ions and substantial losses by charge exchange with the high neutral density may be responsible.

In JIPP T-2 similar experiments with 32 kW at 35.5 GHz and resonance field $B_o = 1.27$ T have been carried out with $\iota_o = 0.12$. A particle confinement time of about 15 ms was deduced from the density decay.

Fig. 16. CLEO.

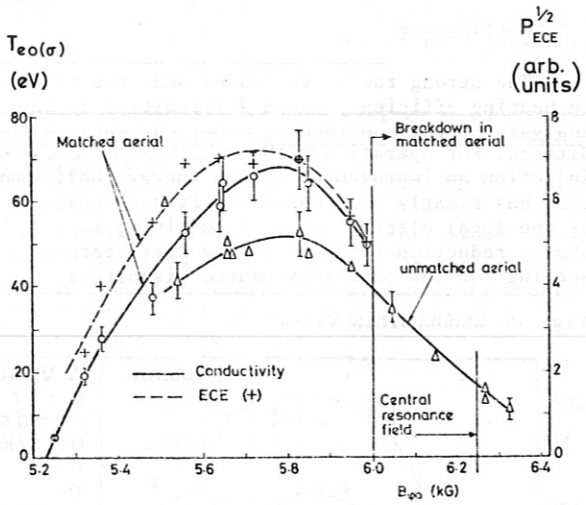

FIG. 16a

Dependences on $B_{\phi O}$ of $T_{eO(\sigma)}$ and $P^{\frac{1}{2}}_{ECE}$, where $T_{eO(\sigma)}$ is the peak electron temperature measured by probing the plasma conductivity and P_{ECE} is the second harmonic electron cyclotron emitted power; $\bar{n}_e = 1.5 \times 10^{18}$ m^{-3} (matched aerial), 1.8×10^{18} m^{-3} (unmatched aerial).

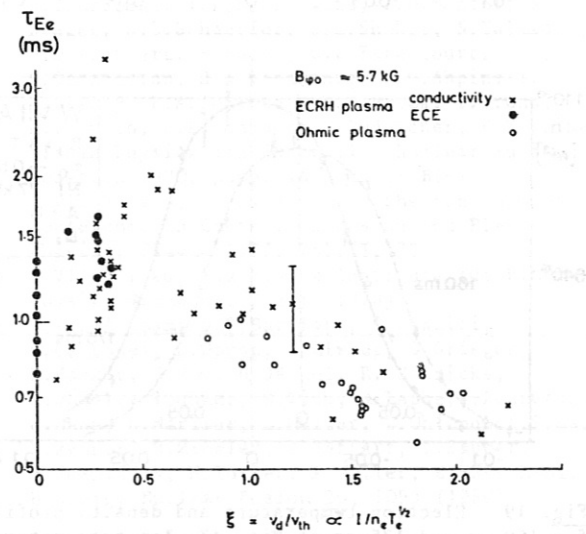

FIG. 16b

Dependence on the drift parameter ξ of the electron energy confinement time, for ECRH and ohmic plasmas.

HELIOTRON E used ECRH to initiate and sustain a discharge. The 28 GHz generator produces 200 kW. At 1 T field, a plasma of average density $\bar{n} = 5 \cdot 10^{12} cm^{-3}$ and electron temperature $T_e \simeq 500$ eV has been obtained. The pulse duration for the source (10 msec) is not long enough to establish thermal equilibrium between electrons and ions. An analysis of the afterglow plasma shows a confinement agreeing with preditions of neoclassical theory. In this afterglow regime, $T_e \simeq 200$ eV, $T_i \simeq 150$ eV; and the energy confinement time is 35 ms.

B. Neutral Injection Heating into WENDELSTEIN VII-A

For the application of neutral injection a target plasma has to be produced by ohmic heating. In the transition to currentless operation, the plasma current was reduced during the injection phase. In this operation, if the q = 2 surface $\iota_o + \iota_p|_a < 0.5$ stays inside the confinement region, the plasma pressure is limited to $\beta_\theta \leq 8$, where $\beta_\theta \sim W/I_p^2$. Further increase of beam power only results in abrupt decrease of plasma energy. Beam deposition at the edge modifies the current profile and destabilizes tearing modes. Thus the fast rising (2,1) mode at the q = 2 surface causes a severe decrease of the electron temperature [19].

Fig. 17 WENDELSTEIN VII-A

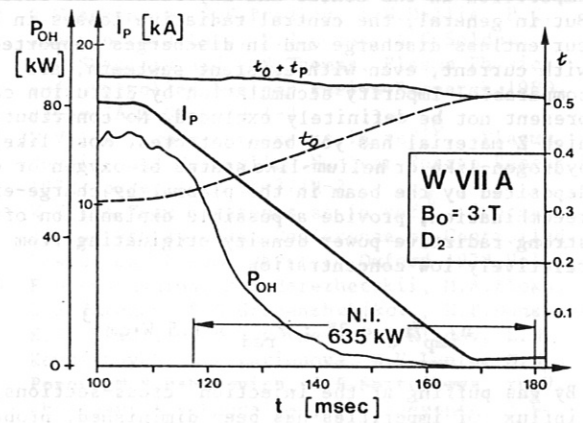

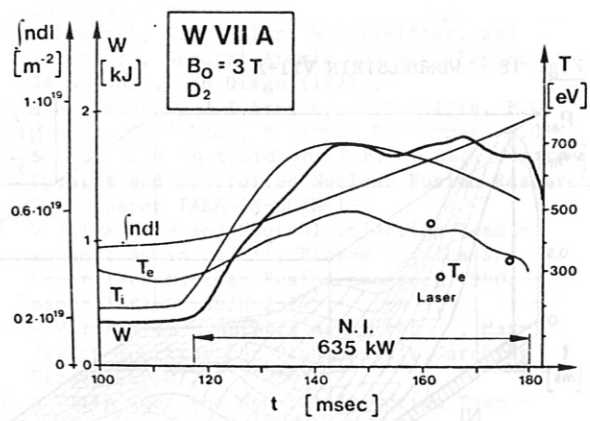

Fig. 17 Transition to currentless operation in WENDELSTEIN VII-A during neutral injection. As shown: P_{OH} ohmic power, external transform ι_o, rotational transform $\iota_o + \iota_p|_a$, line density, electron and ion temperature. 2 Injectors are used: $P_{NI} = 635$ kW.

The dangerous (2,1) mode can be excluded, however, by an increase of the vacuum transform during plasma current reduction so that the condition $\iota_o + \iota_p|_a > 0.5$ is satisfied at all times. This procedure allows a rapid decrease of plasma current, accompanied by a substantial change of the tokamak-like transform profile to the shearless WENDELSTEIN VII-A configuration with $\iota_o > 0.5$. No pronounced MHD phenomena have been observed, if the current is sufficiently low. Fig. 17 presents the main parameters for a discharge with 2 injectors.

Radiation

Under these conditions, a significant increase of radiation power is observed. This severe radiation loss, predominantly in the central region and at photon energies $E_{ph} > 400$ eV, determines the length of the discharge. Fig. 18 presents bolometric measurements (in agreement with soft X-ray measurements) for the discharge of Fig. 17. As can be seen on the profiles of Fig. 19, the strong radiative power density in the center diminishes the electron temperature at later time. A strong impurity influx during the injection phase by beam contamination or beam-wall interaction, combined with good confinement properties, is probably the reason for the high radiative losses. At higher plasma current, sawtooth instabilities seem to counteract the accumulation of impurities in the center and may reduce the rate. But in general, the central radiative losses in the currentless discharge and in discharges supported with current, even with existent sawteeth, are comparable. Impurity accumulation by diffusion can at present not be definitely excluded. No contribution of high Z material has yet been detected. Most likely hydrogen-like or helium-like states of oxygen or carbon, deposited by the beam in the plasma, by charge-exchange recombination, provide a possible explanation of the strong radiative power density originating from relatively low concentration

$$n_{imp}/n_e < 3\% : P_{rad} > 1.5\ W \cdot cm^{-3}$$

By gas puffing at the injection cross-sections, the influx of impurities has been diminished, probably due to formation of a cold gas layer.

Fig. 18 WENDELSTEIN VII-A

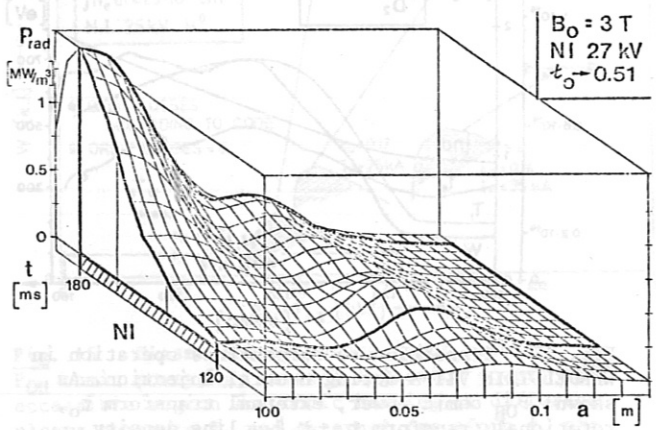

Fig. 18 Radiative power density by means of bolometer for conditions of Fig. 17.

Starting with a target plasma, careful adjustment of -dI/dt and dn/dt during neutral injection allows a transition to currentless operation at $\iota_o > 0.5$. Control of dn/dt is necessary to avoid reduction of the temperature $T_e < 150$ eV, which characterizes a radiation barrier. To heat a plasma from lower temperatures appears impossible.

High plasma pressure $\beta(o) \geq 0.5\%$ at 3 T has been achieved with two injectors at $P_N = 635$ kW, with $n_e = 10^{14} cm^{-3}$, $T_e > 330$ eV, $T_i = 550$ eV. Preliminary results with higher injection power indicate a further increase of the plasma pressure without introducing MHD limitations in the shearless configuration $t_o > 0.5$. For these discharges further increase of radiation determines the length of the discharge [20].

Confinement

The strong radiative losses and uncertainties in heating efficiency cause difficulties in the analysis of the confinement under currentless conditions. For operation with ohmic current and neutral injection an improvement of the energy confinement time has clearly been observed. Even calculations of the local electron heat conductivity seem to show a reduction compared to the drift parameter scaling for the ohmically heated discharges.

Fig 19 WENDELSTEIN VII-A

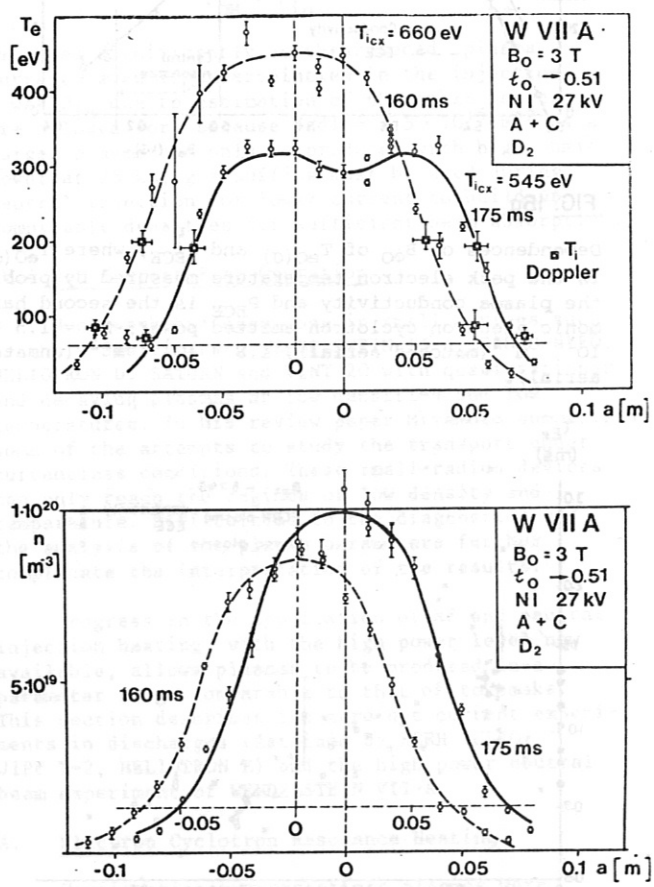

Fig. 19 Electron temperature and density profiles for 160 ms and 175 ms of Fig. 17, Ion temperatures are indicated: for the central region by charge exchange measurements, at the edge region derived from Doppler width measurements.

In the currentless plasma the power balance indicates a more efficient power transfer from the beam to the plasma than predicted by the ODIN code. This is indicated by

i) The radiation power exceeds the calculated input power;

ii) The energy transfer from the hot ions to the colder electrons is larger than the beam power deposition to the ions in the central region.

A higher heating efficiency seems to be possible by taking into account radial electric fields. These fields lead to better confinement of the highly energetic ions, thus reducing the orbit losses. Experimentally, there is evidence for plasma rotation, which may be a result of an electric field of 1 kV across the plasma radius.

The observation of beam excited ion cyclotron waves suggests their importance for the ion heating by anomalous slowing down.

When the radiative loss is subtracted from the beam input power the energy confinement time in these discharges is $\tau_E \sim 35$ ms. The ion heat conduction should determine the plasma confinement. Indications of a significant reduction of the electron heat conduction may be seen in the dramatic drop of the fluctuation level observed by CO_2 laser scattering in agreement with 2 mm microwave scattering at $k \sim 10\,cm^{-1}$ during the currentless phase. The absence of any MHD modes may also contribute [19].

References

1 K.Miyamoto, Nucl. Fusion 18, 243 (1978)

2 M.S.Rabinovich, G.S.Voronov, Proceedings of the 9th European Conference on Controlled Fusion and Plasma Physics, Oxford 1979, Vol.II, 223

3 D.T.Anderson, J.D. Callen, J.A.Derr, J.H.Harris, D.J.Hoffman, T.W.Kruckewitt, T.D.Mantel, S.C. Prager, R.C.Schaeffer, J.L.Shohet, N.Talmadge, J.D.Treffert; F.Bauer, O.L.Betancourt, P.Garabedian, J.A.Tataronis; J.G.Aspinall, L.Lidsky, P.A.Politzer, R.E.Potok; T.K.Chu, H.P.Furth, J.L.Johnson, C.Ludescher, K.E.Weimer, Plasma Physics and Controlled Nuclear Fusion Research 1980, paper IAEA-CN-38/BB-1

4 W VII-A Team, Proceedings of the 8th European Conference on Controlled Fusion and Plasma Physics, Prague 1977, Vol.II, 73

5 W VII-A Team, Max-Planck-Institute für Plasmaphysik, Garching, 2/241 (1978)

6 W VII-A Team: D.V.Bartlett, G.Cannici, G.Cattanei, D.Dorst, A.Elsner, G.Grieger, H.Hacker, J.How, H.Jäckel, R. Jaenicke, P.Javel, J.Junker, M.Kick, R.Lathe,F.Leuterer, C.Mahn, S.Marlier, G.Müller, W.Ohlendorf,F.Rau, H.Renner, H.Ringler, J.Saffert, J.Sapper, P.Smeulders, M.Tutter, A.Weller, E.Würsching, H.Wobig, Nuclear Fusion 20, 1093 (1980)

7 J.Fujita, S.Itoh, K.Kadota, K.Kawahata, Y.Kawasumi, O.Kaneko, T.Kuroda, K.Matsuoka, K. Matsuura, K.Miyamoto, N.Noda, Y.Oda, K.Ohkubo, K.Sakurai, K.Sato, M.Sato, S.Tanahashi, Y.Terashima, K.Toi, Plasma Physics and Controlled Nuclear Fusion Research,1980 paper IAEA-CN-38/H-3-2

8 K.Ohasa, J. Phys. Soc. Japan 48, 1731 (1980)

9 T.K.Chu, Nucl. Fusion 20, 803 (1980)

10 W VII-A Team: G.Cannici, G. Cattanei,A.Cavallo, D.Dorst, A.Elsner, G.Grieger, H.Hacker, J.How, H.Jäckel, R.Jaenicke, P.Javel, J.Junker, M.Kick, F.Leuterer, C. Mahn, S.Marlier, G.Müller, W.Ohlendorf, F.Rau, H.Renner, H.Ringler, J.Saffert, J.Sapper, P.Smeulders, M.Tutter, O.Vollmer, A.Weller, E.Würsching, H.Wobig, M.Zippe, Plasma Physics and Controlled Nuclear Fusion Research 1978, paper IAEA-CN-37/H-3

11 W VII-A Team: D.V.Bartlett, G.Cannici, G.Cattanei, D.Dorst, G.Grieger, H.Hacker, J.How, H.Jäckel, R.Jaenicke, P.Javel, J.Junker, M.Kick, R.Lathe, J.Meyer, C.Mahn, S.Marlier, G.Müller, W.Ohlendorf, F.Rau, H.Renner, H.Ringler, J. Sapper, P.Smeulders, M.Tutter, B.Ulrich, A.Weller, E.Würsching, H.Wobig, M.Zippe, and Neutral Injection Team: D.Cooper, K.Freudenberger, G.Lister, W.Ott, E.Speth, Plasma Physics and Controlled Nuclear Fusion Research 1980, paper IAEA-CN-38/H-2-1

12 D.W.Atkinson, J.E.Bradley, A.N.Dellis, P.C. Johnson, D.J.Lees, P.J.Lomas, A.C.Selden, P.A.Shatford,and P.R.Thomas, Plasma Physics and Controlled Nuclear Fusion Research 1980, paper IAEA-CN-38/H-1-2

13 W VII-A Team - authors as in ref [10], Plasma Physics and Controlled Nuclear Fusion Research 1978, paper IAEA-CN-37/H-2

14 W VII-A Team - authors as in ref [6], Proceeding of the 9th European Conference on Controlled Fusion on Plasma Physics, Oxford 1979,Vol.I,4

15 E.D.Andrukhina, M.S.Berezhetskii, M.A.Blokh, G.S.Voronov, S.E.Grebenshchikov , N.P.Donskaya, K.S. Dyabilin, B.I.Kornev, S.V.Kladov, L.M. Kovrizhnykh, N.F.Larionova, N.V.Lunin, S.N. Popov. M.S.Rabinovich, I.S.Sbitnikova, Yu.V. Khol'nov, A.V.Khudoleev, O.I.Fedyanin, I.S. Shpigel, S.V.Shchepetov. Plasma Physics and Controlled Nuclear Fusion Research 1980. paper IAEA-CN-38/H-3-1

16 G.E.Guest, R.L.Miller, W.W.Pfeiffer, and R.E.Waltz, General Atomic Company, Report GA-A 14831, San Diego (1978).

17 D.W.Atkinson, J.E.Bradley, A.N.Dellis, P.C. Johnson, D.J.Lees, B.Lloyd, P.J.Lomas, A.C. Selden, P.A. Shatford and P.R. Thomas, Plasma Physics and Controlled Nuclear Fusion Research 1980, paper IAEA-CN-38/H-1-1

18 W VII-A Team and Neutral Injection Team - authors as in ref [11], Plasma Physics and Controlled Nuclear Fusion Research 1980, paper IAEA-CN-38/H-2-2

19 W VII-A Team - authors as in ref [11], Max-Planck-Institut für Plasmaphysik,Garching Report IPP 2/250 (1980)

20 W VII-A Team and Neutral Injection Team - authors as in ref [11], and O.Vollmer - 2nd Intern. Symposium on Heating in Toroidal Plasmas, Como (1980)

V. THEORY

Introduction

Introduction

Stellarators having no net current can be viewed as a system with external confinement. This means that the plasma equilibrium can be achieved by a steady-state externally imposed magnetic field, with currents in the plasma merely modifying the shape of the magnetic surfaces. This is in contrast to a tokamak, where a non-zero net toroidal current is essential to provide the necessary $J \times B$ force. From this point of view as well as from that of actually producing such plasmas it is natural to consider a series of equilibria starting with a vacuum magnetic field and extending to as high values of β as possible or as desired. As it is well known, axisymmetric fields cannot confine a plasma without a net toroidal current. Therefore one has to consider in principle the large variety of three-dimensional fields. We shall, however, restrict the consideration to fields which are periodic, i.e., which are invariant under rotation by an angle $2\pi/m$ (m = natural number) around the z-axis.

The plasma must be confined in such a way that an almost isotropic velocity distribution can be maintained nearly everywhere. Therefore the ideal MHD equilibrium conditions must be satisfied closely, and ideal MHD stability theory will presumably be adequate as far as gross modes of possible instabilities are concerned. The consideration of transport processes and the prediction of the confinement of injected neutrals, of the high energy tail of the D- and T-distribution responsible for the thermonuclear reactions, and of the confinement of the α-particles make the evaluation of particle trajectories necessary. It is sufficient to consider these trajectories in the guiding center approximation, and use can also be made of the second adiabatic invariant when it exists.

In the MHD picture there exists a set of nested toroidal surfaces which are both magnetic surfaces and isobaric surfaces, while the pressure decreases monotonically from its maximum on the toroidal magnetic axis. Nontrivial three-dimensional analytical solutions of this type are unknown, and, indeed, the existence of such solutions has not been proven. Mathematical difficulties exists at those magnetic surfaces whose rotational transform ι (ι = twist number) is rational. However, solutions are known for cases where all magnetic lines of force close upon themselves after a finite number of turns. Then ι is a constant rational number. The condition that the pressure p be constant on those field lines for which $\oint dl/B$ is the same is necessary for these equilibria. In general this condition and the condition that p = constant on magnetic surfaces are contradictory when the limit is approached under which both the conditions of unique existence of magnetic surfaces and rational twist numbers are fulfilled. One might ignore these difficulties, if the simple rational twist numbers (in particular 0, 1, 1/2 etc.) are exluded and it is assumed that some shear is always present and that this shear makes the rational surfaces of high order (i.e., closure after many turns) innocuous.

Stellarators, being non-axisymmetric devices have a basic problem as regards theoretical work; there is no ignorable coordinate. Thus, much work must be done with either various expansion techniques or with complex numerical approaches. In this chapter, a discussion of the various approaches will be made. Section V.1 treats MHD equilibrium and stability and points out several methods for their calculation. Section V.2 presents a scheme for developing an "optimized" configuration in which the secondary currents are minimized. Section V.3 presents a discussion of orbits and transport in which the neo-classical theory based on a random walk approximation and recent Monte-Carlo calculations are compared. A discussion on the existence of bootstrap current is included.

V.1 MHD Equilibrium and Stability

As with all other devices, the use of fluid models has provided significant insight into the macroscopic behavior of stellarators. This has been more pronounced than for many other systems because the complicated field configurations have made analysis using models containing more physics particularly difficult. The standard MHD equations can successfully model the observed plasma behavior, even at low values of collisionality. The major questions that can be studied with fluid models concern MHD equilibrium and stability.

The equilibrium problem is the determination of solutions of the simple fluid condition[1]

$$(\nabla \times \underset{\sim}{B}) \times \underset{\sim}{B} = \nabla p, \quad \nabla \cdot \underset{\sim}{B} = 0 ,$$

with the magnetic field lines forming reasonable magnetic surfaces. This is not particularly simple. Indeed, useful configurations exist only

for very special magnetic field designs. The most essential requirement is that a path be provided so that electrons can flow from a region where $B \times \nabla B$ drifts have created an excess to where there is a deficiency. This follows from the condition that the current be divergence-free,

$$\underset{\sim}{B}\cdot\nabla\underset{\sim}{J}\cdot\underset{\sim}{B}/B^2 = (\underset{\sim}{B} \times \nabla p\cdot\nabla B^2)/B^4.$$

If the magnetic field lines close on themselves, the right-hand side of this relation must have a zero average value. This can be shown to require that $p = p(\oint d\ell/B)$. If the lines form magnetic surfaces, this restriction is not so severe. Currents perpendicular to the field are set up by the particle drifts with current flow along the field lines which cancels the charge buildup.[2] These secondary currents, commonly called Pfirsch-Schluter currents, generate vertical magnetic fields that, as β is increased, move the magnetic axis outward away from the major axis of the system. At the same time they bring a second closed line or stagnation line in towards the plasma from the center of the system at an even faster rate than the magnetic axis moves. At some critical β this separatrix approaches the plasma surface.

This aspect of the equilibrium problem has led to a study of how to minimize these secondary currents by properly shaping the field lines so that $\int d\ell/B$ over one toroidal field period is nearly the same for any azimuthal position on a magnetic surface.[3] Techniques for accomplishing this by properly combining two or more helical fields were developed in connection with the high β stellarator program (Scyllac and Isar) and are being used at present to accomplish this.

On the other hand, stability studies (both theoretical and experimental) have tended to show that minimum average B configurations are highly desirable[4] and are probably essential for steady state operation. The outward shift of the magnetic axis due to the secondary currents can provide this property,[5] so that it is not clear that the complete elimination of them is desirable. Furthermore, some of the techniques for minimizing the variation of $\int d\ell/B$ tend to increase the vacuum magnetic field at the magnetic axis, making this problem even worse. It is possible that magnetic shear may provide sufficient stabilization.

There have been some stability calculations based on specific models so that a good intuitive feeling for what to expect exists. On the other hand, general quantitative results are not available so that it is difficult to provide explicit scaling laws to guide reactor studies or provide the necessary input to machine design.

The three-dimensional nature of stellarator configurations has limited the possibilities for treatment. It has even been surmised that stellarator equilibria do not exist.[6] Existence proofs to all orders in various small expansion parameters have been found, and both numerical and experimental studies have provided justification for such work.

Since stellarators will probably have a large aspect ratio, progress can be made by ignoring toroidicity and treating the system as helically invariant. In this case the equilibrium equations reduce exactly to a Grad-Shafranov type elliptic problem.[7] Numerical codes have been developed to determine these equilibria. These have been used both to evaluate equilibrium and localized stability properties of these systems and to provide a calibration for more general three-dimensional codes. The ERATO stability code has been modified for MHD stability studies of these equilibria.[3]

Almost all three-dimensional MHD stellarator studies can be classified into three categories: magnetic field ordering expansions, expansions about the magnetic axis, and three-dimensional numerical approaches. The first method is based on the fact that in many stellarator embodiments there exists a periodicity length smaller than the distance around the torus such that averaging over the behavior on this short length scale reduces the problem to a two-dimensional one. This approach is discussed under the label "stellarator expansion". Much progress has been made with the second approach which is to write all the variables in terms of the distance from the magnetic axis and to determine the expansion coefficients. In some sense, this can be visualized as a large aspect ratio expansion. The difficulty with this method is in connecting to external boundary conditions. Frequently one must carry the expansion to very high orders to treat plasma behavior well away from the axis where the transform and shear may be much different than elsewhere in the system. Finally, progress can be made with the third method by attacking the complete three-dimensional problem directly, without utilizing any formal expansion. The latest generation of computers has made this approach useful, but it suffers from the disadvantage of requiring very large amounts of both computer memory and computer time, and may not have sufficient resolution to investigate certain phenomena. The following material is a more detailed discussion of these techniques.

A. Stellarator Expansion

The earliest analytic treatment of stellarator equilibrium and stability was the work at Princeton where the stellarator expansion was developed.[7,8] The magnetic field is written as

$$\underset{\sim}{B} = \underset{\sim}{B}_o + \underset{\sim}{B}^{\delta} + (\underset{\sim}{B}^{K} + \underset{\sim}{B}^{\beta} + \underset{\sim}{B}^{\sigma} + \underset{\sim}{B}^{\delta\delta}) + \ldots$$

where $\underset{\sim}{B}_o$ is a uniform axial field,

$$\underset{\sim}{B}^{\delta} = B_o \nabla \sum_p \sum_\ell \frac{\varepsilon_\ell}{ph} I_\ell(phr) \sin(\ell\theta - phz),$$

is a vacuum field with a shorter periodicity length than the length of the system,

$$\underset{\sim}{B}^{K} = - B_o \frac{r}{R} \cos\theta \underset{\sim}{e}_z$$

is the modification of the toroidicity associated with toroidal curvature,

$$\underset{\sim}{B}^{\beta} = - (p/B_o)\underset{\sim}{e}_z$$

is the field due to diamagnetic currents associated with the pressure,

$$\underset{\sim}{B}^{\sigma} = \underset{\sim}{e}_z \times \underset{\sim}{\nabla} A^{\sigma}$$

is the lowest order component of the field perpendicular to the z-axis and independent of z, so that it can be expressed in terms of a stream function A^{σ}, and $\underset{\sim}{B}^{\delta\delta}$ is a vacuum field which varies over the short periodicity length $2\pi/h$. We assume that $(B^{\delta}/B^{o})^2 \sim (B^{\kappa}/B_o) \sim (B^{\beta}/B_o) \sim (B^{\sigma}/B_o) \sim (B^{\delta\delta}/B_o) \sim hR \sim a/R << 1$. Then, from the axial component of $\nabla \times \underset{\sim}{B} = \underset{\sim}{J}$, we see that

$$\nabla^2 A^{\sigma} = J^{\sigma};$$

by expanding $\underset{\sim}{B} \cdot \nabla\Psi$, we obtain

$$\Psi^{o} = \langle B_{\theta}^{\delta} \int B_r^{\delta} dz \rangle - A^{\sigma};$$

and from $\underset{\sim}{\nabla} \cdot \underset{\sim}{J} = 0$, we find

$$J^{\sigma} = - p'(\Psi^{(o)})\, \Omega + G(\Psi^{(o)})$$

with

$$\Omega \equiv \langle B^{\delta 2} \rangle / B_o^2 - 2(r/R)\cos\theta.$$

Here the brackets $\langle\ \rangle$ denote an average over the short periodicity length. Thus, this expansion has reduced the equilibrium problem to one similar to a high - β large-aspect ratio tokamak formulation. With this expansion the stability problem is also reduced to a relatively simple formalism:[9]

$$2\delta W = \int \left[Q_{\perp}^2 + \underset{\sim}{J}_{\parallel} \times \underset{\sim}{\xi}_{\perp}^{(o)*} \cdot \underset{\sim}{Q}_{\perp} + \underset{\sim}{\xi}^{(o)} \cdot \nabla p \underset{\sim}{\xi}_{\perp}^{(o)} \cdot \nabla\Omega \right] d\tau,$$

$$\underset{\sim}{Q}_{\perp} = - inB_o \underset{\sim}{\xi}_{\perp}^{(o)} + (1/2\pi R)\, \underset{\sim}{e}_z \times \nabla(\underset{\sim}{\xi}_{\perp}^{(o)} \cdot \nabla\Psi^{(o)}).$$

In the lowest orders of the expansion, the perturbation had to be made constant over the short period, $\underset{\sim}{\xi}_{\perp}^{(o)} = \underset{\sim}{\xi}_{\perp}^{(o)}(r,\theta,z/R)$, and $\nabla \cdot \underset{\sim}{\xi}_{\perp}^{(o)} \approx 0$ so that it could be expressed in terms of a stream function, and some variation of $\underset{\sim}{\xi}_{\perp}^{(1)}$ had to be introduced so that the perturbation can follow the modulation associated with the B^{δ} field. The first term in this equation clearly represents the stabilization energy associated with bending the magnetic field lines. It is similar to that obtained in analyses of tokamaks except that the rotational transform due to external currents enters the expression for $\underset{\sim}{Q}_{\perp}$. The second term represents the energy available from expansion or interchange of the plasma. The only difference from a tokamak is the additional field line curvature term associated with $\langle B^{\delta 2} \rangle$ in Ω. The last term is the energy associated with the interaction of the force-free current with the perturbed magnetic field and is responsible for kink and tearing modes in tokamaks. The advantage of this particular ordering results from the fact that any other ordering can be inferred from it. For example, the toroidal curvature terms were left out of it in the earliest stellarator work. Consideration of the behavior of the Euler-Lagrange equation, obtained by minimizing δW near a singular surface where $\iota \approx n/m$ leads to a Mercier-type stability criterion. Similarly, if both pressure and toroidal curvature are neglected, the Euler-Lagrange equation can be used to construct stability diagrams for ohmically heated stellarators. Considerable work has been done with this equation using different current distributions, and this formalism has even been used for stability discussions of heliotron and torsatron configurations where the original ordering assumption is invalid.

This reduced set of equations is still second order so that results cannot be obtained trivially. It is clear that the equations can be made homogeneous by restricting $p(\Psi^{(o)})$ and $G(\Psi^{(o)})$ to be linear. Then a quadrature solution can be written.[8] The $\beta = 0$ solution in a pure $\ell = 3$ stellarator system with an aspect ratio of 20 has concentric circular $\Psi^{(o)}$ surfaces as in Fig. 1. (The helical perturbation is of higher order.) As the pressure is increased the surfaces are shifted outwards as in Fig. 2, which corresponds to $\beta = 2.5\%$. A carefully selected vertical field $B^{\sigma}/B_o = 5\%$ shifts the vacuum magnetic surfaces inward as in Fig. 3. For this particular field, increasing β to 2.5% does not change the shape of the surfaces. This can be understood from the fact that $\int d\ell/B$ along a field line over one periodicity length is nearly the same all the way around the flux surface so that Ω is a function of $\Psi^{(o)}$ and one does not need secondary currents to keep the current divergence-free. One can see from Fig. 4 that V'', a measure of the average magnetic field line curvature, is unfavorable for this configuration. The outward shift observed in Fig. 2 produces an average magnetic well and thus good properties concerning interchange instabilities.

Another assumption where progress has been made is by treating the $(r/R)\cos\theta$ term as small and by carrying out further expansion.[10] The most interesting thing that comes from such a study is that there exists a critical β at which the shift of the magnetic axis from the center of the coil system becomes infinite. Although equilibria with higher values of β can be found, they are unstable with respect to a nearly rigid shift.

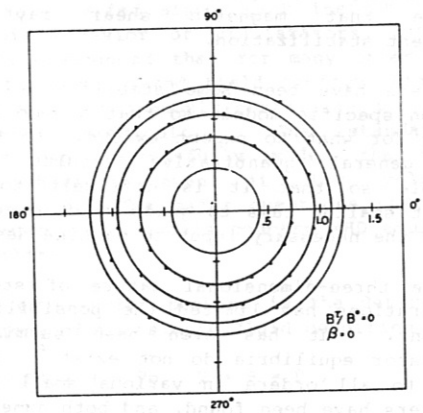

Fig. 1. Zeroth-order magnetic surfaces when a multipolar field with $\ell = 3$, $(\varepsilon^{\delta})^2 = 10$, $hR = 20$ is present. $B^{\tau}/B^{o} = 0$; $\beta = 0$.

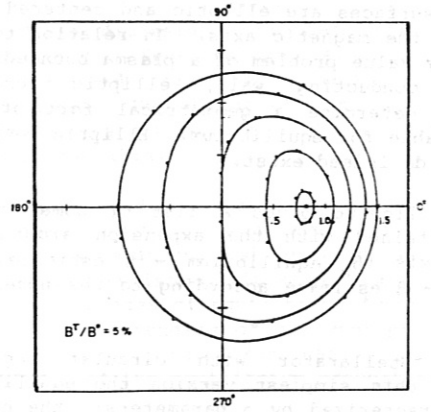

Fig. 2. Zeroth-order magnetic surfaces for the configuration of Fig. 1 but with $\beta = 0.025$.

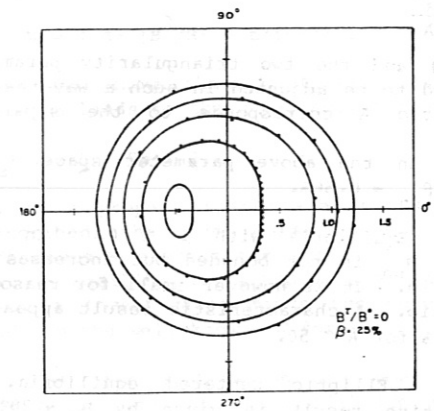

Fig. 3. Zeroth-order magnetic surfaces for the configuration of Fig. 1, but with $B^T/B^O = -0.05$; $\beta \leq 0.025$.

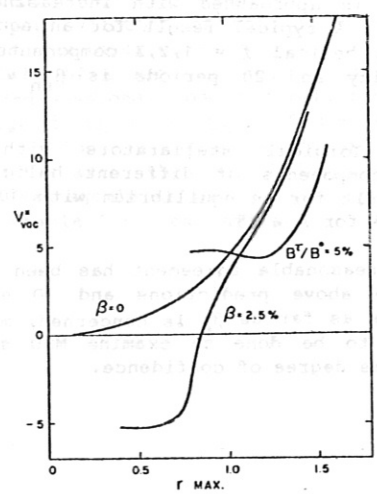

Fig. 4. $V''_{vac}(\psi)$ as a function of the maximum radius of a magnetic surface for the configurations of Figs. 1-3.

A slightly different ordering[11] with

$$B^{\beta}/B_o \sim B^{\kappa}/B_o \sim B^{\sigma}/B_o \sim a/R,$$
$$B^{\delta}/B_o \sim (a/R)^{4/3}, \quad \text{phr} \sim (a/R)^{2/3}$$

has been treated because it makes the magnetic field ripple associated with the toroidal field the same order as that due to the helical windings. In the standard ordering the helical ripple dominates. Use of this ordering allows analytic treatment that can provide insight into the nature of particle confinement in three-dimensional systems.

A different limit where considerable work has been done is obtained by treating the pressure as finite.[12] It is clear from the expression for J^{σ} that in this case Ω must be a function of Ψ; otherwise the force-free current which would be necessary to keep J divergence free would create such large fields that the equilibrium would not exist. Most of the effort here has been to find combinations of the B^{δ} fields so as to achieve this. In much of the work, the curvature has been assumed of order δ^3 so that the lowest order magnetic surfaces can be circular. This system is unstable to an $m = 1$, $n = 0$ mode, although considerable effort has been expended to provide wall stabilization.

This type of expansion has been used in many applications. In the Soviet literature it is known as the Method of Averaging.[13]

An initial value computer code can be written utilizing reduced equations obtained by introducing the expansion about a uniform axial field into the usual fluid equations and carrying through the averaging procedure. Numerical codes of this type have been developed[14] and are being used to investigate the behavior of specific stellarator devices.

This discussion has been restricted to a study of the ideal MHD equations for a static system with a scalar pressure and no resistivity, viscosity, or finite gyration radius effects. The stellarator expansion can be used to include such additional physics. Indeed, an early study of resistive instabilities based on it[15] provided the first explicitly derived expression for the resistive interchange and tearing mode criteria. Similarly, this expansion was used in the initial discussions of the buildup of radial electric fields and plasma rotation in a stellarator.[16] It was found that this buildup could be limited either by viscous effects or would lead to the development of a shock. The stellarator model was also used in making estimates of the effect of finite gyration radius on the interchange instability.[17] A stellarator expansion formulation of the equilibrium problem has been made using a formalism where fluid concepts are introduced to treat behavior normal to the magnetic field but the distribution function description is retained to treat behavior along the field.[18] This provides a mechanism for studying the effect of anisotropic pressure and trapped particles on equilibrium.

B. Expansion Around Magnetic Axis

A second approach that has led to significant progress is to expand all functions in powers of the distance from the magnetic axis. This method was first proposed by Mercier[19] and has been used with significant results by Lortz and Nührenberg.[20] In its most simple version this expansion is carried to third order in the distance from the magnetic axis.

Restricting the description to the case of vanishing toroidal current, the scope of this expansion in terms of the possible functions is as follows. The plasma β enters via the derivative of the pressure with respect to volume on the magnetic axis, $\dot{p}(0)$, which is adequate for approximately parabolic profiles. The magnetic axis is given by its curvature and torsion, $\kappa(\ell)$, $\tau(\ell)$, the form of the axis being related to the $\ell = 1$ fields of the configuration. The magnetic field on axis, $C_o(\ell)$ is related to the $\ell = 0$ field; the half-axis ratio $e(\ell)$ of the (in lowest order) elliptic plasma cross section and its turning angle $\alpha(\ell)$ are related to $\ell = 2$ fields. The triangularity functions of the surfaces, $\delta^*(\ell)$, $\Delta^*(\ell)$ are related to $\ell = 3$ fields; because of the equilibrium equations, instead of δ^* and Δ^* two shift functions $S_a^*(\ell)$, $S_b^*(\ell)$ could equivalently be used, which describe the shifts of the surfaces with respect to the magnetic axis and one of which is the well-known Shafranov shift in the osculating plane of the magnetic axis. The interpretation of $C_o(\ell)$, $e(\ell)$, $\alpha(\ell)$, $\delta^*(\ell)$, $D^*(\ell)$ in terms of $\ell = 0, 2, 3$ fields requires one to think of these fields as being centered on the magnetic axis. In third order in the distance from the magnetic axis δ^*, Δ^*, S_a^*, S_b^* give rise to stagnation points in the flux surfaces and thereby limit the available volume to the separatrix volume V_s. Thus, a consistent equilibrium (average value) β estimate may be obtained

$$\beta = -\frac{\dot{p}(0) V_s \int d\ell / C_o}{\int C_o d\ell} .$$

Furthermore, the above information about the equilibrium suffices to calculate necessary and sufficient stability criteria, i.e. the limiting value of β as the magnetic axis is approached. Thus, the stability criteria may serve two purposes. Given the equilibrium functions in the neighborhood of the axis, they indicate stability or instability. In order to estimate stable β values they are properly used as side conditions in the equilibrium β estimate.

Not included in this simple version of the expansion around the magnetic axis are the effects on equilibrium and stability of the detailed p(V) profile, of the shear, of the fourth order transverse fields (ℓ>4) and of external modes (as far as they are not ruled out by evaluation of a sufficient stability criteria).

An application of this theory is the concept of elliptic, centered equilibria. From the fact that an increase of $\dot{p}(0)$ for fixed rotational transform moves the stagnation points of the flux surfaces towards the magnetic axis, one may ask for toroidal equilibria in which sizable values of the equilibrium β can be reached without deformation of the outer flux surfaces, i.e. in which the surfaces are elliptic and centered with respect to the magnetic axis. In relation to the 3D boundary value problem of a plasma bounded by a perfectly conducting wall, elliptic centered equilibria determine a geometrical form of the wall favorable for equilibrium. Elliptic centered equilibria do indeed exist.

The following gives a list of some of the results obtained with the expansion around the magnetic axis (β_e equilibrium - β estimate, β_{sn} stability - β estimate according to the necessary criteria).

i. Stellarator with circular magnetic axis. In this simplest version the equilibrium can be characterized by 5 parameters: the number of periods, the rotational transform (or, equivalently, $1/q$), $\dot{p}(0)$, and two triangularity parameters. An approximate scaling of β_e is given by

$$\beta_e \approx \frac{\varkappa^2}{A}$$

where $\dot{p}(0)$ and the two triangularity parameters are assumed to be adjusted in such a way that the aspect ratio A corresponds to the separatrix volume.

In the above parameter space β_{sn} is bounded: $\beta_{sn} \approx 0.66\%$.

ii. Equilibria with $\varkappa \equiv 0$. In these equilibria β_{sn} is not bounded but increases with aspect ratio. It is however small for reasonable aspect ratio. A characteristic result appears to be $\beta_{sn} \sim 2\%$ for $A \sim 50$.

iii. Elliptic centered equilibria. A representative result is given by $\beta_e \approx 20\%$ for $A \approx 20$ with the local aspect ratio given by the local curvature not smaller than 3.

iv. Toroidal equilibria near helical equilibria in the sense that a helically symmetric equilibrium is approached with increasing number of periods. A typical result for an equilibrium with strong helical $\ell = 1,2,3$ components of the same helicity and 20 periods is $\beta_{sn} \approx 17\%$ for $A \approx 50$.

v. Toroidal stellarators with strong $\ell = 1,2,3$ components of different helicity. A typical result for an equilibrium with 10 periods is $\beta_{sn} \approx 10\%$ for $A \approx 25$.

While reasonable agreement has been obtained between the above predictions and 3D numerical code results as far as β_e is concerned, much more work needs to be done to examine MHD stability with the same degree of confidence.

C. Full Three-Dimensional Calculations

Three dimensional problems pose significant complexity. Nevertheless, significant progress can be and has been made using general techniques. The advent of the latest generation of computers is making a direct attack on the problem feasible.

It is useful to note that the use of a Hamada coordinate system has allowed for evaluation of dispersion relations and determination of criteria for localized instabilities in terms of magnetic surface averages of equilibrium functions.[21] Thus a good understanding of the MHD properties of a stellarator or torsatron can be obtained from knowledge of its equilibrium properties.

At present there exist two major three-dimensional codes to study the MHD properties of stellarators by numerical techniques.[3,22] Both determine equilibrium configurations by minimizing the potential energy

$$W = \int d\tau \, [B^2/8\pi + p/(\gamma-1)].$$

It is well known that the first variation of this function leads to the usual equilibrium equation

$$\underset{\sim}{J} \times \underset{\sim}{B} - \nabla p = 0,$$

or, if a proper kinetic energy normalization is prescribed, the usual normal mode equations. In both cases a viscous term is introduced to ensure that an equilibrium is approached. Stability can also be investigated since the second variation leads to the well-known δW formalism.

The main application of these programs has been to investigate the equilibrium and stability properties of systems of resonating ℓ and $\ell + 1$ helical fields such that the secondary currents are reduced. Applications to the Wendelstein VII-A and Heliotron E configurations have also been made with indications of stability for significant β-values. They have also been used to investigate nonlinear evolution of various modes, both free-surface and bounded modes. As an example, the stability of several modes, as calculated by the full 3-dimensional code for Heliotron E, is shown in Fig. 5 as a function of the average plasma beta. As long as the curves do not pass below the horizontal axis, the equilibrium is stable. Thus, up to average betas of 5%, the equilibrium seems to be stable for these modes.

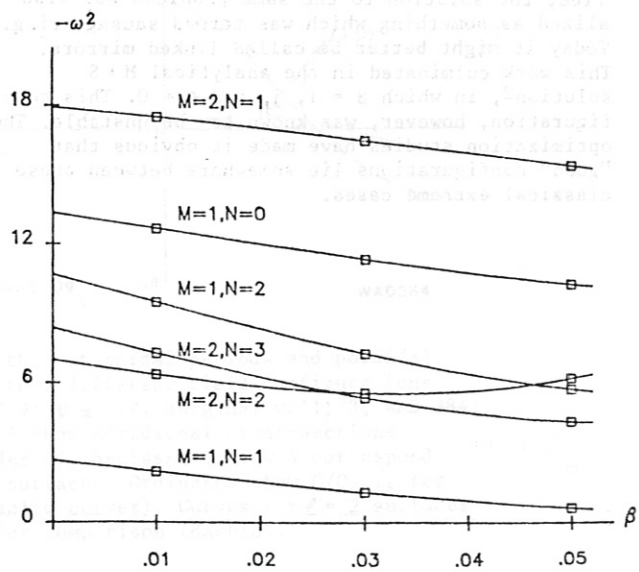

Fig. 5. Instability growth rate as a function of β for Heliotron E.

References

1. M. D. Kruskal and R. M. Kulsrud, Phys. Fluids 1, 265 (1958).
2. L. Spitzer, Jr., Phys. Fluids 1, 253 (1958).
3. R. Chodura, W. Dommaschk, W. Lotz, J. Nührenberg, A. Schluter, R. Gruber, F. Herrnegger, W. Kerner, W. Schneider, and F. Troyon, Plasma Physics and Controlled Nuclear Fusion Research 1980, paper IAEA-CN-38-BB2.
4. A. H. Glasser, J. M. Greene, and J. L. Johnson, Phys. Fluids 18, 875 (1975).
5. A. B. Mikhailovskii and V. D. Shafranov, Soviet Physics - JETP 39, 88 (1974).
6. H. Grad, Phys. Fluids 10, 137 (1967).
7. J. L. Johnson, C. R. Oberman, R. M. Kulsrud, and E. A. Frieman, Phys. Fluids 1, 281 (1958).
8. J. M. Greene and J. L. Johnson, Phys. Fluids 4, 875 (1961).
9. J. L. Johnson and J. M. Greene, Phys. Fluids 4, 1417 (1961).
10. J. M. Greene, J. L. Johnson, and K. E. Weimer, Plasma Physics (J. Nucl. Energy Pt. C) 8, 145 (1966).
11. D. R. Dobrott and E. A. Frieman Phys. Fluids 14, 349 (1971).
12. H. Weitzner, Phys. Fluids 14, 658 (1971).
13. A. I. Morozov and L. S. Solov'ev in Reviews of Plasma Physics (Consultants Bureau, N.Y. 1966) Vol. 2, p. 1.
14. H. R. Strauss and D. A. Monticello, Phys. Fluids (in press).
15. J. L. Johnson, J. M. Greene, and B. Coppi, Phys. Fluids 6, 1169 (1963).
16. J. M. Greene, J. L. Johnson, K. E. Weimer, and N. K. Winsor, Phys. Fluids 14, 1258 (1971).
17. R. M. Kulsrud, Phys. Fluids 6, 904 (1963).
18. D. R. Dobrott, J. M. Greene, and J. L. Johnson, Phys. Fluids 13, 795 (1970).
19. C. Mercier, Nucl. Fusion 4, 213 (1964).
20. D. Lortz and J. Nührenberg, Z. Naturforsch 34A, 167 (1979).
21. J. M. Greene and J. L. Johnson, Phys. Fluids 5, 510 (1962).
22. F. Bauer, O. Betancourt, and P. Garabedian, "A Computational Method in Plasma Physics (Springer-Verlag, N.Y. 1978).

V.2 Optimization of Stellarator Configuration

A. General Procedure

An approach to the design of a stellarator starts by selection of a suitable vacuum field which possesses nested toroidal magnetic surfaces and a sufficiently "irrational" twist of the fields on these surfaces. The vacuum field determines then to lowest order in pressure p (i.e. in β) the distribution of the electric current, and in particular the ratio $\langle j_\parallel^2 \rangle / \langle j_\perp^2 \rangle$, where $j_\perp = |\nabla p|/B$ and the averages over one field period are taken over each magnetic surface separately. To go beyond first order in β, 3D numerical codes have to be employed. MHD stability for $\beta \to 0$ can be secured by satisfying the average minimum B condition. The determination of the stability β limits is as yet not in a satisfactory state though analytical expansion around the magnetic axis and the numerical codes give some indications. The MHD considerations allow also to determine the magnitude and pattern of the external electric currents necessary to produce the field and to calculate the forces on these currents so that the constraints of practical feasibility can be observed. The sufficiently close coincidence of the drift surfaces of passing (circulating) particles with the magnetic surfaces is achieved simultaneously with a reduction of $j_\parallel$. For the sufficient containment of the so-called trapped particles the invocation of finite β effects may be necessary if in vacuum fields it cannot be made good enough.

B. Classical Approaches

Analyses of many of the common stellarator configurations (see e.g. ref. [1] and refs. cited therein) lead to the conclusion that their equilibrium- and stability-β limits are too low for practical application. Moreover, near the β_{equ} - limit, $j_\parallel$ is comparable to that of a tokamak with the same twist of the magnetic field. Conventional stellarators seem also to show too poor a particle confinement in the long mean free path limit. In the original Göttingen approach to net current free confinement, when the Princeton stellarator work was still classified, the solution to the same problems was visualized as something which was termed sausage-ring. Today it might better be called linked mirrors. This work culminated in the analytical M + S solution[2], in which $\beta = 1$, $j_\parallel$ and $\iota = 0$. This configuration, however, was known to be unstable. The optimization studies have made it obvious that "good" configurations lie somewhere between these classical extreme cases.

C. Configuration Studies

The following demonstrates in section (a) a method to obtain vacuum field configurations with finite ι, an at least marginal magnetic well, and an acceptable aspect ratio with the parallel current density reduced as compared to the classical stellarator. Section (b) is concerned with the problem to find the current geometry to generate a given field configuration. Section (c) gives results on computation at finite beta, and section (d) is concerned with particle containment.

a) Vacuum Field Configurations for Reduced Parallel Current Density

For small twist number ι the parallel current density is governed by the variation on magnetic surfaces of

$$Q = \int dl / B$$

where the integral is performed along a field line over one field period. This variation is characterized by

$$S = \langle Q^2 \rangle - \langle Q \rangle^2$$

where $\langle \ldots \rangle$ indicates the appropriate average on the magnetic surface, or by S_{rel}, which is the variation of Q normalized to the corresponding value of the pure $\ell = 2$ stellarator.

Vacuum field configurations have been obtained in which S_{rel} is small and in which the low-β stability requirement of an average magnetic well can be satisfied. The search in configurational space was performed as follows. A complete set of explicit harmonic fields[3] is used to compose vacuum field configurations. To satisfy the above requirements, sets of these fields which typically represent $\ell = 0, \ldots, 3$ corrugations have to be used so that the parameter space has a typical dimension of 10 -20. The numerical optimization in this space with respect to the above goals was performed with constraints, e.g. on the geometry of the flux surfaces and the value of ι. This technique has also been used to strive for other containment conditions (see d).

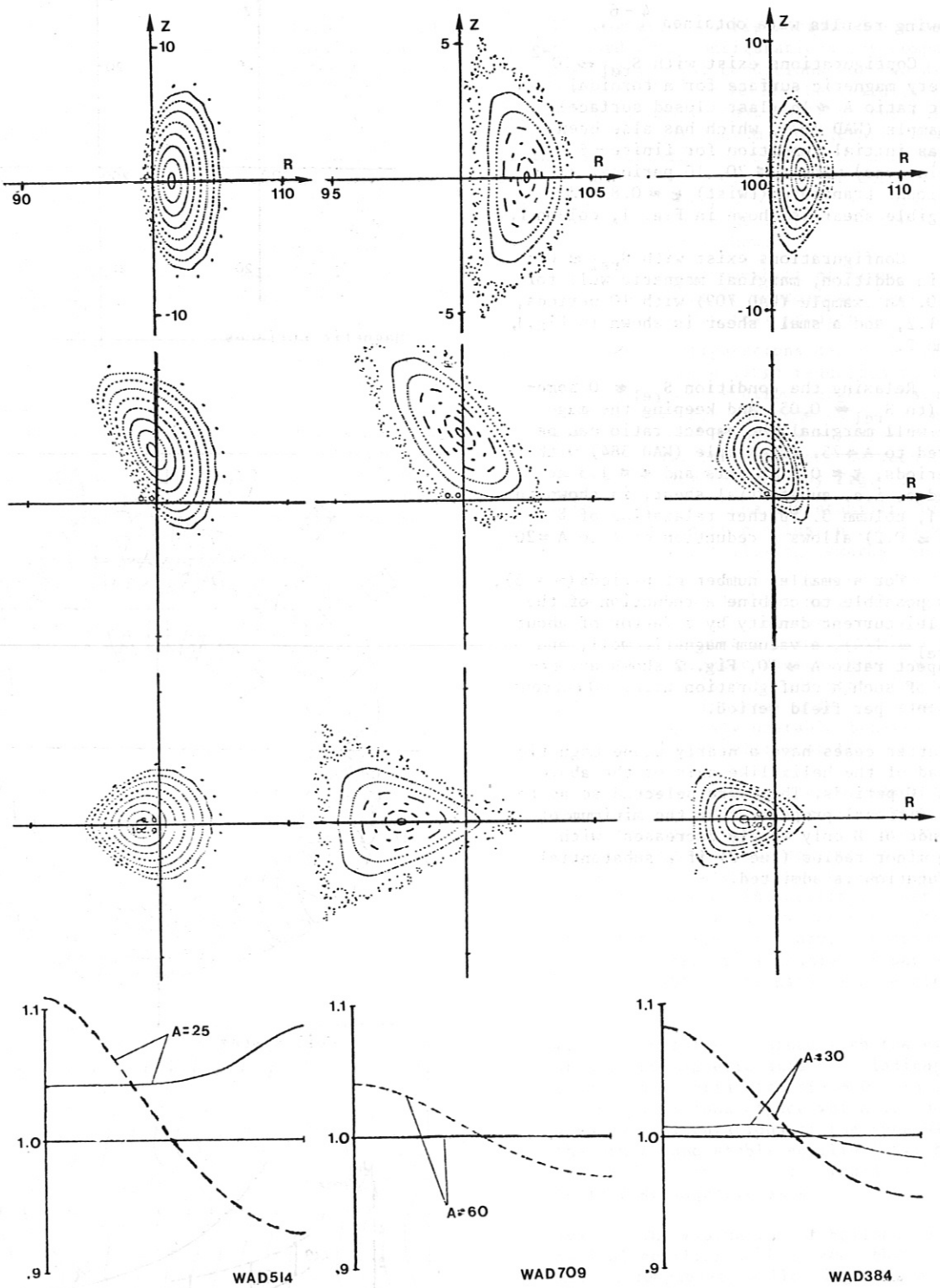

Fig. 1: Magnetic surfaces of vacuum fields with 10 toroidal periods and poloidal variation of Q. Columns 1 to 3 belong to 3 different field configurations (1, WAD 514: $\iota \approx 0.8$, no well; 2 WAD 709: $\iota \approx 1.2$, marginal well; 3, WAD 384: $\iota \approx 0.8$ to 1.3, with well). Rows 1 to 3 show meridional cross-sections separated by 1/4 of a period. Left sides of abscissas in row 4 correspond to radially outward directed parts of surfaces. Ordinates show Q/Q_{axis} for surfaces with various aspect ratios (solid curves). Curves for $\ell = 2$ surfaces (with the same value of ι) are shown for comparison (dashed).

The following results were obtained [4-6].

i) Configurations exist with $S_{rel} \approx 10^{-2}$ on every magnetic surface for a toroidal aspect ratio A ≈ 16 (last closed surface). An example (WAD 514 , which has also been used as initial condition for finite - β calculations) with A ≈ 20, 10 periods, total rotational transform (twist) $\iota \approx 0.8$ and negligible shear is shown in Fig. 1, column 1.

ii) Configurations exist with $S_{rel} \approx 0$ and, in addition, marginal magnetic well for A ≈ 40. An example (WAD 709) with 10 periods, $\iota \approx 1.2$, and a small shear is shown in Fig. 1, column 2.

iii) Relaxing the condition $S_{rel} \approx 0$ somewhat (to $S_{rel} \approx 0.05$) and keeping the magnetic well marginal, the aspect ratio can be lowered to A ≈ 25. An example (WAD 384) with 10 periods, $\iota \approx 0.8$ on axis and $\iota \approx 1.3$ at the edge, i.e. substantial shear, is shown in Fig. 1, column 3. Further relaxation of S ($S_{rel} \approx 0.2$) allows a reduction of A to A ≈ 20.

iv) For a smaller number of periods (m = 5), it is possible to combine a reduction of the parallel current density by a factor of about 2 ($S_{rel} \approx 1/4$), a vacuum magnetic well, and an aspect ratio A ≈ 10, Fig. 2 shows an example of such a configuration using 10 current filaments per field period.

The latter cases have a nearly plane magnetic axis instead of the helix-like axis of the above cases with 10 periods. They were selected so as to have the additional property that the minimum of the magnitude of B only weakly decreases with increasing minor radius (see d) if a substantial $\ell = 0$ corrugation is admitted.

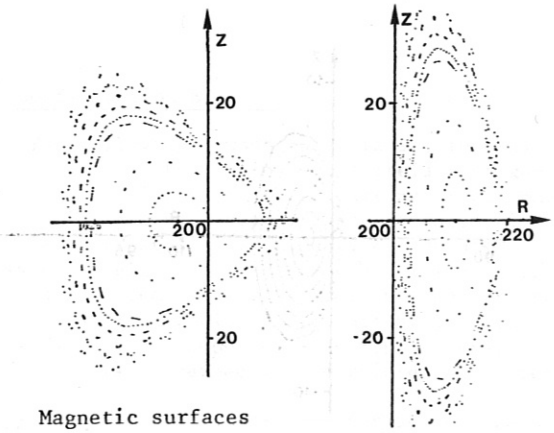

Magnetic surfaces

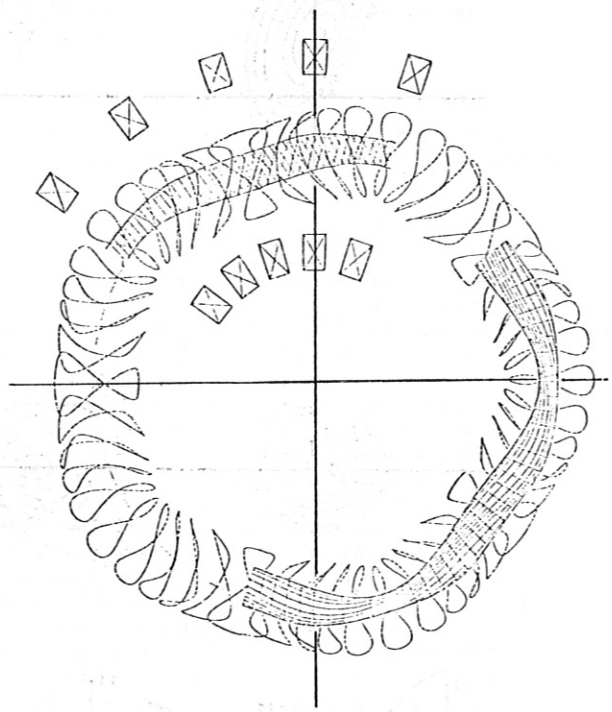

Coil system

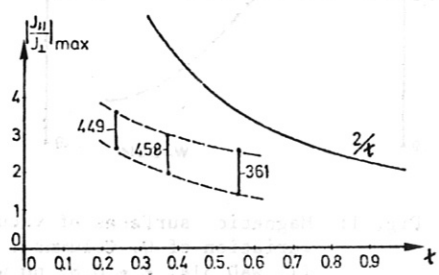

Fig. 2: Magnetic surfaces and coil arrangement of configuration with reduced secondary currents, having an aspect ratio A ≈ 10 and a magnetic well ≈ 1%. The lower part of the figure shows the ratio of secondary to perpendicular current density of this configuration in comparison to that of the classical stellarator (2/ι).

b) Boundary Value Problems for Vacuum Fields [7]

i) The surface current density on a closed toroidal surface which generates a given magnetic configuration inside this surface was computed.

Fig. 3 shows as example for WAD 514 a case where the current carrying surface is taken to be a torus with $\ell = 1$ corrugation and a turning elliptical cross-section with A ≈ 12. The main result of calculations with different toroidal surfaces was:

- A qualitative adjustment of the current carrying surface to the magnetic surfaces (at lower aspect ratio) leads to a large reduction of the toroidal excursions of the current density lines as compared to the result obtained with a circular axisymmetric toroidal surface.
- For an aspect ratio as low as about one half of that of the magnetic configuration, the geometrical form of the current density lines seems to be acceptable for all of the examples of (a) if the enclosing surface is adjusted.
- A simple discretization of the continuous current density is obtained if a finite number of line currents lying on the original current density lines is used. Typically 8 line currents per period were necessary to adequately approximate the original magnetic configurations.

ii) For a given closed toroidal surface the magnetic configuration with its normal component $B_n \equiv 0$ on the inside of this surface was computed. This boundary value problem was useful to obtain configurations with a flux surface geometry as predicted by analytical theory [8,9] to be advantageous for the optimization goals for (a).

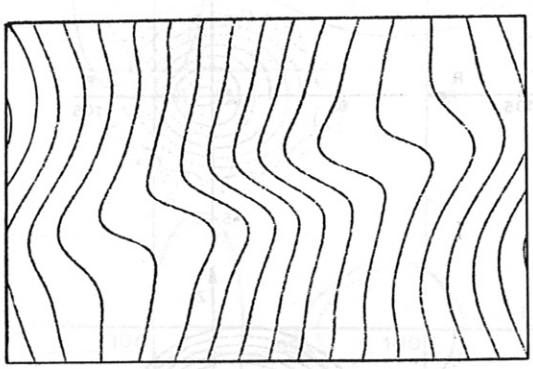

Fig. 3: Current density lines on a non-axisymmetric torus with aspect ratio 12. This current density generates WAD 514. The ordinate is the poloidal angle, the abscissa the toroidal angle over one field period.

c) Finite - β Calculations

The magnetic configurations described in (a) and standard $\ell = 2$ configurations for comparison were used as initial conditions for two different 3D MHD codes [10,11] to verify the validity of the approach outlined in (a). While in the Eulerian code [10] the actual vacuum configurations were used as initial conditions (together with an appropriate pressure distribution), the outer form of the flux surfaces, the twist profile, and a pressure distribution are used as inputs for the Lagrangian code [11]. Both codes show:

i) The Shafranov-shift of finite - β, $\ell = 2$ stellarators is in approximate agreement with the simple analytical prediction (see Fig. 4);

ii) The configurations described in (a) indeed lead to a large reduction of the toroidal shift and thereby allow larger β-values (factor 2-4) for the same values of aspect ratio and rotational transform than $\ell = 2$ stellarators (see Fig. 4). The agreement between the codes is clearly demonstrated by Fig. 5.

With respect to the MHD stability of these equilibria no definite conclusion can as yet be drawn. However, the following remarks can be made:

i) Most of the vacuum configurations considered have at least a marginal magnetic well. The residual shift observed in the finite - β equilibria creates a magnetic well (beyond the trivial diamagnetic deepening of the well). Although this is not sufficient for the stability of all internal modes, it should at least remove the grossly unstable behavior of the straight $\ell = 2$ stellarator [12].

ii) There is numerical evidence from the results obtained with the Lagrangian code that, e.g., the case shown in the second row of Fig.5 cannot be grossly unstable to internal modes. Whereas this case relaxes to equilibrium without any indication of instability, other cases with β - values of only a few percent, a different form of the outer boundary, but otherwise the same characteristics (number of periods, aspect ratio, rotational transform) were clearly unstable.

iii) Results obtained with the expansion around the magnetic axis [9] indicate Mercier stable equilibria with $\langle\beta\rangle \approx 0.1$ in that part of configurational space which is characterized by configurations of the type WAD 384. On the other hand stable equilibria with $\langle\beta\rangle > 0.01$ have not been found without a helix-like magnetic axis.

iv) The evaluation of ballooning modes in helical equilibria [13] shows that $\langle\beta\rangle \gtrsim 0.1$ can be completely ballooning stable if $\ell = 1, 2, 3$ corrugations are admitted. Preliminary evaluations of gross internal modes in these configurations with the HERA code [12] verify the stability against internal modes.

In summary it can be stated that the evidence as of yet does not exclude the possibility of stable equilibria with $\langle\beta\rangle \gtrsim 0.05 - 0.1$.

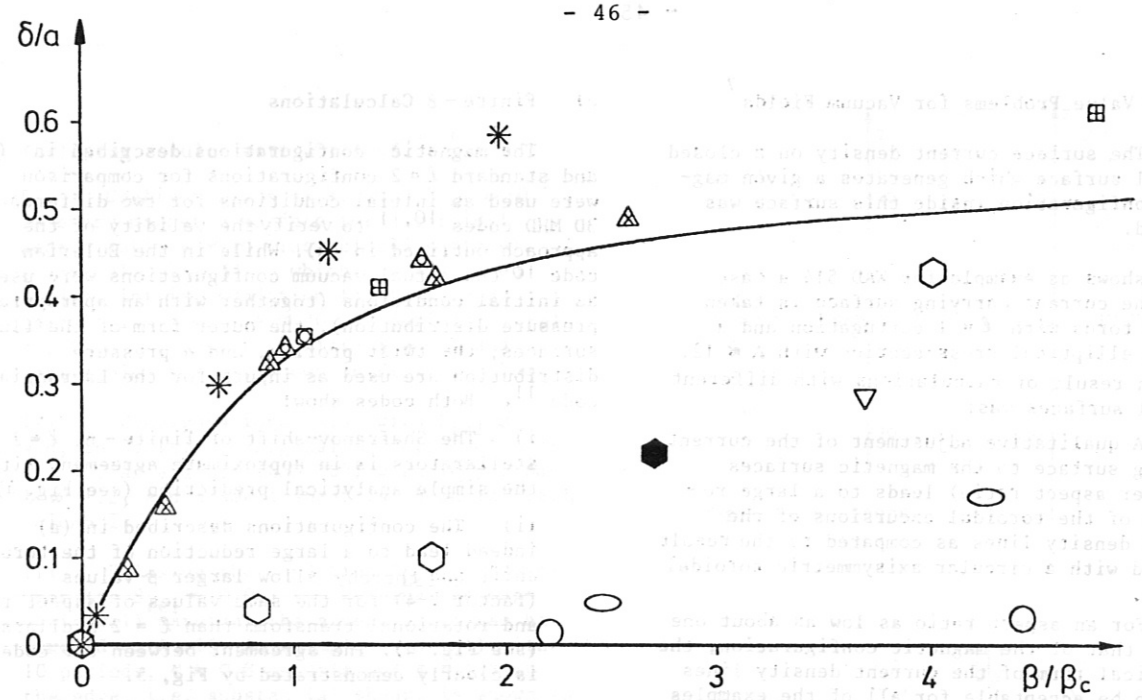

Fig. 4: Toroidal shift of the magnetic axis relative to the plasma radius as function of the ratio of the β-value to $\beta_c = 2\ell^2/A$. The values of the shifts are measured with respect to the position of the magnetic axis for β = 0. The curve shows the Shafranov-shift (analytical value) for $\ell = 2$ stellarators. Numerical results obtained with

Chodura-Schlüter Code:

m = 5 : $\ell = 2$ stellarator, various aspect ratios △ □ and rotational transform + X ○

m = 10: ▽ WAD 514, $\beta_c = 0.05$; ⬭ WAD 384, $\beta_c = 0.03$

NYU - Code:

✱ only $\Delta_2 \neq 0$; $\Delta_2 = 0.35$, $\iota = 1.1$; $\beta_c = 0.13$

⬡ $\Delta_2 = 0.23$, $\Delta_1 = 0.28$, $\iota_o = 0.8$, $\beta_c = 0.07$, $\Delta_o = 0.05$, $\Delta_3 = -0.03$, $\Delta_{20} = -0.07$, $\Delta_{30} = 0.01$, $\Delta_{22} = -0.08$, $\Delta_{33} = -0.02$

○ $\Delta_2 = 0.23$, $\Delta_1 = 0.28$, $\iota_o = 0.4$, $\beta_c = 0.02$, $\Delta_o = 0.1$, $\Delta_3 = -0.02$, $\Delta_{10} = 0.1$, $\Delta_{20} = -0.06$, $\Delta_{30} = 0.01$, $\Delta_{22} = -0.08$, $\Delta_{33} = -0.02$

⬢ The surfaces of this configuration are shown in lower row of Fig. 5.

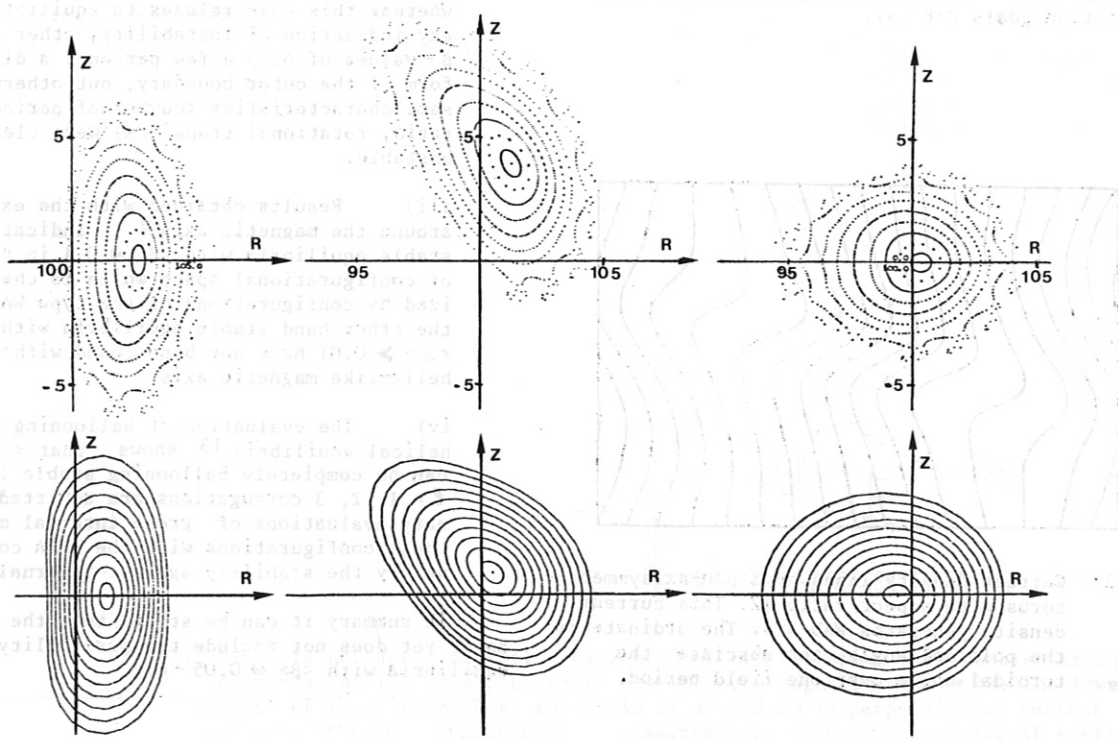

Fig. 5: Magnetic surfaces of finite-β equilibria. Same representation as in Fig. 1, but as a row for each configuration. First row with CS-Code: WAD 514, $\beta_o = 0.18$, second row with NYU-Code: $\beta_o = 0.18$, parameters of the boundary see Fig. 4; ⬡

d) Particle Containment

In vacuum field configurations with $S_{rel} \approx 0$ the deviation of circulating particles from magnetic surfaces should be reduced by one order in the relative variation $\delta B/B$ on magnetic surfaces to the order $|(\delta B/B)^2|$. Numerical guidung center computations verify for all circulating particles that the deviation from a magnetic surface is of the order of the gyroradius. Fig. 6 shows the comparison of the configuration WAD 514 with an equivalent $\ell = 2$ stelarator for a barely circulating particle.

On the other hand trapped particles mostly drift outof the region of closed magnetic surfaces, because, for the configurations considered, the various helical ripples of different helicity are larger than the toroidal ripple. Therefore, considering only the maximal possible loss cone, the containment of trapped particles could be too poor. Monte-Carlo simulations for these configurations are underway.

The systematic optimization of field configurarations (see (a)) was also used to influence the containment of trapped particles directly by selection of configurations in which the minimum of mod B on a magnetic surface decreases from the magnetic axis to the outer flux surfaces by only a small fraction of the 1/R decrease of the field of a tokamak or a classical stellarator. Under these circumstances the minimum of $|B|$ should increase in the corresponding finite-β equilibrium because of the diamagnetic effect and the configuration should show absolute minimum B confinement properties. This influence on the trapped particle behavior is being investigated.

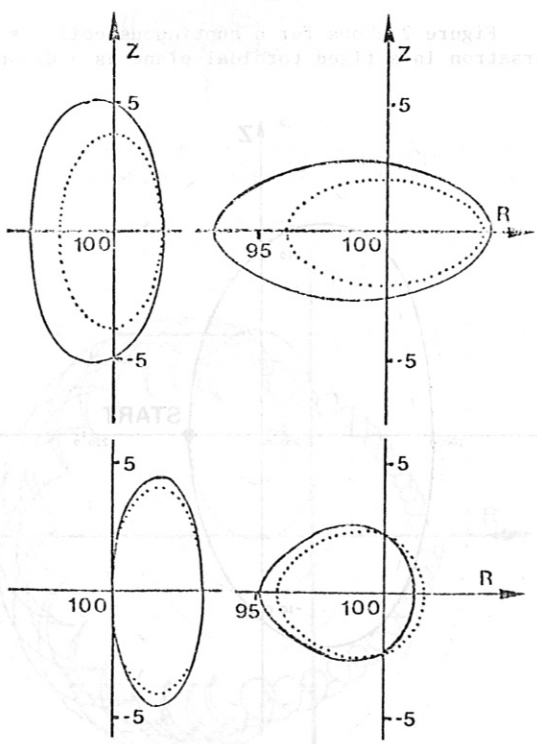

Fig. 6: Magnetic surfaces and drift surfaces of a barely circulating particle in an $\ell = 2$ stellarator which is equivalent (ι,A) to WAD 514. Shown are two meridional sections. Second row: the same for WAD 514.

References

1 R. Chodura, A. Schlüter, M. Kaufmann, W. Lotz, Plasma Physics and Controlled Fusion Research 1978 (Proc. 7th Int. Conf. Innsbruck, 1978), Vol.II, IAEA, Vienna (1979) 335, D.Lortz, J. Nührenberg, Plasma Physics and Controlled Nuclear Fusion Research 1978 (Proc.7th Int. Conf., Innsbruck, 1978), Vol.II, IAEA, Vienna (1979) 309

2 F. Meyer, H.U. Schmidt, Z. Naturforsch. 13a (1958) 1005

3 W. Dommaschk, Max-Planck-Institut für Plasmaphysik, Garching, Report 0/38 (1978)

4 R. Chodura, W. Dommaschk, W. Lotz, J. Nührenberg, A. Schlüter, Proc. of the Workshop on Optimization of Toroidal Confinement 1980, Inst. Fusion Theory, Hiroshima University, 1980, HIFT-25, p. 20

5 W. Dommaschk, J. Nührenberg, A. Schlüter, Proc. of the Annual Meeting on Theoretical Aspects of Contr. Thermonucl. Res., Tucson, 1980, paper 3A7

6 R. Chodura, W. Dommaschk, W. Lotz, J. Nührenberg, A. Schlüter, Plasma Physics and Controlled Nuclear Fusion Research 1980, Brussels, IAEA-CN-38, paper BB2

7 W. Dommaschk, Z. Naturforsch. 36a (1981)

8 D. Lortz, J. Nührenberg, Z. Naturforsch. 34a (1979) 167

9 J. Nührenberg, Proc. of the Annual Meeting on Theoretical Aspects of Contr. Thermonucl. Res., Mount Pocono, Pa., IC20 (1979), and J. Nührenberg, Proc. of the Symposium on Stellarators with Three-Dimensional Magnetic Axis, Sendai (1979), I

10 R. Chodura, A. Schlüter, Max-Planck-Institut für Plasmaphysik, Garching, Report I/180(1980) and J. of Comp. Phys. (1981), in print

11 F. Bauer, O. Betancourt, F. Garabedian A Computational Method in Plasma Physics, Springer Verlag (1978)

12 R. Chodura, R. Gruber, F. Herrnegger, W. Kerner, W. Schneider, F. Troyon, Plasma Physics and Controlled Nuclear Fusion Research 1980, Brussels, IAEA-CN-38, paper BB2

13 J. Nührenberg, Proc. of Int. Conf. on Plasma Physics, Nagoya, 1980, paper 10b-I-03

FIG. 1a

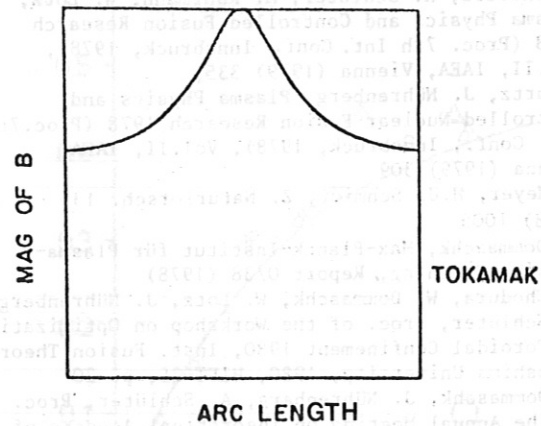

FIG. 1b

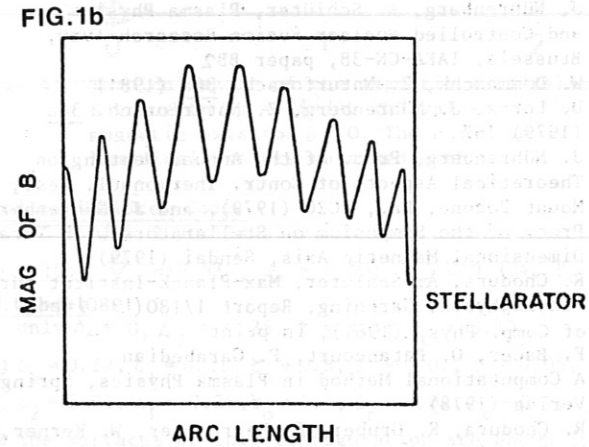

FIG. 1c MODULAR STELLARATOR

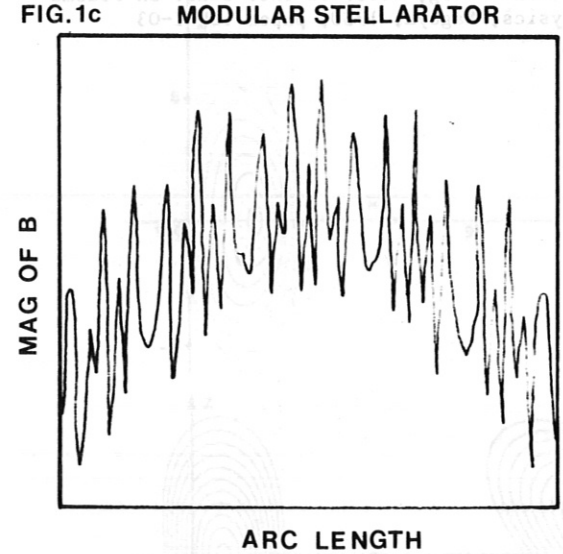

Fig. 1. Dependence of the magnitude of B vs the arc length of a field line

Fig. 1a. for a tokamak.
Fig. 1b. for a stellarator.
Fig. 1c. for a modular stellarator.

V.3 Orbits and Transport in Stellarators

A. Orbits

Single particle orbits in stellarator configuration can be computed by solving the Lorentz equation (or guiding center drift equation) in the three-dimensional magnetic field. For an attempt to obtain a qualitative picture, we may write an approximation for the magnetic field as follows:

(a) For a tokamak $B = B_o(1 - \varepsilon_r \cos\theta)$

(b) For a stellarator with continuous coils[1] $B = B_o(1 - \varepsilon_r \cos\theta - \varepsilon_h \cos(\ell\theta - m\phi))$

(c) For a modular stellarator[2] $B = B_o(1 - \varepsilon_r \cos\theta - \varepsilon_{h_1} \cos(\ell\theta - m\phi) - \varepsilon_{h_2} \cos(\ell\theta + 2m\phi) + \varepsilon_M \cos(M\phi))$

In the above expression, $\varepsilon_r \sim \frac{a}{R}$ refers to the toroidal modulation of the magnetic field, ε_h is the helical modulation amplitude produced by a continuous helix, ε_{h_1} and ε_{h_2} refer to the helical modulation produced by the effective oppositely wound helices and ε_M the toroidal ripple. The latter quantity is produced by M separate modular coils. Figure 1 shows a plot of the magnitude of B along the arc length of a field line according to the above types of modulation.

In tokamaks, collisionless particles follow circulating or toroidally trapped (banana) orbits. Such orbits also exist in torsatrons and in stellarators, along with some additional types.

Figure 2 shows for a continuous coil $\ell = 2$ torsatron in a fixed toroidal plane as a drawn curve

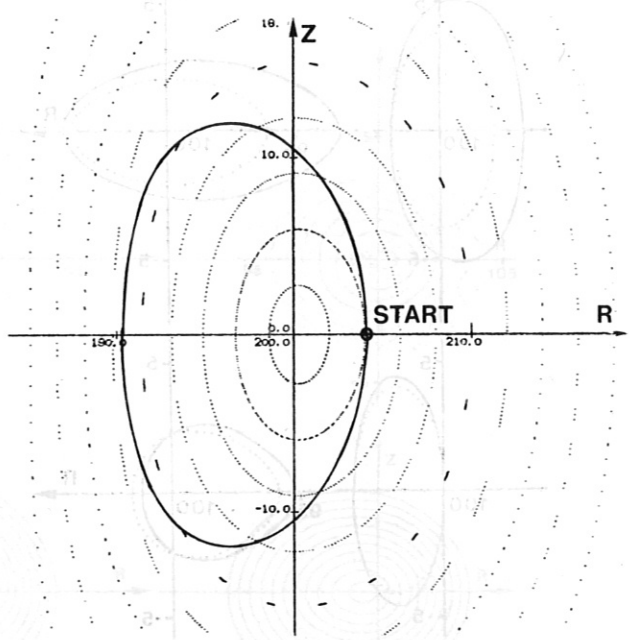

Fig. 2. Intersection of flux surfaces (dotted) and a drift surface (drawn curve) for an $\ell = 2$ torsatron. Passing particle with start point identified.

the intersection of the orbit of a passing particle (drift surface) along with the system of nested flux surfaces (dotted). Note the marked radial shift of the drift surface which is of the order of ρ/ι, where ρ is the Larmor radius, and ι is the rotational transform.

Figure 3 shows the projection of a toroidally trapped orbit (banana) in a continuous coil stellarator.[3] Note that the particle follows the "retrograde" motion of the field line trajectories until it is toroidally reflected. Note the appearance of the given orbit depends upon the type of representation used.

Figure 4 shows a projection of an orbit in a continuous coil stellarator that is initially circulating and then becomes helically trapped.[3] The helical trapping motion deviates significantly from the retrograde trajectory of a field line.

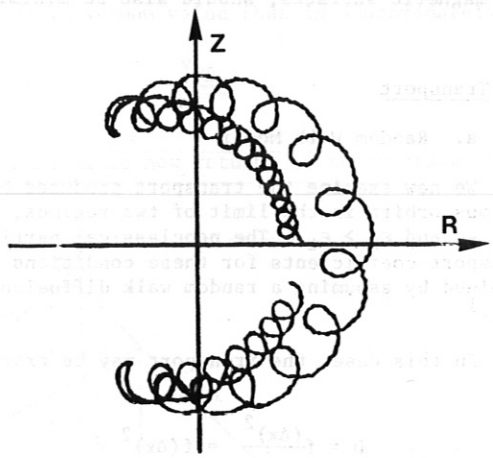

Fig. 3. Projection of a toroidally trapped banana in a continuous coil stellarator.

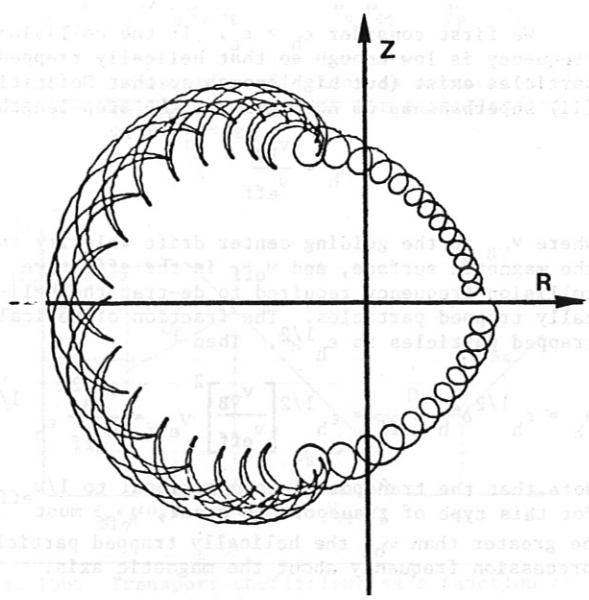

Fig. 4. Partially helically trapped particle.

Figure 5 shows an orbit that is always helically trapped and precesses around the magnetic axis. A third type of orbit is shown in Fig. 6. Here, the particle is both toroidally and helically trapped.[3] Figure 7 shows an orbit in an $\ell = 3$ modular stellarator. The particle is trapped between two modules and drifts out[4]. Such orbits do not appear in continuous coil devices.

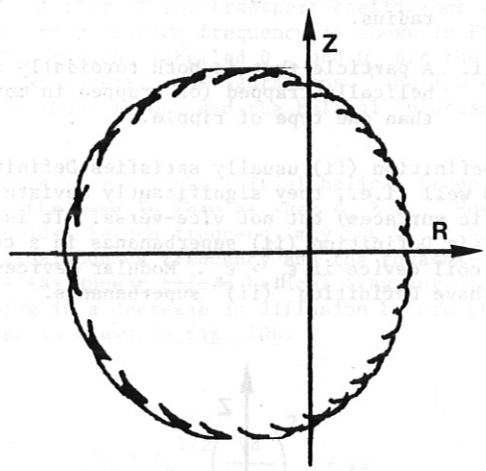

Fig. 5. Always helically trapped particle.

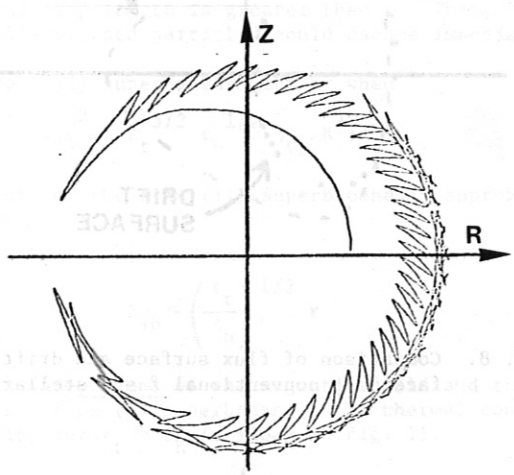

Fig. 6. Toroidally and helically trapped particle.

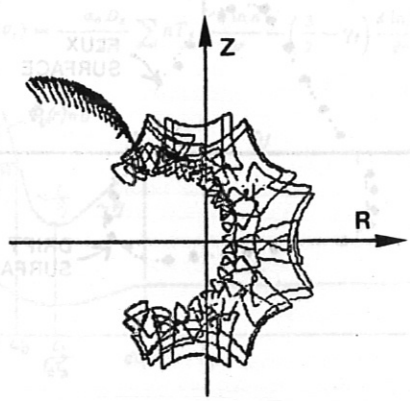

Fig. 7. Orbit in an $\ell = 3$ modular stellarator; trapped between two modules and then lost.

The orbits shown in Figs. 4 to 7 are qualitatively different from either completely circulating or banana orbits. They have all been called "superbananas". Two definitions for a superbanana can be given:

i. A particle whose deviation from a flux surface does not go to zero in the limit of infinite magnetic field or zero gyroradius.

ii. A particle that is both toroidally and helically trapped (or trapped in more than one type of ripple.

Definition (ii) usually satisfies Definition (i) as well (i.e., they significantly deviate from magnetic surfaces) but not vice-versa. It is hard to obtain Definition (ii) superbananas in a continuous coil device if $\varepsilon_h > \varepsilon_t$. Modular devices may often have Definition (ii) superbananas.

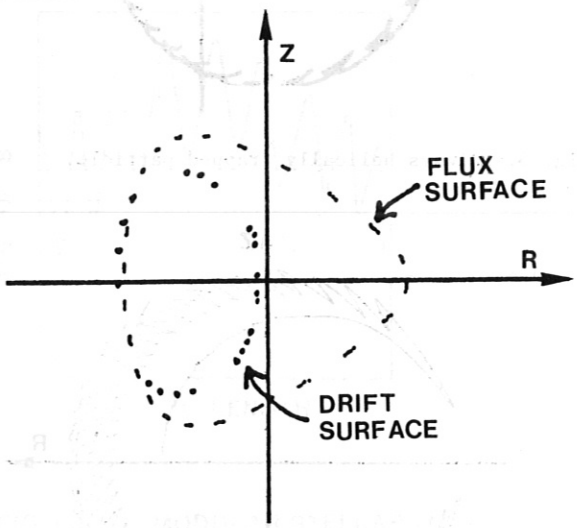

Fig. 8. Comparison of flux surface and drift surface of a conventional $\ell = 3$ stellarator.

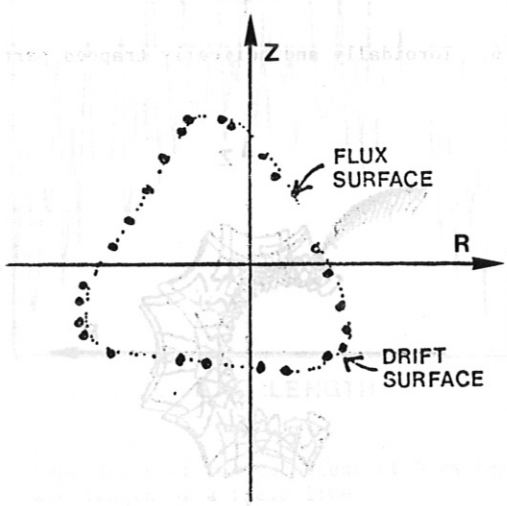

Fig. 9. Close coincidence of flux and drift surfaces in a drift-optimized system.

The deviation of particle orbits from magnetic surfaces causes much of the enhanced transport predicted to occur in low collisionality regimes.

Accordingly, if the deviation of the orbits from the magnetic surfaces could be minimized, less transport would occur. Definition (i) superbanana orbits can be made to approach the magnetic surfaces in the limit of infinite aspect ratio, or possibly by minimizing the poloidal variation of the length of the magnetic field lines in the configuration. Such "drift-optimized" configurations also offer significant improvements in transport and critical beta, see Section V.2.

For an $\ell = 3$ system, a comparison of flux surfaces and drift surfaces is given in Fig. 8 for a conventional stellarator, and in Fig. 9 for a drift-optimized modular stellarator.

Since there the magnetic surfaces appear to approximate a straight configuration, the Pfirsch-Schlüter currents that produce an outward shift of the magnetic surfaces, should also be minimized.

B. Transport

a. Random Walk Model

We now examine the transport produced by the various orbits in the limit of two regimes, $\varepsilon_t < \varepsilon_h$ and $\varepsilon_h > \varepsilon_t$. The neoclassical particle transport coefficients for these conditions may be obtained by assuming a random walk diffusion process.[1]

In this case, the transport may be expressed as

$$D \simeq f\frac{(\Delta x)^2}{\tau} = f(\Delta x)^2 \nu$$

where f is the fraction of particles that are under consideration, Δx is the step-length for the transport, and τ is the time between collisions (ν is the collision frequency).

We first consider $\varepsilon_h > \varepsilon_t$. If the collision frequency is low enough so that helically trapped particles exist (but high enough so that Definition (ii) superbananas do not appear), the step-length is

$$\Delta_h = \frac{v_{\nabla B}}{\nu_{eff}}$$

where $v_{\nabla B}$ is the guiding center drift velocity for the magnetic surface, and ν_{eff} is the effective collision frequency required to de-trap the helically trapped particles. The fraction of helically trapped particles is $\varepsilon_h^{1/2}$. Then

$$D_h = \varepsilon_h^{1/2}\Delta_h^2 \nu_{eff} = \varepsilon_h^{1/2}\left[\frac{v_{\nabla B}}{\nu_{eff}}\right]^2 \nu_{eff} = \frac{v_{\nabla B}^2}{\nu_{eff}} \varepsilon_h^{1/2} \quad (1)$$

Note that the transport is proportional to $1/\nu_{eff}$. For this type of transport to occur, ν_{eff} must be greater than ω_h, the helically trapped particle's precession frequency about the magnetic axis.

In an axisymmetric device, such as a tokamak, one may write a similar expression for the plateau diffusion coefficient as

$$D_P \simeq \left[\frac{\sqrt{\pi}\, qR\, \nu_{eff}}{V_T}\right]\left[\frac{v_{\nabla B}}{\nu_{eff}}\right]^2 \nu_{eff} \qquad (2)$$

The difference between Eqs. (1) and (2) is the difference between axisymmetric plateau diffusion and helically trapped particle diffusion. It is only in the term for the fraction of particles that are in the axisymmetric plateau regime or are helically trapped, respectively. Both diffusion processes exhibit a $v_{\nabla B}$ drift away from a magnetic surface and require a collision frequency high enough so the drifting particle does not return to the magnetic surface before it makes a collision.

The increase in D predicted by Eq. (1) as collision frequency is decreased does not occur without limit. The deviation from the magnetic surface is limited to a maximum value that is approximately

$$\frac{v_{\nabla B}}{\omega_h},$$

since the particle now returns to the surface by completing the precession before it makes a collision and thus

$$D \to D_{hp} = \frac{\varepsilon_t^2}{\varepsilon_h} R\, v_{\nabla B} = \frac{r^2}{R\varepsilon_h^{1/2}} v_{\nabla B}$$

where R is the major radius and r is the minor radius. A plot of the transport coefficient as a function of collision frequency is shown in Fig. 10a. The regions labelled D_{ps} and D_p are the same as for axisymmetric configurations. The $1/\nu$ dependence is shown as D_h, and the helical "plateau" as D_{hP}.

Where $\varepsilon_t > \varepsilon_h$, the initial helical trapping remains the same in form as when $\varepsilon_h > \varepsilon_t$. However, the toroidal bounce frequency may now be higher than the helical bounce frequency and the tokamak-type bananas may appear before helical trapping occurs, resulting in a decrease in diffusion before the $1/\nu$ increase as shown in Fig. 10b.

Thus

$$D_h = \varepsilon_h^{1/2}\left(\frac{v_{\nabla B}}{\nu_{eff}}\right)^2 \nu_{eff}$$

When ν_{ei} becomes small enough so that $\nu_{ei} < \frac{v_{\nabla B}\varepsilon_h}{r}$, then the step length is greater than r. Then, helically trapped particles could escape immediately.

Type (ii) superbananas appear when

$$\nu_{ei}^2 < \varepsilon_t^{3/2}\, \varepsilon_h^{1/2}\, v_{\nabla B}\, R^2/a^2$$

The width of the type (ii) superbanana is approximately

$$\Delta_{sb} \sim \left(\frac{\varepsilon_t}{\varepsilon_h}\right)^{1/2} r$$

This is independent of the magnetic field and thus is a true type (i) superbanana. The thermal conductivity for $\varepsilon_t > \varepsilon_h$ is shown in Fig. 11.

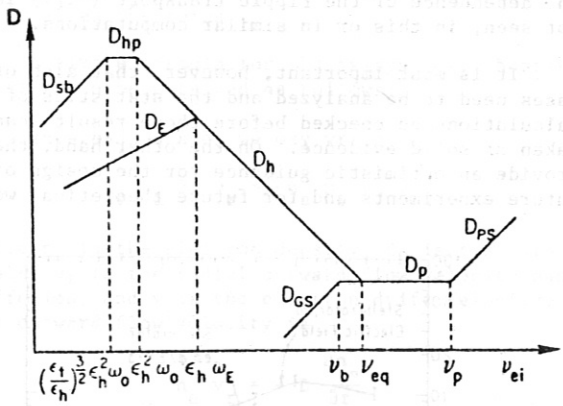

Fig. 10a. Transport coefficient as a function of collision frequency for a stellarator with $\varepsilon_t < \varepsilon_h$.

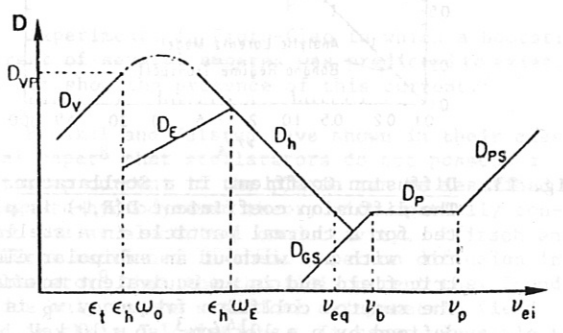

Fig. 10b. Transport coefficient as a function of collision frequency for a stellarator with $\varepsilon_t > \varepsilon_h$.

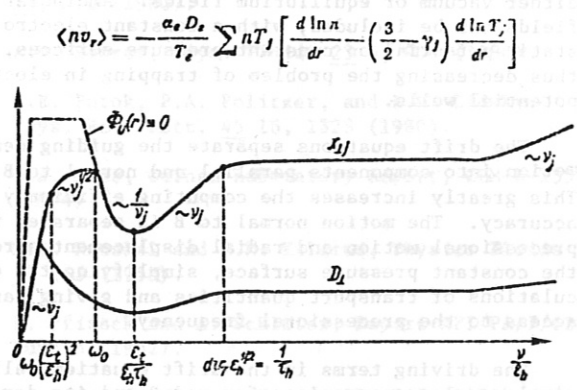

Fig. 11. Thermal conductivity for $\varepsilon_t > \varepsilon_h$.

Much of the above discussion is based on some assumptions regarding the second adiabatic invariant, the action, J.

$$J = \oint m v_{\parallel} \, dS_{\parallel}$$

Figure 12 shows the action calculated for the orbit shown in Fig. 4. Note that J is not conserved, except in a "piecewise" fashion. The jumps in the action occur when the particle makes transitions between circulating and helically trapped states.

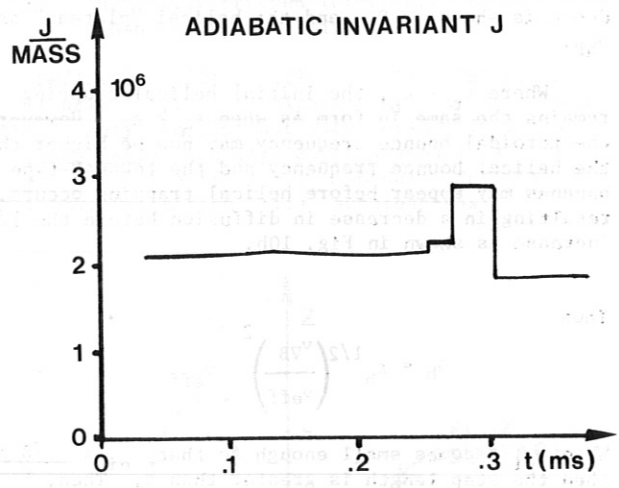

Fig. 12. Computation of the adiabatic invariant J for the orbit of Fig. 4.

b. Monte-Carlo Transport Calculations

Transport calculations based on a numerical Monte-Carlo approach have recently been undertaken. The orbits of a large number of particles launched on magnetic surfaces are statistically analyzed. Collisions are introduced as a random change in velocity occurring at a random time. The particle diffusion coefficient may be obtained in the following way:[5]

First, magnetic coordinates are used. The "radial" coordinate is the flux inside a constant pressure surface. The method can be applied to either vacuum or equilibrium fields. Ambipolar fields can be included, with a constant electrostatic potential on constant pressure surfaces, thus decreasing the problem of trapping in electric potential wells.

The drift equations separate the guiding center motion into components parallel and normal to B. This greatly increases the computing efficiency and accuracy. The motion normal to B is separated into precessional motion and radial displacement across the constant pressure surface, simplifying the calculations of transport quantities and giving easy access to the precessional frequency.

The driving terms in the drift equations allow simple scalar expressions for mod-B and its derivatives. The rotational transform, shear, and various ripple harmonics can be included explicitly as simple functions of the toroidal flux.

Fitting of these expressions to actual fields can be accomplished through a field-line tracing technique, followed by a Fourier transform operation. As accurate a fit as desired can be obtained by increasing the number of terms retained in the Fourier representation.

Figure 13 shows as an example the normalized diffusion coefficient D/D_{NC} versus the normalized collision frequency ν/ν_R for stellarators with and without an electric field. For comparison, the results of a computation for an equivalent tokamak are also given, along with the prediction of an analytic model in the banana regime (dashed line).

Another approach[6] calculates the thermal conductivity χ_i from the expression:

$$\chi_i = \frac{\frac{1}{t}\int \frac{1}{2}(x - x_o)^2 U_i(x,t)dx}{U_i(x,t)dx}$$

where

$$U_i(x,t) = \int f_i(x,v,t) \, \frac{1}{2} m_i v^2 \, d^3v$$

x_o is the initial coordinate of the particle (on the flux surface). x is the coordinate after a fixed time t, and f_i is the ion velocity distribution at time t and at point x. Figure 14 shows as an example the ion thermal conductivity calculated for a torsatron with coil aspect ratio $R_o/a = 12$. The dependence of the ripple transport ($\sim 1/\nu$) is not seen, in this or in similar computations.

It is most important, however, that also other cases need to be analyzed and the statistics of the calculations be checked before those results can be taken as solid evidence. On the other hand, they provide an optimistic guidance for the design of future experiments and for future theoretical work.

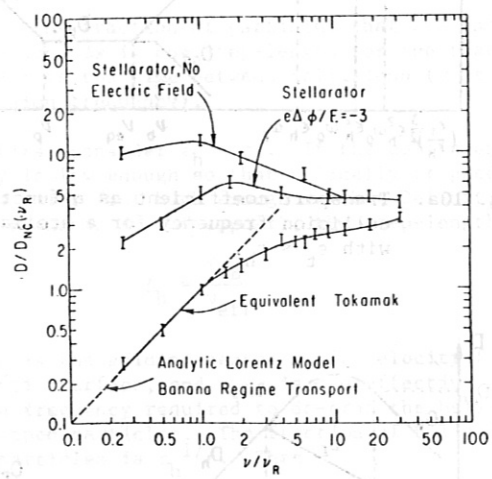

Fig. 13. Diffusion Coeffient in a Stellarator. The diffusion coefficient $D(E,\psi)$ is plotted for a thermal particle in a stellarator with and without an ambipolar electric field and in an equivalent tokamak. The reactor collision frequency ν_R is defined by $n = 10^{14}/cm^3$, T = 10 keV, B = 50 kG. The symbol $D_{NC}(\nu_R)$ means the value of the neoclassical diffusion at $\nu = \nu_R$. The parameters of the stellarator were $\ell = 2$, m = 6, $\varepsilon = 1/7$, and q = 2.

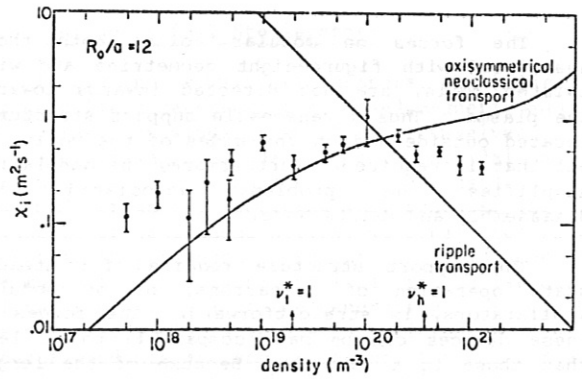

Fig. 14. Ion thermal conductivity of a torsatron with coil aspect ratio $R_o/a = 12$.

C. Bootstrap Current

The bootstrap current, which is a net toroidal current driven by diffusion, could be measured in a net current free stellarator, if it exists. This should appear in the collisionless regime where toroidally trapped orbits appear. If the density of banana orbits varies with minor radius, then a net current might exist, since the motion of a banana orbit is not balanced by an oppositely directed orbit along the torus.

A simple formula for the axisymmetric bootstrap current can be obtained as follows:

In steady state, we may write

$$n_e q_e B_p v_r = -n_e m_e v_{\parallel} \nu_{ei} \qquad (3)$$

where n_e is the electron density, B_p is the poloidal field, v_r is the radial outward flow velocity due to diffusion, and $v_{\parallel}$ is the electron drift velocity. The outward flow velocity is

$$n_e v_r = - D \frac{\partial n_e}{\partial r}$$

Using the expression for electron transport in the collisionless regime, we obtain

$$j_b = - \frac{\epsilon_t^{1/2}}{B_p} \frac{\partial p}{\partial r}$$

Experiments in Proto-Cleo in which a bootstrap current of several amperes was predicted to exist, did not show the presence of this current.[7]

Kruskal and Kulsrud have shown in their classical paper[8] that stellarators do not possess a bootstrap current if the plasma can be described by a magneto-hydrodynamic theory with spatially constant scalar electrical conductivity. Pfirsch and Schlüter mentioned in their paper on diffusion in a stellarator[9] that the toroidal current they found is due only to the artifical axisymmetric field used in their calculations. It seems plausible that any microscopic theory should give the same results in the collision-dominated regime. It might be argued that a magneto-hydrodynamic theory with spatially constant scalar electrical conductivity σ is not the proper limit for high-collision frequencies and large magnetic fields. For scalar plasma pressure p, it can, however, easily be shown[10] that the result of Kruskal and Kulsrud also holds if the parallel conductivity $\sigma_{\parallel}$ differs from the perpendicular conductivity $\sigma_{\perp}$ and if $\sigma_{\parallel}$ is allowed to vary from pressure surface to pressure surface, i.e., $\sigma_{\parallel} = \sigma_{\parallel}(p)$; $\sigma_{\perp}$ may even be an arbitrary function of the space coordinates. Of course, this result only applies to the collisional regime with high magnetic fields which includes a scalar pressure. It shows, however, that no general relation exists between the diffusion flux and a toroidal current, but that the special field geometry enters such a relation. The helical field in a net current free stellarator has, at first glance, the somewhat paradoxial property of simultaneously possessing a rotational transform and having

$$\oint \underline{B} \cdot \underline{dl} = 0$$

small circumference.

It is this property that is responsible in a self-consistent way for the vanishing also of the bootstrap current in the collision-dominated regime. One could therefore expect this current to vanish also in the neo-classical regimes rather than to be similar to the bootstrap current in axisymmetric configuration.

On the other hand, calculations of neoclassical transport of stellarators [11] clearly indicate that changes in population of trapped particles associated with pressure gradients should provide these currents. Although some arguments against this have recently been advanced, it is often believed they should exist.

Therefore, from the theoretical point of view the question concerning the existence of a bootstrap current in a stellarator is still an open one.

References

1. K. Miyamoto, Plasma Physics for Nuclear Fusion MIT Press (1980).

2. J.A. Derr, Bull. Am. Phys. Soc. 25, 830 (1980).

3. J.A. Derr and J.L. Shohet, Phys. Rev. Let. 43, 1730 (1979).

4. R.A. Schill and J.L. Shohet, Bull. Am. Phys. Soc. 25, 870 (1980).

5. A.H. Boozer, Phys. Fluids 23 5, 904 (1980).

6. R.E. Potok, P.A. Politzer, and L.M. Lidsky, Phys. Rev. Lett. 45 16, 1328 (1980).

7. D.J. Lees, Culham Laboratory Report, CLM-R-135 (1974).

8. M.D. Kruskal and R.M. Kulsrud, Physics Fluids 1, 265 (1958).

9. D. Pfirsch and A. Schlüter, Report MPI/PA/7/62, Munich (1962).

10. D. Pfirsch, Nuclear Fusion 12, 727 (1972).

11. T.E. Stringer, Toroidal Symposium (Garching, 1973) Paper F1.

VI. COIL CONFIGURATIONS

Introduction

To confine plasma in a closed system with a toroidal field, it is necessary to provide a twist, or rotational transform, of the magnetic field lines. By suitable adjustment of the twist, nested closed toroidal magnetic surfaces can be obtained. This is accomplished in tokamaks by passing a toroidal current in the plasma to create a poloidal field. A stellarator can be defined as a device where this rotational transform is provided solely by coils outside the plasma so that steady-state operation can be achieved.

The original stellarator concept[1] used the torsion associated with a nonplanar magnetic axis, such as in a figure-eight shape, to provide this transform. It can be seen quite easily by following a magnetic field line around such a system that it returns at a rotated position on the same magnetic surface. The need for shear to stabilize MHD interchange instabilities led to the classical stellarator concept[2] where the magnetic axis can be planar; the poloidal field is provided by a set of 2ℓ toroidally continuous helical windings with current flowing in opposite directions in adjacent windings, and the toroidal field is obtained from currents in planar poloidal coils. The torsatron[3] is a straightforward extension of this classical stellarator where the current goes in the same direction in the ℓ helical coils and provides both the poloidal and toroidal fields. The idea of deforming the poloidal coils either into an elliptic shape with a planar cross section[4] or by warping[5] so that they provide both components of the field has also evolved. All of these techniques for obtaining stellarator configurations with useful magnetic surfaces have considerable flexibility and many variations.

Classical stellarator coils suffered from two problems: the large, inwardly directed force acting on one set of the helical coils, and the interlinked geometry of the toroidal field coils and the helical windings. Both problems are alleviated in torsatrons where the access can also be improved.

The forces on modular coils, both those associated with figure-eight geometries and with twisted coils, are not directed inwards towards the plasma. Thus a reasonable support structure, located outside and on the sides of the coils, is all that is required. Furthermore, the modularity simplifies the problems associated with disassembly and maintenance.

The support structure required for steady-state operation of torsatrons, or of modular stellarators, is straightforward. The forces in these devices can be made comparable to or less than those in a tokamak. Because of the larger aspect ratio envisioned in stellarators, the fields at the coils as well as the forces on them are reduced significantly.

In the following sub-sections we treat coil configuration studies, first for continuous coils, and then for modular ones.

References

[1] L. Spitzer, Jr., Phys. Fluids 1, 253 (1958).
[2] J. L. Johnson, C. R. Oberman, R. M. Kulsrud, and E. A. Frieman, Phys. Fluids 1, 281 (1958).
[3] C. Gourdon, P. Hubert, and D. Marty, Compte Rendes Hebd. Seances Acad. Sci. II, 271, 843 (1970).
[4] S. N. Popov and A. P. Popryadukhin, Soviet Physics - Tech. Phys. 11, 284 (1966).
[5] S. Rehker and H. Wobig, in Proceedings of the 7th Symposium on Fusion Technology, Grenoble (1972) p. 345.

VI.1 Continuous Coil Stellarators

In continuous coil stellarators, the helical magnetic field necessary for closed magnetic surfaces is generated by windings which are themselves helical, linking the plasma in both toroidal and poloidal directions. Such windings are used on almost all presently operating stellarators. The advantage of continuous helical windings lies in the fact that the strength of the helical component of the magnetic field is proportional to the largest helical component(s) of the generating current. Thus the poloidal field is generated efficiently. Continuous windings are separable into two categories, depending upon whether the helical windings are also used to generate a net toroidal magnetic field.

In the "classical" stellarator configuration, 2ℓ windings carrying currents in alternate directions are used to produce a stellarator field with ℓ-fold poloidal symmetry without a net toroidal field. Therefore additional toroidal field coils are required. Figure 1 shows a schematic of an $\ell = 2$ stellarator. In all classical stellarators built thus far, the toroidal field coils are located outside of the helical windings, but this is not necessary in principle. Examples of existing classical stellarators are WENDELSTEIN VII-A, CLEO, L-2, JIPP T-2, and many others (see Annex for full list). One of the advantages of the stellarator configuration is the flexibility associated with the possibility of independence of the helical and toroidal field components. This feature allows a wide range of configurations in a single experimental device, and has made possible studies of the transition from tokamak-like configurations (rotational transform produced entirely or almost entirely by toroidal plasma currents) to pure stellarator configurations (with no net toroidal plasma current).

FIG. 1

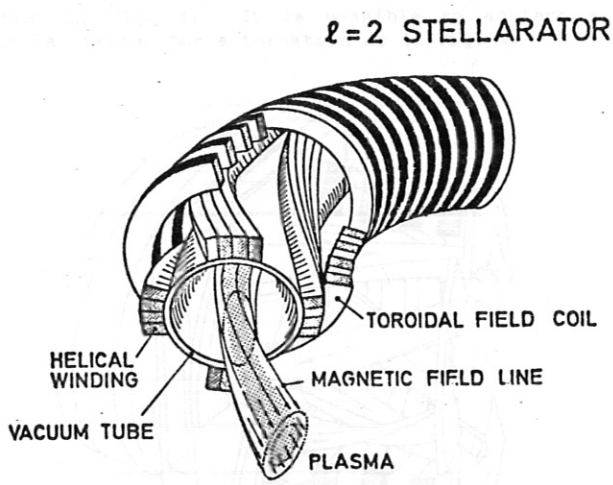

A particular disadvantage of the classical stellarator configuration arises from the interaction between the toroidal field coils and the helical windings. If the helices are imbedded in a large toroidal magnetic field, large radial forces appear which alternate in direction from one helix to the next. Thus, for large devices with significant confining fields, the problem of supporting the helices becomes very serious, as relatively little space is available for structure. For one set of the helical windings the support structure must be placed under the coil, between it and the plasma.

For a stellarator reactor this would make an economic design difficult. Since the field falls rapidly with decreasing radius, the coils must be near the plasma and this loss of space is indeed severe. Since the helical windings and the toroidal field coils are interlinked the disassembly and maintenance would be difficult.

This problem can be alleviated somewhat by placing the helical windings outside of the toroidal field coils. However, the helical current then must increase as the ℓ-th power of the radius of the winding.

Some of these difficulties of the classical stellarator are alleviated in the torsatron configuration. Here, a field with ℓ-fold poloidal symmetry is generated by ℓ helical windings, all carrying current in the same direction. The torsatron thus generates both toroidal and poloidal field components, and, in principle, no other coils are needed. Furthermore, the complication with two sets of interwoven windings is eliminated. Problems associated with disassembly and maintenance still exist due to the toroidal continuity of the helical coils but are less severe. Since in torsatrons one set of ℓ windings is used (rather than the 2ℓ windings of a stellarator) the access can be improved.

The torsatron coils usually generate an average vertical field which opens the vacuum flux surfaces. Thus, unless a specific winding law is selected (the "ultimate" torsatron law), an additional compensating vertical field coil set is needed. Furthermore, the basic torsatron configuration lacks experimental flexibility (i.e., variation of rotational transform, well depth, etc.), because of the use of a single set of windings. This flexibility can be restored with the use of an additional small vertical field, an additional small toroidal field, or by allowing variation in the helical harmonic content. Examples of the torsatron configuration are HELIOTRON E (which uses an added toroidal field), PROTO-CLEO, VINT-20 (an $\ell = 1$ torsatron), and URAGAN III (under construction).

Among the advantages of the torsatron configuration is the possibilty of significant reduction of the forces on the helical windings. The forces tend to be directed radially outward, so that the support structure is no longer a severe problem. Indeed, it is possible to transfer the average outward forces onto external Helmholtz coils far from the plasma.

For a torsatron with a certain winding law of the helical coils the radial force averaged over a field period even may be reduced to zero. For this case large forces appear on the compensation coils, but these can be located where there is adequate space for support structure.

In the following the different winding laws will be discussed in more detail. This discussion applies for the continuous coils of stellarators and torsatrons. For the magnetic field computations the helical windings usually are represented by one or more current filaments.

A continuous winding is defined in terms of a curve on a toroidal surface: $(m/\ell)(\phi - \phi_{oi}) = f(\theta)$, where m is the number of toroidal field periods, ℓ is the number of poloidal field periods, and ϕ_{oi} is the starting toroidal angle of the i-th filament. The winding law is subject to the periodicity condition that

$$\phi\,(\theta + 2\pi) = \phi\,(\theta) + 2\pi\ell/m$$

If the winding lies on a circular torus of major and minor radii R and a respectively, the local pitch angle is

$$\zeta = \cot^{-1}\left[\frac{R+a\cos\theta}{a}\;\frac{d\phi}{d\theta}\right]$$

In discussions of various winding laws, it is useful to expand $f(\theta)$ in a Fourier series:

$$\frac{m}{\ell}\,(\phi - \phi_{oi}) = \theta + \alpha_1 \sin\theta + \alpha_2 \sin 2\theta + \ldots$$

Some special cases are:

a) $d\phi/d\theta$ = constant
For this winding law $\alpha_1 = \alpha_2 = \ldots = 0$.
A torsatron with this winding requires a large compensating vertical field approximately given by

$$B_V \simeq -\frac{1}{2}\,B_{Ho}\,\frac{\ell}{m}\left[\ln\frac{8R}{a} - \frac{1}{2}\right]$$

where $B_{HO} = \mu_o\, m\, I/2\pi R$ is the average toroidal field produced for a current I in each winding.

b) ζ = constant
This winding law represents the geodesic winding on a circular torus. In the series expansion, $\alpha_1 \simeq -a/R$, and the needed compensating vertical field in a torsatron is

$$B_V \simeq -\frac{1}{2}\,B_{HO}\,\frac{\ell}{m}\left[\ln\frac{8R}{a} - \frac{3}{2}\right]$$

c) Self-compensating ("ultimate")
A torsatron with this winding law needs no additional vertical field compensation. The coefficient of sin Θ is

$$\alpha_1 \simeq -\frac{a}{R}\left[\ln\frac{8R}{a} - \frac{1}{2}\right]$$

Analysis of the vacuum fields generated by continuous helical windings in toroidal systems requires a fully three dimensional numerical treatment. Many different configurations have been examined, but no systematic study of the dependence of topological parameters (rotational transform, shear, well depth, useful volume, separatrix shape, thickness of ergodic layer, etc.) on winding law has been reported. In fact, most generalizations and intuition regarding the properties of stellarators are based on straight stellarators (infinite aspect ratio) which can be solved analytically as this is a strictly two dimensional system.

Because of the variability of the winding law, a continuous winding may generate a broad spectrum of helical harmonics, so it is an oversimplification to refer to a "pure" helical field structure (e.g., $\ell = 2$ alone). However, from analysis of straight systems and of a wide variety of toroidal configurations, some features of the magnetic topology can be associated with the presence of specific helical harmonics.

a) $\ell = 2$ contributions: give large transform in the central region of the plasma; shear depends on the relative pitch of the windings - short pitch gives large shear but lower transform per period (as in HELIOTRON E), while long pitch gives negligible shear but higher transform per period (as in WENDELSTEIN VII-A).

b) $\ell = 1$ contributions: give helicity to the magnetic axis, and are otherwise similar to $\ell = 2$; generate relative displacements of inner and outer magnetic surfaces which can be adjusted to minimize parallel currents and to improve beta limits ("drift optimized systems").

c) $\ell \geq 3$ contributions: give very small transform in the central region of the plasma, but a large transform near the edge, yielding high shear. Since the poloidal field varies as $r^{\ell-1}$, the higher order contributions can be used to control conditions near the plasma edge (e.g., the shape of the last closed surface and the shear at the edge) without affecting the topology near the center. In general, the size of the last surface increases with increasing ℓ, and also with shorter pitch lengths. In combining helical harmonics in a given system, it is important to take into account the fact that toroidal effects can couple different harmonics due to the basic $\ell = 1$ dependence of a toroidal system.

VI.2 Modular Stellarators

A. Introduction

The term modular stellarator refers to a generalized stellarator configuration of nested magnetic surfaces with multiple helicity achieved by a system of discrete coils which provides both toroidal and poloidal fields. Since there is no net toroidal current, no vertical-field coils are needed. A modular stellarator, therefore, has no toroidally continuous windings; the confinement coil system is modular. Furthermore, there is no force directed inwardly towards the minor axis. Thus the support structure can be located outside and on the sides of the coils.

Modular stellarators can be classified into two types: those in which the magnetic axis has significant torsion and is thus spatial, and those with a nearly circular, planar axis. The non-planar configurations are characterized as having a large $\ell = 1$ poloidal Fourier component of the magnetic field. The other type has $\ell > 2$. The $\ell = 1$ configuration requires only circular, planar toroidal field coils; the rotational transform is obtained by deforming the geometric axis of the coil system from a two-dimensional ring into a three-dimensional curve. For m = 2, where m is the toroidal field-period number, the configuration is a figure 8 stellarator. For m > 2, the geometric axis is a toroidal helix.

One possible approach to modularize the coils would be to segment the usual stellarator windings, combining the helical and toroidal field coils as in Fig. 1.[1] This has the difficulty that the inwardly directed coil forces are large. One could equally well visualize construction of discrete coils by superposing opposing torsatron windings with different pitches as in Fig. 2.[2] An improvement of this approach can be achieved with an evolution of the twisted coil concept[3,4] as shown in Fig. 3. It is possible to achieve a similar design for a torsatron as in Fig. 4.[2]

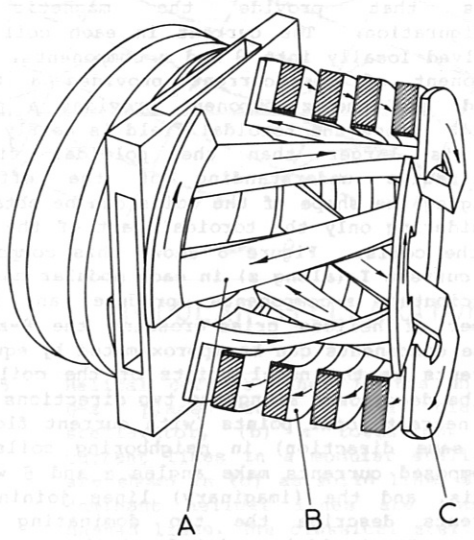

Fig. 1 Modularized classical stellarator coil for an $\ell = 3$ system. A, helical segment, B, toroidal field coil, C, connection of helical segment.

This section describes the ideas leading to optimization of a particular planar, $\ell \geq 2$, system. The $\ell = 1$ system involves only planar coils and is relatively simple. It should be noted that an $\ell = 2$ configuration can also be obtained by using planar, elliptically shaped coils.[5] Successive coils are rotated and each coil is tilted from the plane perpendicular to the geometric axis. Similarly, an $\ell = 3$ configuration can be obtained by using planar triangular coils. The rotational transform obtained with such coil systems is usually small. The modular-coil concept based on deforming the planar coil enhances greatly the rotational transform.

The basic concept of modular coils was first proposed by Rehker and Wobig.[3] An analytic-numerical analysis of a straight system was given by Ohasa and Miyamoto.[6] A modularized helix was introduced by Streibl.[7] Recent work[2,4,8,9] shows that substantial strengthening of the rotational transform can be obtained by improving the helical symmetry in the winding law, and that rotational transforms of confinement interest can be obtained without greatly deforming the toroidal field coils from being planar. The divertor feature of the coil system has also been examined.[10]

Part B of this section describes the basic principle of the Rehker-Wobig coil where the winding contains only the fundamental component of the poloidal field-period number ℓ. Part C describes the effect of harmonics in the winding law by (a) an analytic-numerical analysis and (b) a geometric analysis. Part D discusses types of coils, and Part E presents the different kinds of magnetic configurations that are achievable in modular stellarators. Types of profiles of rotational transforms are presented in Part F. The structure of ripples and their origin are discussed in Part G.

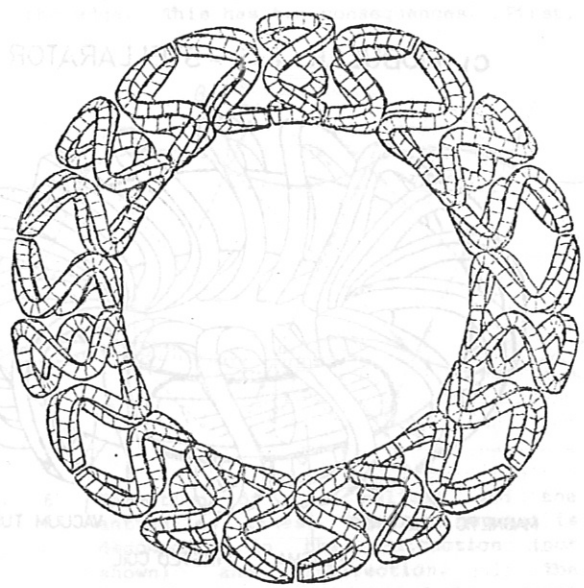

Fig. 2 Modular $\ell = 3$ twisted coil system approximating opposing torsatron windings. This IMS configuration is being investigated as a modification of PROTO-CLEO.

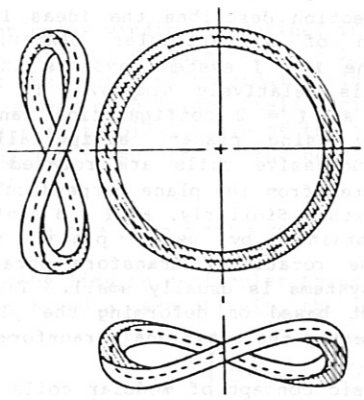

a) ℓ=2 COIL

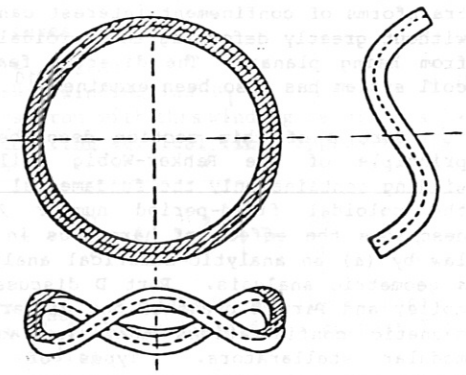

b) ℓ=3 COIL

c) MODULAR ℓ=2 - STELLARATOR

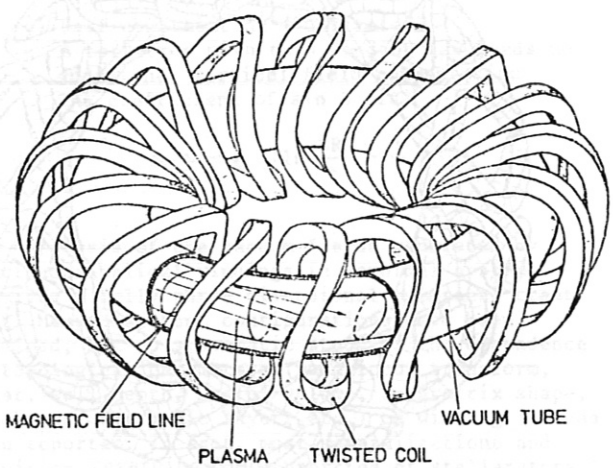

Fig. 3 (a) An ℓ = 2 modular coil, (b) an ℓ = 3 modular coil, and (c) coil arrangement in an ℓ = 2 modular stellarator.

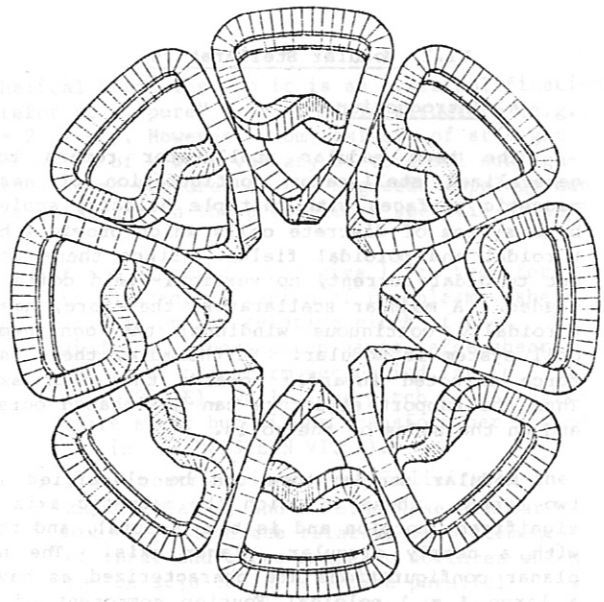

Fig. 4 Modular torsatron.

B. Basic Principle of Rehker-Wobig Coils

In classical stellarators and torsatrons, the windings providing the rotational transform are toroidal helices. These helical lines are shown in Fig. 5 in the unfolded θ-z plane, where z is the distance along the toroidal direction. In a simple modular stellarator, the N windings are sinusoidal curves in the θ-z plane, and they are discrete in z. A good qualitative picture of the nature of these stellarators can be obtained by considering this system and decomposing the currents into superpositions of helical current lines that provide the magnetic field configuration. The current in each coil can be resolved locally into θ and z components. The θ-component of the current provides a toroidal field, and the z-component provides a poloidal field. Since the toroidal field is nearly uniform and is larger than the poloidal field, a qualitative understanding of the effect of changing the shape of the coils can be obtained by considering only the toroidal part of the current in the coils. Figure 6 shows this component of the current I (along z) in each modular coil. The distributed z-components produce an infinite number of helices criss-crossing the θ-z plane. These components can be approximated by equivalent currents at the nodal points of the coil. They can be decomposed along the two directions joining the nearest nodal points (with current flowing in the same direction) in neighboring coils. The decomposed currents make angles α and β with the z-axis, and the (imaginary) lines joining these currents describe the two dominating helical lines. It should be pointed out that, except for certain geometric configurations, the helical lines are not lines joining the sloping parts of the sinusoidal curves in the θ-z plane.

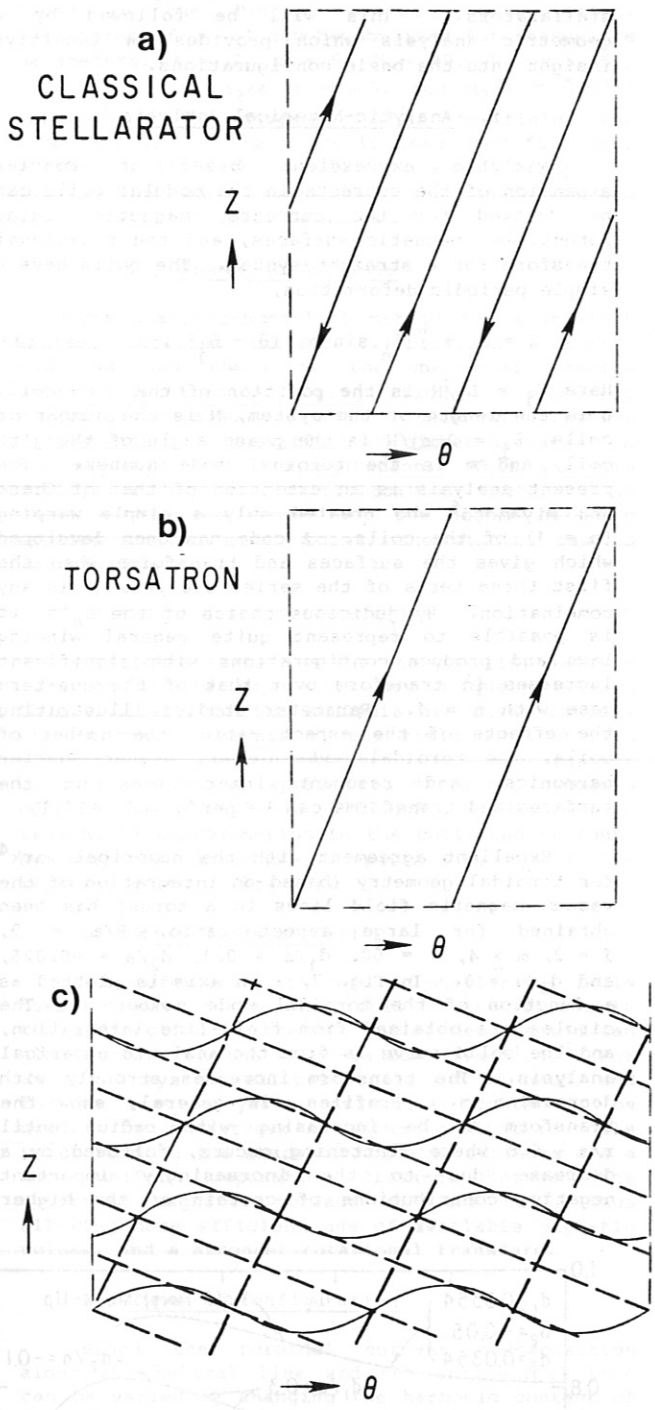

Fig. 5 Helical current lines in the unfolded θ-z plane in (a) a classical stellarator, (b) a torsatron. The current lines in a modular stellarator are shown in (c) as solid lines and the dominant helical lines are shown as dashed lines. The classical stellarator configuration of (a) has additional TF coil windings, and the torsatron configuration of (b) has vertical field windings. These windings are not shown in the figure.

The smaller angle α corresponds to the pitch angle of the helical windings in a classical stellarator, and

$$p_\alpha \equiv \tan \alpha = \frac{a}{R}\frac{m}{\ell} \quad . \qquad (1)$$

The larger angle β corresponds to a second stellarator helical winding with

$$p_\beta \equiv \tan \beta = \frac{a}{R}\frac{m}{\ell}\left(\frac{N}{m} - 1\right) = \frac{a}{R\ell}(N - m). \qquad (2)$$

Equations (1) and (2) describe the two dominant helices among the complex array of modes in modular stellarators. The characteristics of the modular stellarators can be described approximately by these two stellarator helical components.

The two sets of helical lines give opposing transforms. (The α-angle lines will be designated as the helical lines and the β-angle lines as the antihelical lines.) The helical lines depend only on the geometric configuration of the torus and not on the number of modular coils. The antihelical lines, in addition, depend on the number of modular coils. Both pitch angles are independent of the amplitude of the deformation of the coil. The pitch angle of the antihelical lines corresponds to a set of windings whose number of toroidal field periods is (N/m) - 1 times that of the helical lines. Because of this higher toroidal field-period number, the contribution to the rotational transform from the antihelical lines is relatively small in the interior but becomes significant near the edge. Also, with fewer modular coils, the opposing transform contributed by the antihelical lines is stronger. The lowest integer N/m value which gives non-zero rotational transform is 3. For N/m = 2, $\beta = \alpha$ and there is no transform for the purely sinusoidal coil.

The antihelical lines "unwind" the field lines and give an opposing transform especially near the edge. This has two consequences. First,

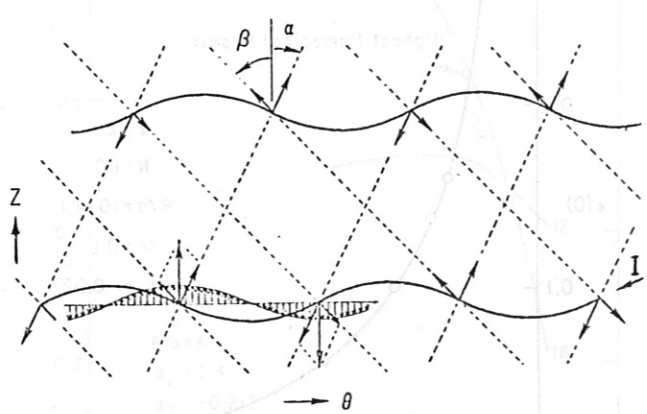

Fig. 6 Formation of the helical and the antihelical lines. The coil current is decomposed in the θ-direction (not shown) and z-direction. The distributed z-components of the current are represented by their values at the nodal point, and these are resolved along lines joining nodal points (with current flowing in the same direction) in neighboring coils.

the rotational transform of a modular stellarator is generally lower than that achieved with the helical lines (α-angle lines) alone. Second, the separatrix is held at a larger radial position than that achieved with the helical lines alone. A modular stellarator thus has lower edge transform and larger usable magnetic volume than a classical stellarator.

In summary, a simple modular stellarator can be regarded as being nearly equivalent to (1) a set of planar toroidal field coils and (2) two sets of stellarator helical windings giving opposing transforms. This decomposition is by no means unique. For instance, for special choices of the geometric parameters, a modular stellarator can also be interpreted as being essentially four sets of torsatron windings, two of the sets giving unequal positive transform, and the other two unequal negative transform. A change of the winding law from being simply sinusoidal modifies these considerations by changing the harmonic content. When certain harmonics are present a modular stellarator can produce fields similar to a simple stellarator[1], Fig. 1, or fields roughly equivalent to two opposing torsatron windings with different pitch angles.[2,11] A specific example of this is the IMS configuration, Fig. 2.[12]

C. Harmonic Content

In this section, we discuss the effect of changing the harmonic content of the winding so as to increase the rotational transform and to obtain field configurations with different helical symmetry and rotational transform profiles. This additional degree of freedom enables the modular stellarator to achieve many different magnetic field configurations, some of which cannot be achieved by classical stellarator or torsatron windings. We will first give some analytic-numerical results for straight modular stellarators. This will be followed by a geometric analysis which provides an intuitive insight into the basic configurations.

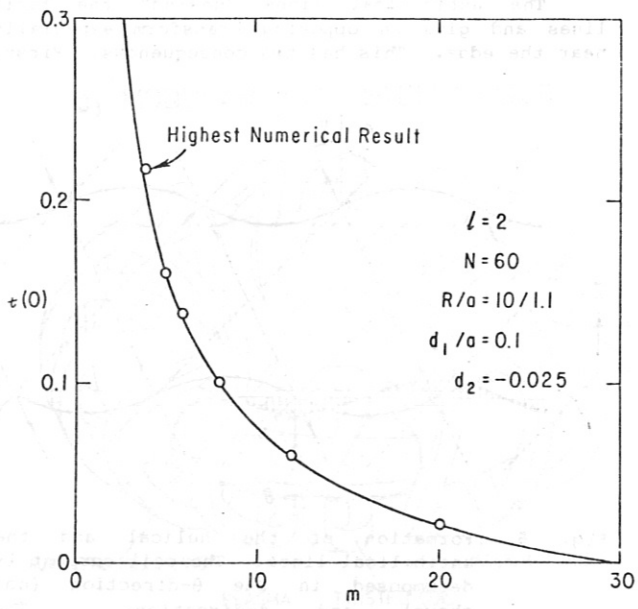

Fig. 7 Analytic-numerical results of on-axis rotational transform for a straight system (curve), and numerical results for a toroidal system (discrete points) when the toroidal field-period number m is varied.

i. Analytic-Numerical Analysis

Analytic expressions based on Fourier expansion of the currents in the modular coils can be derived for the currents, magnetic scalar potentials, magnetic surfaces, and the rotational transform for a straight system. The coils have a simple periodic deformation,

$$z = z_j + \sum_n d_n \sin n\,(\ell\theta - \theta_j) \,. \qquad (3)$$

Here $z_j = Lj/N$ is the position of the j'th coil, L is the length of the system, N is the number of coils, $\theta_j = 2\pi mj/N$ is the phase angle of the j'th coil, and m is the toroidal mode number. The present analysis is an extension of that of Ohasa and Miyamoto[6] who treated only a simple warping (n = 1) of the coils. A code has been developed which gives the surfaces and transforms when the first three terms of the series are present in any combination. By judicious choice of the d_n's, it is possible to represent quite general winding laws and produce configurations with significant increases in transform over that of the one-term case with n = 1. Parameter studies illustrating the effects of the aspect ratio, the number of coils, the toroidal mode number, higher Fourier harmonics, and resonant interactions on the surfaces and transforms can be performed readily.

Excellent agreement with the numerical work[4] for toroidal geometry (based on integration of the vacuum magnetic field lines in a torus) has been obtained for large aspect ratio, R/a = 9, $\ell = 2$, $m \geq 4$, N = 60, $d_1/a = 0.1$, $d_2/a = -0.025$, and $d_3/a = 0$. In Fig. 7, ι on axis is plotted as a function of the toroidal mode number m. The circles are obtained from field-line integration, and the solid curve is from the analytic-numerical analysis. The transform increases strongly with decreasing m. Profiles, in general, show the transform to be increasing with radius until r/a ~ 0.6 where flattening occurs, followed by a decrease due to the increasingly important negative contributions of certain of the higher

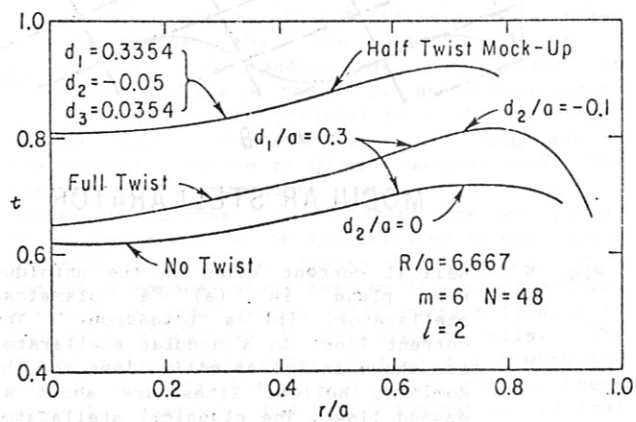

Fig. 8 Analytic-numerical results of rotational transform profiles for a straight $\ell = 2$ system for different combinations of the d_n's.

modes in the Fourier series representation. Transforms of $\iota \sim 1$ can be obtained for reasonable parameters: $\ell = 2$, $m = 6$, $N = 48$, $R/a = 6.667$, $d_1/a = 0.3354$, $d_2/a = -0.05$, and $d_3/a = 0.0354$ (Fig. 8). The agreement with the field line computations for the torus is less good for these parameters since the stellarator expansion used to obtain the expressions for the surfaces and transform is not well satisfied.

ii. Geometric Analysis

The analytic-numerical method for a straight system, outlined in Sec. (i) provides a useful modeling and check of the numerical results obtained for toroidal configurations. A geometric analysis can also be made to gain an intuitive understanding of the effect of higher harmonics on the magnetic field configuration. This analysis employs a harmonic multiplication factor s so that, within the segment of the higher harmonic applied at the nodal point, the winding law is described by

$$Z = Z_j + d \sin s\,(\ell\theta - \theta_j) . \qquad (4)$$

The rotational transform and its profile, and the location of the separatrix are uniquely related to s. Details of the analysis are given in Ref. 13. An exact analysis of the field configuration similar to that described in Sec. (i) for different s values applied to different segments of the same coil is difficult. However, a reasonable approximation to the coils can be found by properly choosing the parameters d_n in the representation of Eq. (3).

D. Other Types of Coil

The deformation in modular stellarator coils does not have to be restricted to distortions in the z-direction of the θ-z plane; deformation can also be made in the minor-radius direction.[8] For an $\ell = 2$ system, elliptic coils can be used, and for an $\ell = 3$ system, triangular coils can be used. The advantages of using noncircular coils to conform to the shape of magnetic surfaces are a more uniform separation distance between the outermost magnetic surface and the coil, thus allowing more efficient use of available magnetic volume, and a stronger rotational transform.

E. Types of Configuration

Since the toroidal current decomposition along the helical line and the antihelical line can be varied by changing the harmonic content of the winding law at and near the nodal points, configurations with varying degrees of helical symmetry and different profile shapes of rotational transform can be obtained. Further, by varying the geometry of the helical and the antihelical lines, magnetic surfaces can be made to contain a multiplicity of ℓ-modes, thus producing a vacuum magnetic field which has a magnetic well (or hill). It is possible to minimize the azimuthal variation of the geodesic curvature in a magnetic surface and thus reduce the secondary current. This section discusses types of magnetic field configurations that can be achieved with modular coils.

i. General Configuration

A simple modular stellarator has both helical and antihelical lines. For an $\ell = 2$ configuration, the rotational transform is therefore high near the center and decreases radially outward. In an $\ell = 3$ modular stellarator the contribution to the rotational transform from the helical and antihelical lines are similar, but the rotational transform profile, like that in a classical stellarator, is zero at the center and increases outward.

ii. Flexibility of Design

A striking feature of these modular coils is that minor changes in shape allow significant modification in the configuration. The angles α and β are affected by geometry and by the positioning of the coils. This can be seen in Fig. 7, where the rotational transform decreases with increasing rotation of the consecutive coils, or increasing m. Similar improvement of the rotational transform with increasing number of coils is shown in Fig. 9. This figure provides a good demonstration that saturation sets in as N gets large; the configuration approaches that of a classical stellarator. It is possible to obtain almost any desired set of values of current along

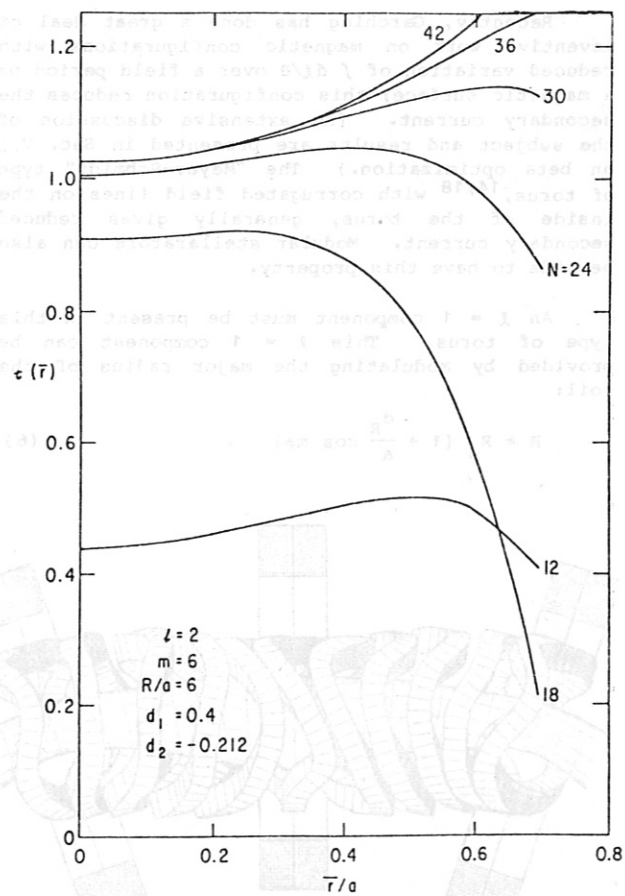

Fig. 9 Analytic-numerical results of rotational transform for a straight $\ell = 2$ system for different N.

α and β by varying the harmonic content in Eq. (3). This enables one to obtain quite different types of configurations. The limiting cases are the classical stellarator, which has a single helicity and thus possesses highest helical symmetry, and the case with N/m = 3, which has the highest contribution from the antihelical lines.

iii. Magnetic Well Formation

By varying the geometry of the α-angle lines, a non-zero local vertical field can be produced. This vertical field causes differential shifts of the magnetic surfaces from (or towards) the major axis thus producing a magnetic well (or hill). A coil deformation which accomplishes this purpose is a deformation in the θ-direction of the θ-z plane so that the α-angle lines are determined from

$$\phi = \frac{\ell}{m} (\theta + \gamma \sin \theta) \qquad (5)$$

where ϕ is the toroidal angle. We note that winding laws similar to Eq. (5) have been used in torsatrons. Rau[14] obtained magnetic well and hill formation in torsatrons by using positive and negative γ's, respectively. For negative γ's, a torsatron configuration with no additional vertical field windings for maintaining plasma equilibrium can also be obtained.[15-17]

iv. Configuration with Reduced Secondary Currents

Recently, Garching has done a great deal of inventive work on magnetic configurations with reduced variation of $\int d\ell/B$ over a field period on a magnetic surface; this configuration reduces the secondary current. (An extensive discussion of the subject and results are presented in Sec. V.2 on beta optimization.) The "Meyer-Schmidt" type of torus,[14,18] with corrugated field lines on the inside of the torus, generally gives reduced secondary current. Modular stellarators can also be made to have this property.

An $\ell = 1$ component must be present in this type of torus. This $\ell = 1$ component can be provided by modulating the major radius of the coil:

$$R = R_o \left(1 + \frac{d_R}{a} \cos m\phi\right) \quad . \qquad (6)$$

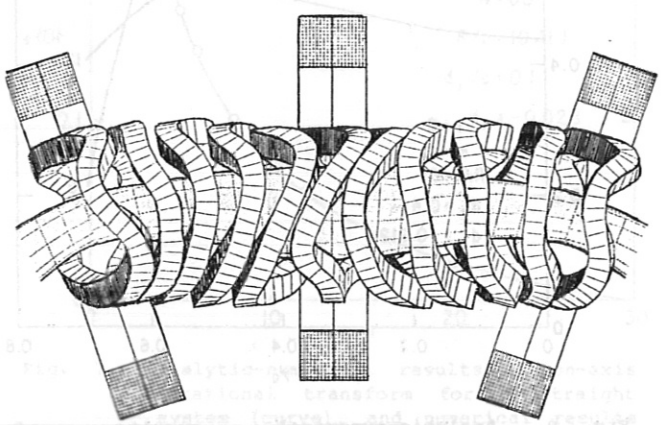

Fig. 10 Configuration with reduced secondary current.

In this case the geometric axis wriggles in the horizontal plane providing the possibility of minimizing the deviation of $\int d\ell/B$ from its average value over a transit around the machine. This can provide a configuration possessing a magnetic well and having a reduced drift.[13] Figure 10 shows the top view of a coil arrangement that also produces a configuration with reduced secondary current.

F. Types of Rotational Transform Profiles

By varying the current components along the α and β angle lines, profiles of rotational transform can be varied from positive $d\chi/dr$ to negative $d\chi/dr$. The profile with negative $d\chi/dr$ cannot be achieved by simple stellarator or torsatron windings having a single poloidal field period number ℓ. Configurations with this type of profile have a larger usable magnetic volume. If an ohmic-heating current is used, the resultant transform profile will retain the feature of monotonic decrease; no bumpy profile will result.

G. Ripples

Modular stellarators have toroidal, helical and modular ripples. The origins of the modular ripples are the discreteness of the coils and the finite poloidal rotation in successive, discrete coils. Because a modular stellarator inherently contains multiple helicity, its helical ripples have multiple-helicity structure. For the simple Rehker-Wobig coil, the helical ripples consist of those due to the helical lines (the α-angle lines) and the antihelical lines (the β-angle lines). The ripple amplitude for each component of helicity increases radially outward. The amplitude of modular ripples can be reduced by improved winding methods.[8]

Summary

Considerable progress has been made in the design of modular stellarator coils since the concept was first proposed. A good qualitative understanding of the fields generated by these coils can be obtained by decomposing the toroidal component of the current into components along directions joining the nodal points (with current flowing in the same direction) of neighboring coils. Improved coil shaping can be designed from geometric studies of these current decompositions as well as from quasi-analytic models obtained by Fourier analyzing the currents into helical components. It is thus possible to design modular systems with large rotational transform. Systems with either radially increasing or decreasing transform as well as with minimum average fields can be obtained.

References

[1] S. Hamberger, L. E. Sharp, and L. F. Peterson, 9th European Conference on Controlled Fusion and Plasma Physics, Oxford, (1979) Paper BP-20.

[2] D. T. Anderson et al., in Plasma Physics and Controlled Nuclear Fusion Research (Brussels, 1980) Paper IAEA-CN-38/BB-1.

[3] S. Rehker and H. Wobig, Proceedings of 7th Symposium on Fusion Technology, Grenoble (1972) p. 345; Max-Planck Institut fur Plasmaphysik Report IPP 2/215 (1973).

[4] T. K. Chu, H. P. Furth, and C. Ludescher, Bull. Am. Phys. Soc. II 24, 956 (1979).

[5] S. N. Popov and A. P. Poyryadukhin, Soviet Physics - Technical Physics 11, 284 (1966).

[6] K. Chasa and K. Miyamoto, Jap. J. of Applied Physics 16, 813 (1977).

[7] B. Streibl, Nineth Symposium on Fusion Technology, Garmisch-Partenkirchen (Pergamon Press, Oxford, 1976) p. 217.

[8] C. Ludescher, T. K. Chu, and H. P. Furth, Bull. Am. Phys. Soc. II 25, 869 (1980).

[9] K. E. Weimer and J. L. Johnson, Bull. Am. Phys. Soc. II 25, 869 (1980).

[10] J. Derr, University of Wisconsin Report ECE-80-36 (1980).

[11] K. Chasa and K. Ikuta, Nuclear Fusion 17, 473 (1977).

[12] D. T. Anderson, J. A. Derr, and J. L. Shohet, Bull Am. Phys. Soc. II 25, 869 (1980).

[13] T. K. Chu, H. P. Furth, J. L. Johnson, C. Ludescher, and K. E. Weimer (to be published).

[14] F. Rau and W VII-A Team, 9th European Conference on Controlled Fusion and Plasma Physics, Oxford, (1979); Paper BP-22; also, Private communication.

[15] C. Gourdon, P. Hubert, and D. Marty, Comptes Rendus Seances Acad. Sci. Series B, 271 843 (1970).

[16] S. M. Hamberger, L. E. Sharp, A. Malein, J. Bradley, W. McKay, in Plasma Physics and Controlled Nuclear Fusion Research 1974 (International Atomic Energy Agency, Vienna, July 1975) Vol. 2, p. 21.

[17] T. W. Kruckewitt, J. L. Shohet, Nuclear Fusion 20 1375 (1980).

[18] R. Chodura, W. Dommaschk, W. Lotz, J. Nuhrenberg, A. Schluter, R. Gruber, F. Herrnegger, W. Kerner, W. Schneider, and F. Troyon, Plasma Physics and Controlled Nuclear Fusion Research 1980, paper IAEA-CN-38-BB2.

VII SURVEY OF PRESENT STELLARATOR REACTOR STUDIES

Introduction
A. UWTOR-M
B. Modular Stellarator Reactor (MSR)
C. T-1 MIT Design
D. HELIOTRON

Introduction

Early stellarator reactor designs[1-6] concluded that the coupled problems of high coil cost and low system power density (i.e., low beta) were particularly severe for the classical stellarator. The more recent torsatron[7,8] and modular-coil configurations[11 - 13], however, show strong promise in alleviating the coil problem per se. For these reasons, the overall coil performance represents a major element in the more recent reactor survey and systems analyses.[12,13]

The pioneering Princeton Model-D design[1] represents one of the most comprehensive extrapolations of a confinement concept to the reactor stage. Experimental and theoretical work during the 1950s, however, established that several of the physics and technology assumptions upon which the Model-D design was based were untenable (e.g., average beta of 0.75, "figure-8" topology and copper coils).[2,14] The Model-D design, however, set a precedent for Stellarator-like reactors that was prominent until the publication of the T-1 Torsatron design[8]: the tendency for Stellarators to produce large amounts of thermal power (i.e., > 5 GWt). Attempts to impose equilibrium and stability limits on beta led to reactor survey calculations at Culham[4,5]. The assumed scaling of beta with plasma aspect ratio (equilibrium limit) in toroidal geometry, when coupled with the conservative transport scaling assumed, resulted in systems with high peak magnetic field strengths in the inboard region of the coils. Three additional stellarator reactor designs, given in Refs. 8-10, invoke the Torsatron coil configuration. The Heliotron-C design[9] is based upon a large beta value, which in a system of large major radius also leads to large power output. This situation exists for the Kharkhov design point[10].

The more recent MIT T-1 Torsatron design[8] reflects an attempt to reduce the total power output to $\lesssim$ 4 GWt under the assumption of conservative beta limits. The assumed Alcator (empirical) transport scaling allows moderate on-axis field strength, and the large aspect ratio reduces the corresponding peak field on the inboard region of the coil. Because of the monolithic helical coils required for this $\ell = 3$ Torsatron reactor, modularity could be achieved only by proposing demountable superconducting breaks within the coil structure and modules that weigh on the order of 1000 tonne. The otherwise favorable performance of the T-1 reactor design is used as a benchmark for ongoing Stellarator reactor studies[12,13] with an emphasis being placed on improved modularity of reactor construction and operation. It is emphasized that the issue of stability remains important for these more recent stellarator/torsatron reactor designs[12,13], although the use of appropriately distorted modular coils considerably enhances the reactor prospects of this steady-state, disruption-free device.

References

1. L. Spitzer, D. Grove, W. Johnson, L. Tonks and W. Westendorp, "Problems of the Stellarator as a Useful Power Source," USAEC Report NYO-6047 (1954).

2. R. G. Mills, "Economic Prospects for Thermonuclear Reactors," Princeton Plasma Physics Laboratory report MATT-60 (February, 1961).

3. K. Miyamoto, "Recent Stellarator Research, " Nucl. Fus., 18, 243-284 (1978).

4. A. Gibson, "Permissible Parameters for Economic Stellarator and Tokamak Reactors," Proc. BNES Nuclear Fusion Reactor Conf. at Culham Laboratory, 233-241 (September, 1969).

5. A. Gibson, R. Hancox and R. J. Bickerton, "Economic Feasibility of Stellarator and Tokamak Fusion Reactors," Proc. 4th Inter. Conf. on Plasma Physics and Controlled Nuclear Fusion Research, IAEA-CN-28/K-4, III, 375-392 (June 17-23, 1971).

6. H. C. Cole, J. W. Hill and M. J. Terry, "Plasma Heating by Neutral Injection in a Stellarator Reactor," Proc. 6th Symp. on Fusion Technol., Aachen, FRG, EURATOM report EUR 4593e, 479-484 (September, 1970).

7. C. Gourdon, D. Marty, E. K. Maschke and J. Touche, "The Torsatron without Toroidal Field Coils as a Solution of the Divertor Problem," Nucl. Fus., 11, 161-166 (1971).

8. P. A. Politzer, L. M. Lidsky and D. B. Montgomery, "Torsatrons and the TOREX Proof of Principle Experiment," Massachusetts Institute of Technology report PFC/TR-79-1 (March, 1979).

9. A. Iiyoshi and K. Uo, "Heliotron as a Steady Fusion Reactor," Proc. 5th Inter. Conf. on Plasma Physics and Controlled Nuclear Fusion Research, IAEA-CN-33/G4, III, 619-630 (November 11-15, 1974).

10. A. V. Georgievskii, Yu. M. Loktionov and V. A. Suprunenko, "Characteristics of a Hypothetical Thermonuclear Stellarator Reactor in the 'Plateau' Regime, "Kharkhov Physico-Technical Institute report KhFTI 76-38 (1976), (English Translation in UKAEA Culham Laboratory report CTO/1299 (November, 1976)).

11. W. Wobig and S. Rehker, "A Stellarator Coil System without Helical Windings," Proc. 7th Symp. on Fusion Technology, Grenoble, France, 333-343 (October 24-27, 1972).

12. R.L. Miller and R.A. Krakowski, "The Modular - Stellarator Fusion Reactor Concept", Los Alamos National Laboratory report (to be published, June, 1981).

13. I.N. Sviatoslavsky, University of Wisconsin, private communication (January 1981).

14. R. G. Mills, "Thermonuclear Power and Superconductivity," Engineering Aspects of Magneto-hydrodynamics, Columbia University Press, NY, 514-520 (1962).

A. UWTOR-M, University of Wisconsin Design

The University of Wisconsin Fusion Engineering Group has been looking at some engineering problems of stellarator or torsatron power reactors. The aim is not to come up with a self-consistent design of a power reactor as much as to investigate and assess the engineering implications of maintainability.

Three coil configurations were investigated: helical coils, modular torsatron coils and twisted stellarator coils. Although the viability of the first two configurations has not been ruled out, it was decided to pursue the twisted stellarator coil option because of its more attractive possibilities for maintainability.

According to the present cost of energy, any economical power reactor must produce at least 1000 MW_e. We thus chose as a starting point 3000 MW_{th} as the power output. Arbitrarily selecting an average β of 5%, setting the maximum field at the conductor at 9.5 tesla, selecting a multipolarity of 3 and starting out with a plasma aspect ratio of $\approx$ 10, several coil design iterations were made. As soon as it appeared that the desired conditions were approached, refinements were made for other constraints not originally imposed. The resulting parameter list is given in Table I.

TABLE I. Main Parameters of UWTOR-M

Major radius (m)	24.1
Average coil radius (m)	4.77
Coil aspect ratio	5.05
Average β (%)	5.
Multipolarity	3
Field on axis (T)	5.5
Max. field on conductor	9.5
Coil current (MA)	35.
No. of field periods	6
Coils for period	3
No. of coils	18
Plasma minor radius (m)	1.35
Plasma aspect ratio	14
Rotational transform at edge	1.125
Plasma volume (m^3)	1408.
Avg. neutron wall loading (MW/m^2)	1.72
Thermal power output (MW_{th})	5500.

At the present the effort is concentrated in three primary areas: the coil conductor and structure, the design of the divertor, and the maintainability approach. Since a choice was made to minimize the number of coils, we are finding that the required current density and the amount of structure needed to react the forces makes the coil design very challenging. This is further complicated by the need to transfer forces across warm junctions between adjacent coils. This is necessitated by the chosen maintainability approach which requires that individual coils can be moved out radially to provide access for blanket replacement.

The topology of the divertor has been established and several design approaches are being pursued with the aim of prolonging the periods between divertor target change-out. Should it prove necessary to replace divertor targets more frequently than the blanket modules, then this is planned to be done without a major disassembly.

In the chosen maintainability approach, an evacuated annular tunnel houses the reactor. Every third coil will be located in line with an access port. The access port leads to the service tunnel which also circumvents the reactor. During routine maintenance, the access port is unsealed and opened, and the coil is rolled out radially into the service tunnel. A specially designed carriage is then rolled back in place to the coil to disconnect and extract the blanket modules within the two coils adjacent to the removed one. Simultaneously, the blanket module within the extracted coil will also be removed and replaced.

The advantages of such a scheme are listed below:

- Minimal disassembly of reactor components
- Allows two coils/period to be within a common dewar
- Undisturbed vacuum stations within reactor tunnel
- Neutral beams located between access ports will not be disturbed
- External seal on access ports lends itself to many conventional sealing techniques.

B. Modular Stellarator Reactor (MSR) Studies - Los Alamos / Princeton

The Los Alamos/Princeton Modular Stellarator Reactor (MSR) study to date has focused on the development and evaluation of a simplified but general systems model that quantifies the relationship between the performances of plasma (equilibrium and stability beta limits, plasma power density), coils (stress, current density, modularity) and reactor (wall loading, engineering power density, total power, maintainability). Key design parameters for the MSR are summarized in Table II. The procedure used to arrive at this interim design point is elaborated upon in Annex IV.

Parametric trade-off calculations have led to the consideration of an $\ell = 2$, $m = 6$ system with $N = 24$ modular coils. Present understanding of equilibrium and stability limits imposed on the average beta, $\langle\beta\rangle$, for such a configuration allows a marginally acceptable value of $\langle\beta\rangle \sim 0.04$ for a plasma aspect ratio $A = 11$. This relatively low value for $\langle\beta\rangle$ is the key MSR disadvantage identified to date. It is emphasized, however, that the imposed beta limits are conservative. Specifically, the equilibrium limit is determined in the usual manner by equating to the plasma radius the outward toroidal shift of the plasma column as induced by the Pfirsch-Schlüter current and the associated vertical magnetic field. The separate stability limit is simultaneously imposed by gross kink modes associated with diffusion-driven currents. The evolution of an acceptable reactor design point on the basis of these conservative assumptions of equilibrium and stability $\langle\beta\rangle$ limits is viewed as encouraging for the MSR approach.

Positioning of the stagnation-point radius, r_s, behind the nominal combined blanket and shield thickness of ~ 1.5 m allows for a modest, low-shear value of average rotational transform, $\iota \sim 0.66$, which is nonetheless consistent with the value of $\langle\beta\rangle$ cited above. The MSR design is proposed to operate with a pumped-limiter impurity control scheme, rather than with a magnetic divertor acting at the last closed magnetic surface, in order to define the plasma boundary and maximize the volume utilization (i.e., plasma filling factors within the volume enclosed by the first wall) within the first-wall radius, r_w.

Each of the modular coils has a maximum lateral distortion, $d/r_c = 0.3$, which is constrained by the finite coil cross-section required to carry an overall current density in the range 12-20 MA/m^2 and also by the number of coils which must be accommodated in the toroidal configuration. Higher-harmonic coil distortion will be required to achieve values of $\iota \sim 0.66$ beyond the $\iota \sim 0.25$ attainable with the first-harmonic (Rehker-Wobig) coil configuration.

Ignited (i.e., low recirculating power) DT operation with Alcator transport scaling gives a plasma radius, $r_p \sim 1.84$ m, such that the major radius for A = 11 becomes $R_T = 20.2$ m. A fraction $f_\alpha = 0.88$ of the fusion-product alpha-particle power is assumed to be retained in the plasma for self-heating.

The thermal power output of the MSR is 4.0 GWt, and the 14-MeV neutron first-wall loading is 1.5 MW/m^2. Assuming that the thermal conversion efficiency is $\eta_{TH} = 0.35$ and the fraction of the gross electrical power output devoted to plant auxiliary equipment is $f_{AUX} = 0.08$, the net electrical power output of the MSR is $P_E = 1.3$ GWe. No additional recirculating power is required to sustain the ignited plasma. An average plasma temperature of 8 keV and average density of $1.7 \cdot 10^{20}$ m^{-3} result in an on-axis magnetic-field strength $B_o = 6.4$ T. The Lawson parameter is $n\tau_E \sim 3.7 \cdot 10^{20}$ s/m^3.

Dominant coil forces (~ 60 MN) are directed radially outward from the minor axis, with smaller lateral forces (~ 30 MN) acting to increase the lateral coil deformation. Manageable peak stresses are estimated to be ~ 200 MPa, corresponding to ~ 0.1% strain in the internal coil support structure.

An MSR reactor module would consist of a single modular coil and underlying blanket and shield components. Limiter, vacuum and fueling access would occur at the interface between two adjacent modules at the outboard side of the torus. A single coil (including internal structure and thermal insulation) would have a mass ~ 100-200 tonne/coil.

The Los Alamos/Princeton MSR design emphasizes the elucidation of attractive reactor operating points within the constraints imposed by physics and engineering. Towards this goal the design parameters of Table II are being subjected to detailed magnetics and electromechanical analyses that in turn are being performed in conjunction with well-documented goals for first-wall/blanket/shield performance and overall system modularity/maintainability/reliability. As a consequence of this iteration between the simpler analytic approach adopted by the systems model and the more detailed numerical analyses of coil performance, the interim parameters of Table II will develop into a more reliable reactor prognosis for this approach. Additionally, the physics assumptions related to transport, equilibrium and stability are being examined throughout the course of this study in preparation for a detailed conceptual engineering design and economic evaluation of the MSR approach to magnetic fusion energy.

Table II

INTERIM MSR DESIGN PARAMETERS

Stellarator Parameters	
Poloidal field periods, ℓ	2
Toroidal field periods, m	6
Rotational transform, ι	0.66
Average plasma radius, r_p(m)	1.84
Major radius, R_T(m)	20.2
Plasma aspect ratio, $A = R_T/r_p$	11.0
Mean coil radius, r_c(m)	4.58
Coil aspect ratio, R_T/r_c	4.41
Average separatrix radius, r_s(m)	3.98 (~ r_c)
Plasma Parameters	
Radial profile index, ν	3
Average temperature, $\langle T\rangle$ (keV)	8.0
Average density, $\langle n_i\rangle$ (10^{20}/m^3)	1.72
Average beta, $\langle\beta\rangle$	0.04
(Alcator) confinement time, τ_E(s)	2.2
Lawson parameter, $\langle n\rangle\tau_E$ (10^{20}s/m^3)	3.7
On-axis magnetic field, B_o(T)	6.4
Plasma power density, p_F(MWt/m^3)	~3.0
Alpha-particle loss fraction, $1-f_\alpha$	0.12
Alpha-particle partial pressure, p_α/p	0.25
Scrape-off parameter, $x = r_p/r_w$	0.74
Effective charge, $Z_{eff}(n_\alpha/n_i = 0.056)$	1.1
Magnet Parameters	
Number of coils, N(m = 6, ℓ = 2)	24
Coils per field period, N/m	4
Average coil radius, r_c(m)	4.58
Coil current, I_c(MA)	26.9
Coil current density, j_c(MA/m^2)	19.0
Coil lateral distortion, d/r_c	0.3
Coil thickness and width, δ_c(m)	1.19
Peak field at conductor, B_c(T)	~13
On-axis magnetic field, B_o(T)	6.4
Coil volume/mass (m^3/tonne)	44./110.
Stored magnetic energy, E_M(GJ)	~200.
Reactor Parameters	
Total thermal power, P_{TH}(GWt)	4.0
First-wall radius, r_w(m)	2.48
Major radius, R_T(m)	20.2
Plasma volume, V_p(m^3)	1340.
Neutron first-wall loading, I_W(MW/m^2)	1.5
System power density, p_S(MWt/m^3)	0.37
Blanket/shield thickness, Δb(m)	1.5
Blanket energy multiplication, M_N	1.1
Impurity control	pumped limiter

C. T-1 MIT Design

This reactor is a steady-state, large aspect ratio, modular, beam ignited torsatron, possessing natural divertors with continuous helical windings in a nearly force free configuration. With conservative engineering and plasma physics assumptions, this reactor produces 1520 MW_e of electric power with $\bar{n}\tau_E = 3 \times 10^{20}$ sec m^{-3}.

The notable feature of this reactor is that it is modular while possessing continuous near force free helical coils. This is accomplished by having 20 identical modules consisting of demountable coil segments containing the blanket and shield. The coil itself is superconductive but the joints between modules are resistive. The conductors, which are 2 cm wide and 80 cm deep overlap each other at the joint by 40 cm. Calculations indicate that the refrigeration system required to dissipate the heating at the resistive joints can be operated with about 3% of the plant electrical output.

The thickness of the blanket and shield is 1.5 m, adequate for tritium breeding and coil shielding. The blanket consists of subdivided liquid lithium zones cooled by flowing molten salt. The lithium is slowly circulated only to extract tritium. This design is suited for torsatrons where the strong magnetic field will inhibit the rapid flow of a liquid metal.

The shape of the separatrix is such as to divert part of the plasma to recessed wall regions. In these regions charged particle collectors are installed. The resultant neutral gas is pumped out throughout vacuum manifolds outside the blanket.

The reactor is contained within an evacuated enclosure. Disassembled modules are lifted vertically by an overhead crane and then transported circumferentially to an exit hatch. They are then taken to a separate building for disassembly and maintenance while a new module is being installed.

The reactor parameters are listed in Table III.

Table III. T-1 Reactor Parameters

Major coil radius (m)	29.2
Minor coil radius (m)	4.0
Multipolarity	3
Coil current (MA)	36.5
Coil current density (A/cm^2)	3000
Field on axis (T)	5
Max. field on conductor (T)	8.7
Stored energy (GJ)	460
Plasma radius (m)	2.3
Plasma volume (m^3)	3240
Avg. β(%)	3.54
$n\tau_E$(sec m^{-3})	3×10^{20}
Plasma power density (MW/m^3)	1.18
Thermal power output (MW_{th})	4320
Electrical power putput (MW_e)	1500

D. HELIOTRON - Kyoto Design

A pre-conceptual design of a heliotron power reactor has been carried out at the Kyoto Plasma Physics Lab. in Japan.

The magnetic field configuration is for $\ell = 2$ continuous helical coils with no toroidal coils and with a built-in divertor. By choosing the optimum geometry of the helical coil, a high rotational transform and strong shear is obtained. For an estimated maximum β of 0.1 - 0.2, the diffusion remains near the plateau regime of neoclassical theory.

The outstanding feature of this reactor is that it employs a breeding blanket only between the coils. In this way, the coils can be closer to the plasma and thus, presumably would be less costly to build. Obviously the coils still have to be shielded. An extensive neutronic analysis has been carried out where it was determined that the damage to the copper stabilizer will be $\sim 5 \times 10^{-6}$ dpa/yr. The concept of an Internal Spectral Shifter and Energy Converter is used as part of the coil shield. This is in the form of a molybdenum zone 6 cm thick immediately facing the plasma. It was also determined that a breeding ratio of 1.12 can be achieved while using only the blanket regions between the helical coils.

Maintainability of the blanket in the heliotron reactor is assured because of its easy accessibility. A disadvantage of this design is that it makes the coil virtually not maintainable.

Table IV below gives a partial parameter list of the heliotron reactor.

Table IV. Heliotron Reactor Parameter List

Plasma β(%)	10
Avg. neutron wall loading (MW/m^2)	1.0
Distance from plasma to helical coil (m)	1.46
Total thermal power (MW_{th})	4961
Field on axis (T)	3.6
Plasma major radius (m)	20.9
Avg. plasma minor radius (m)	2.09
Plasma ion temp. (keV)	15
Ion density (m^{-3})	1.1×10^{20}

VIII. TASKS

Introduction

1. Reactor Considerations
   Summary of Tasks
2. Plasma Performance
   A. Theory
      Summary of Tasks
   B. Experiments
      Summary of Tasks

Introduction

The stellarator concept offers an immense variety and richness of possible magnetic configurations. Its distinguishing feature is that closed, nested magnetic surfaces are provided in the vacuum by windings outside the plasma. Thus the magnetic topology can be prescribed by the choice of winding configuration. In this section, we draw upon experimental and theoretical results to indicate programmatic directions which should be followed in order to fully develop this concept.

It is, first of all, useful to summarize the topics and questions which have bearing on this program. None of these topics can be considered in isolation. Choices made to improve one aspect of stellarator operation may have an adverse effect on other aspects. In considering these questions, we make extensive use of information and understanding developed in the total magnetic confinement program. A number of questions and problems in stellarator research which appeared to be intractible ten years ago are now well in hand and the program is now ready to concentrate on the unique aspects of stellarators.

VIII.1 Reactor Considerations

The technological and economic problems associated with toroidal fusion reactors have been well defined in the tokamak reactor studies. Proceeding outward from the plasma, we find that conditions of neutron, charged particle, neutral particle, and radiation fluxes at the first wall will be comparable in stellarators and tokamaks. Similarly, the conditions of power deposition and irradiation of the first wall, blanket, and shield are very much the same. Finally, the magnetic field levels and currents in the coils are also comparable. Thus no separate stellarator programs for first wall materials, shield and blanket module development, or basic magnet technology are needed. On the other hand, there are significant large scale differences between stellarators and other toroidal confinement devices. The existence of vacuum magnetic surfaces rests on the presence of a helical component of the current in the confining field coils. This leads to either continuous helical windings or modular coils. Modular coils have the conceptual advantage of allowing possibly easier disassembly of the reactor for repair and maintenance. The principal consequence of the presence of closed vacuum magnetic surfaces is the possibility of steady-state operation of stellarators.

Another feature of stellarators is the presence of a magnetic separatrix which can be used as a divertor for control of impurities, regulation of boundary conditions, and helium ash removal. Although there is still discussion in the tokamak community about the need for a divertor, this discussion is grounded in recent recognition of the difficulty of providing a divertor in the restricted space available. With stellarators, the separatrix is generated with no additional windings. However, there are other questions regarding divertors that must be addressed. In general, the separatrix in a stellarator is not a well defined magnetic surface, but is a volume traversed ergodically by magnetic field lines. The influence of such an ergodic boundary region on reactor plasma operation is unknown, as is its effect on design of the divertor. Furthermore, it may be necessary to place the divertor collector region in the blanket, or to use additional coils to guide the diverted plasma to a more remote collector. Either of these conditions may increase the complexity of the reactor system.

While steady state operation greatly alleviates the effects of cyclic stresses on a reactor structure, it has other implications as well. For example, it may be that the requirements placed on the heating system needed to heat the plasma to ignition temperatures at the start of a burn are eased significantly (e.g., the power needed for startup may be drawn directly from the power net reducing the necessity for large and efficient energy storage systems). Also, the heat removal system for the blanket and first wall may be simpler if the burn time is very long. Other problems associated with long burns need less specific considerations. The questions of fueling, impurity buildup, and ash removal are common to all toroidal devices with burn times exceeding particle confinement times.

Although locally the first wall, blanket and shield of a stellarator may look the same as in a tokamak, the three-dimensional field structure of stellarators influences these reactor elements. In stellarator configurations the plasma shape varies in the toroidal direction. Furthermore, they also can have a large variation of the magnetic field strength along the plasma column. The influence of these variations on wall loading, and on blanket and shield structure should be examined.

Finally there is the question of size. The minor radius of the reactor is determined primarily by plasma confinement and wall loading requirements, but the choice of major radius has a number of interacting constraints. From the point of view of reactor engineering, there are conflicting requirements. There is interest in making the major radius small, in order to reduce the unit size and power output, but the maintainability requirement indicates interest in larger systems. Furthermore, there are indications from theory that plasma performance improves as the aspect ratio is increased. Little experimental information is available as existing stellarator devices all have similar aspect ratios. The dependence of reactor cost and reliability as well as plasma performance on aspect ratio needs to be quantified.

Summary of Tasks: Reactor Studies

i) Determine what constraints are imposed on the physics by reactor technology and economics (e.g., beta limits and confinement margins).

ii) Study the quantitative changes in cost and reliability as the size and scale are varied.

iii) Investigate the feasibility of continuous helical windings.

iv) Examine the feasibility of modular coil systems, including construction, structural support requirements, modular coils and maintenance.

v) Investigate the advantages and disadvantages for divertor design. Consider the possibility of pumped limiters. Determine whether divertor collectors can be placed within the blanket region and, if they are outside, what additional coil systems are needed to study the possibilities and limitations imposed by these two alternate systems.

vi) Design an adequate blanket which accommodates a nonsymmetric plasma column.

vii) Consider the advantage of the low duty cycle of the start-up heating system in reducing cost and reliability requirements.

VIII.2 Plasma Performance

The fundamental goal of any magnetic confinement system with respect to plasma performance is to provide a high beta, stable plasma, with a long enough energy confinement time. There are basically three problem areas: macroscopic equilibrium and stability, transport, and heating. In designing a stellarator to optimize operation in these areas there are a number of variables associated with magnetic topology which can be controlled: aspect ratio, helical periodicity and harmonic content, other magnetic ripples (e.g., due to discrete coils), rotational transform, shear, geodesic curvature, and well depth. It is clear from this list that the option space available for stellarators is much larger that that for tokamaks. It is this feature more than any other which makes the stellarator distinct from the tokamak, and greatly enhances the prospects for significant improvement.

A. Theory

Stellarator theory has been proceeding on a broad front, but progress has been limited largely by the availability of resources and manpower. Both analytic and numerical techniques are available. Because of the complication of the problem and the number of independent parameters that can be varied, it is essential that both approaches, with a great deal of interfacing and interaction, be utilized. The various areas where effort is needed can be catagorized into the usual subjects ; MHD behavior, transport, microscopic behavior,and heating.

The first considerations in MHD studies must concern configuration design, concentrating on properties of the vacuum fields. Analytic considerations of desired magnetic properties (e.g., rotational transform, shear, magnetic well, constancy of $\int d\ell\ /B$ on the magnetic surfaces, harmonic content and magnitude of magnetic field ripples, etc.) provide the incentives and guidance for the studies but the efforts are largely numerical. One successful approach being actively persued is to select a particular field from a set of expansion functions, then to determine the current on a prescribed surface which will give this field, and finally to approximate this with currents in discrete coils. The other is to follow magnetic field lines for specific coil specifications and from this obtain reasonable modular or continuous coils that provide useful magnetic configurations. Although coils can be found to generate any field desired, only certain coil configurations are suitable for either large experiments or for reactor scale devices. In fact, the requirements of these two kinds of systems are different. For reactor scale systems, the ability to vary the magnetic configuration is not needed, but cost and maintainability become primary issues. For experimental research devices on the other hand, the more important considerations are the ability to vary the configuration over a reasonable range of parameters, and access for diagnostics and heating. Therefore, the present attempts to systematize the analyses of stellarator fields need to be expanded in order to determine which regions of parameter space are accessible with realistic windings.

Once the magnetic fields are prescribed, the MHD equilibrium and stability properties can be investigated so as to get an understanding of critical pressures that can be maintained. Again both analytic and numerical techniques must be employed. Harmonic analysis coupled with application of the stellarator expansion, or expansion about the magnetic axis can give some understanding of both equilibrium and stability properties. Three-dimensional numerical codes can also be employed. Because of the need for fine meshes and large amounts of computer time for even a single computer run, these codes can at present primarily provide confirmation or denial of ideas developed from more approximate, analytic, or intuitive models. Use of these codes may be viewed as numerical experiments, which provide detailed information about specific properties of specific stellarator configurations. Clearly more work on developing analytic methods and improving codes is needed, as well as much more application of existing techniques to obtain an understanding of the effect of changing magnetic field parameters. Little effort has been expended on the nonlinear evolution of MHD instabilities. To a large extent, the intuition developed in tokamak research can be carried over to stellarators bodily. An optimistic indication of the prospects for MHD stability of stellarators comes from recent tokamak results with intense neutral beam heating. Although regimes have been reached in which pressure driven ballooning modes are expected to be unstable, it appears that these modes have a soft onset, and do not have a catastrophic effect on confinement. Tokamak and stellarator experiments operate well with a wide variety of unstable modes present, possibly because of the innocuous character of the saturated states of these modes.

Both analytic and numerical studies of transport have been made with an understanding of how they compare and differ only now beginning to emerge. The Monte Carlo transport calculations tend to be more optimistic than the earlier analysis. In particular, the inverse dependence of thermal conductivity on collision frequency is much less severe than that which was predicted by the analytic theory. Preliminary calculations indicate that the behavior of transport coefficients may be even more complex. Their dependence on collisionality may be significantly influenced by the harmonic structure of the confining magnetic field. In this regard, the role of collisionless transitions between different types of particular orbits should be examined in detail. Part of the difference between those numerical and analytic results is that the particles do not stay trapped in the magnetic field ripples as long as assumed in the analysis. Also, much of the enhanced loss is associated with the very high energy particles which were not fully incorporated into the numerical work. Since the plasma behavior is significantly affected by small changes in magnetic topology, it is important that extensive work, both analytic and numerical, be done to clarify the nature of the transport processes.

In this connection, it should be noted that the effect of the ambipolar electric field on transport is large, but a self-consistent treatment of this field has not yet been formulated. Other problems associated with transport which have not been solved include an understanding and estimate of size of the bootstrap current, which could be particularly important for MHD stability considerations, the behavior of trapped particles in systems where the variation of $\int d\ell / B$ in a magnetic surface has been minimized, and the confinement of high energy particles. Analytic techniques developed for treatment of transport in two-dimensional systems as in noncircular tokamaks could easily be generalized to stellarators, although the averaging over the magnetic surfaces at each step to determine the correct diffusion coefficients would probably stretch present-day computers. Because of their three-dimensional character, stellarators will probably have more and larger ergodic regions than tokamaks and a proper treatment of these should be incorporated into the calculations. In this connection, some effort on the microscopic fluctuations and instabilities in stellarators is needed as they will provide some anomalous diffusion.

Theoretical work in the area of radio frequency heating of stellarator plasmas needs considerable expansion. While there are efforts under way on low frequency heating, the influence of the stellarator geometry on heating at higher frequencies should be studied in great detail. As experiments on current free plasmas become more important, it will be necessary to use expensive high power systems efficiently. In particular, the frequency ranges which depend on magnetic field variation, such as electron and ion cyclotron frequency heating, should be examined. These ranges have shown promise in tokamak experiments, and it may be that the stellarator configuration can allow more effective coupling and control of power deposition. Therefore, the influence of geometry on high frequency waves needs detailed study. Similarly, the effect of geometry on the efficiency of neutral beam trapping is very important. As experiments with current-free plasmas become increasingly important, it is essential to have theoretical guidance in the choice and design of the heating techniques.

Summary of Tasks: Theory

i) Investigate the accessible parameter ranges for vacuum magnetic surface properties obtained with reasonable continuous or modular coils (e.g., transform, shear, magnetic well, aspect ratio, field ripple, Pfirsch-Schlüter current, available volume).

ii) Determine how the equilibrium limitations on beta depend on these magnetic parameters.

iii) Study the stability limitations on beta. Investigate the relative importance of magnetic well, and that of ballooning modes. Consider the nonlinear behavior of instabilities.

iv) Determine the single particle containment and transport properties of stellarators. Investigate the importance of reduction of secondary currents for transport. Examine the nature of the neoclassical transport coefficients including their dependence on the toroidal and helical ripples. Study the mechanism for bootstrap current and estimate its magnitude. Study the importance of microinstabilities for providing anomalous transport. Examine the nature and role of self-consistent electric fields. Explain the discrepancy between analytic transport theory and the Monte Carlo calculations.

v) Investigate the effect of stellarator field structure on radio frequency heating efficiency and on neutral beam injection.

B. Experiments

Steady progress has been made in the understanding of the behavior of plasma in medium-sized stellarators, both with ohmic heating and with currentless plasmas. Some of the more important results are listed as follows:

i) Stability. It is known that the application of sufficient external transform inhibits major disruptions in an ohmic-heated plasma. The maximum beta value obtained approaches 1%. If, however, rational ι values are present in a low shear configuration the confinement becomes deteriorated.

ii) Transport. With ohmic heating electron thermal conductivity appears anomalous as in the tokamak, but with lower factors, if the current is small enough. Ion thermal conductivity is only a few times greater than neo-classical. In general, thermal insulation is improved as the ohmic current is reduced.

iii) Non ohmic-heating, i.e., neutral injection and ECRH, has produced hot currentless plasmas with energy containment times as long as predicted by neo-classical theory, but the scaling laws are at present unknown. Some problems have been encountered, however, which make the interpretation of results in current-free plasmas more difficult. These include the effect of impurities, energy deposition profiles, the low density with a consequent difficulty of diagnostics, and the small parameter variation possible. All the recent results have been limited to the plateau regime. There are, however, previous measurements made in small stellarators at reduced plasma parameters which appeared to show agreement with the recent predictions of Monte Carlo code calculations, namely that the effect of helically trapped particles at low collisionality may be less than was previously thought.

The present status of stellarator experiments is such that the program is ready for new experimental investigations at the level of presently operating tokamaks. The questions that need to be addressed are, globally, those of confinement, stability and heating at parameters approaching those needed for a tritium burning device. Thus, the target densities should be of the order of 1×10^{20} m^{-3}, temperatures of the order of a few keV, energy confinement times of the order of 0.1 seconds, and beta values in the range of a few percent.

The selection of a suitable non-ohmic method of effective plasma heating requires some thought, since each technique has its merits and disadvantages. Similarly the choice of configuration, i.e. its shear, transform and optimization properties, is particularly important, since it is intended to study beta limits, stability, transport and trapped particle effects under optimum conditions. In addition, it is desirable to have as large a minor radius as possible, not only to achieve the greatest containment times, but also to ensure that the inner core of the plasma is free of the atomic physics of wall interaction. Furthermore, since a primary advantage of the stellarator is the possibility of steady-state operation, the questions of long pulse operation, impurity accumulation, and divertor operation urgently need study, particularly under zero net current conditions.

This experimental program must confront the increased costs of constructing and operating major facilities. On one hand, experimental investigations are required under a wide variety of conditions and configurations. On the other hand, the resources available are limited, and must be used wisely. It appears, however, that two sequential generations of a small number (relative to the number of major tokamaks) of carefully designed and integrated systems can provide the information needed.

Summary of Tasks: Experiments

i) Determine the transport properties in the long mean free path, net current free regime.

ii) Investigate the experimental limitations on beta.

iii) Optimize the various possible heating mechanisms.

iv) Determine the experimental parameters that affect electric fields in the plasma.

v) Study the mechanism of impurity transport, and develop techniques for control.

vi) Investigate the dominant plasma wall interactions.

vii) Study how a divertor operates.

viii) Measure diffusion driven currents if they exist.

ix) Investigate plasma start-up without ohmic heating.

x) Extend the experiments to steady-state operation (based on the time required to reach equilibrium with the walls).

xi) Investigate the effects of changing magnetic topology, including shear, magnetic well and harmonic content, on plasma confinement.

xii) Demonstrate the feasibility of modular configurations.

IX RECOMMENDATIONS

It follows from the data base documented in this report that the stellarator program is ready to advance and to investigate systems promising further essential improvements. New and major decisions should be taken in the following fields:

A. Experiments

New and modern stellarator devices are required to allow access to regimes adequate for properly investigating the relevant issues. They should incorporate advanced stellarator-configuration ideas or techniques that drive the classical stellarator to its full advantage. They should be able to operate in the collision-free regime and have ample separation between the plasma boundary and the wall. Sufficient heating power must be provided. Utilization of modern diagnostics is essential.

The program should incorporate parallel development and use of several experimental devices and subsequently at least one large feasibility experiment. This should have hydrogen operation with plasma parameters envisaged in a fusion reactor in order to prove the reactor potential of the stellarator.

B. Theory

Configuration studies are producing significant results at an acceptable rate. The level of effort on beta limits and transport properties, with all their three-dimensional implications, is inadequate and needs to be expanded. Adequate manpower and computer time must be provided and a proper balance between numerical and analytic approaches has to be ensured.

C. Reactor Studies

Questions regarding engineering and reactor developments have been, and are, of prime importance for stellarators. Therefore, some stellarator reactor studies with modest industrial involvement are necessary to identify the most essential reactor properties and to provide a focus for the theoretical and experimental programs.

D. Technology

No special technology program is required for stellarators at this time because the basic technologies can be transferred from other parts of the fusion development program. Some small-scale work might be required, however, to include the specific stellarator geometry into these technologies.

ANNEX

I Present Stellarator Devices

II Stellarator Principle

III UWTOR-M, a Conceptual Design Study of a Modular Stellarator Power Reactor

IV The Los Alamos/Princeton Modular Stellarator Reactor (MSR) Point Design

V The T-1 Self Consistent Point Design

ANNEX I

PRESENT STELLARATOR DEVICES

The following is a list of stellarators, operating or under construction as per end of 1980.

NAME	LOCATION	COMMENTS R = major radius; r = radius of last closed magnetic surface B_ϕ = toroidal magnetic field ℓ = number of poloidal field periods
Wendelstein II-A	Bochum, FRG	R = 50cm, r = 5cm, B_ϕ ~ 8kG, ℓ = 2. RF plasma.
Wendelstein II-B	Garching, FRG	R = 50cm, r = 5cm, B_ϕ ~ 7.5kG steady state, 15kG, pulsed mode. ℓ = 2.
Wendelstein VII-A	Garching, FRG	R = 200cm, r = 10 cm, B_ϕ ~ 40kG, ℓ = 2.
Heliotron DM	Kyoto, Japan	R = 50cm, r = 5cm, B_ϕ ~ 10kG.
Heliotron D	Kyoto, Japan	R = 105cm, r = 10 cm, B_ϕ ~ 5kG.
Heliotron E	Kyoto, Japan	R = 220cm, r ≅ 21 - 40 cm, B_ϕ ∿ 20 kG, ℓ = 2.
JIPP-I	Nagoya, Japan	R = 50cm, r = 7cm, B_ϕ ~ 4kG, ℓ = 2 and 3.
JIPPT-II	Nagoya, Japan	R = 91cm, r = 17cm, B_ϕ ~ 30kG, ℓ = 2.
Cleo	Culham, UK	R = 90cm, r = 13.5cm, B_ϕ ~ 20kG, ℓ = 3.
IMS	Madison, USA	R = 40cm, r = 5cm, $B_{\phi\ max}$ = 6kG, ℓ = 3 Modular stellarator, under construction.
Proto-Cleo	Madison, USA	R = 40cm, r = 5cm, B_ϕ ~ 5kG, ℓ = 2 and 3, ℓ = 3 Torsatron
Chrystall-2	Kharkov, USSR	R = 36cm, r = 8.7cm, B_ϕ = 25kG, ℓ = 3 Torsatron, superconducting, under const.
Uragan-II	Kharkov, USSR	Race track of length 1035cm, r = 10cm, B_ϕ = 20kG.
Uragan-III	Kharkov, USSR	R=100cm, r = 17cm, B_ϕ = 30-45kG, ℓ = 3 Torsatron, under construction
Sirius	Kharkov, USSR	Race track of length 600cm, r = 10cm, B_ϕ = 20kG.
Saturn-1	Kharkov, USSR	R = 36cm, r = 8.7cm, B_ϕ = 10kG.
VINT-20	Kharkov, USSR	R = 31.5cm, r = 7.2cm, B_ϕ = 20kG Torsatron, ℓ = 1.
M-8	Kurchatov, USSR	Figure-8 device. r ≅ 8cm.
L-2	Lebedev, USSR	R = 100cm, r = 11cm, B_ϕ = 20kG, ℓ = 2.
R-O	Sukhumi, USSR	R = 50cm, r = 5cm, $B_{\phi\ max}$ ~ 8kG, ℓ = 3.
RT-2	Sukhumi, USSR	R = 65cm, r = 4cm, $B_{\phi\ max}$ ~ 20kG, ℓ = 2.

ANNEX II

STELLARATOR PRINCIPLE

A stellarator is a toroidal magnetic confinement device in which plasma confinement is made by generating closed toroidal magnetic surfaces. Unlike the tokamak however, stellarators generate their confining surfaces entirely by means of currents flowing in external conductors. For a general overview of stellarators in greater detail the reader is referred to the excellent work by Miyamoto [1].

I. Introduction

In order to generate closed magnetic surfaces in a torus to compensate outward drifts and to provide MHD equilibrium, it is necessary to keep the magnetic field lines from closing on themselves after one pass around the torus by introducing a twist in the poloidal direction. Figure 1 shows a coordinate system useful for describing these configurations. We call the angle phi the toroidal angle and the angle theta the poloidal angle.

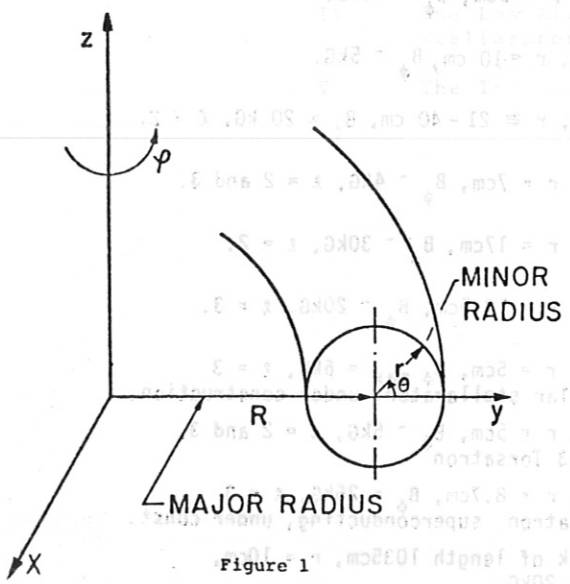

Figure 1

Tokamaks provide the necessary twisting of the magnetic field lines by passing a current in the toroidal direction through the plasma. Stellarators provide the twisting by means of either deformation of the torus itself, e.g., twisting the torus into a Figure 8, or by utilizing a set of twisted helical coils. Figure 2 shows an artist's view of the similarities and differences between a stellarator and a tokamak.

Examination of Figure 2 shows that classical stellarators still require toroidal field coils. This can be seen physically as follows. In the stellarator shown in Figure 2, the currents in adjacent helical windings flow in opposite directions. A qualitative picture of the magnetic fields generated by these helical windings can be obtained by noting that a helical winding is really a loosely wrapped solenoidal winding. That is, a single

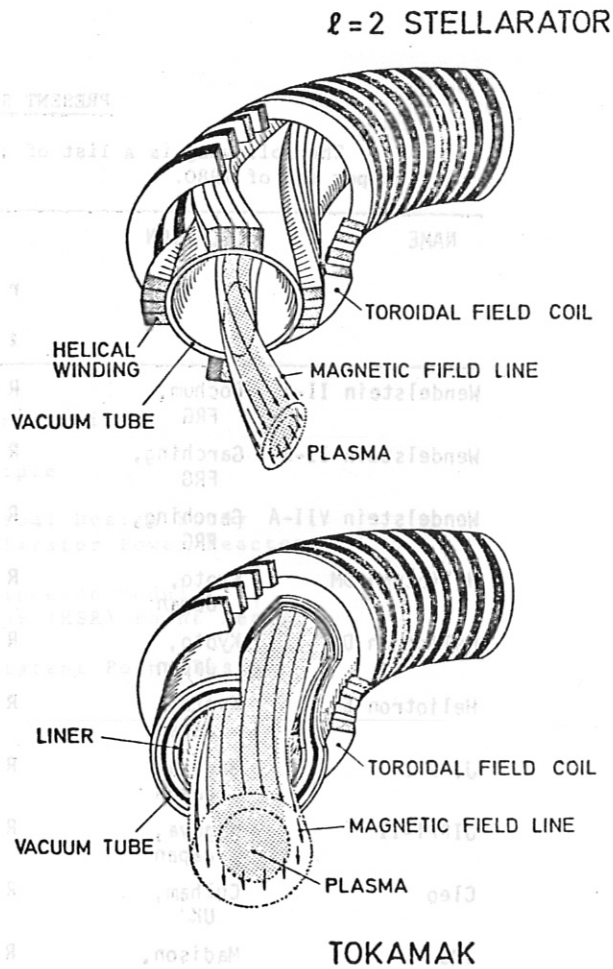

FIG. 2

helical winding generates a toroidal field and vertical field of its own as well as a poloidal field. The vertical field appears because the helix is not only a loosely wrapped solenoid, but a loosely wrapped vertical field coil as well, as can be seen by looking down on the torus. Therefore, currents flowing in opposite directions in adjacent helices (of the same pitch) cancel out each other's vertical fields and toroidal fields on the average. Thus, the need for a separate set of toroidal field coils exists. The toroidal field is needed to provide a magnetic "connection" between adjacent sections of the torus and to provide the basis for generating the toroidal magnetic surfaces.

What is not cancelled from the helical windings are the poloidal fields and fluxes. The combination of the poloidal fields from the helical windings and the toroidal fields from the separate set of toroidal field coils results in a net flux which twists the magnetic field lines as they pass around the torus. Figure 3 shows a trajectory of a field line as it passes around the torus, projected on a fixed poloidal plane. Figure 4 shows the same trajectory looking at the side of the torus. Each time the line moves downward it is passing near a helical coil carrying current in the "+" direction, but there is a net drift of the line in the poloidal

[1] Miyamoto, K., Nucl. Fusion 18 (1978) 243

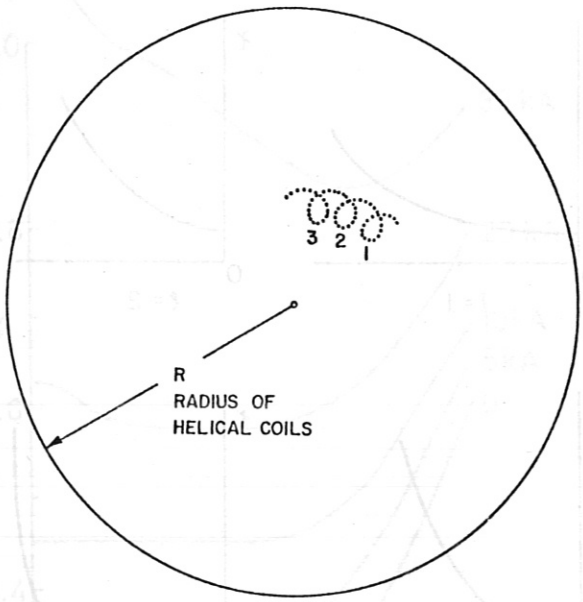

Figure 3

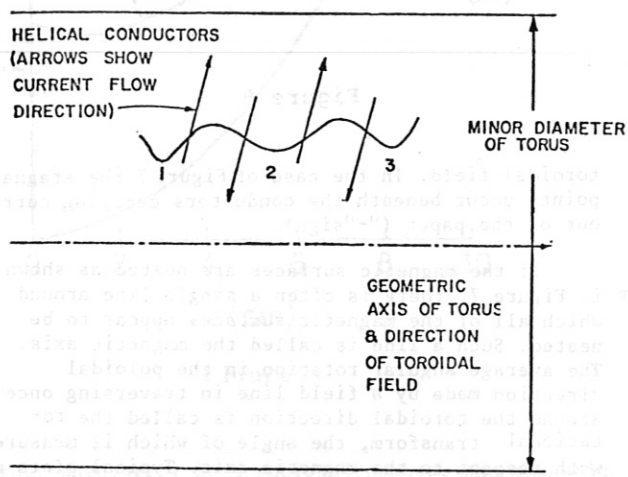

Figure 4

direction in the direction of the "wrapping" of the helical windings. The net drift occurs because the toroidal field of the helical coils alternately adds to or subtracts from the external toroidal field without affecting the poloidal field, thus changing the direction of the field line as shown in Figure 4. If the stellarator windings are designed properly, the magnetic field line can pass many times around the torus before it closes upon itself and can thus generate a toroidal closed surface, which is called a magnetic surface. Figure 5 shows the intersection (and the projection) of the particular field line of Figure 3 with a fixed plane. This intersection is what the magnetic surface looks like at that plane. This surface rotates as the field line moves around the torus as seen in Figure 2. The trajectory of the line always lies between two circles; the inscribed and circumscribed circles of the magnetic surface shown in the Figure. Due to toroidal effects these circles are not concentric, however. Figure 6 is a 3-dimensional plot of the magnetic surface.

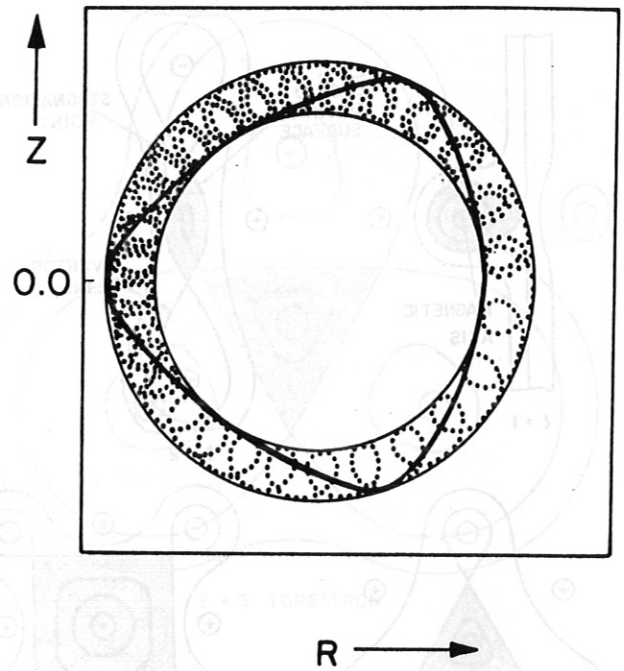

Figure 5

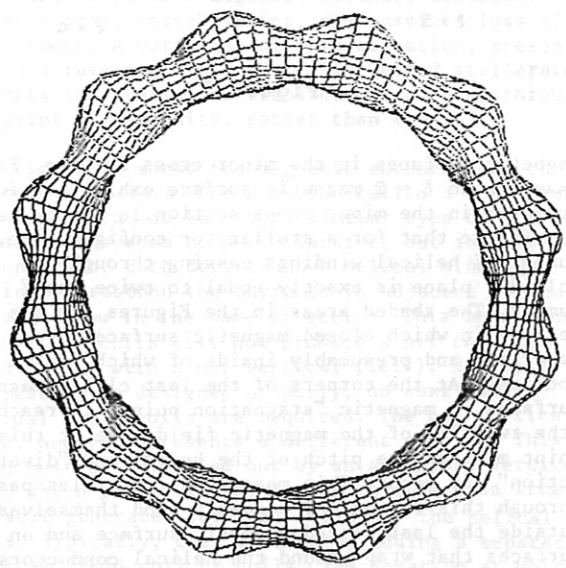

Figure 6

Each magnetic surface is generated by a different magnetic field line. Often the amount of twist of each field line is different from that of other field lines. Optimization of the magnetic configuration will result in a set of nested toroidal magnetic surfaces. Figure 7 shows several types of magnetic surfaces that can be generated by stellarator windings.

The 4 different surfaces in Figure 7 are labelled $\ell = 1$, $\ell = 2$, $\ell = 3$, $\ell = 4$ surfaces, respectively. The ℓ numbers refer to the apparent symmetry of the

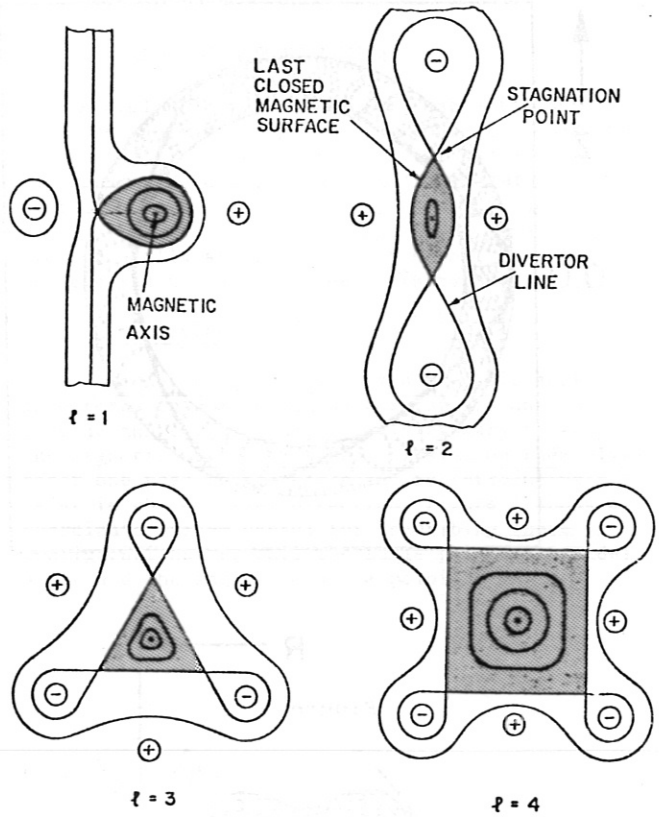

Figure 7

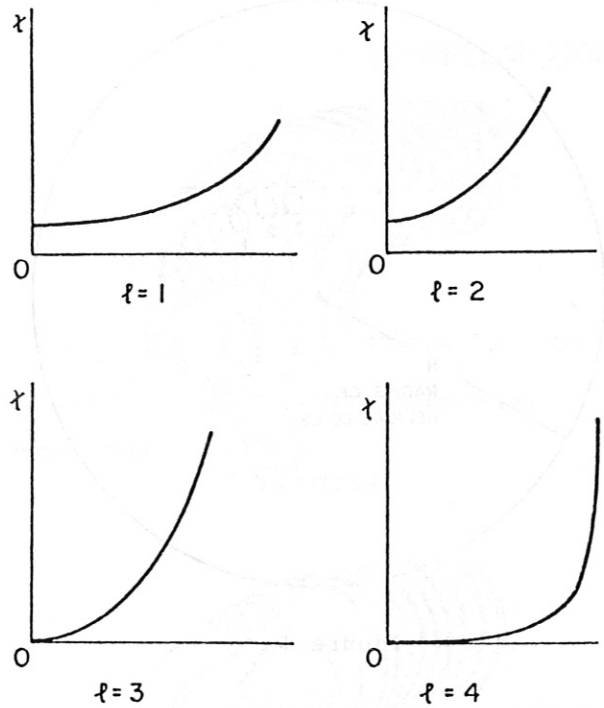

Figure 8

magnetic surfaces in the minor cross section. For example, an $\ell = 2$ magnetic surface exhibits 2-fold symmetry in the minor cross section. It can be seen from the Figure that for a stellarator configuration, the number of helical windings passing through the poloidal plane is exactly equal to twice the ℓ number. The shaded areas in the Figures are the regions in which closed magnetic surfaces are generated and presumably inside of which plasma is confined. At the corners of the last closed magnetic surfaces, a magnetic "stagnation point" is reached, (the twisting of the magnetic field line at this point matches the pitch of the helix) and "divertor action" may occur. This means that particles passing through this region may suddenly find themselves outside the last closed magnetic surface and on the surfaces that wrap around the helical conductors, where they may be collected. Outside of the last closed magnetic surface, the field lines wrap around the individual conductors.

Often, the last closed magnetic surface is called a separatrix. Strictly speaking, however, this only can exist in the limit of infinite toroidal aspect ratio because toroidal effects tend to spread the last closed magnetic surface into a broader region of "ergodic" (not well behaved) magnetic field lines. In Figure 7, the toroidal field is assumed to point out of the paper, and the helical windings wrap from the outside to the inside of the torus over the top of the torus. The signs of the currents refer to their direction with respect to the toroidal field. The net twisting of the magnetic field lines always occurs in the same direction as the wrapping of the helical windings regardless of the direction of the toroidal field. In the case of Figure 7 the stagnation points occur beneath the conductors carrying currents out of the paper ("-"sign).

If the magnetic surfaces are nested as shown in Figure 7, there is often a single line around which all of the magnetic surfaces appear to be nested. Such a line is called the magnetic axis. The average angular rotation in the poloidal direction made by a field line in traversing once around the toroidal direction is called the rotational transform, the angle of which is measured with respect to the magnetic axis. Typical plots of the average rotational transform angle for the four magnetic surface configurations shown in Figure 7 are shown in Figure 8. The transform profiles of the $\ell = 3$ and $\ell = 4$ devices begin at zero transform on the magnetic axis, whereas $\ell = 1$ and $\ell = 2$ begin at non-zero values. In all cases, the transform increases monotonically out to the last closed magnetic surface. Since the $\ell = 1$ and $\ell = 2$ configurations have non-zero transform on the magnetic axis, it is possible to design a device in which the transform is constant out to a very large value of minor radius. Such a configuration is said to have no shear. A convenient definition of the shear parameter is

$$L_s = \frac{R}{2\pi r} \frac{d\iota}{dr}^{-1} \qquad (1)$$

In equation (1) ι is the rotational transform value in radians. Often ι is normalized with respect to 2π and then written as ν. When ν is unity, the transform is 2π and the field line should close upon itself after one pass around the torus the long way, provided that the minor radius of the field line does not change when it completes the pass around the

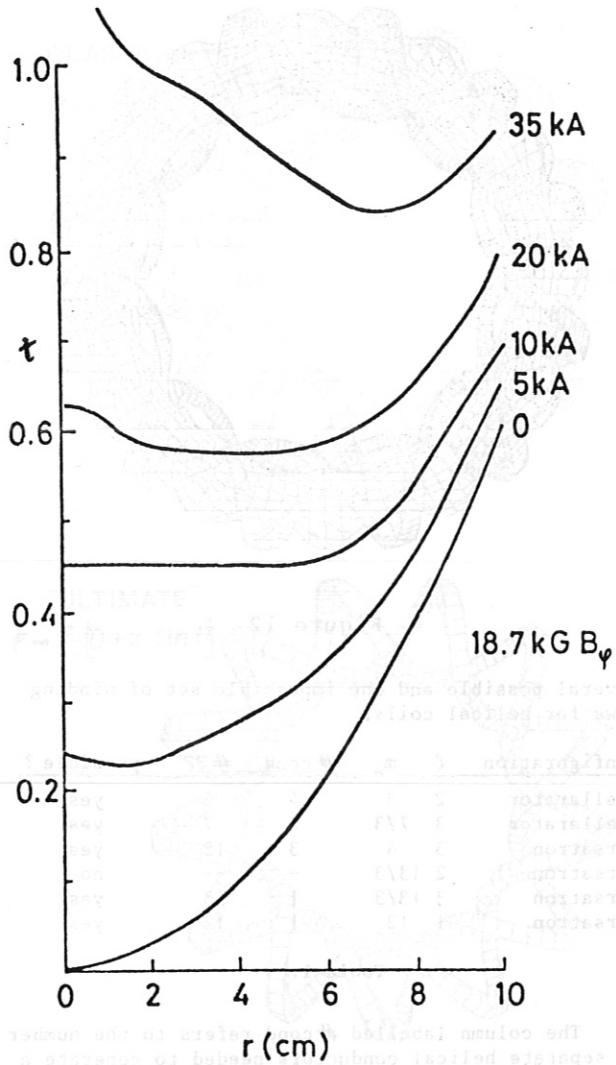

Figure 9

torus. Whenever ι is a rational number, the magnetic field line closes upon itself after a finite number of passes and generates a closed line configuration (not a closed magnetic surface). Often confinement is poor if there is no shear and ι is rational, especially if ι is an integer near unity. With shear, both rational and irrational values of ι appear and confinement tends to be improved.

In contrast to tokamaks, ι increases as minor radius increases. If it is recalled that $q = 1/\iota$ then it can be seen that the q profile for stellarators tends to decrease as minor radius increases. This means that the lowest value of q tends to be on the outside of the plasma, and thus it is fairly easy to avoid q = 1 surfaces appearing inside the plasma, which can lead to instabilities and possible loss of confinement. However, if ohmic heating is added, the transform profile gradually becomes more tokamak-like with increasing ohmic heating current and eventually begins to decrease with minor radius as shown for an $\ell = 3$ stellarator in Figure 9. If the ohmic and helical transforms are made to oppose each other, it is likely that the point $\iota = 0$ will appear inside the plasma away from the magnetic axis. This

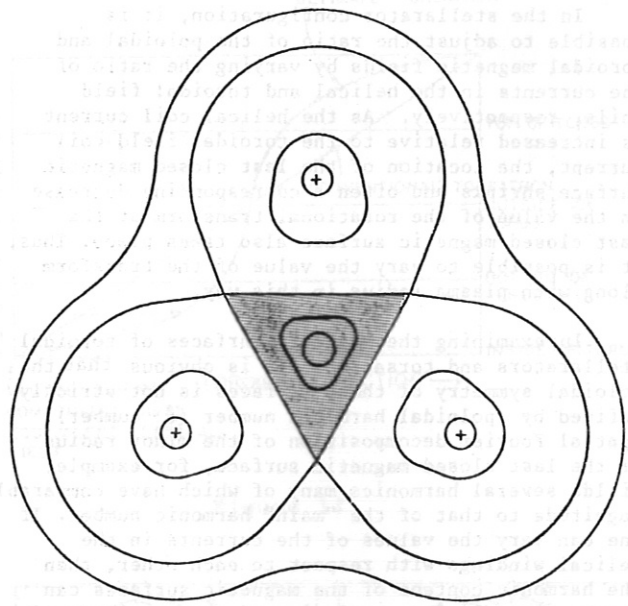

$\ell = 3$ TORSATRON

Figure 10

will tend to produce magnetic islands, secondary magnetic axes, instabilities, and possible loss of confinement. A variation of this situation, presently called a reversed field ohmically heated stellarator, attempts to reverse the transform by passing through the point ι = infinity, rather than $\iota = 0$.

Figure 10 shows the magnetic surfaces and the helical conductors for a device called a torsatron. This configuration is a very similar type of confinement system to a stellarator, but is simpler to construct. Both devices have helical windings, but in a torsatron the currents in adjacent helical windings flow in the same direction. This means that the helical coils will now produce a net toroidal field (along with a net vertical field). Hence, if a torsatron is designed properly, no auxiliary toroidal field coils are required. The net vertical field, however, presents a different problem. This field must be cancelled out by an auxiliary vertical field which points in the opposite direction from the self-generated vertical field of the helical coils. Typically, this is done by adding a separate vertical field coil or coils. The location at which the average vertical field is cancelled defines the magnetic axis. If the vertical field could not be cancelled at this point, the line defining the magnetic axis would not be able to close upon itself after on pass around the torus. If the vertical field coils are located outside of the helical coils and have a radius larger than the maximum major radial position of the helical coils, then the current flowing in the vertical field coils should be oppositely directed to that flowing in the helical coils. If the vertical field coils are located towards the major axis of the torus, then the current must go in the same direction as that in the helical coils. It is also obvious that the currents in the vertical field coils must be comparable to the currents flowing in the helical coils.

In the stellarator configuration, it is possible to adjust the ratio of the poloidal and toroidal magnetic fields by varying the ratio of the currents in the helical and toroidal field coils, respectively. As the helical coil current is increased relative to the toroidal field coil current, the location of the last closed magnetic surface shrinks and often a corresponding decrease in the value of the rotational transform at the last closed magnetic surface also takes place. Thus, it is possible to vary the value of the transform along with plasma radius in this way.

In examining the magnetic surfaces of toroidal stellarators and torsatrons, it is obvious that the poloidal symmetry of these surfaces is not strictly defined by poloidal harmonic number (ℓ - number). Spatial Fourier decomposition of the minor radius of the last closed magnetic surface, for example, yields several harmonics, many of which have comparable magnitude to that of the "main" harmonic number. If one can vary the values of the currents in the helical windings with respect to each other, then the harmonic content of the magnetic surfaces can change. In addition, variation of the magnitude of the compensating vertical field can shift the position of the magnetic axis, change the harmonic content of the magnetic surfaces, and vary the transform profile. Figure 11 shows the Fourier components of the last closed magnetic surface of an $\ell = 3$ stellarator.

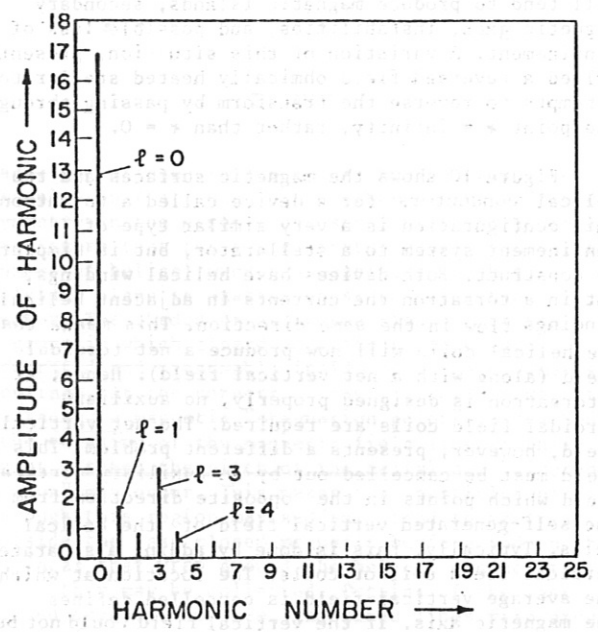

Figure 11

In addition to the absence of a separate set of toroidal field coils, torsatrons also require only half the number of helical coils for the same ℓ number as do stellarators. In fact, it is possible to create a torsatron with only a single helical coil. Typically, a winding law for helical coils is of the form:

$$m_c \vartheta = \Theta \qquad (1)$$

m_c is always a rational number, but not necessarily an integer. For example, Table I lists several possible and one impossible set of winding laws for helical coils.

Figure 12

Configuration	ℓ	m_c	#cond	#FP	possible ?
Stellarator	2	3	4	6	yes
Stellarator	3	7/3	2	7	yes
Torsatron	3	4	3	12	yes
Torsatron	2	13/3	-	--	no
Torsatron	3	13/3	1	13	yes
Torsatron	1	12	1	12	yes

Table I.

The column labelled #cond refers to the number of separate helical conductors needed to generate a complete set of windings. The column #FP refers to the number of field periods, that is, the number of times the magnetic surfaces repeat in going around the major axis of the torus. One field period is not, in general, a 360 degree rotation of the surface, but rather only a poloidal rotation sufficient to have the shape of the surfaces repeat. Figure 12 shows such a set of surfaces in perspective, together with a set of torsatron helical windings. The number of field periods is exactly the product of ℓ and m_c. Any of the stellarator configurations may be turned into a torsatron configuration of the same ℓ number provided that the currents in the adjacent coils are shut off and, of course the toroidal field coils are also shut off and a vertical field is added. (Otherwise the ℓ number would be doubled, if the currents all flow in the same direction). Only a torsatron configuration, therefore, may be wound from a single conductor. Other winding laws, such as constant pitch or other toroidal geodesics are also used, but the basic relationship between the ℓ number and the number of field periods remains the same. If a separate set of toroidal field coils are added to a torsatron such a configuration is called a heliotron.

A further interesting simplification of the torsatron configuration is called the "ultimate" torsatron. The winding law for the helices in the ultimate torsatron differs from that shown in equation (1) in that the pitch is modulated as per the following, but non-unique, relation .

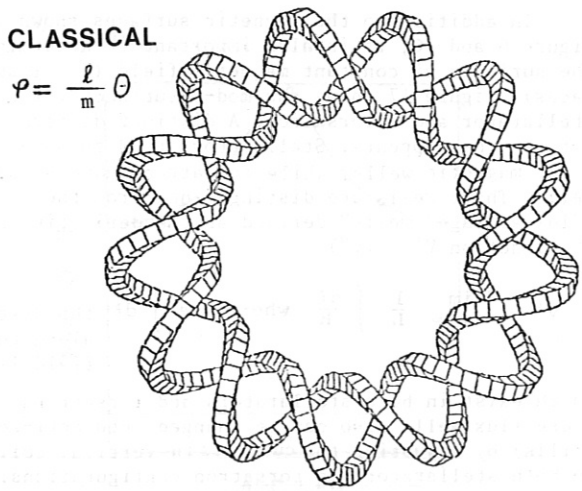

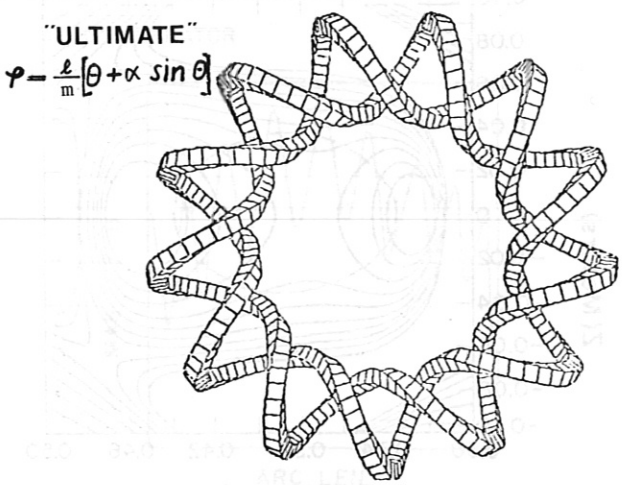

Figure 13

$$m_c \varphi = \theta + \alpha \sin \theta \qquad (2)$$

The purpose of the modulation of the winding law is to produce a net compensating vertical field directly from the helical winding itself. Figure 13 shows the comparison between an ultimate and a conventional torsatron winding. It is clear that the modulation results in a winding that is more like a toroidal field coil on the outside and more like a vertical field coil on the inside of the torus than a conventional torsatron winding. Laying out both of these windings on a graph (Figure 14) in which the horizontal axis is proportional to toroidal angle and whose vertical axis is proportional to poloidal angle, the conventional torsatron winding is a straight line. The ultimate torsatron winding is the sinusoidal waveform shown in the Figure. The top, bottom, inside, and outside of the torus are marked. It can be seen that at the top and bottom of the torus, the direction of the current in the conventional winding is identical to the direction of the current in the ultimate winding. However, at the inside and outside of the torus, the direction of the current in the ulitmate torsatron

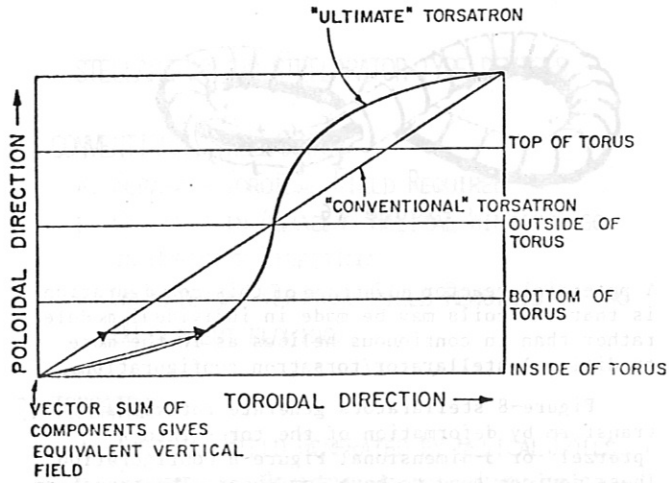

Figure 14

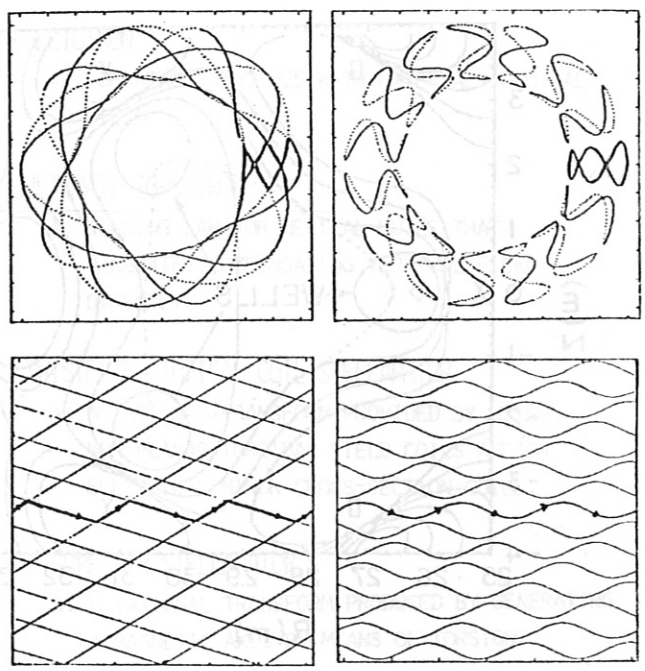

Figure 15

winding differs from the conventional winding in just such a way as to produce a component of current in the same direction as that of an appropriate compensating vertical field coil. This is the case on both the inside and outside, since the net vertical field from both deformed parts is in the same direction. An ultimate torsatron only needs a small vertical field trim coil to be used to vary the transform profile, etc., if desired.

Another method used to produce stellarator configurations is the "twisted-coil" stellarator. Figure 15 shows a plan of a sketch of such a device. Basically, a twisted coil stellarator is made of a set of deformed toroidal coils, that are bent in such a way as to simulate sections of intersecting helices wound with opposite twist and different pitch. The heavy line in the figure corresponds to the traces of the effective helices.

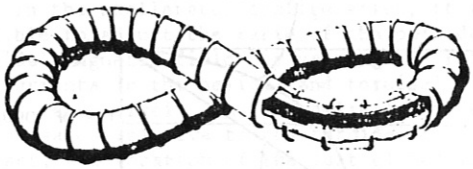

Figure 16

A potential reactor advantage of this configuration is that the coils may be made in individual modules, rather than in continuous helices as in the more traditional stellarator/torsatron configurations.

Figure-8 stellarators generate rotational transform by deformation of the torus into a "pretzel" or 3-dimensional Figure-8 configuration. These devices tend to have low shear. The transform is proportional to the deformation of the torus. A sketch is shown in Figure 16. Extensions of this concept have resulted in stellarators whose magnetic axis varies spatially around a torus.

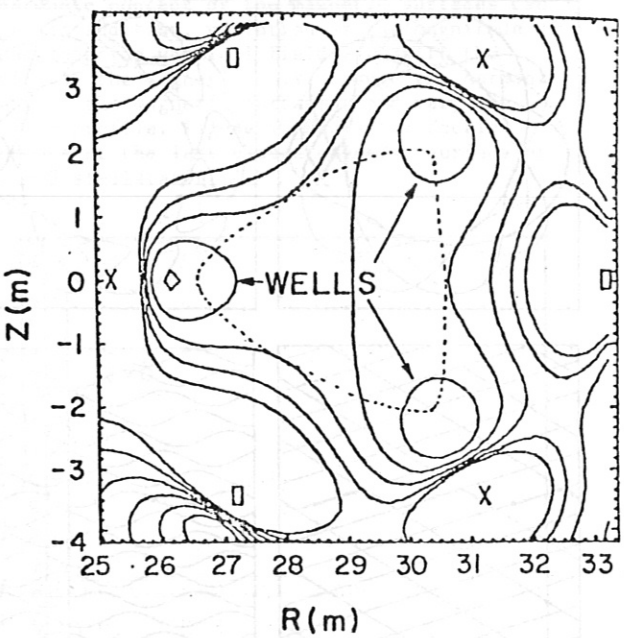

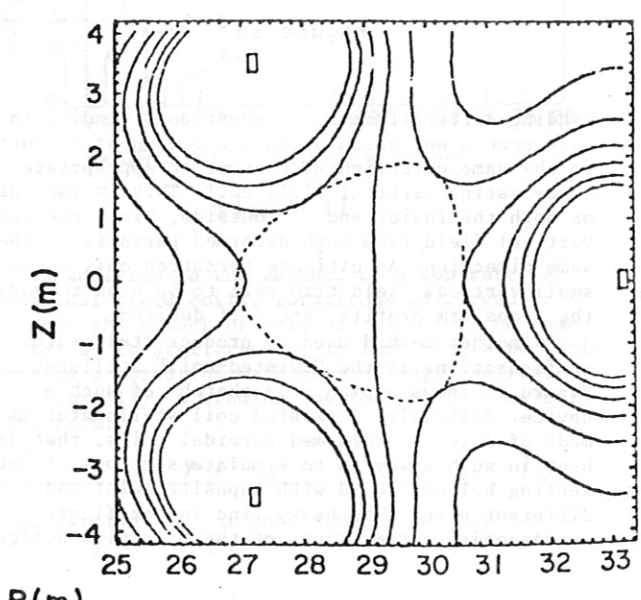

Figure 17

In addition to the magnetic surfaces shown in Figure 6 and 10, it is also important to determine the surfaces of constant magnetic field (mod-B surfaces). Figure 17 shows the mod-B surfaces for a stellarator and a torsatron. A distinct difference between them appears. Stellarators tend to have local magnetic wells, while torsatrons have no such wells. These wells are distinguished from the "flux-averaged wells" defined as the derivative of the function V' (V")

$$V' = \lim_{L\to\infty} \frac{1}{L} \int \frac{d\ell}{B} \quad \text{where } L = \int d\ell \text{ the distance along the field line}$$

which exist in both stellarators and torsatrons. These flux wells also can be changed into anti-wells (hills) by adjusting the currents in vertical coils in both stellarator and torsatron configurations.

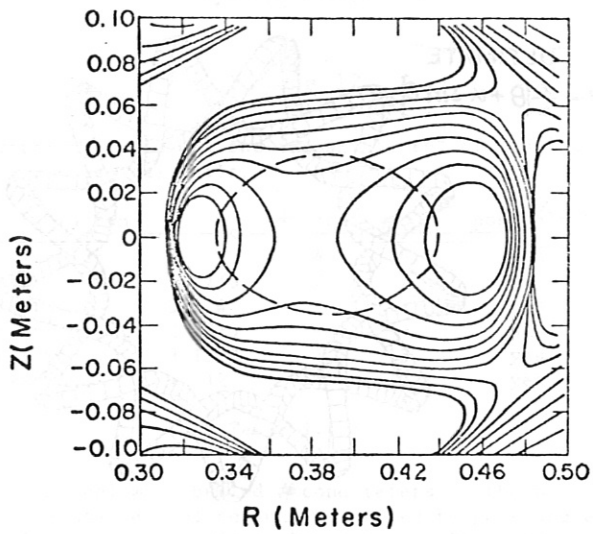

Figure 18

A maximum-B stellarator not only has local wells as shown in the Figure, but will also have a global mod-B surface that is also closed, of roughly the same area as the last closed magnetic surface. This is shown in Figure 18.

A final property of stellarator/torsatrons is observed in examining the value of the magnitude of the magnetic field as a magnetic field line is followed around the torus. Figure 19 shows a comparison between a tokamak, a stellarator and a torsatron.

One can see that a toroidal magnetic mirror appears in all three devices, but the latter two configurations have both toroidal and local mirrors (helical mirrors). Although a tokamak may have ripple that looks like the ripple of a stellarator or torsatron due to the fact that all tokamaks generate their toroidal field from spaced coils, the ripple is really quite different, since only in the case of a stellarator/torsatron is the ripple truly helical. Table II shows a summary of the various stellarator/torsatron configurations discussed in this section.

TOKAMAK

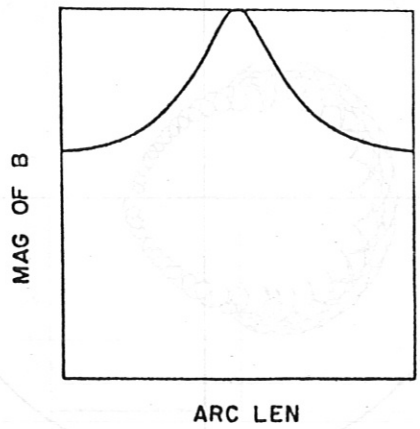

STELLARATOR

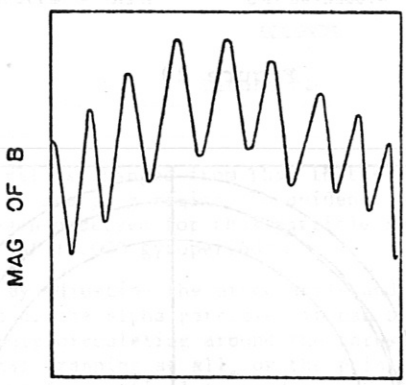

ULTIMATE
TORSATRON

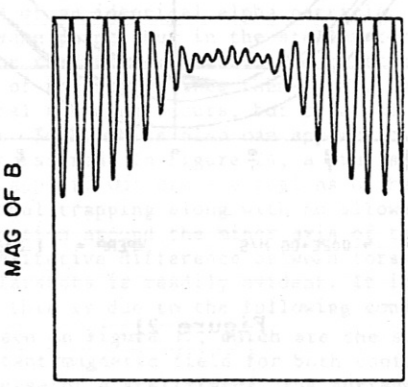

Figure 19

STELLARATOR AND STELLARATOR-TYPE DEVICES

1. CONVENTIONAL STELLARATOR
   - A. SEPARATE TOROIDAL FIELD REQUIRED
   - B. CURRENTS IN ADJACENT HELICAL WINDINGS GO IN OPPOSITE DIRECTIONS
   - C. NO EXTERNAL VERTICAL FIELD REQUIRED (IF NO OH CURRENT FLOWING)

2. TORSATRON
   - A. TOROIDAL FIELD GENERATED BY HELICAL COILS
   - B. CURRENTS IN ADJACENT HELICAL WINDINGS GO IN SAME DIRECTION
   - C. EXTERNAL VERTICAL FIELD REQUIRED

3. HELIOTRON
   - A. TORSATRON WINDINGS WITH EXTERNAL TOROIDAL FIELD

4. ULTIMATE TORSATRON
   - A. WINDING LAW FOR HELICAL COILS THAT GENERATES COMPENSATING VERTICAL FIELD DIRECTLY

5. TWISTED/ELLIPTICAL COIL STELLARATOR
   - A. ROTATIONAL TRANSFORM PROVIDED BY USING NON-PLANAR TOROIDAL FIELD COILS AND/OR ELLIPTICAL MINOR CROSS-SECTION COILS.

6. FIGURE - 8 STELLARATOR
   - A. ROTATIONAL TRANSFORM PRODUCED BY GENERATING A MAGNETIC AXIS BY MEANS OF TORSION.

7. MAXIMUM-B STELLARATOR
   - A. IN ADDITION TO THE CLOSED MAGNETIC SURFACES, CLOSED SURFACES OF CONSTANT-B CONTOURS ARE GENERATED, ALONG WITH LOCAL MAGNETIC WELLS. IMPROVES CONFINEMENT OF TRAPPED PARTICLES AND PROVIDES PATH TO CYCLOTRON RESONANCE IN INTERIOR OF PLASMA.

Table II

II. Particle orbits in stellarators and torsatrons

In order to compute particle orbits in non-axisymmetric devices as stellarators and torsatrons, it would be very helpful to have some kind of ignorable coordinate. As yet, such ignorable coordinates have not been found for stellarator and stellarator-type devices. As a result, to compute the orbits, it is necessary to solve the equation of motion for charged particles in the magnetic field configuration desired. Usually, the energy and the magnetic moment of the particle can be assumed constant so that a guiding center approximation can be made. However, in this section, we do solve the full Lorentz equation of motion for alpha particles in both a stellarator and a torsatron reactor.

A qualitative description of the orbits in stellarators and torsatrons will now be undertaken. Basically, three types of orbits should be present. The first type are circulating particles, as in the case in a tokamak, i.e., particles that pass entirely around the torus without making a reflection. The second type, helically trapped particles, reflect in the local mirrors of the helical field, and finally,toroidally trapped particles (bananas) that reflect (as is also the case in a tokamak) in the mirrors of the toroidal field. It is possible for a particle to exhibit some or all of the characteristics of these three types of orbits at various times and positions in the device. A helically trapped particle that is also toroidally trapped is called a "super-banana" particle. Helically trapped particles are sometimes called helical bananas while purely toroidally trapped particles are the same as "banana" particles in tokamaks. The trapping of charged particles in the various ripples of the magnetic field is an important consideration in studies of particle and energy transport in stellarators and torsatrons. Naturally, the collision frequency of the charged particles must be low enough so that evidence of helical and/or toroidal trapping can be seen. If this is not the case, the transport properties differ but little from that of a tokamak. The orbits calculated for stellarators and torsatrons in this section are for devices that are of such size as might be possible fusion reactors. The orbits are those of 3.5 MeV alpha particles. The basic orbit types, however, exist in scaled-down geometries as well. The magnetic surfaces and rotational transforms for both devices were made as nearly identical as possible in order to determine whether qualitative differences exist between the two configurations. It is found that the nature of the orbit of the 3.5 MeV alpha particles is primarily determined by the pitch angle of the particle and its launch point.

Figure 20 shows the poloidal projection of an alpha particle orbit for the torsatron geometry. The figure shows helical trapping on the inside of the torus, and no trapping on the outside of the torus. Thus this orbit is partly circulating. The circular paths in the untrapped region correspond closely to the rotations of the magnetic field line as it passes around the torus in the toroidal direction. Figure 21 shows a toroidal projection of the same orbit. The region of helical trapping is clearly evident. In particular, it can be seen that this alpha particle is trapped in one particular helical ripple, but when it is not helically trapped it drifts entirely around the torus. A plot of the

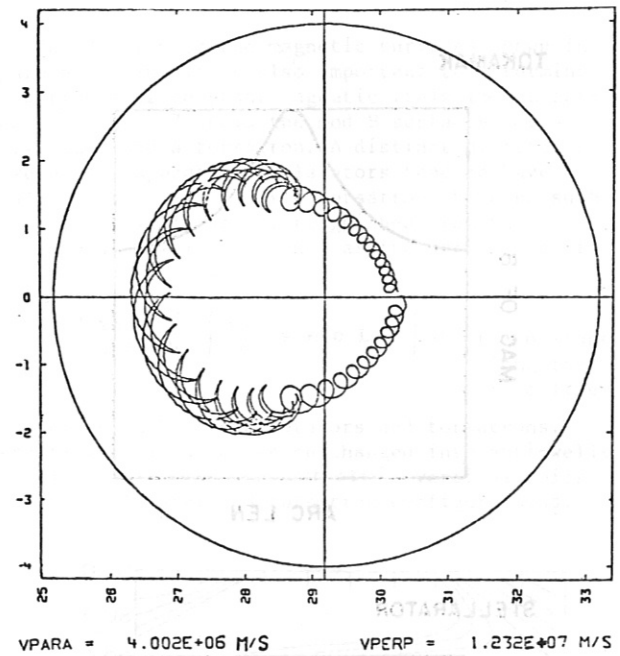

Figure 20

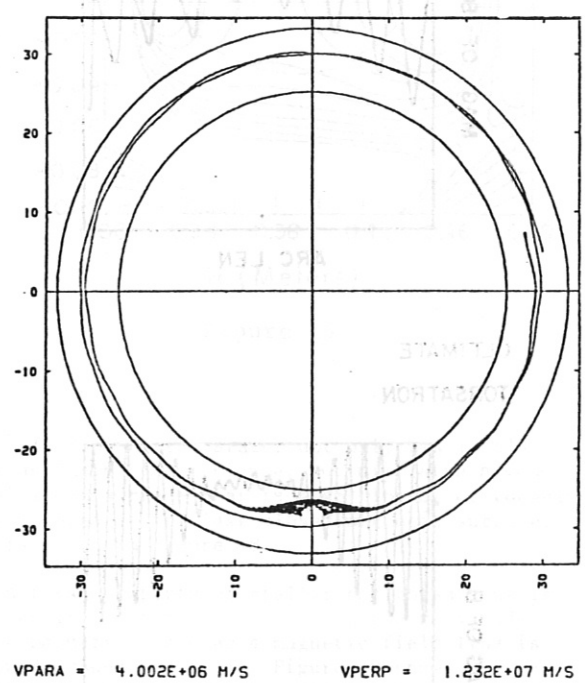

Figure 21

action, J, defined as $\oint M V_{\parallel} dV_{\parallel}$ over a helical bounce shows that it is conserved only when the particle is helically trapped and not conserved when it is untrapped (Figure 22). If the action was always conserved it could provide an ignorable coordinate. Furthermore, when the alpha particle enters a new region of helical trapping, the value of the action

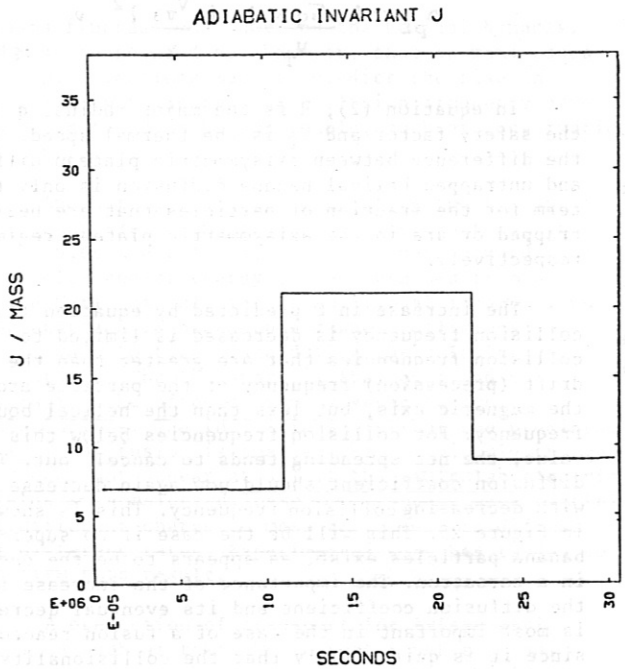

Figure 22

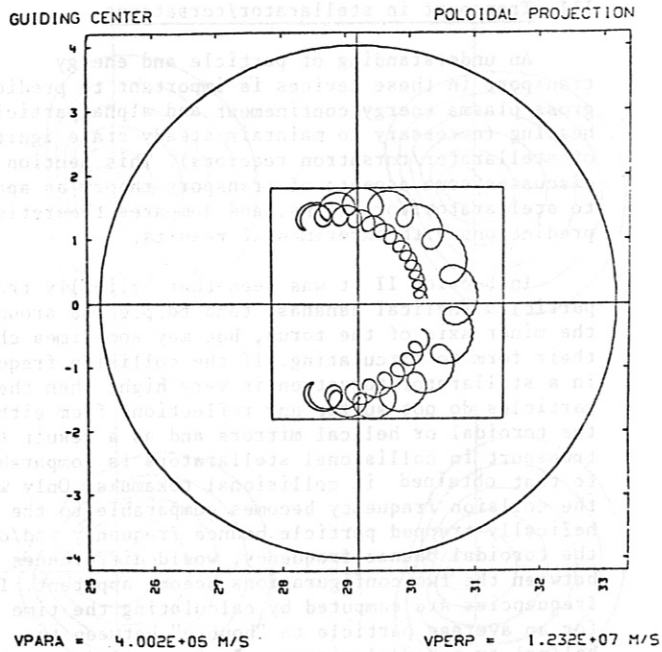

Figure 23

integral is changed from that in the previous helical trapping region. No evidence of outward drift has been observed for this particle for times of the order of 12.000 gyroperiods.

By adjusting the pitch angle and/or the launch point of the alpha particle, it can be made to be entirely circulating around the torus, with no helical trapping at all, or the point at which it changes from helical trapped to circulating can be changed. For this geometry, no orbit was found that was toroidally trapped as well as helically trapped. Thus, super-banana orbits do not appear to exist in the torsatron configuration.

A comparison with the equivalent geometry for a stellarator can now be made. Figure 23 shows the orbit of an identical alpha particle, launched at the same point, but in the stellarator rather than in the torsatron geometry. The twisting shown is that of the field lines themselves. Here, no helical trapping occurs, but toroidal trapping does occur. Such orbits also can appear in the case of the torsatron. In Figure 24, a true super-banana does appear. One can see regions of helical and toroidal trapping along with no allowed complete precession around the minor axis of the torus. Thus, a qualitative difference between torsatrons and stellarators is readily evident. It is believed that this is due to the following condition which is seen in Figure 17, which are the surface of constant magnetic field for both configurations. In the case of a stellarator, the surface of constant magnetic field have local magnetic wells, in which the helically trapped particles can be reflected, thus making super-banana. Such wells are readily seen to be absent in the case of a torsatron.

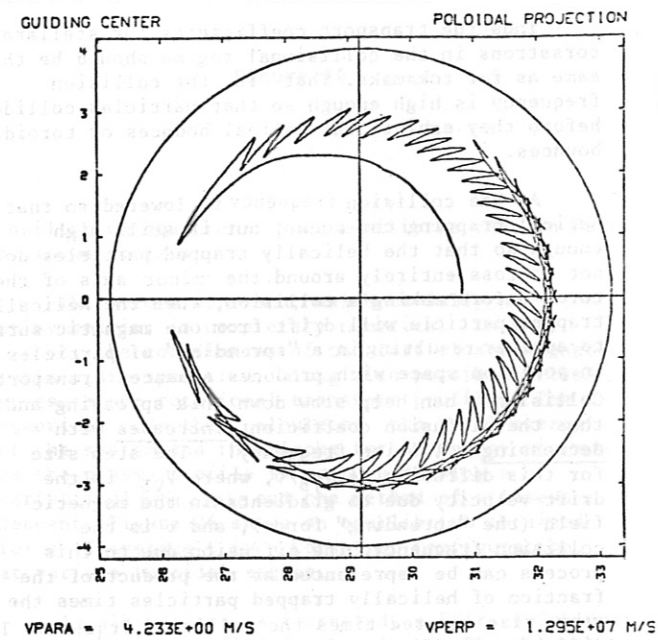

Figure 24

III. Transport in stellarator/torsatrons

An understanding of particle and energy transport in these devices is important to predict gross plasma energy confinement and alpha particle heating (necessary to maintain steady state ignition of stellarator/torsatron reactors). This section discusses some aspects of transport theory as applied to stellarator/torsatrons, and compares theoretical predictions with experimental results.

In Section II it was seen that helically trapped particles (helical bananas) tend to precess around the minor axis of the torus, but may sometimes change their form to circulating. If the collision frequency in a stellarator/torsatron is very high, then the particles do not suffer any reflections from either the toroidal or helical mirrors and as a result the transport in collisional stellarators is comparable to that obtained in collisional tokamaks. Only when the collsion frequency becomes comparable to the helically trapped particle bounce frequency and/or the toroidal bounce frequency, would differences between the two configurations become apparent. The frequencies are computed by calculating the time for an average particle to "bounce" between the helical or toroidal mirrors. In fact, if one could construct a straight stellarator, toroidal effects disappear, and it has been shown that the transport in such devices is theoretically equivalent in form to that of a toroidal tokamak.

Thus the transport coefficients for stellarator/torsatrons in the collisional regime should be the same as for tokamaks. That is, the collision frequency is high enough so that particles collide before they exhibit the helical bounces or toroidal bounces.

As the collision frequency is lowered so that helical trapping can occur, but is still high enough so that the helically trapped particles do not precess entirely around the minor axis of the torus before making a collision, then the helically trapped particle will drift from one magnetic surface to another resulting in a "spreading" of particles in position space wich produces enhanced transport. Collisions, can help slow down this spreading and thus the diffusion coefficient increases with decreasing collision frequency! The step size for this diffusion is $V_{\nabla B}/\nu$, where $V_{\nabla B}$ is the drift velocity due to gradients in the magnetic field (the "spreading" force), and ν is the collision frequency. The diffusion due to this process can be represented as the product of the fraction of helically trapped particles times the step size squared times the collision frquency. The diffusion coefficient is thus:

$$D_\nu \sim \left[\epsilon_h^{3/2}\ \epsilon_t^2\right] \left[\frac{V_{\nabla B}}{\nu}\right]^2 \nu \qquad (1)$$

ϵ_h is helical modulation amplitude. Equation (1) shows that the diffusion coefficient is proportional to the square of ϵ_t, the toroidal modulation amplitude. The $1/\nu$ dependence goes away in the limit of infinite aspect ratio, since under this condition ϵ_t approaches zero. Equation (1) is very similar in form to the plateau diffusion coefficient in axisymmetric devices. For the axisymmetric case the corresponding expression is approximately

$$D_{p\ell} \sim \left[\frac{\sqrt{\pi} qR\nu}{V_T}\right] \left[\frac{V_{\nabla B}}{\nu}\right]^2 \nu \qquad (2)$$

In equation (2), R is the major radius, q is the safety factor and V_T is the thermal speed. Thus, the difference between axisymmetric plateau diffusion and untrapped helical banana diffusion is only the term for the fraction of particles that are helically trapped or are in the axisymmetric plateau regime, respectively.

The increase in D predicted by equation (1) as collision frequency is decreased is limited to collision frequencies that are greater than the drift (precession) frequency of the particle around the magnetic axis, but less than the helical bounce frequency. For collision frequencies below this value, the net spreading tends to cancel out. The diffusion coefficient should now again decrease with decreasing collision frequency. This is shown in Figure 25. This will be the case if no super-banana particles exist, as appears to be the case in a torsatron. The importance of the increase in the diffusion coefficient and its eventual decrease is most important in the case of a fusion reactor, since it is quite likely that the collisionality of such devices may place them well into the region of increase and eventual decrease in diffusion. It is important for future experiments to investigate this regime in detail.

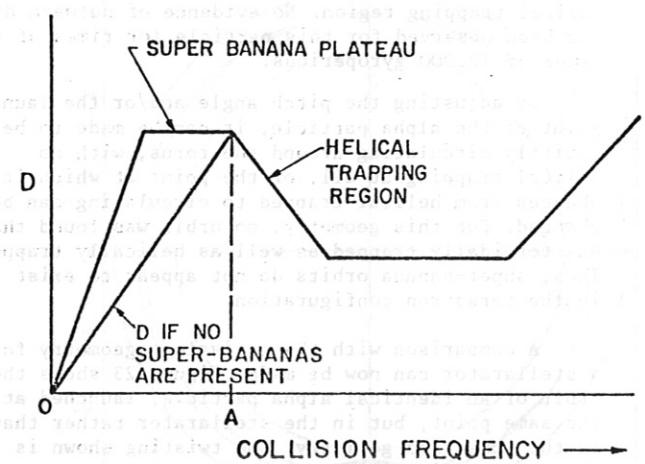

Figure 25

In the case of a stellarator, with super-bananas being present, the diffusion coefficient will not decrease directly, but will probably exhibit a super-banana plateau and then decrease. This is also shown in Figure 25. The decrease in the diffusion coefficient for a stellarator begins approximately at the super-banana bounce frequency.

Thermal diffusion exhibits a similar dependence on collision frequency as does the particle diffusion. However, like particle collisions, rather than unlike particle collisions, tend to dominate the thermal transport. The increase in diffusion in the helical banana regime has been discussed by many authors although several have predicted that it will not be serious in the reactor regime, because either ambipolar electric fields limit the transport, or

plasma fluctuations "untrap" the helical bananas. It must be pointed out however, that in many cases the approximations made to predict the rise in diffusion with decreasing collision frequency have not been found to be applicable, such as conservation of action.

Another approach to calculating the transport is to utilize a numerical procedure. That is, once the orbits are calculated, then a net outward flux particles and/or energy can be obtained from a Monte-Carlo calculation of collisonal interactions. The approach is based upon random collisions being made to take place during the calculation of the orbits. The transport is then obtained by averaging the effects on many separate orbit calculations. The indications are that the predicted rise in diffusion is smaller than previously thought and does not appear at all if the ambipolar electric fields are considered. These fields appear when particles of different charge to mass ratio tend to diffuse at different rates. Experimental work has tended to confirm this result.

A prediction of transport for axisymmetric devices such as tokamaks is that a net toroidal current, termed the bootstrap current, should be driven by diffusion especially in the collisionless regime. It is a consequence of the conservation of angular momentum about the major axis of the torus of the individual particles. In a non-axisymmetric device such as a stellarator, however, the angular momentum of the individual particles is not conserved, and thus the bootstrap current may not exist. The simplest way in which one could attempt to measure the bootstrap current in any toroidal configuration is to operate it as a net-current-free device in the collision-less regime. At this moment, only small stellarator devices have been operated in this way . As yet, no bootstrap current has ever been seen, even though the devices could be operated well into collisionless regime. It remains a goal of the next generation of these devices to search further for the current.

IV. MHD equilibrium and stability

Often the approach to designing a new stellarator/torsatron experiment is to begin with a desired vacuum magnetic field configuration. However, since the main goal of these configurations is the confinement of plasma at a reasonable β it must be determined whether the plasma can exist in MHD equilibrium for non-zero plasma β and whether that equilibrium is stable.

In the case of axisymmetric devices, it is possible to mathematically prove the existence of MHD equilibria. For non-axisymmetric configurations, however, such a proof remains to be discovered . However, as has been pointed out, the non-existence of the equilibrium may result in loss of equilibrium at such a small rate that it can be ignored in practice.

Two approaches towards calculation of the equilibrium have been and are currently under study. The first, an analytic method utilizes expansion of the magnetic field properties about the magnetic axis, and/or an ordering of the fields so as to develop a set of linearized

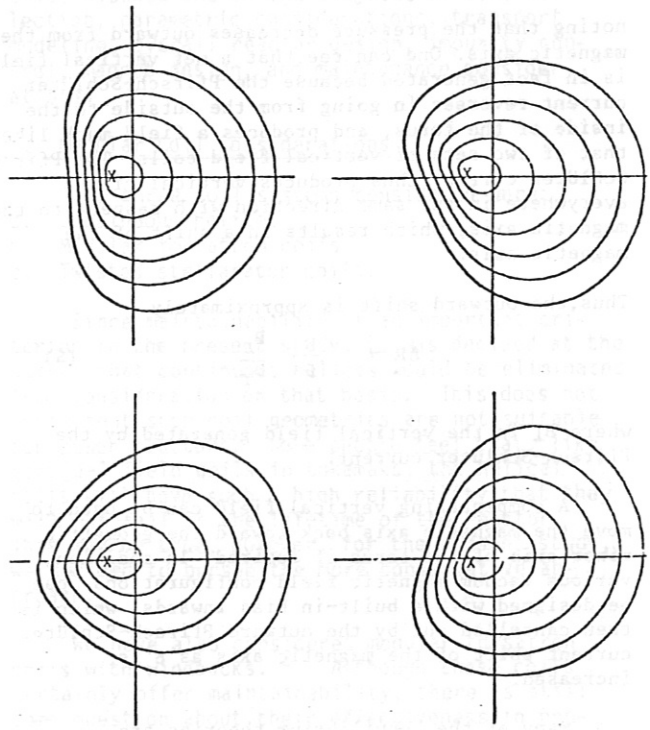

Figure 26

equilibrium equations. Such equilibria can, in fact, be shown to exist.

The second approach, which is fully non-axisymmetric, is completely numerical. In this method, the coordinates of the last closed magnetic surface are specified, along with possible plasma pressure and rotational transform profiles. The numerical code then calculates the total energy of the system and then looks for an energy minimum as the plasma profile is perturbed using a variational principle and the method of steepest descent. Figure 26 shows an equilibrium obtained for a 1% average β in a torsatron configuration, at various toroidal angles.

As plasma beta is increased, a Pfirsch-Schlüter current begins to flow in the plasma. The current is toroidal, but does not have a net value, and is, in rough approximation, of the form:

$$J_{Ps} = \frac{2}{r} \frac{1}{B_T} \frac{\partial p}{\partial r} \cos\theta \qquad (3)$$

p is the plasma pressure, and θ is the poloidal angle. The flow of this current generates a self-vertical field that can move the magnetic axis of the configuration outward, much like the application of an external vertical field. The Pfirsch-Schlüter current is a consequence of the existence of toroidal equilibrium, since it is obtained by solving the time indenpent MHD equilibrium equation:

$$\nabla_p = \bar{J} \times \bar{B} \qquad (4)$$

noting that the pressure decreases outward from the magnetic axis. One can see that a net vertical field is in fact generated because the Pfirsch-Schlüter current reverses in going from the outside to the inside of the torus, and produces a field much like that of two sets of vertical field coils. The Pfirsch-Schlüter current thus produces vertical fields everywhere in the same direction with respect to the magnetic axis, which results in a shift of the magnetic axis.

Thus, the outward shift is approximately

$$\Delta R = \frac{R}{\ell} \frac{B_\perp}{B_T} \qquad (5)$$

where $B_\perp$ is the vertical field generated by the Pfirsch-Schlüter current.

A compensating vertical field can be used to move the magnetic axis back toward the geometric minor axis of the torus if desired. In addition, various vacuum magnetic field configurations can be designed with a built-in bias inwards, which is then cancelled out by the outward Pfirsch-Schlüter current shift of the magnetic axis as β is increased.

Many of the equilibrium theories are considering the effects of increases in beta on equilibrium to determine the critical (maximum) beta for stellarators. Such calculations are necessary both in the design of new experiments, the determination of whether beta may be increased in existing devices, and the eventual size of stellarator fusion reactors.

Knowledge of the maximum beta for equilibrium is not enough, however. Various MHD instabilities may also appear so that an equilibrium, even if it can be shown to exist, may be unstable above a certain value of beta. The numerical and analytical methods described above often can examine the growth rates of various MHD modes as it solves for the equilibrium.

An important theoretical prediction that may limit the beta in stellarators is the onset of a special type of MHD mode called a "ballooning" mode. This mode usually appears in regions of "bad curvature" of the magnetic surfaces. Bad curvature is said to exist wherever the magnetic field lines are curved concave toward the plasma. Typically, the bad curvature region appears on the outside of the torus. This is because the magnetic field decreases outside of the plasma region on the outside of the torus and thus perturbations of plasma tend to grow outward and destroy the equilibrium. The growth of the ballooning modes is often predicted to occur fastest for those wavelengths that are the longest. In this case, the longest wavelength is that distance covered by the magnetic field line in going from a region of good curvature and back to a region of good curvature. In a tokamak this distance, often called the connection length is approximately:

$$\frac{\pi r B_T}{B_p}$$

and is usually greater than the major circumference, $2\pi R$.

Stellarators, normally being devices of somewhat higher aspect ratio than tokamaks would probably have a longer connection length , as defined above, and thus would be considered to be more unstable to ballooning mode growth than tokamaks.

However, if the dot product of the actual curvature vector with the outward normal for the plasma is actually calculated, at least in the case of a torsatron, the connection lengths are actually quite short, of the order of one field period. Figure 27 shows a plot of this quantity for such a configuration as a function of distance along the magnetic field line. It can be seen that "good" and "bad" curvature regions alternate over short distances. Thus, stellarator/torsatrons may actually be more stable against ballooning mode instabilities than previously thought.

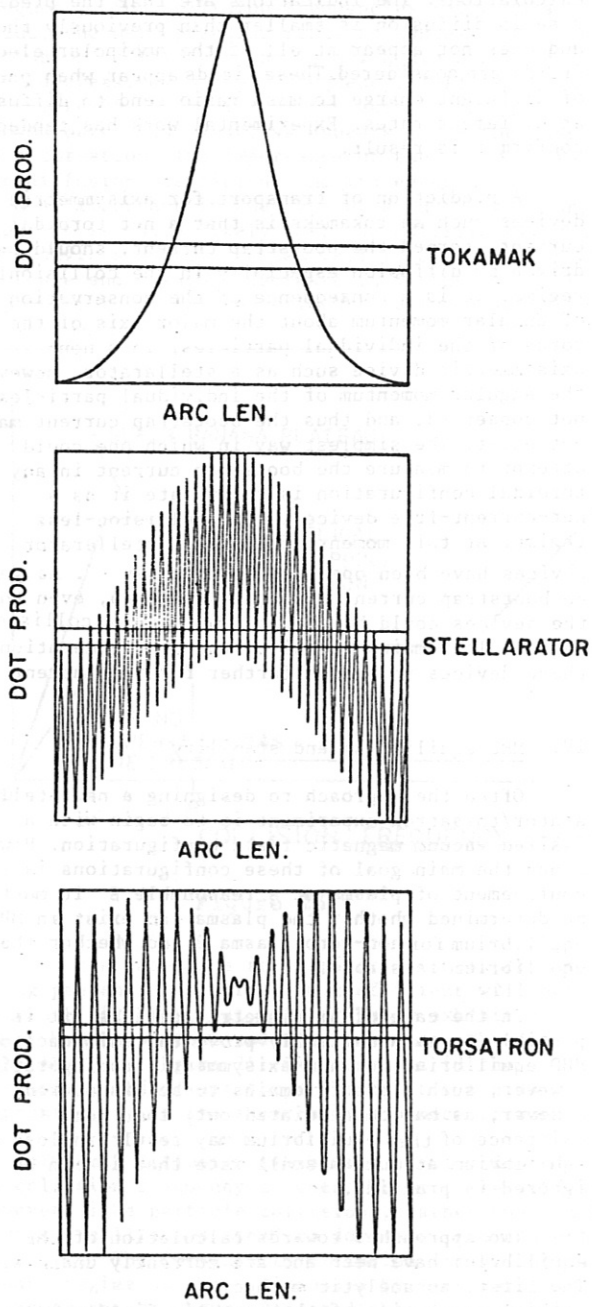

Figure 27

ANNEX III

UWTOR-M, A CONCEPTUAL DESIGN STUDY OF A MODULAR STELLARATOR POWER REACTOR

Abstract

A preliminary design of a 5500 MW_{th} modular stellarator power reactor, UWTOR-M, is presented. Discrete twisted coils are used in an $\ell = 3$ configuration with maintainability as a prime consideration. The natural stellarator divertor is used for impurity control in conjunction with innovative high performance divertor targets. A unique blanket design is proposed which minimizes the overall tritium inventory in the reactor. Finally, a scheme for maintaining the first wall/blanket and other reactor components is discussed.

Introduction

Although the stellarator is one of the earliest proposed magnetic confinement concepts, having been invented in the early fifties, it wasn't until recently that it started to gain recognition in the fusion community. In large measure, this is due to recent encouraging experimental results which show that confinement in a stellarator does not degrade, but in fact improves, when the net plasma current is reduced to a near zero value.[1] These experimental results also verified that above a rotational transform of ~ 0.3, the stellarator does not experience plasma disruption.

In a separate development a breakthrough seems to have taken place in the area of magnets for stellarators. A major early drawback of the stellarator has been the need for continuous helical coils augmented with toroidal field coils making maintainability of both coils and blanket extremely difficult. Recent innovations have shown that the toroidal field coils can be eliminated by using two helical coils of different pitch and opposing currents, producing the so called "ultimate stellarator". Taking this idea a step further it was discovered that the continuous helices can be replaced with a set of discrete twisted coils making the system entirely modular.

The encouraging experimental results and the potential for modularity, coupled with the inherent advantages of stellarators, namely steady state magnetic fields, continuous burn cycle, natural divertor and low recirculating power fraction have rekindled the interest in the fusion community and given the incentive to funding agencies to initiate studies into the technological problems of power reactors based on the stellarator/torsatron concept.

The University of Wisconsin Fusion Engineering Program group has been addressing some of the key technical issues of stellarator/torsatron power reactors. As a result of these deliberations a point reactor design called UWTOR-M has evolved. In the UWTOR-M design we have used an assumed $\beta = 5\%$. We are encouraged that with the favorable rotational transform obtained, this may well be within reach. The following sections give brief discussions on the subjects of coil selection, parametric considerations, transport modeling, overall reactor design, impurity control, magnet design, and maintenance considerations.

A. Modular Coil Considerations

The three coil systems considered were:

a. Continuous helices
b. Modular torsatron coils
c. Twisted stellarator coils.

Since maintainability is an important criterion in the present study, it was decided at the outset that continuous helices would be eliminated from consideration on that basis. This does not imply that such coil geometries are not suitable for power reactors. Some people feel that, like toroidal field coils in tokamaks, the helical coils will have such a high reliability that they will not fail in the lifetime of the reactor. This may be true; however, for the present study, we decided to pursue the more conservative approach.

We have also considered modular torsatron coils with windbacks.[2] Although these coils certainly offer maintainability, there is still some question about their effectiveness in producing stable flux surfaces. Furthermore, the useful magnetic volume in these coil configurations is such a small fraction of the total volume, that it is difficult to imagine they could be competitive with the simpler magnetic confinement systems. For these reasons we chose not to pursue the modular torsatron coils any further.

By the process of elimination we were left with the twisted stellarator coil configuration which we adopted for the present study. These coils have an interesting history. First proposed by workers at the Max Planck Institute of Munich, they became known as Rehker Wobig[3] coils. These coils were wound on a cylinder and were all of identical shape, but simply rotated in pitch to simulate the helical geometry needed. A further improvement entailed taking the windings of an "ultimate stellarator", mapping it on a plane surface and approximating the windings by joining the intersecting points with rounded discrete coils as shown in Fig. 1. This improvement, invented at the University of Wisconsin Stellarator/Torsatron Lab. by J. Derr[4] produces flux surfaces which are as good as or better than those produced by helical coils. However, because these coils are wound on a torus instead of a cylinder, they are not identical. There are in fact only two coil geometries (for $\ell = 3$) needed, as can be seen from Fig. 2, the top view of the coil set adopted for the UWTOR-M point design. There are six field periods, each consisting of three coils. Two of the coils in each field period are identical but are turned around relative to each other. This group of three coils per period will be used in planning the maintainability concept for the reactor which will be described later in the progress report.

B. Parametric Studies

The reactor design presented here incorporates the "natural" helical divertor of the

stellarator configuration as the method of impurity control. This means that the plasma is bounded by the magnetic separatrix. Between the separatrix on the wall will be a scrape-off zone of about 20 cm in width. This choice imposes a constraint on the design of the reactor, since one needs adequate space for the blanket and shield between the outer edge of the scrape-off zone and the inner edge of the magnets. This constraint forces one to coil configurations for which the magnetic volume utilization, η_v (the fraction of the volume inside the coil radius which is occupied by the plasma) is reasonably small, if the reactor size and power level is to be kept to a reasonable value.

We let r_c be the minor radius of the coil centers, r_p the equivalent circular minor radius of the plasma, and R the major radius of torus on which the coils are placed. Then

$$\eta_v = \left(\frac{A_c}{A_p}\right)^2 \qquad (1)$$

where A_c is the coil aspect ratio, R/r_c, and A_p is the plasma aspect ratio, R/r_p. We neglect for simplicity the shift of the magnetic axis of the plasma from the coil axis. Shown in Fig. 3 is the

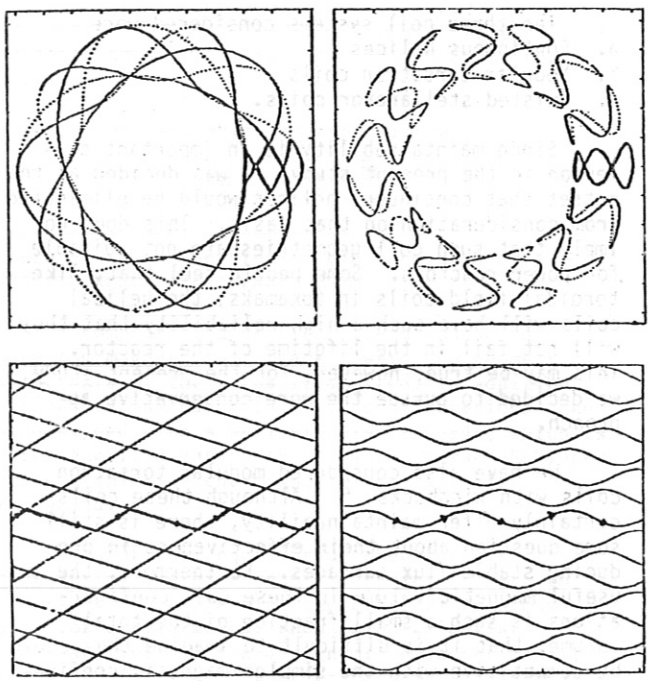

Fig. 1 (a)

Helical coil system of an $\ell = 3$, M = 5 ultimate stellarator (top) and corresponding mapping in the θ-ϕ plane (bottom).

Fig. 1 (b)

Modular coil system from the Fourier series expansion to the ultimate stellarator (top) and corresponding mapping in the θ-ϕ plane (bottom).

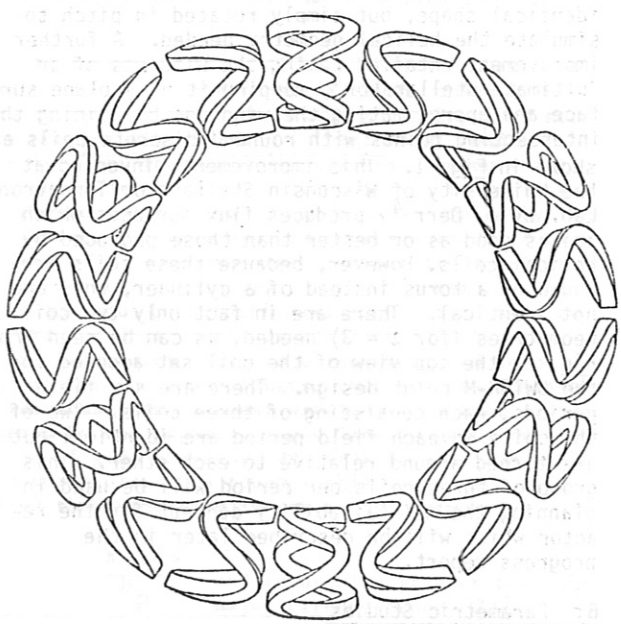

Fig. 2 Top view of UWTOR-M

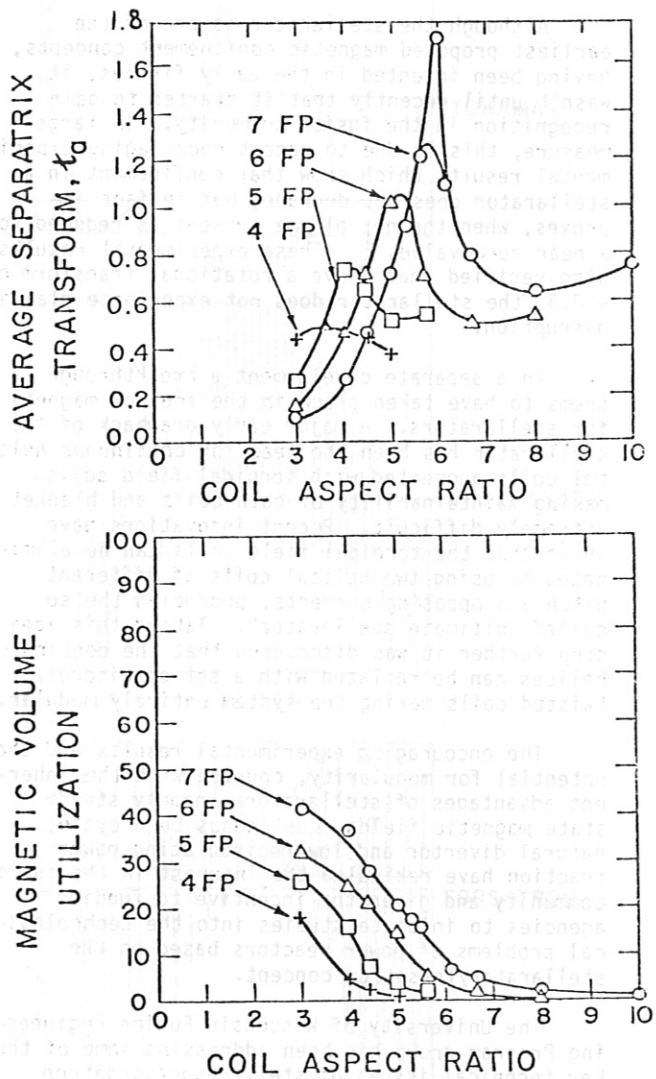

Fig. 3 Rotational transform and magnetic volume utilization as a function of coil aspect ratio for 4,5,6 & 7 field periods

magnetic volume utilization, n_V, and rotational transform versus coil aspect ratio for a particular winding law which appears feasible for reactors.

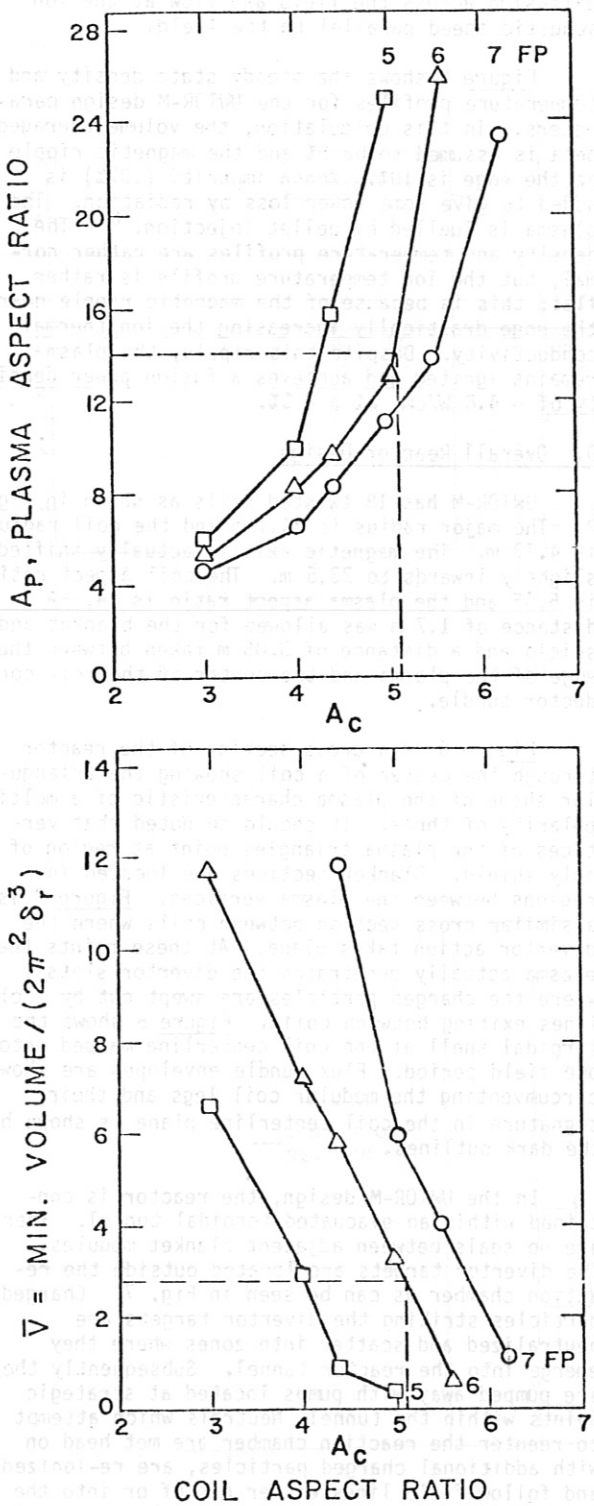

Fig. 4 Plasma aspect ratio and min. volume / $2\pi^2 \delta_r^3$ as a function of coil aspect ratio for 5, 6 & 7 field periods

The plasma radius, r_p, is related to the coil radius, r_c, by

$$r_p = r_c \sqrt{n_V} \quad . \tag{2}$$

Imposing the requirement of adequate space for the blanket and shield gives the relation

$$r_c \geq r_p + \delta_r \tag{3}$$

where the separation, δ_r, is taken to be 3.05 m to allow for the blanket, shield, scrape-off zone, half the coil thickness and required thermal insulation. Equations (2) and (3) imply that there is a minimum plasma volume, given by

$$V_p = 2\pi^2 R r_p^2 = 2\pi^2 \delta_r^3 \frac{A_p A_c^3}{(A_p - A_c)^3} \quad .$$

Shown in Fig. 4 is the plasma aspect ratio and minimum plasma volume for the winding law used in Fig. 3. One sees that the minimum plasma volume scales inversely as the plasma aspect ratio. The normalization factor $(2\pi^2 \delta_r^3)$ equals 560 m^3 if δ_r = 3.05 m; consequently the plasma volume, and therefore the power output, can get rather large if a low plasma aspect ratio is required. A compromise between these two conflicting design considerations must be obtained. For the UWTOR-M design, the point A_c = 5.05, A_p = 14, with 6 field periods, and a plasma volume of 1408 m^3 was chosen. This point is at the peak of the rotational transform curve, Fig. 3, and therefore should have good MHD stability properties, at least according to simple arguments. This, however, needs to be checked by detailed MHD calculatons.

Summary of Parametric Studies

Initial Constraints

- Coil modularity
- Magnetic divertor topology

Additional Design Goals

- High rotational transform
- Effective magnetic volume utilization
- Practical coil system

Choice of Winding Law

- Transform production
- Island formation
- Scrape-off layer, separatrix

Choice of Multipolarity ℓ = 3

- Transform production
- Shear
- Divertor topology

Choice of Field Periods

- Transform production
- Magnetic volume utilization
- Access and number of coils

C. Transport Modelling

A one-dimensional space-time tokamak transport code (the WHIST [5] code) has been modified to model stellarators. The toroidal current is set to zero, and the rotational transform profile is made an input variable. The flux surfaces are assumed to be circular, although one can input the volume between flux surfaces of the actual stellarator configuration without too much difficulty. The code calculates the time evolution of the density, electron temperature, and ion temperature profiles for a given model for the transport coefficients. The model used here assumes that the ion thermal conductivity is neoclassical, but enhanced by the effect of magnetic ripple. [6] The electron thermal conductivity is taken to be 1/5 the alcator [7] scaling value; this reflects the experimental observation that stellarators do somewhat better than the alcator scaling value. The particle diffusion is taken to be 1/5 the alcator scaling value and also includes the effect of ripple. The scrape-off layer of the helical divertor is included in the modelling. The transport in the scrape-off layer is assumed to be Bohm diffusion across the field and flow at the ion acoustic speed parallel to the field.

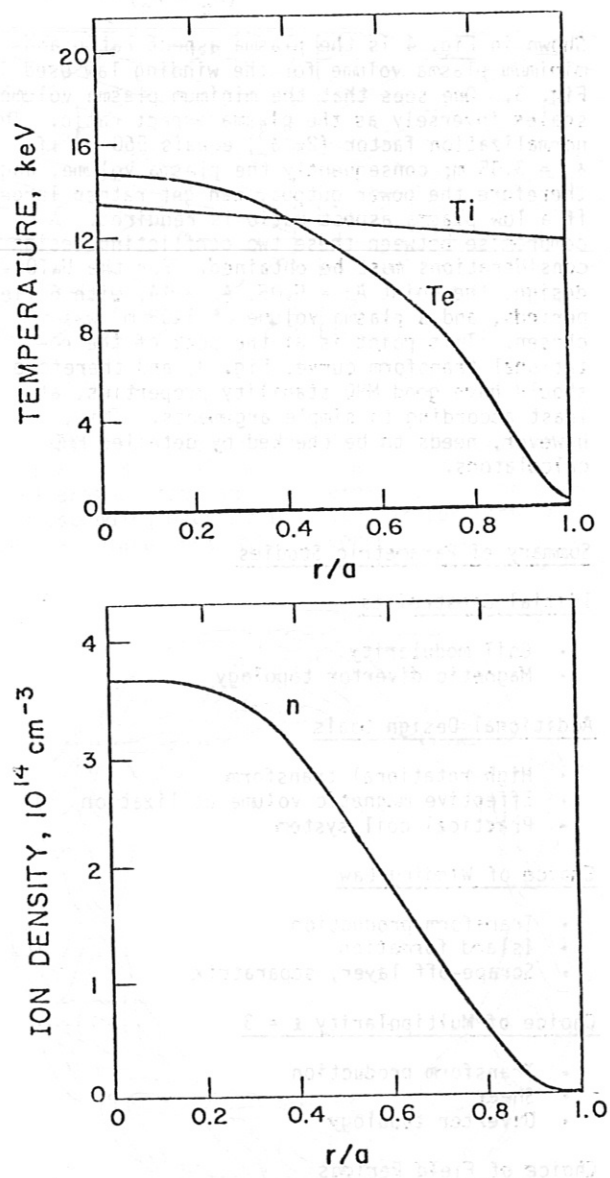

Fig. 5 Electron and ion temperature and ion density as function of the radial distance from plasma center

Figure 5 shows the steady state density and temperature profiles for the UWTOR-M design parameters. In this calculation, the volume averaged beta is assumed to be 5% and the magnetic ripple at the edge is 10%. Xenon impurity (.07%) is added to give some power loss by radiation. The plasma is fuelled by pellet injection. [8] The density and temperature profiles are rather normal, but the ion temperature profile is rather flat; this is because of the magnetic ripple near the edge drastically increasing the ion thermal conductivity. Despite this ripple, the plasma remains ignited and achieves a fusion power density of ~ 4.8 W/cm^2 at β = 5%.

D. Overall Reactor Design

UWTOR-M has 18 twisted coils as shown in Fig. 2. The major radius is 24.1 m and the coil radius is 4.77 m. The magnetic axis is actually shifted slightly inwards to 23.5 m. The coil aspect ratio is 5.05 and the plasma aspect ratio is 14. A distance of 1.7 m was allowed for the blanket and shield and a distance of 3.05 m taken between the edge of the plasma and the center of the coil conductor bundle.

Figure 6 is a cross section of the reactor through the center of a coil showing the triangular shape of the plasma characteristic of a multipolarity of three. It should be noted that vertices of the plasma triangles point at region of only shield. Blanket sections are located in regions between the plasma vertices. Figure 7 is a similar cross section between coils where the divertor action takes place. At these points the plasma actually penetrates the divertor slots where the charged particles are swept out by field lines exiting between coils. Figure 8 shows the toroidal shell at the coil centerline mapped onto one field period. Flux bundle envelopes are shown circumventing the modular coil legs and their signature in the coil centerline plane is shown by the dark outlines.

In the UWTOR-M design, the reactor is contained within an evacuated toroidal tunnel. There are no seals between adjacent blanket modules. The divertor targets are located outside the reaction chamber as can be seen in Fig. 7. Charged particles striking the divertor targets are neutralized and scatter into zones where they emerge into the reactor tunnel. Subsequently they are pumped away with pumps located at strategic points within the tunnel. Neutrals which attempt to reenter the reaction chamber are met head on with additional charged particles, are re-ionized and follow field lines either out of or into the reaction chamber. Like in a pumped limiter, this has a tendency to create a higher pressure of neutral particles in the throat of the divertor targets, thus facilitating their pumping away by the vacuum system. [9]

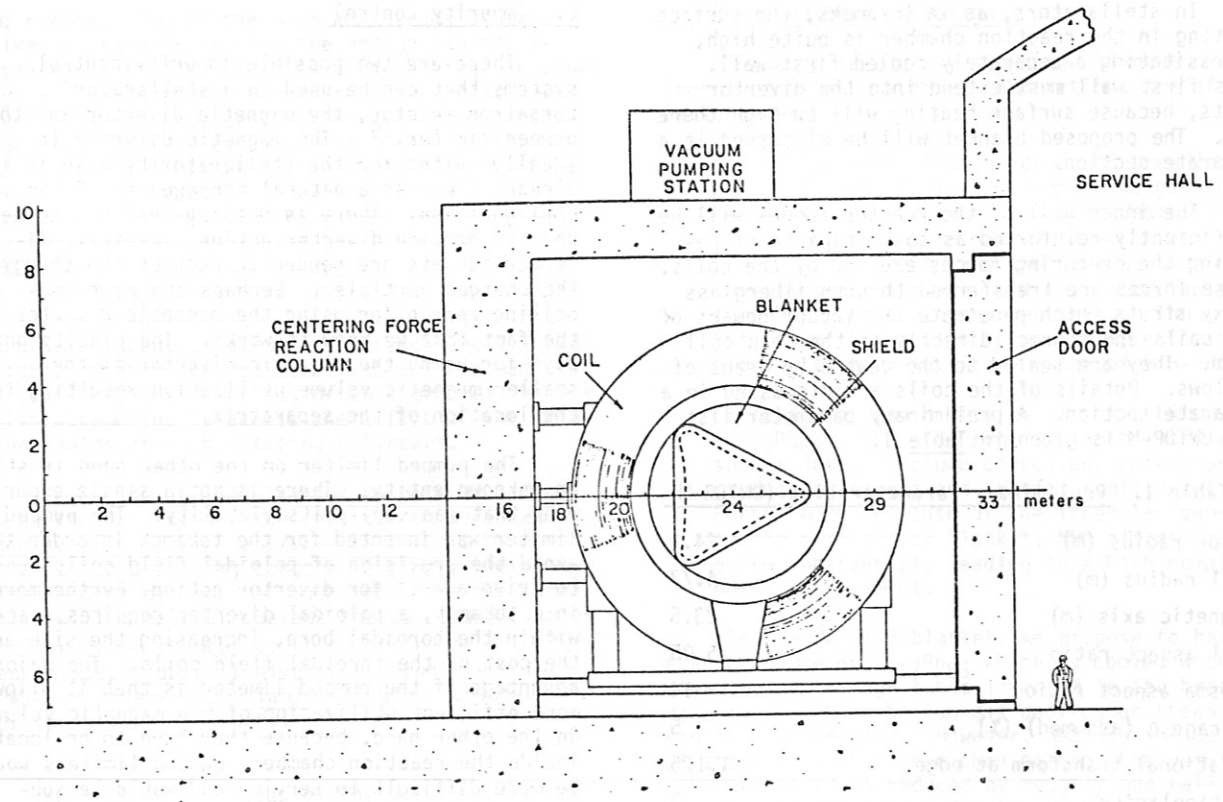

Fig. 6 SIDE VIEW OF UWTOR-M

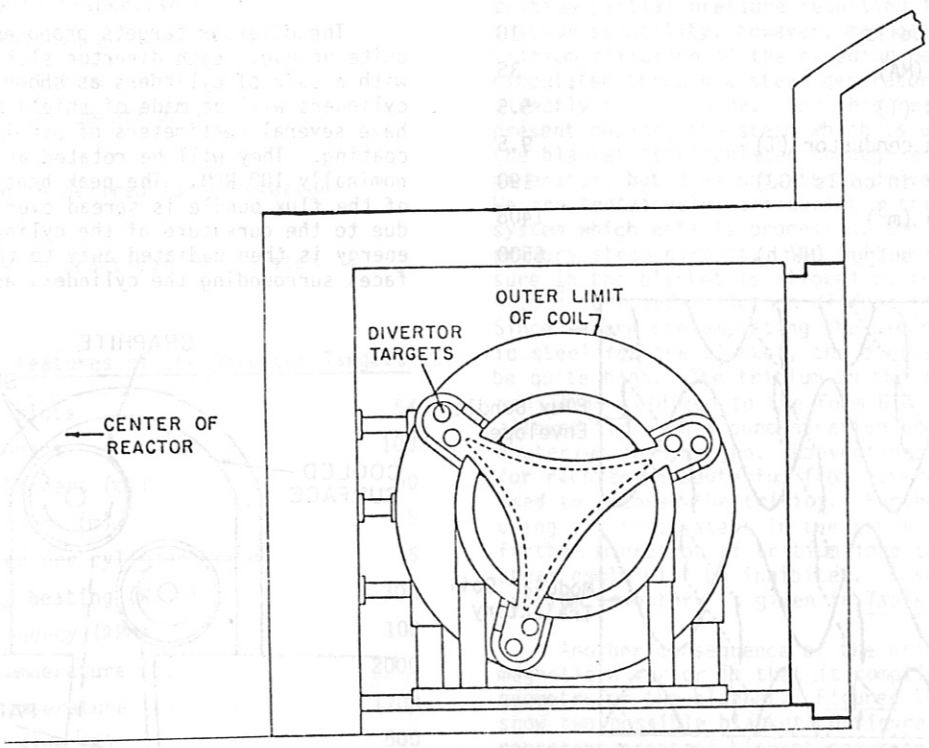

Fig. 7 Side view section between coils showing divertor targets

In stellarators, as in tokamaks, the surface heating in the reaction chamber is quite high, necessitating a separately cooled first wall. This first wall must extend into the divertor slots, because surface heating will be high there too. The proposed blanket will be discussed in a separate section.

The inner wall of the reactor tunnel will be sufficiently reinforced as to be capable of reacting the centering forces exerted by the coils. These forces are transferred through fiberglass epoxy struts which penetrate the vacuum dewars of the coils and connect directly to the cold coil form. They are sealed to the dewars by means of bellows. Details of the coils are discussed in a separate section. A preliminary parameter list for UWTOR-M is given in Table I.

Table I. Preliminary Parameter List (UWTOR-M)

Major radius (m)	24.1
Coil radius (m)	4.77
Magnetic axis (m)	23.5
Coil aspect ratio	5.05
Plasma aspect ratio	14
Average β (assumed) (%)	5
Rotational transform at edge	1.125
Multipolarity	3
No. of field periods	6
Coils/period	3
Total no. of coils	18
Coil current (MA)	35
Field on axis (T)	5.5
Max. field on conductor (T)	9.5
Stored energy in coils (GJ)	190
Plasma volume (m^3)	1408
Thermal power output (MWth)	5500

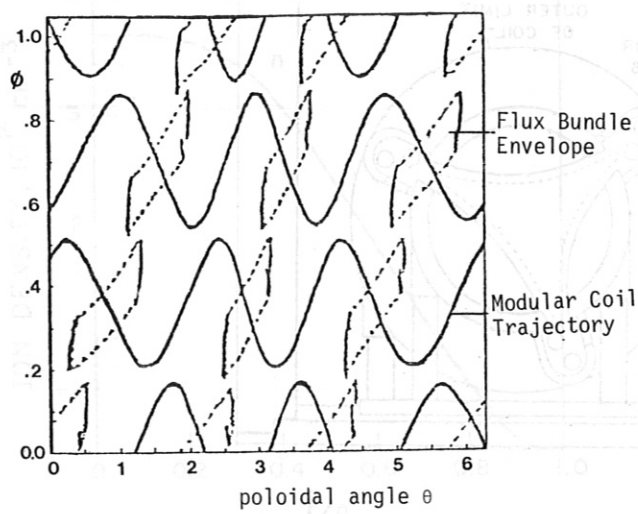

Fig. 8 Emerging flux bundles through the toroidal shell $r_{cutoff} = R_{minor}$, mapped onto one field period $0 \leq \phi \leq 2\pi / 6$

E. Impurity Control

There are two possible impurity control systems that can be used in a stellarator/torsatron reactor, the magnetic divertor and the pumped limiter.[9] The magnetic divertor is ideally suited for the stellarator because it is already there as a natural consequence of the coil configuration. There is nothing that has to be done to provide divertor action. Clearly, divertor targets are needed to recover the energy of the charged particles. Perhaps the most compelling reason for using the magnetic divertor is the fact that we know it works. The penalty one pays for using the magnetic divertor is the smaller magnetic volume utilization resulting from the location of the separatrix.

The pumped limiter on the other hand is still an unknown entity. There is not a single experiment that can verify its viability. The pumped limiter was invented for the tokamak in order to avoid the provision of poloidal field coils needed to drive a null for divertor action. Furthermore, in a tokamak, a poloidal divertor requires space within the toroidal bore, increasing the size and the cost of the toroidal field coils. The major advantage of the pumped limeter is that it allows more efficient utilization of the magnetic volume. On the other hand, because they have to be located inside the reaction chamber, pumped limiters would be more difficult to service and would be subjected to high heat levels and high sputtering rates. Thus, the choice of a magnetic divertor for UWTOR-M represents a conservative option.

The divertor targets proposed for UWTOR-M are quite unique. Each divertor slot will be equipped with a pair of cylinders as shown in Fig. 9. The cylinders will be made of shield material and will have several centimeters of pyrolytic graphite coating. They will be rotated at a slow rate, nominally 100 RPM. The peak heating in the center of the flux bundle is spread over a larger area due to the curvature of the cylinders and the energy is then radiated away to the cooled surfaces surrounding the cylinders as they continue

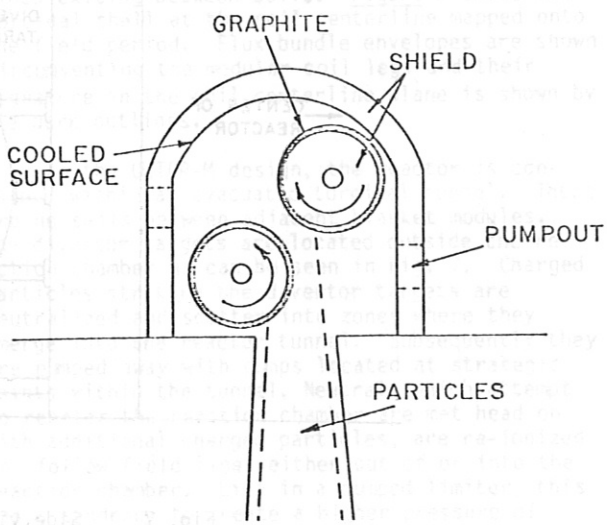

Fig. 9 Graphite covered rotating cylinder divertor targets

to rotate. One of the main advantages of such divertor targets is that the energy can be recovered at a high temperature, improving the power cycle. Furthermore, spreading of the heat load over a larger area prolongs the lifetime of the targets. Initial estimates show that sputtering may not be a limiting factor because of the high energy of the particles due to the flat ion temperature profile on the plasma edge (see Fig. 5). At the operating pressure ($\sim 10^{-4}$ torr) chemical erosion does not appear to be serious either. Because the bulk of the divertor targets are shielding material, they will mitigate the problem of neutron streaming through the divertor slots. Monte Carlo calculations will be made to determine the seriousness of this problem. We are also attempting to access the effect of the fringing fields on such rotating cylinders.

Location of the divertor targets will determine the ease with which they can be serviced. One benefit of such a system is that it is possible to avoid putting targets in places where they are hard to get at. At such locations the particles will simply circumvent the coils and reenter the reaction chamber to be collected at a different place. Table II gives the advantages of the UWTOR-M divertor and Table III gives the features of the divertor targets.

Table II. Advantages of the UWTOR-M Divertor

- No additional coils required
- Compatible with blanket/shield
- Modular, localized collection regions
- Effective for trapped particles
- Well defined scrape-off zone
- Low stray fields
- Compatible with desired large rotational transform
- Compatible with practical coil system

Table III. Features of the Divertor Targets

Number of div. slots	54
Number of cylinders	108
Diameter of cylinders (cm)	60
Length of cylinders (m)	5
Power dissipated per cylinder (MWth)	5
Average surface heating (W/cm)	300
Revolution frequency (RPM)	100
Max. surface temperature (C)	2000
Avg. surface temperature (C)	1700
Temperature of sink (C)	500

F. Proposed Blanket Design

The most frequently suggested blanket breeding/coolant material combinations are of two basic types:

1. Gas cooled solid lithium compound breeding materials, which use a helium purge gas for recovering the tritium. In this design the tritium diffusion mechanism is not clear and the combination of rate limiting steps and radiation effects may lead to unacceptably large blanket tritium inventories. The "Starfire" [10] design for example, estimated a blanket tritium inventory range of 7.8-380 kg.

2. Circulating liquid lithium [11] or lithium lead ($Li_{17}Pb_{83}$). [12] The problems associated with such a design include corrosion, corrosion product transport and tritium confinement. Furthermore, because of the irregular geometry of the stellarator blanket, MHD effects may be quite substantial, leading to a high pumping power requirement.

In the UWTOR-M blanket, we propose to have a static volume of $Li_{17}Pb_{83}$ which is cooled with steam going through tubes immersed in the breeding material. Either helium gas cooling or steam cooling can be used. However, because the density of steam is much higher than helium, the pumping power required is reduced by roughly one half. $Li_{17}Pb_{83}$ is attractive due to its high breeding potential, low activity, low tritium solubility and inertness with respect to water. The high tritium partial pressure resulting from the low tritium solubility, however, may cause excessive tritium diffusion if the breeding material is circulated through a steam generator connected directly to a turbine. For this reason in the present design, the steam which is used to cool the blanket is circulated through another steam generator, but does not itself drive a turbine. We are tentatively considering a tritium recovery system which entails processing the water in the primary steam circuit. The tritium partial pressure in the blanket is allowed to increase to $\sim 10^{-2}$ torr and will then diffuse into the steam. Since we are contemplating the use of HT-9 ferritic steel for the blanket, the diffusion rate will be quite high. The tritium in the steam is immediately oxidized to the form HTO and will be allowed to reach a concentration equal to that of deuterium in hydrogen. Conventional techniques for recovering deuterium from water can then be used to recover the tritium. Furthermore, by using stainless steel in the steam generator, further migration of tritium into the secondary steam cycle will be inhibited. A summary of the tritium inventory is given in Table IV.

Another consequence of the utilization of the magnetic divertor is that it complicates the geometry of the blanket. Figures 10(a) and 10(b) show two possible blanket configurations. They represent areas of blanket coverage if the toroidal shell in the plane of the first wall is mapped out over one field period. The blanket configuration in Fig. 10(a) is more simple, but because of the smaller coverage may not be able to breed sufficient tritium for an overall breeding ratio of one. Fig. 10(b) is more complex, but certainly provides adequate coverage. In the

coming months, a careful analysis will be made to see if a compromise between the two configurations will provide the needed coverage while using a simpler blanket geometry.

Table IV. Tritium Summary

Tritium breeding rate	10^{-2} g/sec
Coolant tube area in the blanket	4×10^4 m^2
Tritium permeability through HT-9	$\frac{1 \text{ mole } T_2 \cdot \text{mm}}{\text{day, m}^2\text{, atm}^{1/2}}$
Tritium partial pressure in $Li_{17}Pb_{83}$	10^{-2} torr
Tritium inventory in $Li_{17}Pb_{83}$	60 g
Water inventory in primary steam circuit	2×10^3 kg
Tritium inventory in primary steam circuit	100 g
Tritium dissolved in blanket structure	4 g
Total blanket system tritium inventory	164 g

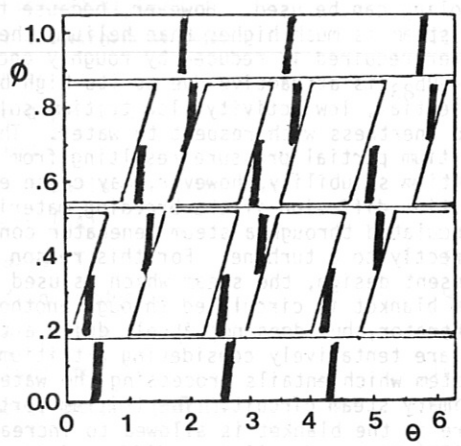

Fig. 10 (a) Simplified blanket configuration with limited coverage of available area

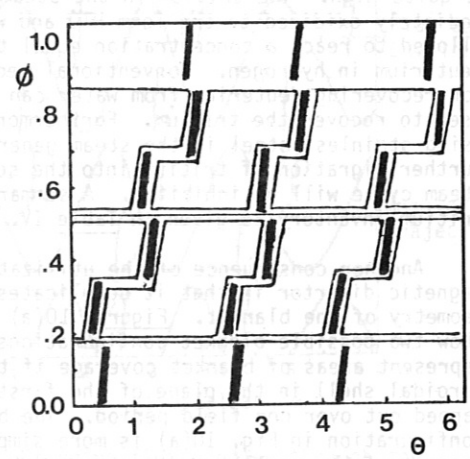

Fig. 10 (b) Complex blanket configuration with more extensive coverage of available area

G. Magnet Design

In the present section we describe a design for the magnet system of a stellarator fusion reactor, UWTOR-M. The basic features of the magnet system are a set of twisted toroidal field coils which approximate helical windings in a classical stellarator. The magnetic fields are moderate ($B_{max} \sim 10$ T) and steady state. Structural support of the magnetic loads are incorporated within the windings and superfluid helium cooling is employed.

1. Magnetic Loads

Magnetic forces on these coils have two principal components, the self force on an individual coil and the interactive force between adjacent coils. In the bend regions, where the coils come in close proximity, the mutually attractive forces dominate, while elsewhere the self force determines the loading.

A schematic representation of the magnetic loading of one coil is shown in Fig. 11. Two components are indicated, radial and toroidal, both having magnitudes of the order 100 MN/m. All components are given on a per unit length of coil basis. Summing the forces gives a net centering force of about 225 MN per coil. This force must be reacted against a central column similar to those proposed for tokamak designs.

Structural containment of the magnetic forces is achieved by combining the load bearing structure as part of the coil case. Since the magnetic loads are high (~ 100 MN/m), the overall current density must be limited to less than 1780 A/cm^2, which has the advantage of limiting the peak fields on the conductor.

2. Coil Design

The major driver for the coil design as presently considered is the structural require-

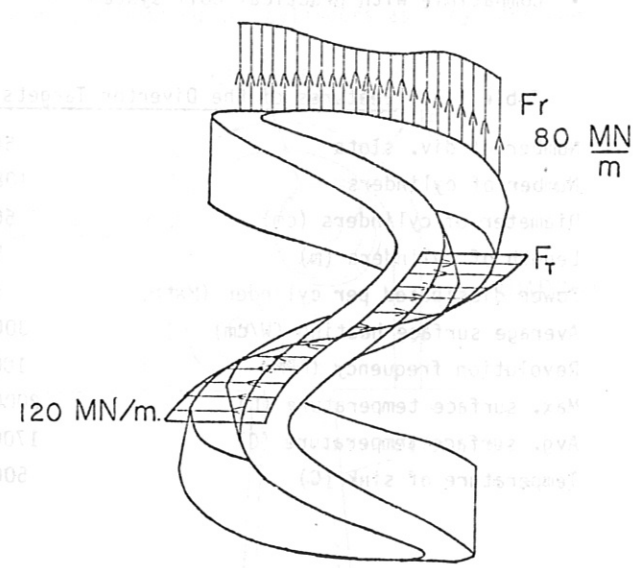

Fig. 11 Radial and toroidal forces on a twisted coil

ment. At an overall current density of 1780 A/cm^2, minimum structural requirements[13] demand that the winding consist of 40% stainless steel stressed to 80 ksi.

An additional complication results from the lack of symmetry axis in these magnets. Unlike most magnet concepts, these coils have regions where the winding procedure demands that the conductor be pushed into place rather than simply wound in tension. This is a construction problem which has been addressed when considering possible structure and conductor design concepts.

Two methods are under consideration for combining the structure with the conductor into one continuous unit. The first employs the imbedded conductor concept introduced in the previous UWMAK[14] designs. Stainless steel subplates are assembled within the winding cross section. Once a complete layer of subplates is installed and welded, an insulated monolythic conductor is embedded into the grooved assembly. On completion of a layer another subplate assembly would be installed. Between layers G-10 CR spacers provide layer-to-layer insulation and insure adequate cooling channels. Alternatively, since the conductors are insulated from the base plates, it may be possible to use stainless steel spacers covering a smaller fraction of the surface. It would then be possible to weld the entire structure on assembly. An admitted difficulty with this approach is that subplates are not interchangeable. However, it provides adequate load transfer from conductor to structure and entails straightforward construction.

The second method of construction uses a winding machine rotating the coil from about a central axis with the conductor fed in at one location while a specially designed set of hydraulic rams continuously conform to the coil contour and hold the conductor into the regions of negative curvature. Mechanical fingers hold the conductor in place while the ram retracts to allow subsequent turns to be added. This scheme provides a simplified conductor but requires a somewhat more complex winding machine. Listed in Table V are the principal design features of the magnet winding.

Table V. Design Features of Torsatron/ Stellarator Magnet Windings

Overall current density	1250 A/cm^2
Structure	304 LN-SS
Max. stress	533 MPA (80 KSI)
Conductor current density	4000 A/cm^2
Current	10 KA
Inductance/coil	30 H
Number of turns	3500
Insulation	G-10 CR
Volume cross section:	
Stainless steel	40%
Copper	43%
Superconductor	2%
Helium	10%
Insulation	5%

3. Conductor Design

Stellarator reactors require DC magnetic fields with $B_{max} \sim 10$ T. The absence of time varying fields allows consideration of monolythic conductors, which may otherwise have prohibitive AC losses. Schematic representation of the current carrying elements is shown in Fig. 12. The present design is for a monolythic composite of NbTi/NbTiTa in 3/4 hard copper. Any instability and induced heat generation must be transmitted through the helium channel to the bath on the sides of the winding. The specific parameters of the conductor design are listed in Table VI.

The relatively high conductor current density necessitates an innovative approach to conductor stability. We are considering the use of a maximum energy depositon criterion based on the enthalpy of the superfluid helium in the region of the normal zone.[15] The approach assumes a steady state normal zone and defines a length of time which the conductor can remain stable before film boiling initiates. Although somewhat less conservative than the fully steady state stability criterion, this approach provides a method of achieving higher conductor current density in large magnet systems. The results of this calculation are listed in Table VI.

Table VI. Conductor Design Parameters

Conductor current density	4000 A/cm^2
Stabilizer	3/4 hard copper
Superconductor	NbTi/NbTiTa
Superconductor current density[16,17]	1500 A/mm^2
Coolant	He II - 1.8 K, 1 atm
Heat generation (Q/ℓ)	3.2 W/cm
Surface heat flux (q)	.95 W/cm^2
Max. energy flux (Ec)	3 J/cm^3 of conductor

CONDUCTOR INSULATION SCHEME

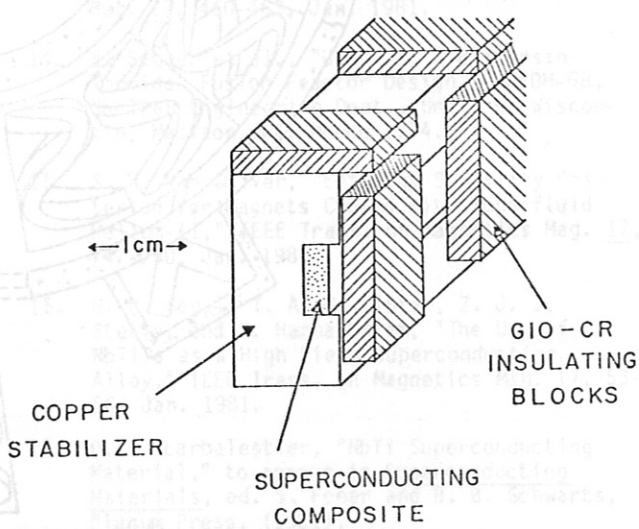

Fig. 12 Proposed conductor and insulation scheme

H. Reactor Maintainability

The major aspects of reactor maintainability have to do with maintaining the blanket and the coils. The advent of modular coils has improved immeasurably the prospects for maintaining both systems.

In the UWTOR-M design, the reactor is contained within an evacuated toroidal tunnel. The reactor tunnel is surrounded by a toroidal service hall and is connected to it by doors located behind each of the "figure 8" coils. Each coil period has three coils, one "figure 8" coil and two identical coils on either side of it. Although the coils are identical in construction, they are turned 180° relative to each other.

The maintenance scheme proposed for this reactor involves the capability of radial extraction of a "figure 8" coil module, consisting of coil, blanket and shield through the door into the service hall. The module is removed to a location where segments of the blanket within it are removed and replaced. At the same time, a specially equipped carriage reenters the reactor tunnel into the place vacated by the extracted module. This carriage can work on blankets on either side, thus reaching the remaining blanket segments within that period. By only moving one third of the coils in the reactor, accessibility has been provided for the whole reactor blanket.

Coils that are adjacent to the "figure 8" coil can also fail and will require servicing. In that event, the failed coil will have to be moved circumferentially first and then radially. Although this operation is by no means simple, provided with guided rails and appropriate stops, it can be performed using present day technology.

Figure 13 shows a coil module which has been extracted from the reactor tunnel. It will be

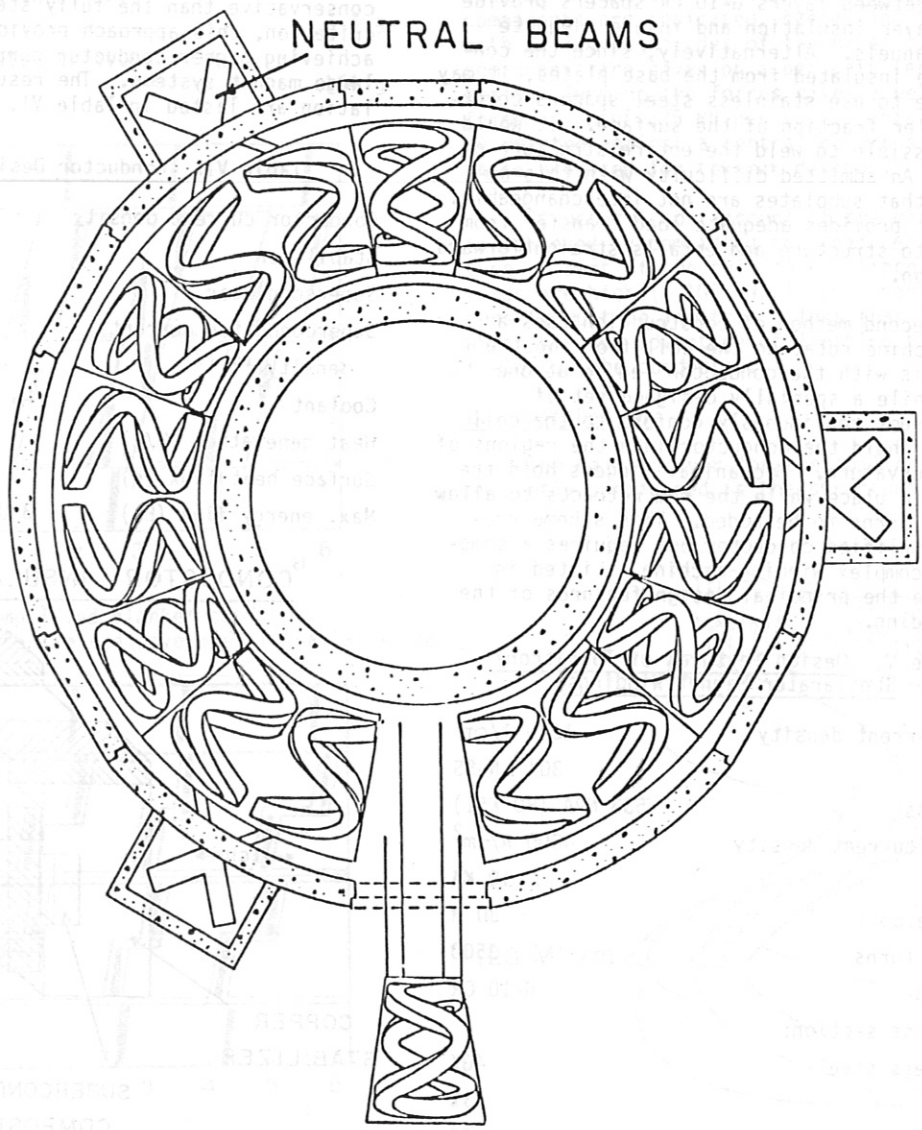

Fig. 13 View showing a coil removed from reactor enclosure into the service hall

noted that the neutral beams can remain in place and need not be disturbed. This is an advantage of such a maintenance scheme. Table VII is a list of parameters relevant to maintenance.

Table VII. Parameters Relevant to Maintenance

Mass of one coil with integral blanket, shield and divertor targets (tonnes)	1400
Outer dimensions (meters)	
Width	10.5
Height	11.5
Depth	11.5
Mass of a blanket unit from one coil (breeding material drained) (tonnes)	40
Outer dimensions (meters)	
Diameter	6.2
Length	9.5
Mass of access door (tonnes)	1400
Outer dimensions (meters)	
Width	12
Height	15
Depth	2

Summary of Maintenance Aspects

- Reactor enclosed in evacuated toroidal tunnel
- Doors spaced every third coil provide access to the reactor
- Retracting one coil with integral blanket and shield provides access for servicing FW/blanket
- Divertor targets serviced the same time as blanket
- If needed coils adjacent to removable one can be translated circumferentially then radially
- Neutral beams remain undisturbed during reactor maintenance. They can be repaired from the service hall.

Conclusions

Preliminary indications are that the engineering issues of modular stellarator/torsatron reactors, although far from being easy, are technically feasible with modest extrapolations of present technology. The special divertor characteristics make possible new and innovative divertor or target designs. Modularity of the system facilitates maintenance of both blanket and coil components. These new developments coupled with the original advantages of the stellarator/torsatron system, are turning it into one of the more attractive magnetic confinement fusion devices.

References

1. H. Renner et al., Max Planck Institute, Plasma Physics and Controlled Nuclear Fusion Research (Brussels, 1980).
2. J. L. Shohet, "Ultimate and Modular Torsatrons," B.3.4. International Workshop on Stellarators, Schloß Ringberg, Lake Tegernsee, Bavaria, FRG, July 1980.
3. S. Rehker and H. Wobig, Proceedings of the Symposium on Fusion Technology, Grenoble (1972), P. 345; Max Planck Institute für Plasmaphysik Report IPP 2/215 (1973).
4. D. T. Anderson et al., Plasma Physics and Controlled Nuclear Fusion Research (Brussels, 1980), IAEA, CN-38/BB-1.
5. W.A. Houlberg and R. W. Conn, Nuclear Science and Technology, 64, 141 (1977).
6. H. E. Mynick, "Verification of the Classical Theory of Stellarator Transport," paper 2A7; J. D. Callen and K. C. Shaing, "Neoclassical Ripple Transport in the Low Collisionality Regime," paper 2C45; Sherwood Theory Mtg., Austin, TX, April 1981.
7. W. A. Houlberg, S. E. Attenberger, A. T. Mense, Nuclear Fusion 20, 811 (1980).
8. W. A. Houlberg, M. A. Iskra, H. C. Howe, S. E., Attenberger, Oak Ridge National Laboratory, ORNL/TM-6549 (1979).
9. R. W. Conn, I. N. Sviatoslavksy, and D. K. Sze, "Limiter Pumping for Divertorless Tokamaks," UWFDM-339, IEEE Meeting on Engineering Problems of Fusion Research, San Fransciso, CA, November 1979.
10. C. Baker et al., "Starfire, A Commercial Tokamak Fusion Power Plant Study," ANL/FPP-80-1, Argonne National Laboratory, Argonne, IL, September 1980.
11. B. Badger et al, "UWMAK-III, A Noncircular Tokamak Power Reactor Design," UWFDM-150, Nuclear Engineering Dept., Univ. of Wisconsin, Madison, WI, July 1976.
12. B. Badger et al., "WITAMIR-I, A Tandem Mirror Reactor Study," UWFDM-400, Fusion Engineering Program, Nuclear Engineering Dept., Univ. of Wisconsin, Madison, WI, September 1980.
13. Y. M. Eyssa and R. W. Boom, "Considerations of a Large Force Balanced Magnetic Energy Storage System," IEEE Trans. on Magnetics Mag. 17, 460-463, Jan. 1981.
14. B. Badger et al., "UWMAK-I, A Wisconsin Toroidal Fusion Reactor Design," UWFDM-68, Nuclear Engineering Dept., Univ. of Wisconsin, Madison, WI, March 1974.
15. S. W. Van Sciver, "Enthalpy Stability Criterion for Magnets Cooled with Superfluid Helium-II," IEEE Trans. on Magnetics Mag. 17, 747-750, Jan. 1981.
16. H. R. Segal, T. A. de Winter, Z. J. J. Stekly, and K. Hammachalam, "The Use of NbTiTa as a High Field Superconducting Alloy," IEEE Trans. on Magnetics Mag. 17, 53-56, Jan. 1981.
17. D. C. Larbalestier, "NbTi Superconducting Material," to appear in Superconducting Materials, ed. S. Foner and B. B. Schwarts, Plenum Press, (1981).

ANNEX IV

THE LOS ALAMOS / PRINCETON MODULAR STELLARATOR REACTOR (MSR) POINT DESIGN.

The Modular Stellarator Reactor (MSR) achieves classic stellarator plasma confinement by means of a modular coil configuration, obtaining a rotational transform in the magnetic field topology by applying a periodic lateral deformation to a set of discrete toroidal field coils. No helical coils are required, resulting in a device with the promise for improved access, maintainability and reliability over traditional stellarator configurations. As a stellarator, the MSR has the advantages of steady-state, disruption-free operation and a plasma start-up on existing magnetic surfaces without the need for driving net internal plasma currents, as is required in a tokamak.

The Los Alamos/Princeton MSR study[1] has focused on the relationships between plasma (equilibrium/stability, beta limits, plasma power density), coil (stress, modularity) and reactor (wall loading, total power, engineering power density, maintainability) performance. This study is the first application of the modular-coil configuration[2,3] in a self-consistent reactor design. The implementation of the abovementioned plasma, coil and reactor constraints on overall system performance has been made by means of a simplified but generalized and interrelated systems model. Imposing the DT ignition requirement for a cubic radial pressure profile and using an empirical (Alcator) transport scaling leads to the choice of the product $\langle\beta\rangle B_o^2 r_p$ and average plasma temperature $\langle T\rangle$, where $\langle\beta\rangle$ is the volume-averaged beta, B_o is the on-axis magnetic field, and r_p is the mean plasma radius. Simultaneous application of simplified, conservative equilibrium and stability beta limits in conjunction with a parametric variation of ℓ, m and N numbers gives the aspect ratio $A = R_T/r_p$, where ℓ is the number of poloidal field periods, m is the number of toroidal field periods and N is the number of coils. A total thermal power, $P_{TH} \simeq 4000$ MWt, and neutron first-wall loading, $I_W \simeq 1.5$ MW/m^2, result. The appropriate limits and/or choices of blanket/shield thickness, $\Delta b = 1.5$ m, coil parameters (current density, radius, coil non-interference) and impurity control scheme (magnetic divertor versus pumped limiter) complete the essential elements needed to specify the MSR design point.

Operation of the MSR with a pumped limiter rather than a magnetic divertor is proposed to maximize the utilization of plasma chamber volume. The limiter, rather than the last closed magnetic surface, defines the plasma boundary. A reactor module would consist of a single coil and underlying blanket/shield components. Limiter, vacuum and fueling access would occur at the interface between two adjacent modules at the outboard side of the torus.

The layout of the MSR is illustrated schematically in Fig. IV-1. The MSR coils would be supported against the net centering forces by leaning against a solid central core. Gimballed supports at the top and bottom of the coil are indicated. Removal of modules would entail decoupling of the support structure at the gimbal mounts, followed by a radially-outward translation. While not yet investigated in detail, access for vacuum, fueling, electrical leads and coolant pipes in this moderte aspect-ratio device appears straightforward and flexible. One option would be to concentrate all access requirements into a wedge-shaped submodules (Fig. IV-1) that serve as interfaces between right-circular-cylindrical coil/blanket/shield modules. The wedge-shaped segment could itself be considered a moveable module or could be fixed to an adjacent

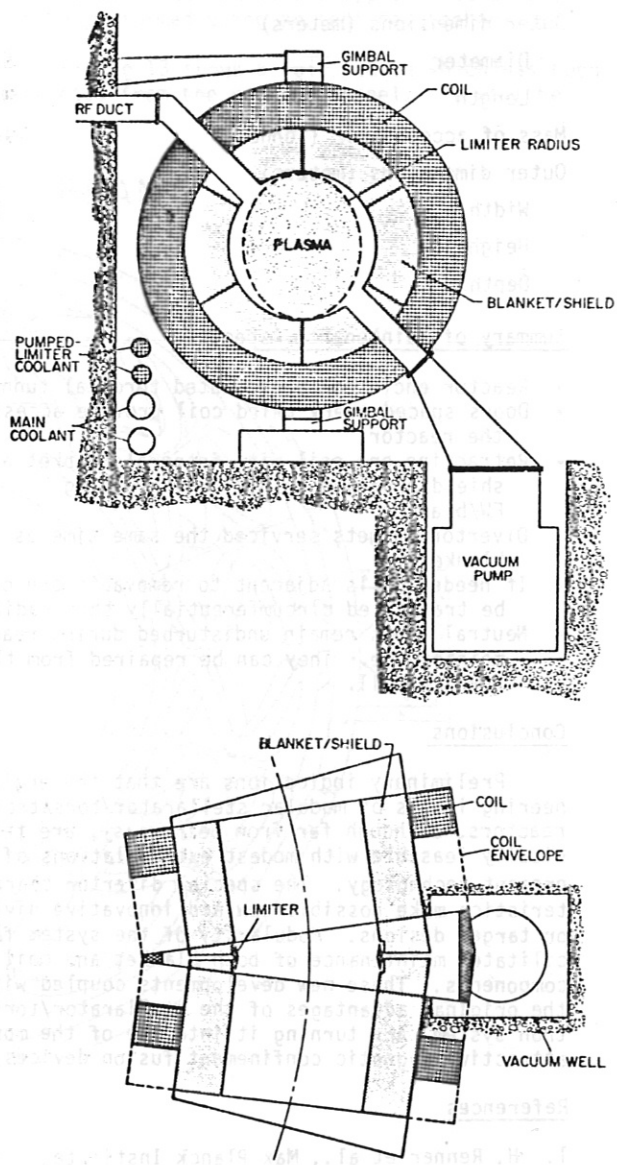

Fig. IV-1. Preliminary MSR layout, showing elevation and equitorial-plane views. Simple right-circular-cylindrical blanket/shield modules are proposed that are connected by wedge-shaped connecting segments through which all penetrations for support systems would occur.

coil/blanket/shield module. The wedge-shaped segment would contain the pumped-limiter impurity-control system and all heating/fueling/vacuum/coolant penetrations and external connections.

Positioning of the stagnation point radius, r_s, near that of the coil, r_c, allows for maximization of the volume utilization (i.e., plasma filling factors within the volume enclosed by the first-wall radius, r_w) and moderate requirements for the average rotational transform. The plasma boundary is defined by the elliptical (for $\ell = 2$) or trefoil (for $\ell = 3$) limiter rather than by the last closed magnetic surface (separatrix), as is illustrated in Fig. VI-2. This configuration has the additional advantage of separating the plasma edge from any magnetic ergodicity that might be expected to occur near the separatrix radius.

A nominal blanket/shield thickness, $\Delta b = 1.5$ m, is imposed between the first-wall radius and the modular coils in order to provide adequate tritium breeding as well as thermal insulation and radiation protection of the superconducting coils. This thickness and the assumed neutron energy multiplication, $M_N = 1.1$, in the blanket are consistent with the designs of other fusion reactors but could be refined and optimized on the basis of specific nucleonics studies.

Present modeling of the MSR assumes ignited operation of a DT plasma. A fraction ($f_\alpha \simeq 0.88$ for a plasma aspect ratio A = 11) of the fusion-product alpha-particle power is balanced against Bremsstrahlung and transport losses to be consistent with supporting calculations for the T-1 Torsatron conceptual design study.[4] Transport scaling is assumed to be described by an empirical (Alcator) scaling given by[5] $\tau_E = 3 \cdot 10^{-21} \langle n \rangle r_p^2$, where $\tau_E(s)$ is the energy confinement time, $\langle n \rangle (m^{-3})$ is the volume-averaged plasma density and $r_p(m)$ is the average plasma radius. A cubic radial profile is typically assumed for the plasma pressure. Based on Fokker-Planck studies of other reactor systems, the suprathermal fusion-product alpha particles are taken to have an equilibrium concentration $n_\alpha/n \sim 0.06$ such that $Z_{eff} = 1.1$. For $T_\alpha/\langle T \rangle = 10$, where $\langle T \rangle$(keV) is the average plasma temperature ($T_i = T_e$), the contribution made by the alpha particles to the total plasma kinetic pressure is substantial (~ 25%), which in turn reduces the productive beta of the device.

Present understanding of the equilibrium and stability limits imposed on $\langle \beta \rangle$ allows a marginally acceptable value of approximately 0.04 for A = 11, $\ell = 2$ and m = 6. The equilibrium limit is determined in the usual manner by equating to the plasma radius the outward toroidal shift of the plasma column as induced by Pfirsch Schluter currents and the associated vertical magnetic field. The separate stability limit is simultaneously imposed by gross kink modes associated with diffusion-driven currents. This relatively low value for $\langle \beta \rangle$ is a key MSR disadvantage insofar as it drives the system to higher magnetic fields and larger coil cross sections, which in turn push the limits for NbTi magnet technology and constrains the allowed lateral coil distortion in a given torus. It is emphasized that these assumptions used to establish the beta limits are conservative in that detailed analyses on specific configurations provide for critical betas that can be a factor of $\gtrsim 2$ above those predicted by the simpler theories. The emergence of an acceptable reactor design point on the basis of these conservative assumptions and constraints, however, is viewed as encouraging for this approach.

Parametric trade-off calculations for the MSR have been directed at identifying attractive systems with modest power output (in contrast to the large reactor systems historically considered for stellarators) and economically viable systems (anticipated for low recirculating power reactors with neutron first-wall loadings $\gtrsim 1$ MW/m^2). These goals are subject to the abovementioned conservative physics assumptions and additional conservative engineering limits and constraints applied to the modular-coil design per se.

Sample parametric results from the MSR survey are shown in Figs. IV-3, IV-4 and IV-5. Figure IV-3 shows the dependence of $\langle \beta \rangle$ on A for a range of m numbers for $\ell = 2$ when the approximate and conservative equilibrium and stability beta limits

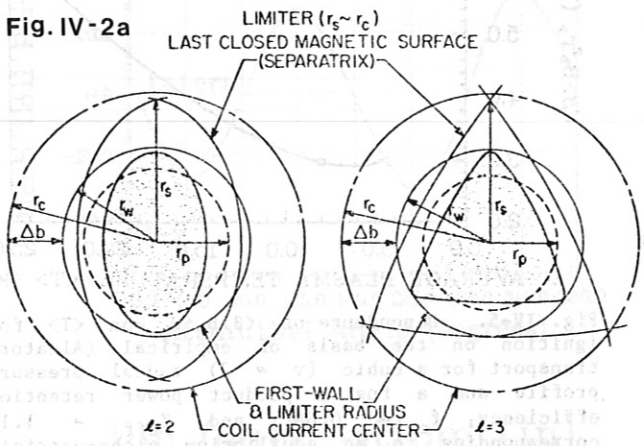

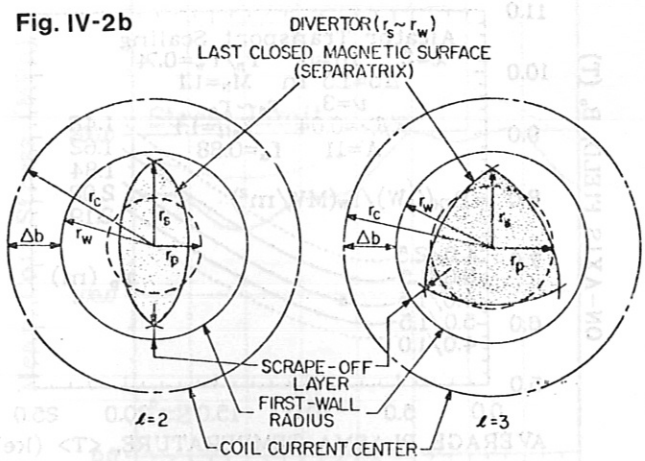

Fig. IV-2. Schematic relation of separatrix radius, r_s, to first-wall radius, r_w, and equivalent plasma radius, r_p, for $\ell = 2$, and $\ell = 3$ configurations assuming a) a limiter acting at $r_w(r_s \simeq r_c)$ and b) a magnetic divertor acting at $r_w(r_s \simeq r_w)$.

are imposed. The dependence of transform at the plasma edge, $\iota(r_p)$, for the first-harmonic lateral coil distortion, $d/r_c = 0.3$, on A is given in Fig. IV-4 for the beta-optimizing values $\ell = 2$ and $m = 6$, when $N = 24$ is selected to avoid coil interference. Lastly, Fig. IV-5 shows the dependence of $\langle\beta\rangle B_o^2 r_p$ on $\langle T\rangle$ required to achieve ignition for the assumed Alcator transport scaling, a cubic radial pressure profile and $f_\alpha = 0.88$. On the basis of this design curve the key interim parameters for the MSR shown on Table IV-I result. A specific value of r_p is obtained for a choice of total thermal output power, $P_{TH}(MW)$, and 14-MeV neutron first-wall loading, $I_W(MW/m^2)$. A value for $\langle\beta\rangle$ results from the imposed equilibrium and stability limits. The value of B_o required for ignition can then be computed as is shown in Fig. IV-6. For a given number of coils, N, the required coil current, $I_c(MA)$ can be estimated. For an overall coil current density, $j_c(MA/m^2)$, the coil thickness, $\delta_c(m)$, results, and a measure of coil interference is obtained. It is emphasized that the choice of P_{TH} and I_W is based on the desire to achieve ignition for a properly constrained set of coil parameters; an economic analysis has not yet been performed. In general, it becomes increasingly difficult to satisfy the coil non-interferance constraint as P_{TH} is lowered or as I_W is raised.

Achievement of a value $\langle\beta\rangle = 0.04$ requires an average rotational transform $\iota \sim 0.66$ for the equilibrium and stability limits imposed on beta. As seen from Figs. IV-3 and IV-4, it is anticipated that these parameters can be accomplished with an $N = 24$, $d/r_c = 0.30$ or an

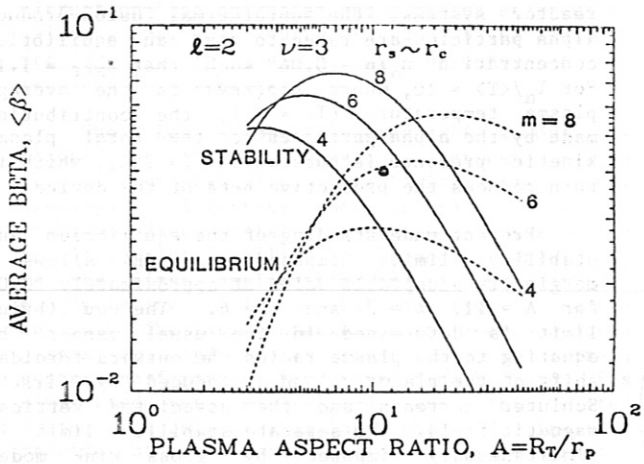

Fig. IV-3. Dependence of average beta, $\langle\beta\rangle$, on plasma aspect ratio, $A = R_T/r_p$, as dictated by simplified stability and equilibrium limits, for a range of toroidal field period numbers, m, with $\ell = 2$ and the use of a pumped limiter ($r_s \sim r_c$).

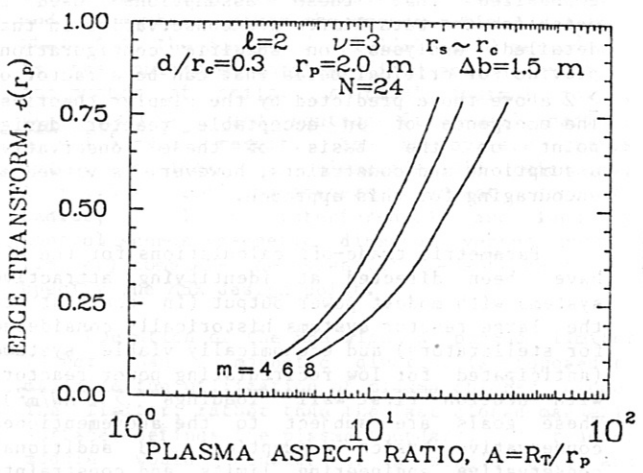

Fig. IV-4. Dependence of edge-plasma rotational transform for the first-harmonic lateral coil distortion, $d/r_c = 0.3$ on plasma aspect ratio, $A = R_T/r_p$, for a range of toroidal field period numbers, m, for an $\ell = 2$, $N = 24$ coil system, with $r_s \sim r_c$ as is appropriate for pumped-limiter impurity control.

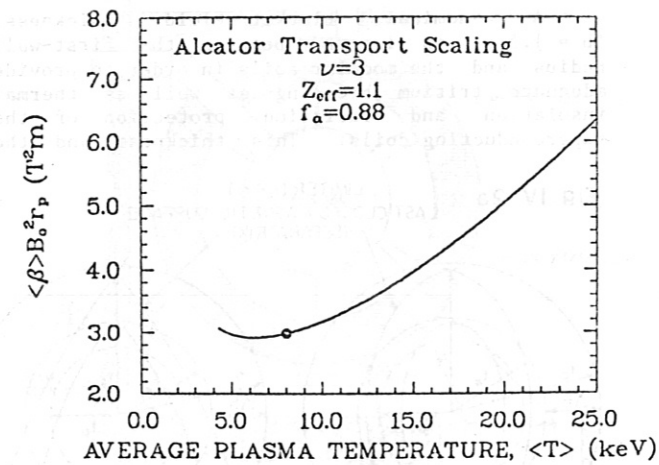

Fig. IV-5. Dependence of $\langle\beta\rangle B_o^2 r_p$ on $\langle T\rangle$ for ignition on the basis of empirical (Alcator) transport for a cubic ($\nu = 3$) radial pressure profile and a fusion product power retention efficiency, $f_\alpha = 0.88$, and $Z_{eff} = 1.1$, corresponding to an equilibrium alpha-particle concentration, $n_\alpha/n_i \sim 0.06$.

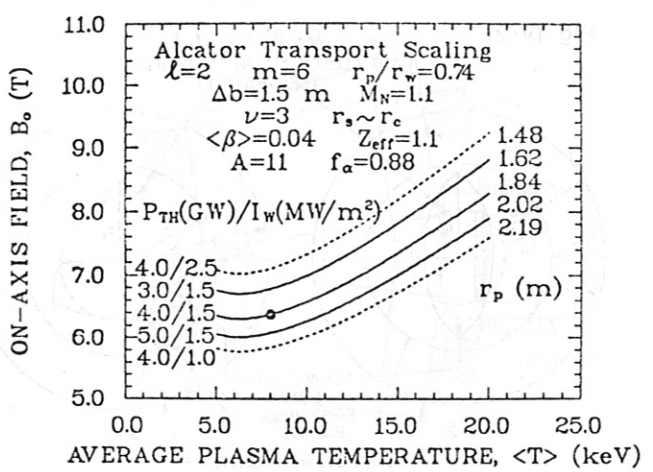

Fig. IV-6. Dependence of on-axis magnetic field, B_o on the average plasma temperature, $\langle T\rangle$, required for ignited MSR operation for the indicated values of the ratio $P_{TH}(MW)/I_W(MW/m^2)$ and corresponding plasma radii, $r_p(m)$, for the indicated fixed parameters.

N = 30, d/r_c = 0.25 coil configuration. Higher-harmonic coil distortion, in addition to the sinusoidal Rehker-Wobig[2] configuration, will be required to achieve the required rotational transform while still maintaining a relatively open, coil set.

The total thermal power output of the MSR point design is ~ 4.0 GWt and the neutron first-wall loading is ~ 1.5 MW/m^2. Ignited operation requires no recirculating power beyond a nominal fraction, f_{AUX} = 0.08, of the gross electrical output devoted to auxiliary plant equipment. Assuming that the thermal conversion efficiency is η_{TH} = 0.35, the net electrical output would be ~ 1.3 GWe, which is consistent with other contemporary fusion reactor conceptual designs and current fission reactor experience.[6]

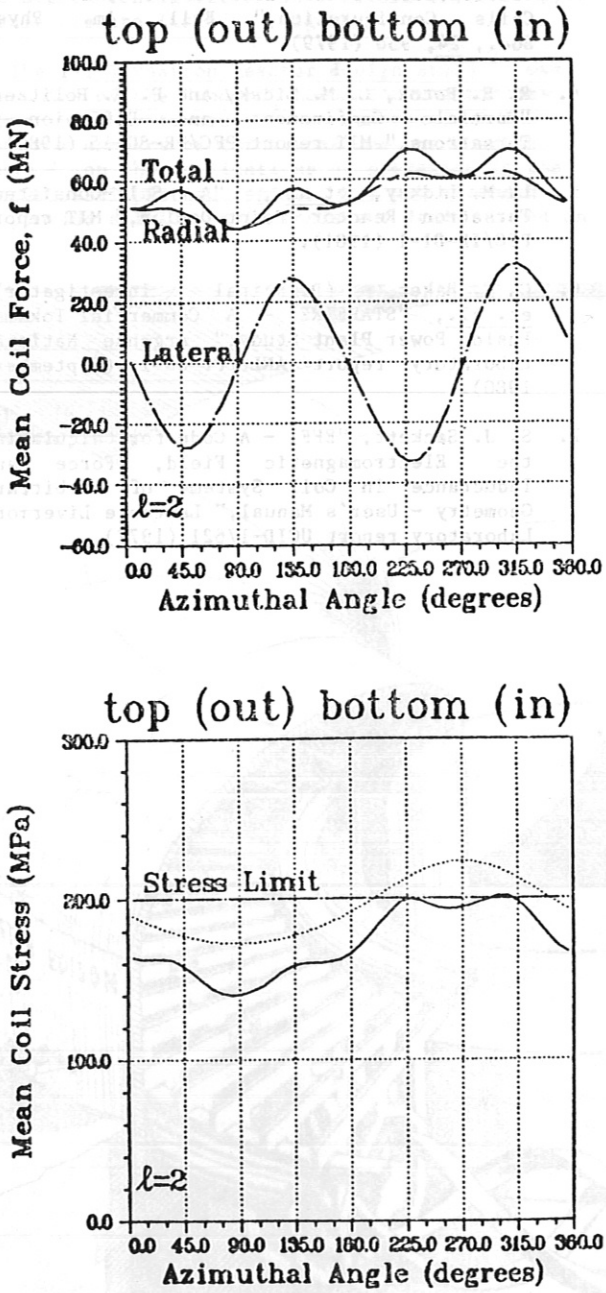

Fig. IV-7. Azimuthal dependence of radial and lateral coil forces and corresponding estimated stresses for the MSR design point summarized on Table IV-I.

A major aspect of the MSR study is the elucidation of the impact of the reactor point design on the engineering features of the required modular coils; the coil forces and stresses are of particular interest. Typical results from the three-dimensional magnetics computation for the MSR design point, using the EFFI code[7], are summarized in Fig. IV-7. Dominant coil forces (~ 60 MN) are directed radially outward from the minor axis, with smaller lateral forces (~ 30 MN) acting to increase the lateral coil deformation. The outward-directed radial forces avoid the need for support structures in the region devoted to the blanket/shield functions. Manageable peak stresses are estimated to be ~ 200 MPa, corresponding to ~ 0.1% strain in the internal coil support structure. The modular-coil configuration, therefore, appears to satisfy basic mechanical design criteria while simultaneously meeting the requirements for modularity and accessibility.

Detailed reoptimization of the MSR design point reported in Table IV-I on the basis of cost, magnetics calibration on the basis of more elaborate models, and engineering systems design are in progress. Additionally, the physics assumptions related to transport, equilibrium and stability are being reexamined by more exact models and contrasted with the predictions of the simplier models used here. The following conclusions have emerged from work to date,

i) A marginally attractive value of beta, as allowed by presently understood equilibrium and stability limits, conservatively applied, is a key limiting factor in MSR performance. Higher allowed values of beta would lead to lower confining fields, reduced coil forces and stresses, smaller systems and/or higher power densities.

ii) Application of conservative assumptions and constraints nevertheless allows the identification of potentially attractive MSR design points that "self-consistently" meet the requirements of stellarator physics performance in modular engineering configurations with maintenance, access and reliability advantages.

iii) A pumped-limiter impurity removal scheme may improve the performance of the MSR over that with a magnetic divertor traditionally associated with the stellarator/torsatron because of better volume utilization within the first wall and by allowing attainment of the assumed beta values at lower values of rotational transform.

iv) Relative to the tokamak, the higher-aspect-ratio stellarator may achieve similiar plasma power densities at lower average beta values for the same magnetic field limits imposed at the coil windings.

TABLE IV-I
INTERIM MSR DESIGN PARAMETERS

Stellarator Parameters	
Poloidal field periods, ℓ	2
Toroidal field periods, m	6
Rotational transform, ι	0.66
Average plasma radius, r_p(m)	1.84
Major radius, R_T(m)	20.2
Plasma aspect ratio, $A = R_T/r_p$	11.0
Mean coil radius, r_c(m)	4.58
Coil aspect ratio, R_T/r_c	4.41
Average separatrix radius, r_s(m)	3.98 ($\sim r_c$)
Plasma Parameters	
Radial pressure profile index, ν	3
Average temperature, $\langle T \rangle$(keV)	8.0
Average density, $\langle n_i \rangle (10^{20}/m^3)$	1.72
Average beta, $\langle \beta \rangle$	0.04
Energy confinement time, τ_E(s)	2.2
Lawson parameter, $\langle n \rangle \tau_E (10^{20} s/m^3)$	3.7
On-axis magnetic field, B_o(T)	6.4
Plasma power density, $p_F(MWt/m^3)$	~3.0
Alpha-particle loss fraction, $1-f_\alpha$	0.12
Alpha-particle partial pressure, p_α/p	0.25
Scrape-off parameter, $x = r_p/r_w$	0.74
Effective charge, $Z_{eff}(n_\alpha/n_i = 0.056)$	1.1
Magnet Parameters	
Number of coils, N(m = 6, ℓ = 2)	24
Coils per field period, N/m	4
Average coil radius, r_c(m)	4.58
Coil current, I_c(MA)	26.9
Coil current density, $j_c(MA/m^2)$	19.0
Coil lateral distortion, d/r_c	0.3
Coil thickness and width, δ_c(m)	1.19
Peak field at conductor, B_c(T)	~13
On-axis magnetic field, B_o(T)	6.4
Coil volume/mass (m^3/tonne)	44./110.
Stored magnetic energy, E_M(GJ)	~200.
Reactor Parameters	
Total thermal power, P_{TH}(GWt)	4.0
First-wall radius, r_w(m)	2.48
Major radius, R_T(m)	20.2
Plasma volume, $V_p(m^3)$	1340.
Neutron first-wall loading, $I_W(MW/m^2)$	1.5
System power density, $p_S(MWt/m^3)$	0.37
Blanket/shield thickness, Δb(m)	1.5
Blanket energy multiplication, M_N	1.1
Impurity control	pumped limiter

References

1. R. L. Miller and R. A. Krakowski, "The Modular Stellarator Fusion Reactor Concept," Los Alamos National Laboratory report (to be published, 1981).

2. S. Rehker and H. Wobig, "A Stellarator Field Produced by Twisted Coils," 6th European Conf. on Controlled Fusion and Plasma Physics, 1, 117-120 (July 30 - August 4, 1973).

3. T. K. Chu, H. P. Furth and C. Ludescher, "Stellarator Fields Based on the Twisted TF Coils Configuration," Bull. Am. Phys. Soc., 24, 956 (1979).

4. R. E. Potok, L. M. Lidsky and P. A. Politzer, "Particle Confinement and Diffusion in Torsatrons," MIT report PFC/PR-80-15 (1980).

5. L. M. Lidksy, et al., "A Self-Consistent Torsatron Reactor Point Design," MIT report PFC/IR-81-1 (1981).

6. C. C. Baker, (Principal Investigator), et. al., "STARFIRE - A Commercial Tokamak Fusion Power Plant Study," Argonne National Laboratory report ANL/FPP-80-1 (September, 1980).

7. S. J. Sackett, "EFFI - A Code for Calculating the Electromagnetic Field, Force and Inductance in Coil Systems of Arbitrary Geometry - User's Manual," Lawrence Livermore Laboratory report UCID-17621 (1977).

Annex V

THE T-1 SELF-CONSISTENT POINT DESIGN

The reference design reactor T-1 is a steady-state, large aspect ratio, modular, beam ignited system, possessing natural divertors, with the helical windings in a nearly "force free" configuration. With rather conservative engineering and plasma physics assumptions (e.g., $\bar{\beta}$ = 3.45%) this reactor produces 1520 MWe with $n\tau_E = 3\times10^{20}$ sec·m^{-3}. Figure 1 is a cutaway view of the reactor illustrating the confinement dome, access between coils, and a single module lifted out for replacement. The system configuration is sketched and the major parameters are listed in Figure 2.

The T-1 Torsatron Reactor design study [1] was the third of the "modern" torsatron reactor designs. The Kyoto study [2] concentrated on the divertor aspects of torsatrons and the Kharkov study [3] on the implications of operation in the neoclassical plateau regime. T-1 was intended to provide a fully self-consistent design based on conservative assumptions regarding both technology and physics. T-1 was not intended to be an optimized system, rather the idea was to see whether a self-consistent design point existed at all, to compare such a design with other potential fusion reactor schemes, to assess the sensitivity of the design to various technological and physics assumptions, and to point out those areas which needed further studies. The most significant results of the T-1 program in addition to the fact that a self-consistent design was possible were the studies of alpha-particle thermalization [4] and ion heat transport [5] performed expressly for T-1. In the following sections, we describe the initial assumptions of the T-1 design, the resulting reactor, the conclusions we draw from the design and the goals of the T-2 design now in progress. The thermodynamics and transport results are reported elsewhere in this document.

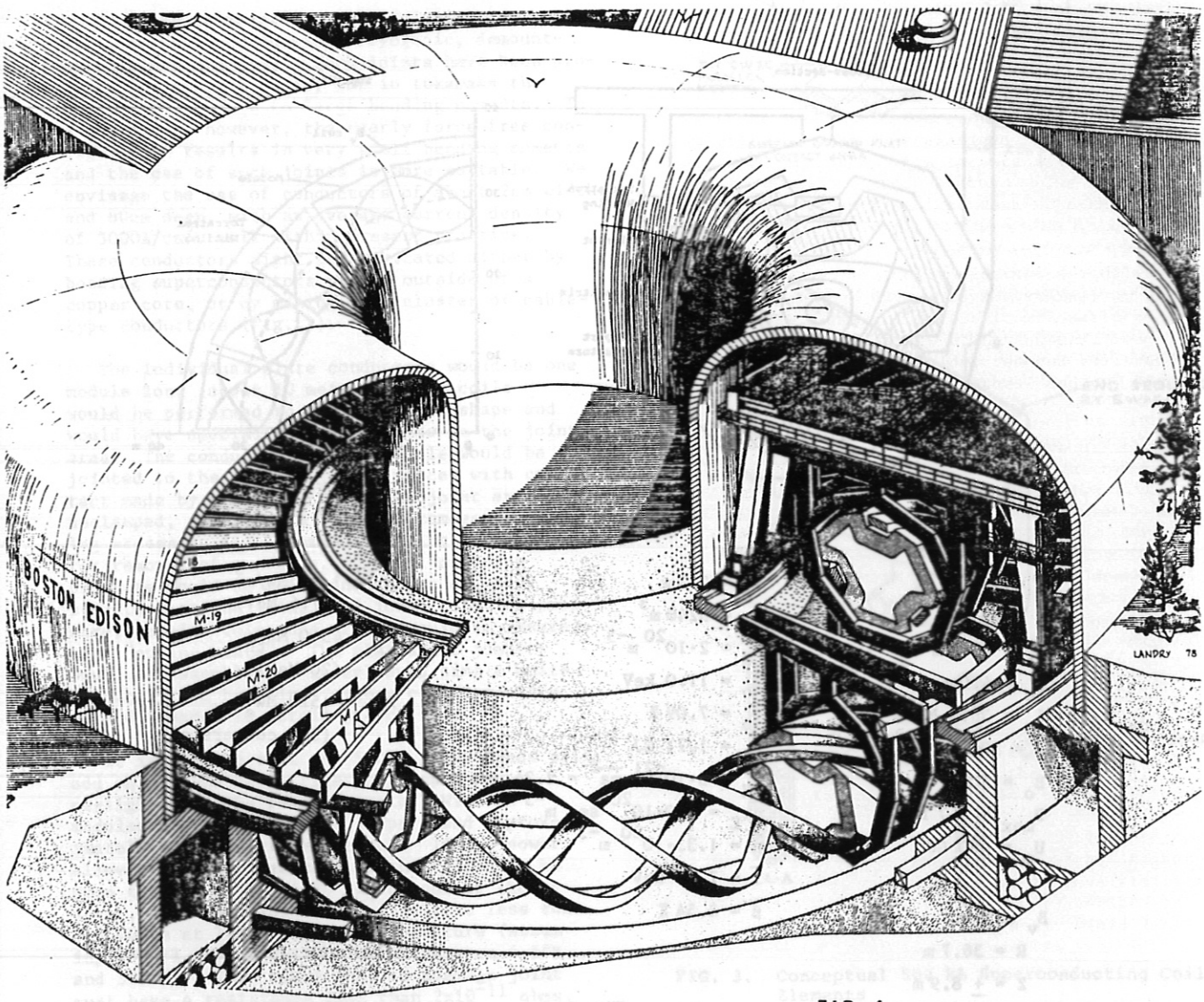

FIG. 1

Design Assumptions

The technological requirements imposed on the T-1 design were:

a. wall loading of 1 MW/m^2,

b. minimum blanket and shield thickness of 1.5m,

c. near force-free winding configuration,

d. modular coil structure,

e. 8.7 tesla maximum field in the conductor.

The physics assumptions were:

a. operation in the neoclassical plateau regime,

b. average plasma beta equal to average vacuum magnetic well,

c. Alcator empirical scaling.

Winding and Modularity

The reactor has an ℓ=3 coil system, with 20 field periods. Thus it is constructed of 20 identical removable modules. The choice of ℓ=3 windings is determined by the requirement that the coil be wound at the force-free pitch, and that there be sufficient room between the separatrix and coil for a scrape-off region, about 0.25m thick and for blanket, shield, and the finite thickness of the coil itself. Following our conservative approach, we have allowed a minimum of 1.5m for blanket and shield. Since average plasma minor radius is set by considerations of β and $\overline{n}\tau_E$ to 2.3m, the minor radius of the windings becomes 4.0m. An ℓ=2 system would give too small a plasma, and ℓ=4 would not leave enough room for blanket and shield. The choice of major radius, and the number of field periods is more flexible. However, in order to maintain the requirement that the reactor structure be made of easily separable modules, the aspect ratio of the winding

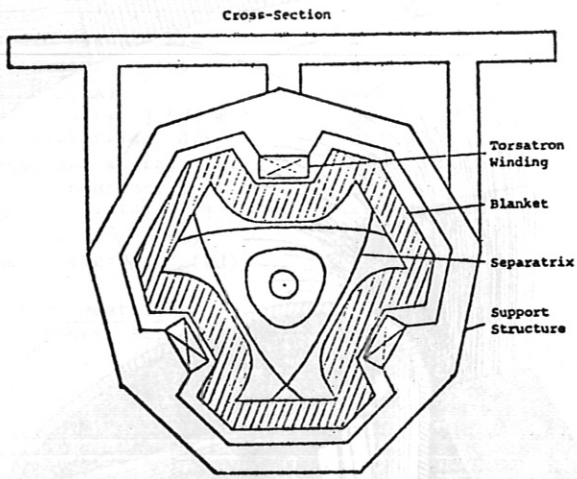

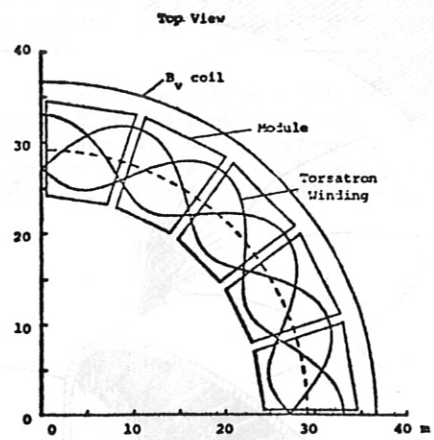

Helical coils:

$\ell = 3$

$N = 20$

$R_o = 29.2\ m$

$a_c = 4.0\ m$

$I_o = 36.5\ MA$

$J = 3000\ A/cm^2$

$B_o = 5\ T$

$B_{max} = 8.7\ T$

$U_m = 460\ GJ$

B_v coils:

$R = 36.7\ m$

$Z = \pm 8.9\ m$

$I = -34.8\ MA$

Plasma:

$\overline{a}_p = 2.3\ m$

$v_p = 3240\ m^3$

$n_o = 2 \cdot 10^{20}\ m^{-3}$

$T_o = 11.0\ keV$

$\beta_o = 7.09\ \%$

$U_p = 1{,}71\ GJ$

$\tau_E = 3 \cdot 10^{-21}\ \overline{n}a^2 = 2.24\ sec$

$\overline{n}\tau_E = 3.0 \cdot 10^{20}\ sec\ m^{-3}$

$\overline{n} = 1.33 \cdot 10^{20}\ m^{-3}$

$\overline{T} = 7.33\ keV$

$\overline{\beta} = 3.54\ \%$

Output:

$\overline{p}_f = 1.18\ MW/m^3$ (17.6 MeV)

$P_f = 4340\ MW_{th}$ (20 MeV)

$P_{el} = 1520\ MW_e$ (35% conversion)

Fig. 2

should be at least 6-8. Furthermore, considerations of particle confinement lead also to aspect ratios in this range. This keeps the toroidal magnetic field ripple (of the order of the inverse aspect ratio) small compared to the helical ripple. In addition, for safety the helical coils should be constructed of one continuous winding , rather than three separate ones, so that if the superconducting winding should go normal, the current decreases uniformlly in the helix, the force reduced characteristics are maintained, and large unsupported forces do not arise. Therefore, we have chosen 20 field periods, compatible with a single conductor making three transits of the system.

As noted, the windings are superconducting. If the nominal magnetic field on the plasma axis is 5.0T, then the maximum field at the winding is 8.7T, allowing the use of NbT_i superconductor. In order to produce this field 36.5MA are required in each winding. Preliminary design studies show that single conductors carrying 500kA can be fabricated, thus each winding consists of 73 turns.

In order to maintain the modularity of the device, normally conducting, cryogenic, demountable joints are used. Such joints have been proposed for tokamak coils, but in tokamaks the joints are subject to large bending moments. In a torsatron, however, the nearly force free configuration results in very small bending moments and the use of such joints is more suitable. We envisage the use of conductors of about 2cm width, and 80cm deep, with an average current density of $3000A/cm^2$, well within present practice. These conductors might be fabricated either by bonding superconductors to the outside of a copper core, or by making up a cluster of cable-type conductors (Fig. 3).

The individual plate conductors would be one module long (about 10 meters). The coils would be performed to the torsatron shape and would have specially prepared ends in the joint area. The conductors in one module would be jointed to the next by jumper pieces with contact made by pressure. When the joint area is unclamped, the jumpers could be removed, giving access to the intermodule joint as required for removal of a module. Overall clamping pressure would be maintained by an external structure at the joint, and local clamping pressure, despite tolerance errors would be assured by a "spring plate". The plates and jumpers would be assembled as interleaved single units to facilitate handling. These considerations were discussed in detail by Uchikawa. [6]

It is notable that the 500kA input leads will add only 1.5MW of refrigerator input power, negligible on the reactor scale. With 20 modules there would be 60 jumpers and approximately 9000 individual joints. If the power allowed for refrigeration of the joints is no more than 1% of the 4340 MW_t output of the reactor, then each joint must dissipate less than 4.9 watts at liquid helium temperature (assuming 1000:1 refrigeration factor between 4.5°K and 300°K). This means that an average joint must have a resistance less than $2x10^{-11}$ ohms. The jumpers in the present design have an overlap of 40 cm, giving a contact area of 3200 cm^2, and requiring a contact resistance of below $6x10^{-8}$ ohm-cm^2. Such values are routinely achieved in small magnets. Thus, although work is needed in scaling present conductors to the 500kA size, the reactor magnet does not require performance beyond that already surpassed in small-scale laboratory tests.

The T-1 design uses a single pair of compensation coils, located at a radius of 36.7m,

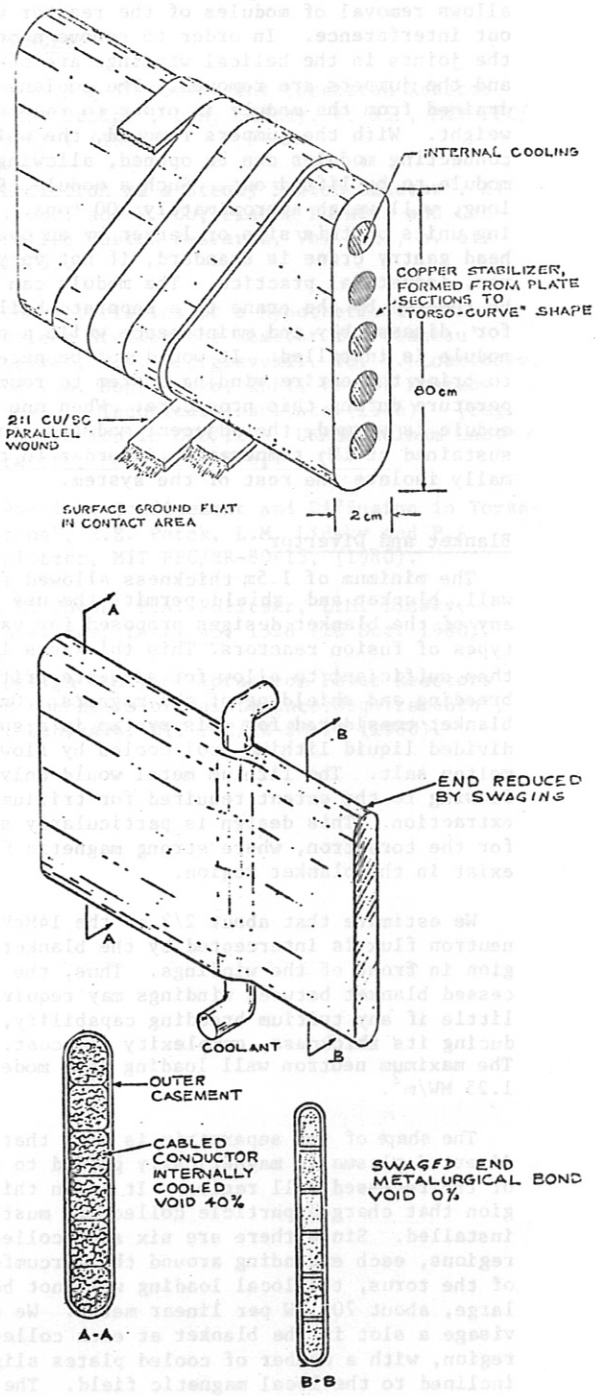

FIG. 3. Conceptual 500 kA Superconducting Coil Elements

and heights of ±8.9m. Each carries a nominal current of -34.8 MA. This arrangement cancels the vertical magnetic field on the geometric axis with the same curvature index as the vertical field generated by the helical windings and provides good cancellation over a large part of the plasma cross-section. In addition, these windings bring the net dipole moment of the torsatron to zero, reducing both the magnetic energy stored and the stray magnetic fields. These coils are 11.6m from the axis of the helix and so are readily supported by the structure of the reactor building. This space allows removal of modules of the reactor without interference. In order to remove a module, the joints in the helical windings are opened and the jumpers are removed. The coolant is drained from the module in order to reduce its weight. With the jumpers removed, the welds connecting modules can be opened, allowing the module to be lifted out. Such a module, 9.17m long, will weigh approximately 500 tons. Lifting units of this size or larger by an overhead gantry crane is standard, if not very common, industrial practice. The module can then be removed by the crane to a separate building for disassembly and maintenance while a new module is installed. It would not be necessary to bring the entire winding system to room temperature during this procedure. When one module is warmed, the adjacent modules can be sustained at LN_2 temperature in order to thermally isolate the rest of the system.

Blanket and Divertor

The minimum of 1.5m thickness allowed for first wall, blanket and shield permits the use of almost any of the blanket designs proposed for various types of fusion reactors. This thickness is more than sufficient to allow for adequate tritium breeding and shielding of the magnets. One blanket considered for this system is a subdivided liquid lithium pool cooled by flowing molten salt. The lithium metal would only be flowing to the extent required for tritium extraction. This design is particularly suited for the torsatron, where strong magnetic fields exist in the blanket region.

We estimate that about 2/3 of the 14MeV neutron flux is intercepted by the blanket region in front of the windings. Thus, the recessed blanket between windings may require little if any tritium breeding capability, reducing its thickness, complexity and cost. The maximum neutron wall loading is a moderate 1.25 MW/m^2.

The shape of the separatrix is such that the diverted plasma is magnetically guided to part of the recessed wall region. It is in this region that charged particle collectors must be installed. Since there are six such collection regions, each extending around the circumference of the torus, the local loading will not be large, about 700 kW per linear meter. We envisage a slot in the blanket at each collection region, with a number of cooled plates slightly inclined to the local magnetic field. The charged particle energy will be deposited on these plates, and the cold gas will be pumped through vacuum manifolds located outside the blanket. A large scrape-off layer, 25cm thick is allowed between the separatrix and the nearest first wall.

Plasma Containment and Heating

The plasma characteristics of particular importance for fusion reactor design are energy confinement time, power density, β, and the confinement of alpha particles. These parameters have been considered on the basis of numerical calculations, some extrapolations from current experimental devices, and some basic theoretical considerations. Conservatism was particularly justified in this regard since detailed theoretical models did not exist at the time of the T-1 design.

Of particular concern is the limiting β in such a device. The most pessimistic estimate of the equilibrium β limit is obtained from calculation of the vacuum magnetic well depth, i.e., the variation in the flux surface average of B^2: $\langle B^2\rangle = \int B d\ell / \int (d\ell/B)$. The flux surfaces in a torsatron with the magnetic axis coincident with the geometric axis are almost identical to those derived for the straight torsatron configuration. For an $\ell=3$ system with coincident axes the rotational transform vanishes on the axis and increases with r^2. $\langle B^2\rangle$ is independent of radius for this case and there is no magnetic well. However, when the magnetic axis is displaced outward, the axis becomes helical, a finite rotational transform is generated on the axis, and a magnetic well is produced. The well depth depends on displacement of the axis, but the exact nature of this dependence is not yet clear. However, well depths exceeding 7% have been calculated for T-1 reactor parameters with acceptable shifts of the magnetic axis. These values are all based on vacuum field calculations. The variation of rotational transform with radius and axis shift is that it is easy to achieve a significant rotational transform on the axis, even of the order of unit, in an $\ell=3$ system.

Since T-1 is a large aspect ratio device, resistive heating of the plasma can be ruled out. The limit on possible plasma current by stability considerations is so low that the power input is negligible. Furthermore, there is strong experimental evidence that the presence of an induced toroidal current degrades the energy confinement time. Heating with electromagnetic radiation is a possibility, but was ruled out in the present reactor design because of insufficient data on its effectiveness. The heating method chosen is energetic neutral beam injection. The physics of energy deposition by such beams is well understood, and the problems of development of high energy, high power sources for reactor scale plasmas are being intensively studied. Approximately, 500MW of beam power would be required to reach ignition conditions.

Estimation of the energy confinement time in any reactor is difficult at best, and any choice of scaling law can be subject to ques-

tion. We used Alcator Empirical Scaling for the T-1 design. The $n\tau$ values derived on this basis were very close to those derived using neoclassical plateau theory although, of course, the scaling was different.

$$\tau_E = 3\times10^{-21}\ \bar{n}a^2 .$$

Many devices show such scaling, often with a coefficient larger than seen in Alcator. We, therefore, take this scaling as a conservative estimate, and obtain, for $\bar{n} = 1.33\times10^{20} m^{-3}$, $\tau_E = 2.24$ sec, and $\bar{n}\tau = 3.0\times10^{20}$ sec$\cdot m^{-3}$. The operating conditions are based on two considerations. First of all, the vacuum well depth indicates that T-1 can contain a central β of about 7 percent. In order to mitigate the possible effects of the large radial excursions undergone by certain classes of trapped particles, the plasma should operate in the "plateau" regime, so the central density is kept relatively high, at 2.0×10^{20} m^3, and the central temperature low, at 11.0keV. These conditions place the bulk of the plasma at the transition between plateau and banana regimes. Assuming a parabolic β profile, and thus broader than parabolic density and temperature profiles gives $\bar{n} = 1.33\times10^{20}$ m^{-3}, $\bar{T} = 7.33$ keV, and $\bar{\beta} = 3.54\%$. These parameters yield an output power of 4340 MWth or 1520 MWe, assuming 20 MeV per fusion event and 35% thermal conversion efficiency.

Conclusions

We draw the following conclusions:

1. The torsatron concept, even with conservative physics and technology constraints, is capable of serving as basis for an acceptable fully self-consistent reactor design.

2. The idea of resistive joints in full scale reactors is technologically feasible without additional development of existing resistive joints. Nonetheless, the detailed working out of this concept shows such joint to be complex; a better solution is desirable.

3. The physical size and net power output of the T-1 reactor are determined by physics assumptions that have been shown to be unnecessarily conservative. The reactor could be improved by operation at lower collisionality and lower aspect ratio. Recent developments in superconducting magnet technology indicate that substantially higher fields are achievable. A design reflecting these factors would presumably be smaller in both output and size with accompanying economic advantages.

4. Although the force free $\ell=3$ winding has attractive features these cannot all be exploited in practice. Advanced winding laws can be used to allow improved access to the blanket as well as simplifying the requirements placed on external field compensating coils.

These considerations will be embodied in our second generation, self-consistent reactor design, T-2. We will maintain the same degree of conservatism in technological constraints except for maximum field intensity. Plateau regime operation will no longer be demanded and the alpha particle trajector code will be used to determine the minimum acceptable aspect ratio. The effect of these changes will be, we think, to reduce the electrical power output to the $600MW_e$ range. We will attempt in this design to develop a helical conductor winding law compatible with the requirements of both particle transport and blanket access through fixed coils.

REFERENCES:

1. "T-1: A Self-Consistent Torsatron Reactor Point Design", L.M. Lidsky, et al., MIT PFC/IR-81-1 (1981).

2. "Heliotron as a Steady Fusion Reactor", A. Iiyoshi and K. Uo, Plasma Physics and Controlled Fusion Research, Vol. III, p. 619 (1975).

3. "Characteristics of a Hypothetical Thermonuclear Stellarator Reactor in 'Plateau' Regime", A.V. Georgievskii, Yu. M. Loktionov, and V.A. Suprunenko, KhFTI 76-38, Kharkov Physico-Technical Institute (1976). [Eng. Translation in CTO/1299, UKAEA Culham Laboratory, November 1976].

4. "Particle Confinement and Diffusion in Torsatrons", R.E. Potok, L.M. Lidsky and P.A. Politzer, MIT PFC/RR-80-15, (1980).

5. R.E. Potok, P.A. Politzer, L.M. Lidsky, Phys. Rev. Lett. 45, 1328 (20 Oct. 1980).

6. "Design Study of Torsatron Power Reactors on the Basis of Maintenance Requirements", T. Uchikawa, MIT PFC/RR-80-20 (1980).